THE EFFECT OF SEASONAL SOIL FROST ON THE ALPINE GROUNDWATER RECHARGE INCLUDING CLIMATE CHANGE ASPECTS

THÈSE N° 2709 (2003)

PRÉSENTÉE À LA FACULTÉ ENVIRONNEMENT NATUREL, ARCHITECTURAL ET CONSTRUIT

SECTION DE GÉNIE CIVIL

ÉCOLE POLYTECHNIQUE FÉDÉRALE DE LAUSANNE

POUR L'OBTENTION DU GRADE DE DOCTEUR ÈS SCIENCES

PAR

Daniel BAYARD

physicien diplômé EPF
de nationalité suisse et originaire de Varonne (VS)

acceptée sur proposition du jury:

Prof. A. Parriaux, directeur de thèse
Prof. P. Germann, rapporteur
Prof. P.-E. Jansson, rapporteur
Dr M. Stähli, rapporteur
Dr P. Turberg, rapporteur
Prof. L. Vulliet, rapporteur
M. F. Zuber, rapporteur

Lausanne, EPFL
2003

A Marie-Noëlle, Eric, Erica, Romaine et Joël.

Acknowledgements

I would like to thank my supervisor, Prof. Aurèle Parriaux, who gave me the opportunity to carry out this research project and let me the freedom to go my own research direction; Prof. Hannes Flühler, who offered me the possibility to work with his team and supported me with technical assistance.

A special thank-you goes to Manfred Stähli who supported me during these three years. He filled my numerous scientific and linguistic gaps and gave me several opportunities to present my work in many parts of Europe.

Also many thanks to:

Pascal Turberg, Véronique Maître and Laurent Tacher, who supported me in Lausanne and introduced me to some concepts of geology. Pascal and Véronique also reviewed part of my thesis.

Patrice Gallay, Hans Wunderli, Hannes Wydler and Jörg Leuenberger, who provided important technical assistance.

Hug Dufumier, for digging and measuring under all possible weather conditions at Gd St Bernard.

Alex Anamatten, for his conscientious work at Hannigalp.

Hermann Rovina, for convincing me to go to this wonderful site of Hannigalp,

Michel Dylsi, for his advice and critical statements about the work.

Alfred Anderau, Shelagh Green and Ruth Borloz. Each of them improved the language of some parts of this work.

The entire team at the Gd St Bernard home for providing a warm and friendly welcome during my numerous stays at the monastery.

The villages of Grächen and Gd St Bernard, as well as the ski-resort of Grächen. In particular I would like to thank Ignatz Amstutz, Simon Ruf and Michel Bregy for they friendly support during my stays in Grächen

Many thanks also to the people from the GEOLEP, with whom I spent the last three years: in particular to Pierre Tullen with whom I shared my office, to Thierry Bussard, Giuseppe Franciosi, Sybille Kilchmann, Sébastien Rotté-Capet, Mike Bensimon, Alina Tomaniak, Xavier Pittet, Bernard Sperandio and all the other for the time spent together ski touring, eating fondues or making other odd things.

Finally, I would like to thank the different persons who accepted to be part of the examining board: Prof. P. German, Prof. P.-E. Jansson, Prof. L. Vulliet and F. Zuber.

Summary

In alpine areas, the snow cover plays an important role as a water reservoir. Water is stored as snow over the winter and released in spring, recharging mountain aquifers through infiltration. These aquifers are essential, especially for supplying water for human activities during dry seasons.

Numerous studies have shown that *locally* soil frost can drastically reduce the water infiltration. However, we know much less about the hydrological impact of soil frost *at a larger scale*, in particular with regard to groundwater recharge. This was our motivation for initiating an extensive field experiment in the southern Swiss Alps. Several methods at different spatial scales were adapted to explore (a) the local effect of a partially frozen ground on the snowmelt discharge in an alpine area, (b) the key processes influencing groundwater recharge during snowmelt periods, such as snow cover and soil frost evolution, snowmelt water runoff types, (c) the large-scale effect of soil frost on the aquifer recharge, and (d) winter situations that are critical with respect to flooding.

In order to take into account spatial, altitudinal and climatic differences, the field study was run for two winter seasons at Gd St Bernard (2500 m), a site with very high winter precipitation and strong winds, and at Hannigalp above Grächen (2100 m), a ski resort with a rather dry winter climate. The different components of the soil water balance (lateral runoff, deep percolation, liquid soil water content) were measured on delimited plots of 5 m^2. Additionally, a dye tracer experiment visualized the snowmelt infiltration patterns into the frozen, respectively non-frozen ground. At Gd St Bernard, investigations of the liquid water content and the soil temperature were additionally conducted at two secondary sites, differing in their orientation, so as to gain a better insight of the spatial soil frost expansion. Finally, an analysis of the water-table variation at the village of Grächen (some 500 m below Hannigalp) during the snowmelt was carried out for a 10-year time period, including our experimental seasons. We complemented our field investigations by using a numerical soil-snow-atmosphere transfer model that simulates the seasonal development of the soil frost and the snow cover, as well as lateral and vertical water flow in the top soil. This model was used as an upper boundary condition to a 2-D groundwater model, to calculate the outlet flow at the base of a simplified alpine aquifer.

The two winters investigated had contrasting meteorological conditions, which resulted in intriguing differences and similarities with respect to the soil physical conditions: the first one having a thick snowpack and hardly any soil frost, and the second one with hardly any snow until January and a deep and persistent soil frost. In spite of a very thick snowpack, the water balance measurements from winter 2000/2001 showed for both sites zero to low surface and subsurface flow due to the fact that soil frost was local and the soil permeability high. During the next winter, approximately 25% of the total meltwater run off laterally. The soil infiltration capacity was mainly reduced by the presence of a basal ice sheet, caused by the freezing of meltwater after a mid-winter snowmelt event.

The field data were used to calibrate and validate a physically-based one-dimensional model. To allow an accurate parameter setting for the water repellent soil of Hannigalp, laboratory infiltration experiments on soil columns were additionally carried out. Using the resultant information, the model predicted correctly most measured soil parameters, in particular good matching was observed between measured and simulated snowmelt discharge. At Gd St Bernard, the simulated results were less satisfactory, especially during the first winter, when large discrepancies were noted between measured and simulated lateral runoff. Apart from the

shortage in the soil parameter characterization, the deviation was a result of the simplified description of the experimental field. The model was, for example, not able to simulate surface runoff generated by a steep slope under unfrozen conditions, as the soil surface is considered by the model to be flat. Nevertheless, results were accurate enough to reproduce the occurrences of snowmelt events and the accumulated values of snow-melt discharge pathways under frozen conditions.

Long-term weather data were used to simulate the soil frost depth at both sites. The simulation results showed that the probability of the occurrence of frozen soils was lowest on slopes with south or north exposure. On southerly exposed plots, the heat stored in the soil during the summer inhibited the development of deep and persistent soil frost, while most pore ice thawed due to underneath heating. On north plots, the building of soil frost was rare, as early snowfall insulated the ground from the atmosphere. However, during snow-poor winters, the frost penetrated deep into the ground, and the low underneath heat flux at that location hardly affected the frost depth until snowmelt. The snow depth and average soil temperature were hence the two components affecting the frost depth extent. The altitude soil frost variation was related to the spatial extent of these two components. The higher the altitude, the higher the precipitation and the lower the mean air/surface temperature. Simulating the whole Grächen recharge area, seasonal soil frost was rare between 1800 m and 2000 m, as the snowpack was thick enough to insulate the ground, and the soil was warm enough to inhibit deep soil frost. In lower areas, the shallow snowpack enabled the soil to freeze during most winters, whereas at higher areas, deep and persistent soil frost was simulated due to the low underneath heating.

A 10-year water-table depth record was used to examine possible large-scale effects of seasonal soil frost. We noted that the water-table rise at snowmelt was lowest at the end of winters with extensive soil frost. However, such winters were characterized by low precipitation, and reduced snow cover. In contrast, winters with little soil frost were mostly snow rich. Consequently, only a reduced number of winters were directly comparable. Considering these winters, the reduction in the water-table rise at snowmelt due to seasonal soil frost varied only between 10 and 30%, as, during snowmelt, most meltwater was able to re-infiltrate into the very permeable ground in lower unfrozen areas. We may assume that a soil with a smaller infiltration capacity can increase the influence of the soil frost on the aquifer recharge.

Finally, we investigated the effect of a changing climate on the hydraulic and thermic regimes at different altitudes in the area of Grächen. We assume an increase in the air temperature of 2°C generates deeper soil frost on lower areas, as the resultant smaller snow cover does not insulate the soil from the atmosphere any more. However, it does reduce the soil frost on higher, snow rich areas, due to the warmer air temperature. As a whole, minor changes were simulated on the mean groundwater recharge, as more/less meltwater was able to infiltrate in higher/lower areas. By increasing additionally the precipitation by 15%, the soil frost diminished slightly over the whole catchment. By combining both climate change scenarios, we may expect an increase in extreme events, as, on the one hand, the rainfall intensity increases, and, on the other hand, rain on snow events over frozen soils occurs more often in lower areas.

In practice, this work shows the importance of better investigating the hydrothermal behaviour of alpine regions. Such a knowledge is necessary, as more and more efforts are put into managing efficiently, durably and globally the available water resources. This work stresses also the necessity to consider seasonally soil frost in alpine risk management. As an example, flooding is mostly a consequence of strong rain precipitation at high altitudes combined with heavy snowmelt. Obviously, the risk of extreme runoff events increases during frozen winters,

when the soil infiltration capacity is further reduced by the soil ice. Also, it has been shown that unstable slopes are mostly related to specific hydrogeological situations, like strong precipitation, which induces a sharp increase in the underneath water circulation. The melt water in spring is hence a potential activating factor, and a frozen soil may reduce the risk of sliding, as less water infiltrates into the ground.

Version abrégée

En région alpine, la couverture neigeuse joue un rôle essentiel en tant que réservoir d'eau. L'eau est stockée sous forme de neige durant l'hiver. Au printemps, l'eau de fonte s'infiltre dans le sol, rechargeant les aquifères alpins sous-jacents. Ces aquifères constituent une source d'eau primordiale comme approvisionnement pour les différentes activités humaines durant la période sèche, lorsque les précipitations sous forme de pluie diminuent ou sont quasiment inexistante.

De nombreuses études ont montré que *localement* le gel partiel dans le sol peut réduire de manière drastique l'infiltration de l'eau. Néanmoins, l'impact hydrologique du gel saisonnier à plus grande échelle, en particulier par rapport à la recharge des eaux souterraines, est moins bien connu. Ce fut le point de départ de cette étude. Plusieurs méthodes à différentes échelles spatiales ont été appliquées afin d'explorer: (a) l'effet local d'un sol partiellement gelé sur les flux de fonte, (b) les processus dominants qui affectent la recharge, tels que l'évolution du manteau neigeux, du gel dans le sol et les différents types d'écoulement de l'eau de fonte, (c) les effets à grandes échelles qu'occasionnent un gel partiel sur la recharge d'aquifères, (d) des situations hivernales qui sont critiques par rapport aux risques d'inondations.

Afin de tenir compte de la variabilité spatiale, climatique, ainsi qu'en fonction de l'altitude, l'étude a été menée durant deux hivers au Gd St Bernard (2500 m), un site avec de fréquentes précipitations et de forts vents, et à Hannigalp (2100 m) au-dessus de Grächen, une station de remontées mécaniques ayant un climat plutôt sec. Les différentes composantes du bilan hydrique du sol (flux latéral, percolation profonde, teneur en eau liquide du sol) ont été mesurées sur des sites spécifiques d'environ 5 m^2. De plus, un essai de traçage a permis de visualiser l'infiltration de l'eau dans un sol respectivement gelé et non gelé. Au Gd St Bernard, des mesures additionnelles de la teneur en eau liquide et de la température du sol ont été faites sur deux sites annexes d'orientation différente. Ces mesures ont permis de caractériser la variation du gel saisonnier en fonction de l'exposition. Finalement une analyse de la variation du niveau piézométrique lors de la fonte de la neige d'un aquifère alpin au village de Grächen (500 m en dessous de Hannigalp) a été effectuée durant une période de 10 ans. Les deux ans de mesures au site de Hannigalp sont inclus dans cette période. A côté des investigations de terrains, un modèle numérique de transfert sol-neige-atmosphère a été utilisé, simulant le développement saisonnier de la profondeur de gel et de la hauteur de neige, ainsi que du flux d'eau latéral et vertical dans la partie supérieur du sol.

Des conditions météorologiques contrastées ont caractérisé les deux années étudiées. En 2000/ 2001 la couverture neigeuse a été profonde et le sol n'a pas gelé. En 2001/2002 quasiment aucune précipitation neigeuse n'a eu lieu jusqu'en janvier, ce qui a permis la formation d'un gel profond et persistant. En 2000/2001, malgré une épaisse couche de neige, très peu d'eau de fonte s'est écoulée latéralement dans la partie supérieure du sol (entre 0 et 10% de l'eau de fonte), le sol très perméable permettant à l'eau de s'infiltrer. Durant l'hiver suivant, environ 25% de l'eau de fonte s'est écoulée latéralement. La capacité d'infiltration du sol a été principalement réduite par la présence d'une couche de glace qui s'est formée sur la surface du sol après différents épisodes de fonte en hiver.

Les données de terrains ont été utilisées afin de calibrer et valider un modèle numérique physique uni-dimensionnel. Afin de permettre une calibration optimale du sol hydrophobe de Hannigalp, des essais d'infiltrations sur des colonnes de sol en laboratoire ont été effectués. En utilisant les informations ainsi obtenues, le modèle a simulé correctement la majorité des paramètres mesurés, dont la fonte de la neige entre autre. Au Gd St Bernard, les résultats de

simulations ont été moins probants, en particulier durant le premier hiver, lorsque des différences notoires se sont produites entre le flux latéral simulé et mesuré. En dehors de l'insuffisance dans la caractérisation des paramètres du sol, cette déviation a été une conséquence de la description simplifiée du site d'expérimentation (par exemple le sol est supposé avoir une pente nulle). Le modèle a sous-estimé le flux de surface lors du premier hiver non-gelé. Néanmoins, les simulations ont reproduit les différents événements de fonte de neige, ainsi que les valeurs cumulées des différents composants du flux de fonte lorsque le sol était gelé.

Des données météorologiques ont été prises en considération afin de simuler la variation de l'état physique du sol sur plusieurs années. Les résultats des simulations ont montré que la probabilité d'apparition du gel était la plus faible dans des régions orientées au sud et au nord. Pour les pentes au sud, la chaleur emmagasinée dans le sol durant l'été s'oppose au développement d'un gel profond et persistant. La majeure partie du sol dégèle durant l'hiver et, lors de la fonte de la neige au printemps, le sol n'est que faiblement gelé. Sur les pentes au nord, l'apparition fréquente d'un manteau neigeux précoce empêche le plus souvent le sol de geler. Néanmoins, durant des hivers pauvres en neige, le gel pénètre profondément dans le sol. Il n'est que faiblement affecté par le flux de chaleur sous-jacent et persiste jusqu'à la fonte de la neige. Les deux facteurs prépondérants pour la formation du gel dans le sol sont l'épaisseur de neige au début de l'hiver ainsi que la température moyenne du sol. Ces deux facteurs varient en fonction de l'altitude. A haute altitude les précipitations sont plus importantes, alors qu'à basse altitude la température moyenne de l'air augmente. Dans la région de Grächen, les résultats des simulations numériques ont montré que le gel saisonnier était le moins fréquent entre 1800 m et 2000 m. A ces altitudes, le manteau neigeux est suffisamment épais pour isoler le sol, alors que la température moyenne du sol est déjà assez haute pour empêcher un gel profond. Dans des régions plus basses, le sol gèle plus souvent à cause d'une faible couverture neigeuse, alors que dans les régions plus élevées, le sol gèle profondément durant les hivers sans neige car le flux thermique sous-jacent est faible.

Des mesures piézométriques ont permis d'examiner à grande échelle les effets d'un gel saisonnier. Durant les 10 années de mesures, l'augmentation du niveau de la nappe au moment de la fonte des neiges était la plus faible durant les années avec un fort gel saisonnier. Ces hivers ont été souvent secs, et la couverture neigeuse est restée mince. En revanche, les hivers sans gel sont, pour la plupart, caractérisés par d'importante précipitation neigeuse. Ainsi, seul un nombre limité d'hivers ont pu être comparé directement. En les comparant, l'augmentation du niveau d'eau à la fonte a été entre 10-30% plus petite que durant les années avec du gel. Cette faible diminution est due au faite qu'une partie de la fonte a pu se réinfiltrer dans des zones de régions dégelées très perméables. Par conséquent, l'influence du gel partiel est certainement plus grande dans des sols possédant une capacité d'infiltration plus réduite.

Finalement, les conséquences d'un changement climatique sur les régimes hydrauliques et thermiques du sol et de la neige ont été étudiées. Quand la température de l'air augmente de 2°C, la hauteur de neige diminue dans les régions moins élevées. Le sol étant moins isolé, il gèle plus profondément. A haute altitude, la couche de neige n'est que marginalement affectée par le réchauffement climatique. L'air étant plus chaud, le sol gèle moins profondément. De manière globale, la recharge des eaux souterraines n'est que peu affectée par un changement climatique puisque l'augmentation de l'infiltration à haute altitude est contrebalancée par la diminution de l'infiltration à basse altitude. En considérant de plus un accroissement des précipitations de 15%, le gel dans le sol diminue légèrement à toutes les altitudes. La combinaison de ces deux scénarios risque d'engendrer une augmentation d'événements extrêmes, car, d'une part,

l'intensité des précipitations va augmenter, et, d'autre part, des événements de pluie sur des sols gelés vont être plus fréquents dans les régions de basse montagne.

Dans la pratique, cette étude a permis de montrer combien il est important de connaître de manière approfondie le comportement hydrothermique des régions alpines. Une telle connaissance est nécessaire, car le problème de l'eau se pose à l'échelle humaine et sera, à l'avenir, une donne socio-politique importante, à savoir comment gérer les ressources en eau de manière efficace, durable et globale. Ce travail démontre également la nécessité de considérer le gel saisonnier du sol dans la gestion des risques alpins. Les inondations sont la conséquence de forte pluie, combinée avec une intense fonte des neiges. Manifestement, le risque d'événement extrême augmente durant les hivers avec du gel, lorsque la capacité d'infiltration du sol est réduite davantage par la glace dans le sol. De plus, il a été démontré que les glissements de pentes sont le plus souvent liés à des processus hydrogéologiques particulier, tels que de fortes pluies, produisant une augmentation abrupte de la circulation de l'eau dans le sol. L'eau de fonte du printemps constitue ainsi un facteur de déclenchement potentiel de glissements de terrain, alors qu'un sol gelé peut réduire ces risques, car la quantité d'eau qui s'infiltre dans le sol est moindre.

Table of content

List of Symbols

NB: All symbols are scalar values.

a_1 ..... : Empirical constant 1 for unfrozen heat conductivity [-]
a_2 ..... : Empirical constant 2 for unfrozen heat conductivity [-]
a_3 ..... : Empirical constant 3 for unfrozen heat conductivity [$m^3 kg^{-1}$]
a_4 ..... : Multiplicative scaling coefficient for heat conductivity [-]
a_A ..... : Parameter 1 for hysteresis effect [s^{-1}]
a_B ..... : Parameter 2 for hysteresis effect [log(Pa)]
a_C ..... : Parameter 3 for hysteresis effect [log(Pa)]
a_D ..... : Parameter 4 for hysteresis effect [-]
a_r ..... : Ratio between the layer thickness and the unit horizontal area [-]
a_{s1} ..... : Parameter 1 for snow albedo function [-]
a_{s2} ..... : Parameter 2 for snow albedo function [s^{-1}]
a_{s3} ..... : Parameter 3 for snow albedo function [C^{-1}]
a_{smin} ..... : Minimum snow albedo [-]
a_{snow} ..... : Snow albedo [-]
a_{surf} ..... : Empirical coefficient for surface runoff [s^{-1}]
b_1 ..... : Empirical constant 1 for frozen heat conductivity [W $m^{-1} C^{-1}$]
b_2 ..... : Empirical constant 2 for frozen heat conductivity [$m^3 kg^{-1}$]
b_3 ..... : Empirical constant 3 for frozen heat conductivity [W $m^{-1} C^{-1}$]
b_4 ..... : Empirical constant 4 for frozen heat conductivity [$m^3 kg^{-1}$]
D ..... : Zero level displacement height [m]
D_w ..... : Effective water diffusivity [$m^2 s^{-1}$]
D_{θ_b} ..... : Water diffusivity at the boundary water content θ_b [$m^2 s^{-1}$]
$D_{\theta_{mi}}$ ..... : Water diffusivity at the current micropore water content [$m^2 s^{-1}$]
d ..... : Diffusion path length [m]
d_f ..... : Parameter giving the amount of liquid water at temperature T_0 [-]
d_2 ..... : Parameter 1 expressing the shape of the freezing point depression curve [-]
d_3 ..... : Parameter 2 expressing the shape of the freezing point depression curve [-]
d_p ..... : Drain spacing [m]
C ..... : Heat capacity of soil [$J C^{-1} m^{-3}$]
C_f ..... : Heat capacity of soil at -5°C [$J C^{-1} m^{-3}$]
C_w ..... : Heat capacity of water [$J C^{-1} m^{-3}$]
c_p ..... : Heat capacity of air [$J C^{-1} kg^{-1}$]
E ..... : Soil heat content [$J m^{-3}$]
E_f ..... : Soil heat content at a temperature of -5°C [$J m^{-3}$]
E_s ..... : Soil surface evaporation [$kg s^{-1} m^{-2}$]
E_{snow} ..... : Snow surface evaporation [$kg s^{-1} m^{-2}$]
e_{air} ..... : Vapour pressure in the air [Pa]
e_s ..... : Vapour pressure at the soil surface [Pa]
e_{snow} ..... : Vapour pressure at the snow surface [Pa]
f_i ..... : Empirical impedance factor [-]
f_{lat} ..... : Fraction of latent heat of ice to the total heat content of soil at -5°C [-]
f_{qh} ..... : Scaling coefficient [-]
$f_{stability}$ ..... : Function governing the influence of atmospheric stability [-]
f_{θ_i} ..... : Damping coefficient [-]
g ..... : Gravitational constant [$m s^{-2}$]

H ..... : Sensible heat content of soil [J m^{-3}]
H_{snow} ..... : Sensible heat flux from the atmosphere to the snow surface [W m^{-2}]
h ..... : Capillary rise [m]
I ..... : Constant [-]
K_b ..... : Maximal soil hydraulic conductivity in the micropore domain [m s^{-1}]
K_{ma} ..... : Soil hydraulic conductivity in the macropore domain [m s^{-1}]
k_h ..... : Soil heat conductivity [W m^{-1} C^{-1}]
k_i ..... : Ratio of the space average of the temperature gradient in particles of kind i and of the one of the surrounding medium ..... [-]
k_{lf} ..... : Soil hydraulic conductivity in the low flow domain [m s^{-1}]
k_{sat} ..... : Saturated hydraulic conductivity [m s^{-1}]
k_{snow} ..... : Snow heat conductivity [W m^{-1} C^{-1}]
k_w ..... : Unsaturated hydraulic conductivity [m s^{-1}]
L_f ..... : Latent heat of fusion [J kg^{-1}]
L_v ..... : Latent heat of vapour [J kg^{-1}]
M ..... : Empirical melting-freezing function [kg s^{-1} m^{-2}]
M_R ..... : Radiation melting-freezing function [kg J^{-1}]
M_T ..... : Temperature melting-freezing function [kg m^{-2} s^{-1} C^{-1}]
m ..... : Van Genuchten parameter [-]
m_f ..... : Temperature melting-freezing parameter [m]
m_{Rmin} ..... : Radiation melting-freezing parameter [kg J^{-1}]
m_T ..... : Temperature melting-freezing parameter [kg s^{-1} C^{-1} m^{-2}]
n ..... : Van Genuchten parameter [-]
n_c ..... : Fraction of cloud cover [-]
n_t ..... : Parameter accounting for pore correlation and flow path tortuosity [-]
P_a ..... : Air pressure [Pa]
P_{phys} ..... : Parameter expressing the maximal hysteresis for each simulated layer [-]
p ..... : Parameter for hydraulic conductivity in macropores [-]
Q_m ..... : Melting energy of snow pack [W m^{-2}]
Q_p ..... : Heat input by rain [W m^{-2}]
Q_q ..... : Temporal change of internal energy storage of snow [W m^{-2}]
q ..... : Liquid water flow [m^3 m^{-2} s^{-1}]
q_D ..... : Darcy water flow [m^3 m^{-2} s^{-1}]
q_f ..... : Amount of water refreezing in the low flow domain [kg s^{-1}]
q_h ..... : Soil heat flow [W m^{-2}]
q_{hf} ..... : Water flow in the high flow domain [m^3 m^{-2} s^{-1}]
q_{input} ..... : Water input flow [m^3 m^{-2} s^{-1}]
q_{output} ..... : Water output flow [m^3 m^{-2} s^{-1}]
q_{perc} ..... : Percolation flow [m^3 m^{-2} s^{-1}]
q_{prec} ..... : Precipitation flow [m^3 m^{-2} s^{-1}]
q_{ssf} ..... : Lateral subsurface flow [m^3 m^{-2} s^{-1}]
q_{sub} ..... : Sublimation flow [m^3 m^{-2} s^{-1}]
q_{surf} ..... : Surface runoff [m^3 m^{-2} s^{-1}]
q_v ..... : Vapour flow [m^3 m^{-2} s^{-1}]
q_w ..... : Water flow [m^3 m^{-2} s^{-1}]
R_{acc} : Hysteresis function that considers the accumulate rate of liquid water content increase [-]
R_{age} ..... : Hysteresis function that considers the time since the start of sorption loop [-]
R_{is} ..... : Atmospheric input of global (short-wave) radiation at the snow surface [W m^{-2}]
R_{lnet} ..... : Net long-wave radiation at the snow surface [W m^{-2}]
R_{long} ..... : Long-wave radiation from the atmosphere [W m^{-2}]

R_{ns} ..... : Net radiation (long-wave + short-wave) at the soil surface [W m^{-2}]
$R_{n,snow}$ ..... : Net radiation (long-wave + short-wave) at the snow surface [W m^{-2}]
R_{refl} ..... : Reflected radiation at the snow surface [W m^{-2}]
R_{shift} ..... : Hysteresis function that considers the shift point pF value [-]
R_{snet} ..... : Net short wave radiation at the snow surface [W m^{-2}]
R_{snow} ..... : Radiation from the snow surface [W m^{-2}]
r ..... : Empiric function giving the shape of the freezing point depression curve [-]
r_{asnow} ..... : Snow aerodynamic resistance [s m^{-1}]
r_{asoil} ..... : Soil aerodynamic resistance [s m^{-1}]
r_{aw} ..... : Radius of meniscus air-water [m]
r_{k1} ..... : Konzelmann parameter 1 [-]
r_{k2} ..... : Konzelmann parameter 2 [C Pa^{-1}]
r_{k3} ..... : Konzelmann parameter 3 [-]
r_{iw} ..... : Radius of meniscus ice-water [m]
r_{ss} ..... : Surface resistance at the soil surface [s m^{-1}]
r_w ..... : Mass ratio of ice and total water or thermal quality [-]
S_{age} ..... : Age of snow since last new snow [s]
S_{ma} ..... : Effective saturation in the macropores [-]
S_{mi} ..... : Effective saturation in the micropores [-]
S_{res} ..... : Water equivalent of the snowpack [kg m^{-2}]
S_w ..... : Exchange rate between micropore and macropore domain [s^{-1}]
S_{wl} ..... : Free liquid water of snowpack [kg m^{-2}]
S_{wlmax} ..... : Maximum free liquid water of snowpack [kg m^{-2}]
s ..... : Saturation [-]
s_1 ..... : Parameter 1 for the empirical melting function [-]
s_2 ..... : Parameter 2 for the empirical melting function [s^{-1}]
s_{dl} ..... : Parameter 1 for the snow density function [kg m^{-3}]
s_{dw} ..... : Parameter 2 for the snow density function [m^{-1}]
s_h ..... : Thermal source/sink term [W m^{-3}]
s_k ..... : Parameter for the snow thermal conductivity [W m^5 C^{-1} kg^{-2}]
s_w ..... : Mass source/sink term [m s^{-1}]
T ..... : Soil temperature [C]
T_f ..... : Temperature where all water is frozen except a residual unfrozen amount [C]
T_0 ..... : Freezing point = 273.15°K [K]
T_{air} ..... : Air temperature [C]
T_{amp} ..... : Amplitude of air temperature [C]
T_{mean} ..... : Mean air temperature [C]
T_{snow} ..... : Snow temperature [C]
T_{ssurf} ..... : Snow surface temperature [C]
T_{sum} ..... : Sum of air temperature exceeding 0°C since last new snow [C]
t ..... : Time [s]
t_{age} ..... : Age of the surface snow [s]
t_{phase} ..... : Time phase shift [s]
u ..... : Wind speed at the reference height z_{ref} [m s^{-1}]
V_w ..... : Specific volume of water [m^3 kg^{-1}]
W_{pool} ..... : Total amount of liquid water in the surface pool [m^3 m^{-2}]
w_{ice} ..... : Mass of water available for freezing [kg m^{-3}]
w_{pmax} ..... : Maximal amount of liquid water stored on the soil surface pool [m^3 m^{-2}]
z ..... : Depth [m]
z_n ..... : Soil layer [-]

z_{ohsnow} ..... : Snow surface roughness length for heat [m]
z_{omsnow} ..... : Snow surface roughness length for momentum [m]
z_{ohsoil} ..... : Soil surface roughness length for heat [m]
z_{omsoil} ..... : Soil surface roughness length for momentum [m]
z_p ..... : Depth of the drains [m]
z_{ref} ..... : Reference height in the calculation of the aerodynamic resistance [m]
z_{sat} ..... : Depth of the saturated layer [m]
α ..... : Van Genuchten parameter [Pa^{-1}]
α_f ..... : Heat transfer coefficient [W m^{-1} C^{-1}]
Δ ..... : Slope of the saturated vapour pressure versus temperature curve [Pa C^{-1}]
ΔT ..... : Change in the air temperature [C]
Δt_{shift} ..... : Time elapsed since last major shift from a desorption to a sorption [s]
$\Delta Prec$ ..... : Change in the precipitation [-]
ΔV_{snow} ..... : Change in snowpack water storage [m^3 m^{-2} s^{-1}]
ΔV_{soil} ..... : Change in soil water storage [m^3 m^{-2} s^{-1}]
Δz ..... : Layer thickness [m]
$\Delta\theta_{sorp}$ ..... : Accumulated increase of liquid water content [m^3 m^{-3}]
ε_a ..... : Porosity [-]
ε_a ..... : Emissivity of the atmosphere [-]
ε_s ..... : Emissivity of the snow surface [-]
Θ ..... : Liquid-solid contact angle [rad]
θ ..... :Water content [m^3 m^{-3}]
θ_b ..... : Liquid water content when micropores are full and macropores empty [m^3 m^{-3}]
θ_i ..... : Volumetric fraction of constituent *i* [-]
θ_{ice} ..... : Liquid water content corresponding to the volume occupied by ice [m^3 m^{-3}]
θ_{lf} ..... : Liquid water content of low flow domain [m^3 m^{-3}]
θ_{ma} ..... : Liquid water content in macropores [m^3 m^{-3}]
θ_{mi} ..... : Liquid water content in micropores [m^3 m^{-3}]
θ_r ..... : Residual liquid water content [m^3 m^{-3}]
θ_s ..... : Liquid water content at saturation [m^3 m^{-3}]
θ_{tot} ..... : Total water content (ice and liquid water) [m^3 m^{-3}]
θ_{wilt} ..... : Liquid water content at a soil water pressure of 4.2 pF [m^3 m^{-3}]
κ ..... : Karmans constant [-]
λ ..... : Pore size distribution index [-]
λ_i ..... : Thermal conductivity of constituent *i* [J m^{-1} C^{-1} s^{-1}]
ρ ..... : Water density [kg m^{-3}]
ρ_a ..... : Air density [kg m^{-3}]
ρ_s ..... : Dry bulk density [kg m^{-3}]
ρ_{smin} ..... : New snow density, assuming dry snow precipitation [kg m^{-3}]
ρ_{snow} ..... : Snow density [kg m^{-3}]
ρ_v ..... : Vapour density [kg m^{-3}]
σ ..... : Stefan Boltzmann constant [W C^{-4} m^{-2}]
σ_{aw} ..... : Surface tension air-water [N m^{-1}]
σ_{iw} ..... : Surface tension ice-water [N m^{-1}]
γ ..... : Psychrometer constant [Pa C^{-1}]
γ_w ..... : Scaling factor [-]
Φ ..... : Soil particles diameter [m]
ψ ..... : Liquid water pressure (also expressed in m) [Pa]
ψ_a ..... : Air entry pressure (also expressed in m) [Pa]
ψ_b ..... Liquid water pressure when micropores are full and macropores empty (al-

so expressed in m) ..... [Pa]
ψ^* .....: Reference value of liquid water pressure (sometimes expressed in m) [Pa]
ω .....: Frequency [s^{-1}]

1. INTRODUCTION

1.1. MOTIVATION

Due to the presence of glaciers and snow, mountains play an important role as water reservoirs for communities. In particular, they supply the water for human activities during dry seasons, either directly through surface runoff or indirectly through infiltration and aquifer recharge. Typically, at the village of Grächen (1600 m) in southern Switzerland, water supply became a problem during winters with little precipitation. This shortage problem was resolved by taking water from the underlying alpine aquifer, recharge of which takes place mainly during the snowmelt in spring. Next to water resources management, snowmelt timing and dynamic is also relevant for hydro power generation, for agricultural production and management (soil erosion and washing away from arable land (Zuzel and Pikul1987, Pikul et al. 1992)) and especially for environmental-impact assessment, as high nutrient loads are often observed during snowmelt in rivers (Williams and Melack 1991). Snowmelt may also be dangerous with regard to hazardous flood events (Petrascheck and Hegg 2000) and be an activating factor for landslides (Tullen 2002).

Knowledge about the different hydraulic and thermal processes related to the snowmelt at both local scale and catchment scale are of central importance. These processes are complicated and need to be further investigated. At a local scale, several dye tracer experiments indicated the occurrence of preferential flow paths in snow (Waldner et al. sub.). However, most numerical model do not include flow instabilities related to finger flow in their setting (Gustafsson et al. sub.). At larger scales, the coupled hydrological and hydrogeological processes are mostly not well understood, due to the spatial variability in the governing climatic and topographical parameters and also because large amounts of meltwater are transported to the stream via subsurface flow (Flerchinger et al. 1994), or interflow (Beven 1989), which is difficult to describe using numerical models.

An additional factor affecting the flow path in the Alps is seasonal soil frost (i.e. ground which is completely unfrozen during the summer). Due to its potential influence on global hydrology, numerous studies have investigated the effect of seasonally frozen ground on the meltwater runoff in cold regions. These studies showed that meltwater was able to percolate through the frozen layer in the remaining ice-free area (Chacho and Bredthauer 1983, Stadler et al. 1996, Stähli et al. 1996, Nyberg et al. 2001). Nevertheless, the reduction of the soil infiltration capacity caused by the pore ice created during specific winters large surface runoff, thereby lowering the underneath groundwater recharge (Sand and Kane 1986, Koren et al. 1995).

Little is known about the effect of seasonal soil frost on the meltwater pathways at local and large scales in the Alps. Until now, most experiments were conducted in Scandinavian or arctic regions, which are characterized by a different soil and snow cover type (Sturm et al. 1995), climate and topography. Additionally, most studies were limited in their interpretation, as only a few numerical models simulating the heat and water transport processes related to the snow and frost depth evolution exist. These models are one-dimensional, and do not include the thermal and hydraulic processes induced by the spatial variation in the soil and snow physical characteristics (Kennedy and Sharratt 1997). Most interest in alpine hydrological processes was focused on glacier and permafrost hydrology (Glen 1982, Tenthorey 1992, Singh and Singh 2001). There is an evident and quite surprising lack of studies as well as tools related to small

and large scale effects of seasonal soil frost on alpine hydrology.

As shown by the Swiss National Research Programme "Climatic changes and natural disasters" (NRP 31) (Fuhrer 1997), mountain environments appear to be very sensitive to long-term climatic changes. As a whole, an elevation in temperature will affect the water resources by globally reducing the amount of snow in winter (Ehrler 1998) and by lowering the reserve of water at altitude (glacier and permafrost) (Chen 1991, Maisch et al. 2000). But on the other hand, it will increase the amount of precipitation and therefore the aquifer recharge. Additional factors should be dynamically taken into account to investigate the effect of climate on groundwater resources. Aquifer recharge primarily takes place during springtime. It is governed by snowmelt conditions, i.e. seasonal alternation of frost and thaw, since frozen soil prevents water from infiltrating and hence increases the surface runoff component. Thus, a warmer climate may influence the spatial seasonal soil frost distribution. Stadler et al. (1997) indicated, for example, that soil frost at lower altitudes may be more pronounced due to a shallow snow cover, but shorter in time because of higher air temperatures.

Therefore, an estimation of the dynamic effect of seasonally frozen soil on the water balance during snowmelt in mountainous areas, as well as an evaluation of the effect of seasonally frozen soils on alpine catchment recharge according to actual and long-term climatic evolution is necessary to ensure suitable water management in future. It is of particular interest as the demand for water in the Alps is expected to increase in the next few years, as, for example, more artificial snow is produced to make up for the lack of snow.

1.2. OBJECTIVES AND STRUCTURE OF THIS STUDY

The overall objective was to evaluate the impact of soil frost on alpine groundwater recharge and to test the aquifer's sensitivity to a climatic change. Special emphasis was put on the conditions representing alpine environments, where melting occurs mainly at the end of the winter.

The study included a two-year measurement programme at two different alpine locations, as well as laboratory experiments in a cold room and numerical modelling. The methodology of the project as well as the different objectives for each chapter are shown in Figure 1.1 and explained below.

Soil frost is a very local phenomenon. It depends on locally defined parameters, such as soil structure, soil water content, air temperature and snow depth at the beginning of the winter. In contrast, recharge of mountain aquifers takes place over large areas, depending on the geology, the morphology and the vegetal cover. Assessing the impact of soil frost on aquifers implies bringing these two scales together. To do so, plot investigations were first carried out on selected sites at Hannigalp close to Grächen (2100 m) and at Gd St Bernard pass (2470 m) in the southern Swiss Alps during two consecutive winters (2000/2001 and 2001/2002) to obtain a database describing water and heat processes. This was done at high altitude from where currently hardly any data are available. The experimental sites are presented in Chapter 4. Chapter 5 presents the climatic characteristics of each experimental site as well as the climatic evolution during the last 30 years at Grächen and 60 years at Gd St Bernard. The aim of the field measurement programme was to quantify the different snowmelt runoff components, as well as to specify which conditions are necessary for soil frost to occur. The observation period was two years and the results are shown in Chapter 6. In addition, a dye tracer experiment was carried

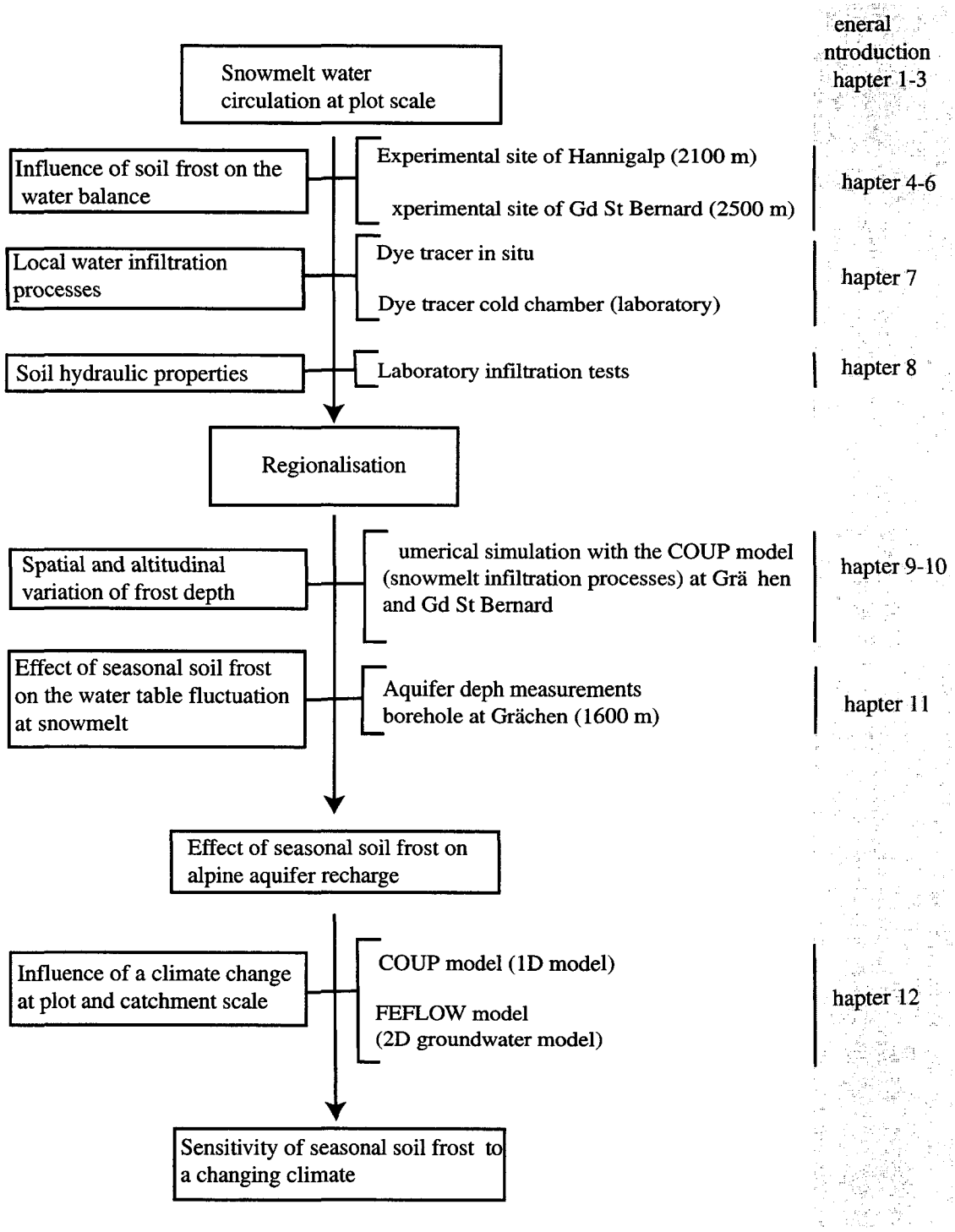

Figure 1.1: Methodology of the project.

out at both experimental sites to investigate the different water infiltration pathways at snowmelt (Chapter 7). We further investigated the soil physical characteristics at Hannigalp because the infiltration pathways from the dye tracer experiments showed intriguing properties. For that purpose laboratory soil column experiments were conducted, and two one-dimensional numerical models, differing in their flow domain, were tested. With this procedure we intended

to clarify which numerical model was best fitted to describe the soil hydraulic behaviour at Hannigalp (Chapter 8). These infiltration tests were carried out in the cold laboratory at the Institute of Terrestrial Ecology (ITÖ) at ETH Zurich in collaboration with Manfred Stähli. Further laboratory studies allowed us to specify the freezing characteristic curve as well as to calibrate and validate the physically based one-dimensional COUP model (Jansson and Karlberg 2001), which proved to be best fitted for our study. This model simulates the heat and water balance as well as the snow depth of a mountainous system. The model was finally applied *in situ*. We compared the results given by an energy balance approach simulating the thermal exchange between the snowpack and the atmosphere with an empirical melting/ freezing approach. The simulation results are shown in Chapter 9. Finally, long-term data were used to simulate the occurrence of soil frost at the two study sites. With that procedure, we aimed at investigating the influence of the altitude and the exposure on the seasonal soil frost extent (Chapter 10).

In a next step, COUP was run using altitudinal-corrected weather data. The objective was to assess soil frost depth at different altitudes of a basin, and to estimate the effect of seasonal soil frost on the water-table rise measured in a piezometer at Grächen some 500 m below the site of Hannigalp (Chapter 11). Finally, long-term scenarios were simulated to evaluate the impact of a climatic change on the groundwater recharge. The COUP model was run using weather data with increased air temperature. The results obtained were introduced in a two-dimensional water model, FEFLOW (Diersch 1996), to assess the sensitivity of groundwater to a changing climate. The results are described in Chapter 12.

The different objectives may be summarized as follows:

1. to quantify the influence of soil frost on local snowmelt runoff at high altitudes at representative alpine sites (Chapters 4 to 6),
2. to investigate locally water infiltration at snowmelt using a dye tracer (Chapter 7),
3. to assess the soil hydraulic characteristics at Hannigalp (Chapter 8),
4. to estimate the impact of the spatial and altitudinal snow depth variability on soil frost and snowmelt, so as to regionalize obtained results (Chapter 9 and 10),
5. to estimate the effect of seasonal soil frost on alpine aquifer recharge (Chapter 11),
6. to evaluate the influence of changing climate on the soil frost depth extent and on the aquifer recharge (Chapter 12).

The literature review is in Chapter 2. Chapter 3 describes the different numerical models, which were used in this study.

1.3. ORGANIZATION AND FINANCIAL SUPPORT

This research was conducted on a scholarship from the Laboratory of Environmental Engineering Geology (GEOLEP). In addition, the Institute of Terrestrial Ecology (ITÖ) at ETHZ provided logistic and material support. The project was split up into two parts, namely a hydrogeological study and soil physical properties characterization. The second part necessitated numerous laboratory experiments, which were conducted at the cold chamber at the ITÖ. Finally there was collaboration with the villages of Grächen and Bourg St Pierre, with the ski-resort of Grächen, as well as with the Gd St Bernard monastery.

2. ALPINE HYDROGEOLOGY: GENERAL REVIEW

2.1. SHORT HISTORICAL REVIEW OF SNOW AND FROZEN SOIL RESEARCH

2.1.1. SNOW STUDIES

A good overview of research in the area of snow hydrology is given by Coldbeck (1987). He divided the development in the area of snow hydrology into four distinctive periods: preparation (pre-1900), discovery (1900-1936), recent (1936-1970), and current (post-1979). The first snow investigation was carried out as early as 1848 when Delesse (1848) studied the petrographic samples of snow. However, before 1900, most research was limited to the development of basic concepts due to lack of available instruments. The interest in mountain hydrology started when management of water resources became of central importance. Observations on snow cover and measurement of the snow inventory were carried out by people like Church (1914) and Seligman (1936). In parallel to these researches, investigations on avalanches were carried out, due in particular to the increased use of motorized transport in the Alps. It was the beginning of establishments like the Swiss Commission on Snow and Avalanche Research and later the foundation of the SLF in Davos. Research was at an early stage, and physical concepts were used as qualitative in sights. After 1936, snow research became more quantitative, international communities were established and physical processes were investigated more thoroughly. Since around 1970, tools became much more sophisticated (efficient computers) and concept from other fields were applied to describe snow related processes.

2.1.2. FROZEN SOIL RESEARCH

The research development in the area of soil frost and snow hydrology was similar. People started investigations on soil frost as early as 1816 (Mac Adam 1816). Most of the early soil frost studies originated from problems related to agriculture and road construction. In 1907 Buckingham (1907) presented a first theoretical approach on how frozen lenses may be created in the soil. A few years later people like Beskow (1935) or Taber (1930) were able to accurately explain this phenomenon. Due to the damaging effect of soil frost on road structure, civil engineers were also involved in these studies. We may quote especially Casagrande (1932), who in 1932 defined the criterion for a soil to be frost-sensitive, a criterion that is still used nowadays.

2.2. HYDROLOGY AND HYDROGEOLOGY IN MOUNTAINS

2.2.1. DEFINITION

Hydrology and hydrogeology in mountain areas include all processes associated with the water movement in the atmosphere, in the snow layer, on the ground surface, in the unsaturated part of the ground, and in the saturated one. The main hydraulic event takes place in spring when the water stored in the snowpack during the winter is released over a few weeks. During this period, the extension of the seasonal soil frost (i.e. a soil which

is unfrozen during the summer), of permafrost zones and of glaciers act on the melt water flow paths (Figure 2.1)..During winters with seasonal soil frost, part

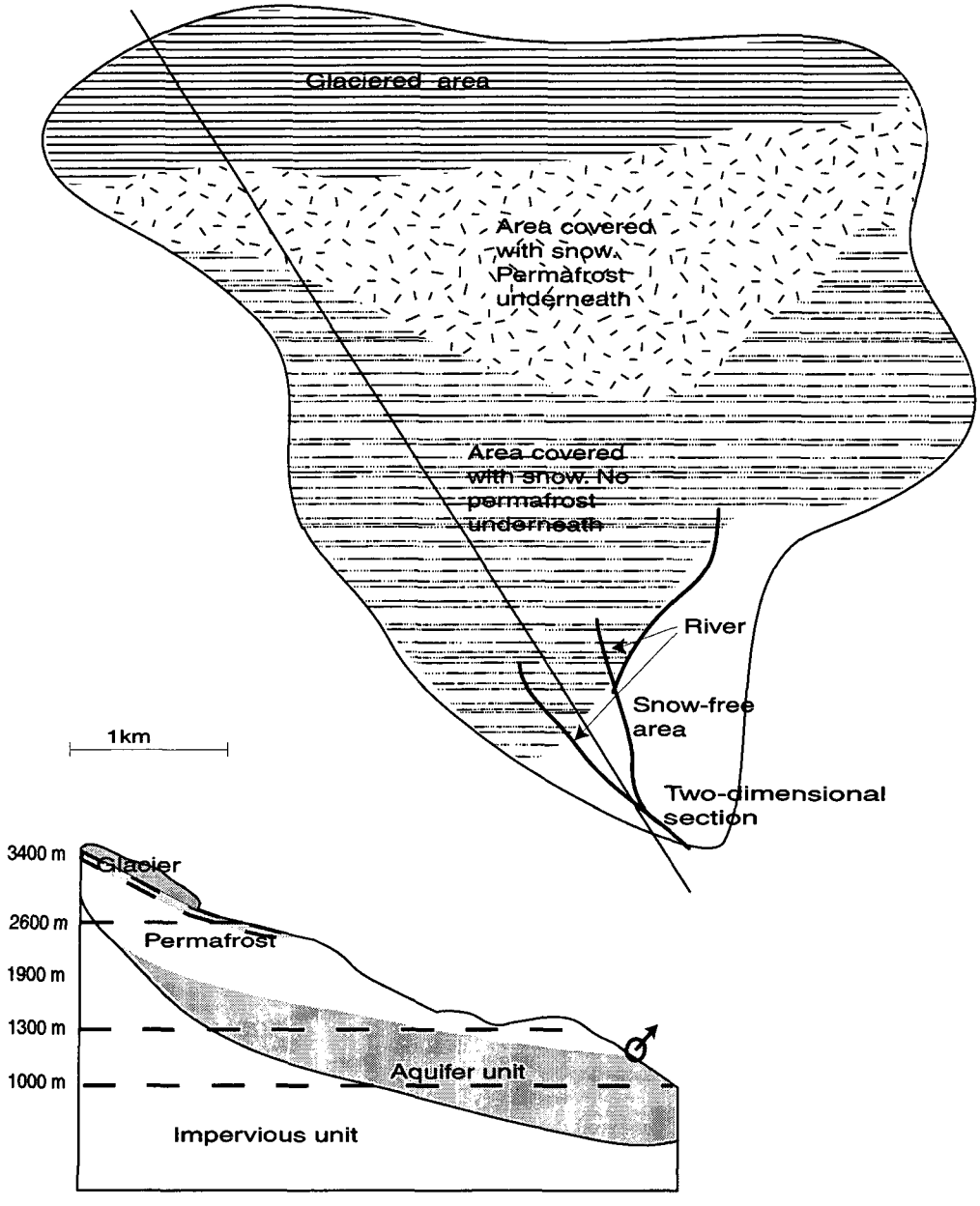

Figure 2.1: Sketches of a mountain catchment in spring during the snowmelt. The catchment is divided into four regions. On the upper part, glaciers are present, followed by a permafrost zone. On the lower zones, the soil is free of permafrost. Snow is encountered everywhere except on the lower end, where the snowpack already melted.

of the melt water runs off as surface or subsurface flow, as the soil infiltration capacity is reduced by the pore ice (Figure 2.2). Quantifying this amount will constitute a major goal of this work.

Hydrology may be subdivided into surface water and groundwater hydrology: surface water hydrology deals with the relations between water and the surface, while groundwater hydrology

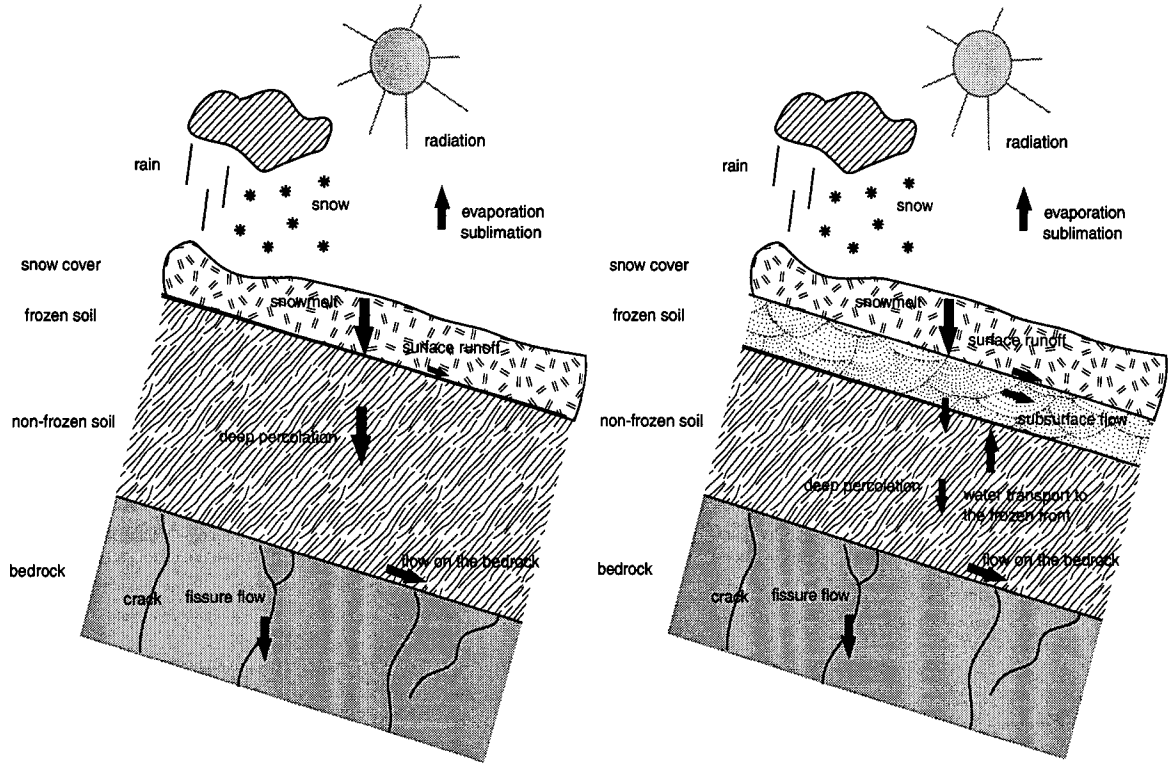

Figure 2.2: Hydrogeologic processes at the plot scale during snowmelt in mountains. The two plots are located outside the glaciered region, free of pergelisol. On the left hand-side the soil remains unfrozen in winter, whereas on the right-hand side the upper 30 cm of soil are frozen.

shows the relations of the water with the lithosphere. These differences in the flow processes reflect themselves in the stream runoff, which we may separate into a flow originating from the groundwater (baseflow) or from direct runoff. In Figure 2.3 the direct runoff was further divided into surface runoff and quick subsurface, while baseflow was divided into delayed subsurface and groundwater runoff. Surface runoff designates the water travelling over the ground surface to a channel. It shows up as sheet flow only when the infiltration capacity of soil is exceeded. As this is rarely the case over the entire catchment, surface runoff is mainly collected and evacuated by first order channels. Subsurface flow is the water, which infiltrates into the soil and moves laterally beneath the soil surface. It occurs in forests or shallow soils, where the upper soil cover is composed partly by roots or rock debris. It also takes place when the soil is unfrozen near the surface but frozen beneath, such as in the active zone of permafrost or in a partly frozen soil. Subsurface flow is not as rapid as surface flow, as the flow is subject to greater resistance. A distinction is made between quick and delayed interflow, with the former merging with surface runoff and the latter with baseflow. Finally, groundwater flow consists in deeply percolated surface water. Groundwater movements are slow in comparison with surface runoff processes and do not generally contribute to the peak discharge of a particular event. In the mountains the recharge of aquifers takes place during snowmelt. During the winter, the water-table steadily lowers as no water percolation exists and therefore no contribution is added to the groundwater.

A distinction has to be made between processes taking place in the snowpack and in the soil. Snowpack evolution is strongly coupled to atmospheric factors, whereas hydraulic processes in the soil depend on the amount of water released by the snowpack, the thickness of the frozen

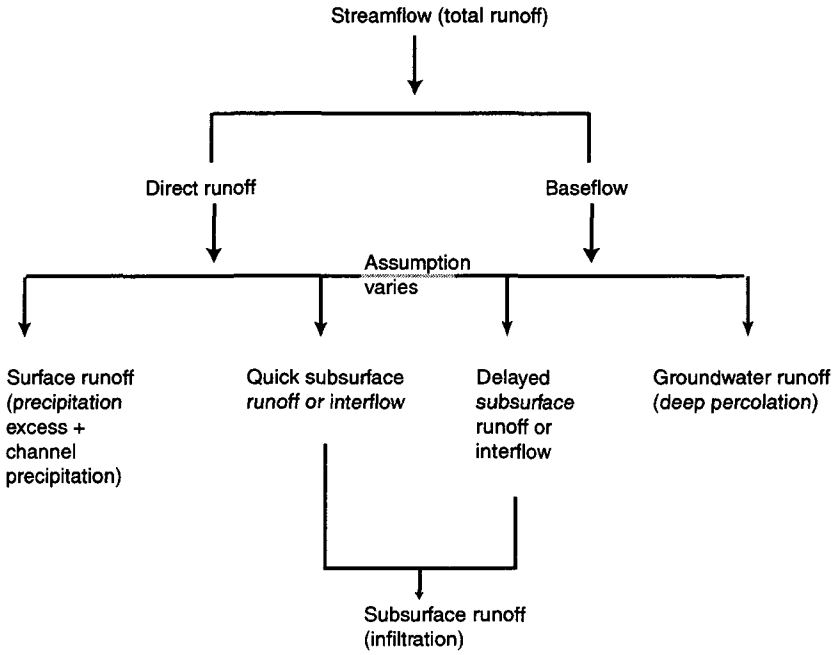

Figure 2.3: Components of streamflow or total runoff along with their sources (Singh and Singh 2001).

layer, and the soil physical properties. In the next part we will hence start to describe these different processes in a first step at plot scale, before dealing with the groundwater recharge over larger areas.

2.2.2. SNOWPACK EVOLUTION

Literature on snow cover evolution and snow hydrology is numerous. For example Singh and Singh (2001) provide an accurate overview of the different snow related processes. We describe shortly the different energetic exchange processes taking place during the winter.

A snowpack is characterized by two properties prior to any melting: (a) the cold content capacity and (b) the liquid water storage capacity. The cold content capacity expresses the energy necessary to heat the snowpack from its actual temperature up to 0°C. The energy is mainly given by latent heat coming from meltwater. In early spring, water melting at the snow surface refreezes in the snowpack and releases latent heat. The liquid water storage capacity is the maximal liquid water content of the snowpack. It is close to zero when snowpack temperatures are below zero. At 0°C the snowpack holds a certain amount of water due to hydroscopicity and capillarity. When water storage potential is reached, the snowpack releases the water excess gravitationally. The liquid water holding capacity is approx. 7%, but this value depends on snow density (U.S. Army Corps of Engineers 1956), ice content and slope.

Percolation through snow occurs in a highly irregular manner. Investigations to understand the vertical movement of the meltwater have been made in numerous studies. These include the influence of ice layers (Colbeck 1973a) or the presence of preferential flow path (flow fingers) during melt period (Colbeck 1978, Waldner et al. sub.) or rain period. Ice layers are

characterized by a variable permeability, which influences the flow pathway. They may break down, creating a highly conductive layer. Water flow-paths in snow occur mainly as flow fingers, which change with time and concentrate nearly all water movement in the snowpack. At the base of the snowpack, water infiltrates the soil until saturation is reached. A saturated layer is then formed in the snowpack and water moves fast along the soil surface as reported by Fujino (1971).

During winter, the snow cover loses mass mainly through sublimation. Energy input due to sublimation may be as much as net radiation, but is usually in the order of 10% (Morris 1989) and hence should not be disregarded. Especially during windy and warm time periods when saturation vapour pressure is high, the snow cover loses rapidly mass due to sublimation. During snowmelt, loss due to sublimation is negligible in comparison with meltwater loss (Hood et al. 1999). At this stage, the snow depth diminishes mainly because of global radiation and sensible energy input. Sensible heat is estimated to be about 40% of the net radiation energy input over a winter.

Calculation of available energy for melting is achieved by solving the energy balance equation for the whole snowpack[1]:

$$Q_m = R_{n,snow} + H_{snow} + L_v E_{snow} + Q_p + q_h(0) + Q_q \qquad (2.1)$$

with: Q_m : melting energy,
$R_{n,snow}$: net radiation energy (see eq. 3.34),
H_{snow} : sensible heat,
$L_v E_{snow}$: latent heat,
Q_p : heat input by rain,
$q_h(0)$: heat input coming from beneath,
Q_q : change of internal energy storage of snow.

Heat input coming from beneath is important at the beginning of the winter when the soil is still warm, but less important during the snowmelt. On the other hand, heat input due to rainfall is essential when the snowpack is still cold (i.e. under 0°C). It is of less importance when the layer has already reached 0°C, rain temperature being close to the freezing point. Rainfall on snow creates major flooding processes, in particular when a combination of melting snow due to mild temperatures and rain is observed. Such a case took place in spring 1999 in Switzerland (Petrascheck and Hegg 2000). Several studies were carried out to estimate the amount and rate of outflow from snowpacks under rain on-snow events (Singh et al. 1997, Singh et al.1998). It was observed that the snowpack acts as a reservoir as long as the water capacity is not reached. However, when heavy rain took place, rainwater travelled several times faster than snowmelt water produced under natural condition (no rain). This is mainly due to changes in the metamorphism of saturated snow as well as to the existence of preferential flow paths and the saturation of the ground surface.

2.2.3. HYDROLOGIC AND THERMAL PROCESSES IN A PARTLY FROZEN SOIL

Literature on this topic is also numerous. We may refer in particular to Williams and Smith (1989) as well as to Dysli (1991), who provide a good overview of the different hydraulic and thermal processes in a partly frozen soil.

1. Unless mentioned, all equations will be written in one dimension.

2.2.3.1. HEAT TRANSFER IN SOIL

Heat is transferred in soil mainly by convection and conduction. Other processes, such as transport of latent heat by water vapour diffusion or heat transfer due to radiation, exist, but will not be explicitly treated, as they are mostly negligible. Heat transfer in soil is given by the energy conservation equation, which will be presented thoroughly in the next chapter (see eq. 3.10).

Heat stocking in the ground is either induced by a change of soil temperature or a change of liquid water content. The phase change between liquid water and ice requires latent heat. As the ratio between sensible and latent heat at a temperature of -5°C is approximately 1:24, the latent heat has a strong impact on the energy conservation equation when freezing takes place. This can be seen in Figure 2.4, where latent heat has to be removed prior to any significant decrease in temperature. The different curves in Figure 2.4 indicate the soil temperature as a function of heat content for different degrees of freezing point depression. Differences in soil texture as well as water solute concentration induce those different curves. Spans and Baker (1996) showed that the freezing-thawing process was comparable to the drying-wetting one. In particular, one can use the soil moisture characteristic curve to deduce the water potential at a given sub-freezing temperature, as soon as the soil moisture is known.

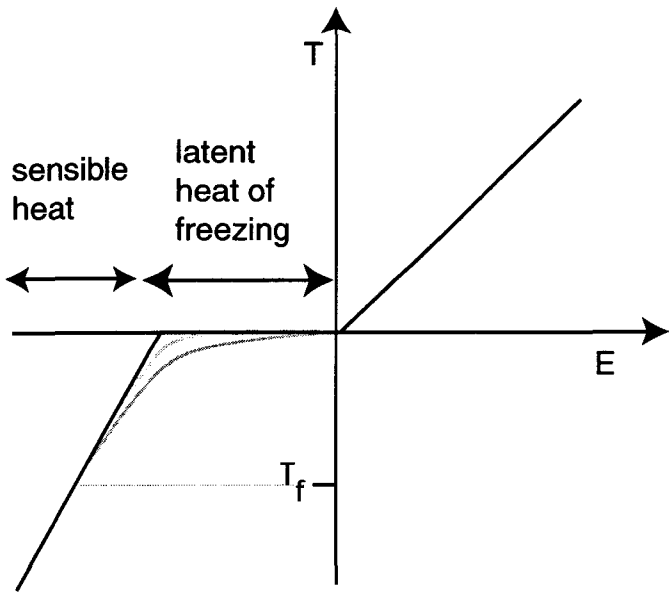

Figure 2.4: Soil temperature (T) as a function of soil heat content (E) for different degrees of freezing point depression. All water is frozen at the temperature T_f exept a residual amount.

Heat conduction is the main energy transfer mechanism in winter when the soil is covered by snow. This process is certainly not as efficient as convection and is related to the soil physical properties of the soil constituents (Ippisch et al. 1998). From de Vries (1975) thermal conductivity is given by:

$$\lambda = \frac{\sum k_i \theta_i \lambda_i}{\sum k_i \theta_i} \tag{2.2}$$

with k_i : ratio of the space average of the temperature gradient in particles

of kind i and the space average of temperature gradient of the surrounding medium,

θ_i : volumetric fraction of constituent i,

λ_i : thermal conductivity of constituent i.

From the differences in the physical properties of liquid water and ice, ice being four times more conductive than liquid water, the thermal gradient is less important in frozen soil than in unfrozen.

Convection is the most efficient heat transfer process. Water circulation due to pressure gradient introduces a large amount of energy into the soil, and hence induces heat transfers over larger distances and over short time periods. Especially at snowmelt when liquid water is released and introduced into a frozen soil layer, soil temperature increases suddenly to 0°C.

To describe the phase change water/ice in the soil pores the Clausius-Clapeyron equation is used:

$$\frac{d\psi}{dT} = \frac{L_f}{(T+T_0)V_w} \tag{2.3}$$

with ψ : liquid water pressure,

T : temperature in °C,

L_f : latent heat of fusion,

T_0 : freezing point in °K (= 273.15°K).

V_w : specific volume of water.

In this equation the pressure of the water is lowered, while the pressure of ice is supposed to be equal to the atmospheric one. If the interest lies with the formation of ice lenses, this assumption is not valid and the ice pressure has to be considered in eq. 2.3. Miller (1980) showed how in that case the ice pressure grows and at some point is equal to the soil load, assuming a constant water flux. At that point the soil particles are no longer held together and an ice lens forms.

The capillary theory for soil moisture in unfrozen soil is also used in freezing theory to explain the difference in the ice and water pressures in frozen soils. From the capillarity theory, the pressure of the water, ψ at the meniscus is given by:

$$P_a - \psi = 2\frac{\sigma_{aw}}{r_{aw}} \tag{2.4}$$

with: P_a : air pressure,

σ_{aw} : surface tension air-water,

r_{aw} : radius of meniscus air-water.

Assuming the same equation when ice replaces air, and combining it with eq. 2.3 produces:

$$T = \frac{V_w 2\sigma_{iw} T_o}{r_{iw} L_f} \tag{2.5}$$

with: σ_{iw} : surface tension, ice-water,

r_{iw} : radius of meniscus ice-water.

This equation expresses the fact that ice penetrates into smaller and smaller pores as the temperature falls. It also becomes clear that the unfrozen water contents are essentially independent of the ice content and therefore also of the total moisture content of the soil. Water is confined in small pores, whereas ice fills up all bigger pores. Anderson and Tice (1972)

showed for example that the unfrozen water content at any temperature is dependent on the specific surface area of the soil and the temperature. For the same pressure, the ratio σ_{iw}/σ_{aw} = 0.42 indicates that the radius meniscus is smaller for frozen soil than for unfrozen, and therefore liquid water is located in smaller pores. Eq. 2.5 is, however, only valid for temperatures within a degree or so of 0°C. At lower temperatures, adsorption forces become more important. This may be expressed by equalling σ_{aw} to σ_{iw} in eq. 2.5. The liquid water pressure for frozen soils is then taken from the retention curve obtained under unfrozen conditions.

2.2.3.2. SOIL WATER FLUXES

The bundle of capillaries model is mostly used to describe soil water fluxes in a soil. Water in partially saturated porous media is considered to be held in a pore space represented by a bundle of cylindrical capillaries. This approach is limited, as it does not take into account the surface forces and films. Other approaches exist, such as the unitary approach (Or and Tuller 1999). Such an approach considers the matric potential as made up by an adsorptive component and a capillary component. Soil pores are represented by angular cross-sections to allow dual-occupancy of wetting and non-wetting phases. In this study the usual approach is considered.

Water flux q in partially frozen soils gets more complicated with the additional ice phase. The flux depends on the flow domains. We distinguish between macropore flux (Beven 1982), flow through cracks (Granger 1984), pipe throughflow (Roberge and Plamondon 1987), and the common micropore flow. In all flows except the last, the flow is mainly gravitational while in the last case (micropore flow), the water flow, q, is given by Darcy's law:

$$q=q_D = -k_w(\psi)\left(\frac{\partial\psi}{\partial z}-1\right) \tag{2.6}$$

with q_D : Darcy flow
k_w : unsaturated hydraulic conductivity,
ψ : liquid water pressure,
z : depth.

If micropore flow is considered, water transport is more efficient if taking place in the previously air-filled coarse pores (microscopic bypass flow) than in the liquid water phase between soil particles and pore ice (microscopic flow) (Stähli et al. 1996). The microscopic permeability of frozen soils was measured with permeameters (Williams and Burt 1974) or air permeameters (Seyfried and Murdock 1997). Conductivities between 10^{-12} and 10^{-8} m/s were reported depending on soil texture. Frozen sandy soils are typically less permeable than frozen silt and clay, as less liquid water is bounded in sand. Micropore bypass flow takes place in larger pores, which are not occupied by ice, but by air. Permeabilities are much higher than microscopic permeability flow, but depend on how much space is free of ice (Kane and Stein 1983, see also "Two-domain flow in a frozen soil", page 31).

Other less significant water displacement mechanisms exist. We may indicate water vapour diffusion, regelation or water flow through microscopic ice channels when the ice is close to 0°C.

2.2.3.3. WATER INFILTRATION IN A PARTIALLY FROZEN SOIL

The amount of water infiltration in a partly frozen soil depends on different factors, which are mostly related between each other: the morphological form of ice (Trimble et al. 1958), the

vegetation, the soil structure (Pikul and Aase 1998), the soil texture and the soil ice content (Kane and Stein 1983, Gray and Granger 1985), the presence of a basal ice sheet (Woo et al. 1982), the spatial variability of soil frost (Stadler et al. 1996) or the frost depth (Hardy et al. 2001). Different structures of soil frost were defined by Trimble et al. (1958), structures, which either inhibit water infiltration (like concrete frost) or which hardly affect snowmelt infiltration (like stalactite frost). Preferential flow paths (like cracks) enhance infiltration. Pikul and Aase (1998) indicated that soil ripping combined with annual cropping improves water infiltration into frozen soil, as ripping creates a system of surface-connected macropores. Kane and Stein (1983) made direct field measurements of infiltration into a seasonally frozen silt soil. They concluded that the drier the soil, the greater the infiltration rate, and that ice-rich soils have relatively low infiltration rates. Basal ice reduces the infiltration capacity of soil as snowmelt water runs on the ice layer. Heterogeneous soil frost distribution, as occurring in forests, affects water infiltration. Several studies pointed out the importance of predicting accurately the frost depth when snowmelt runoff is of interest (Johnsson and Lundin 1991, Stadler et al. 1996). Soil frost has an impact on the different dynamics of soil temperature and soil water content. It may act as a quasi-impervious boundary and water flux is mainly lateral (Burt and Williams 1976). Other investigations showed that meltwater was able to percolate through the frozen layer in the remaining ice-free area (Chacho and Bredthauer 1983, Nyberg et al. 2001).

The ability of soil frost to impede melt water to infiltrate into the ground depends also on the snowmelt intensity and amount (i.e. on the climate). Chacho and Bredthauer (1983) found little lateral runoff yielded during snowmelt, for a continental climate, characterized by low annual precipitation (less than 200 mm per year), very low air temperature, and deep soil frost. In his study about the sub-alpine area of Davos (Switzerland), Stadler et al. (1996) noted that between 60% and 80% of the meltwater infiltrates into the ground, as long as no refreezing takes place. In such areas, the snowpack is thin, the climate temperate, and the soil frost mostly shallow (20-30 cm). In Sweden, Nyberg et al. (2001) established no clear relation between frost effect on runoff, during the three winters examined. In alpine regions, little is known about the hydrogeological behaviour at snowmelt. The common assumption is that an early and insulating thick snowpack inhibits soil to freeze. Singh and Singh (2001) postulated that at snowmelt the meltwater mostly infiltrates directly into the soil and little surface runoff takes place. On the other hand, Waldner et al. (2000) noticed the occurrence of a saturated zone at the bottom of the snow cover creating lateral water runoff even when the soil stayed unfrozen. This study should hence allow to gain a better insight into the thermal and hydraulic processes for such types of areas.

2.2.3.4. SOIL WATER REPELLENCY

In this part we set out some basic concepts of water flux in an (unfrozen) water repellent soil. These notions will be useful to better understand the hydraulic properties at Hannigalp (Chapter 8).

Soil water repellency has been given an increasing consideration during the last years, due to its environmental consequences in particular with respect to agricultural production. Hydrophobic soils tend to produce soil erosion, as well as rapid leaching of agrochemicals (Krammes and DeBano 1965). A common characteristics of water repellent soil, is the ability to generate preferential flow. This behaviour may be problematic, as water bypasses parts of the vadose zone, in particular the biologically and chemically active topsoil.

The definition of water repellency may be given as follows. From the capillary theory the

capillary rise, h, in the bundle of tubes describing the soil is expressed by:

$$h = 2\frac{\sigma_{aw}\cos\Theta}{\rho g r_{aw}} \tag{2.7}$$

with: σ_{aw} : surface tension, air-water,
ρ : water density,
g : gravitational constant,
r_{aw} : radius of meniscus,
Θ : liquid-solid contact angle.

The liquid-solid contact angle Θ specifies the hydrophobicity of the soil. In particular the soil is defined as water repellent when Θ is greater than 90°. **h** becomes then negative, which signifies that water cannot penetrate the soil. If Θ is set to 90° (**h** = 0), the soil is neither hydrophobic nor hydrophilic. A positive value characterizes hydrophilic soils (in eq. 2.4.Θ was set to 0, i.e. the soil was hydrophilic).

In hydrophobic soils, water is redistributed by the organic upper soil layer, leading to large variations in the soil water content and preferential flow patterns. Several studies showed that the wetting front was instable due to the opposite direction of the pressure gradient and the direction of flow (Raats 1973). Nieber (1996) defined (a) the drainage function, as the water retention curve when drainage of an initially saturated sample at zero capillary pressure to residual water content was carried out, and (b) the main wetting retention function, as the relation derived by wetting a sample starting form a dry condition. He showed that fingering (i.e. preferential flow) could only take place when the water entry capillary pressure of the main wetting retention function exceeds or equals the air-entry capillary pressure of the main drainage retention function (Figure 2.5). In water repellent soils, the water entry pressure for the

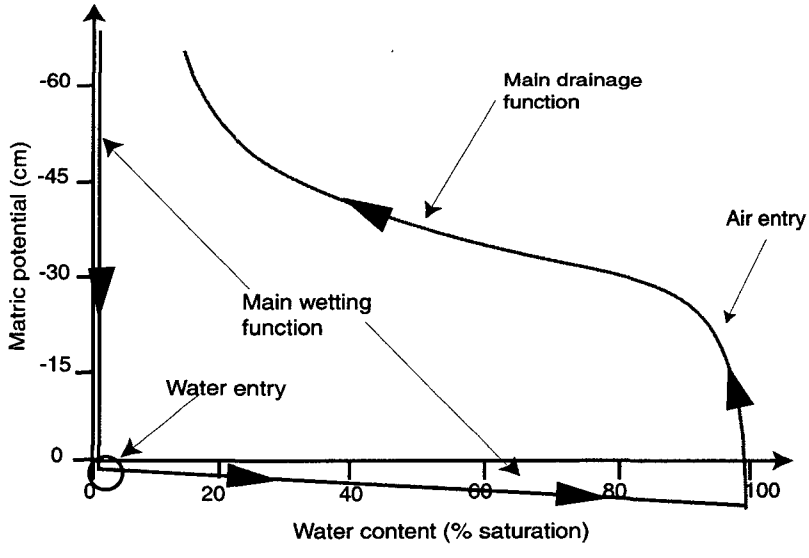

Figure 2.5: Drainage and wetting function of a water repellent soil. The matric potential is lower when the liquid water content is close to saturation in the main drainage function than for a dry soil in the main wetting function.

main wetting retention function is inevitably above zero, whereas the drying curve is similar to that of a hydrophilic soil (Bauters et al. 2000) (i.e. soil air-entry pressure is below zero). As a

result, a positive suction gradient will exist between the flow finger and the dry adjacent zone (the soil suction is higher in the wet zone than in the dry one), inhibiting the infiltrating water to enter into the adjacent dry zone, and explaining the fingering pattern of the water flux. As soon as the hydrophobicity disappears, the gradient becomes negative and the water penetrates into the dry area.

2.2.4. SNOW COVER DISTRIBUTION AND EVOLUTION IN A MOUNTAINOUS CATCHMENT

Over an alpine landscape the interactions among vegetation, topography, precipitation, solar radiation, wind and snowfall produce a highly variable snow cover (Haeberli et al. 1996, Malevsky-Malevich et al. 2001). Air temperature decreases with altitude and influences the snowfall limit as well as the snowmelt amount. Therefore in spring there may be snow ablation in lower parts of the basin, while at a higher location, the snow cover is still growing. Snow melting also differs with the exposure, as during sunny days, melting is mainly dominated by the direct solar heating of the surface (Baker et al. 1999). The vegetation also plays an important role, as the distribution of snow is inhomogeneous in a forest and the sublimation higher than in an open field (Parviainen and Pomeroy 2000).

A major factor of snow distribution in the mountain is the interaction between wind and topography. The different processes affecting snow distribution and displacement due to wind are shown in Figure 2.6. Snow transport at basin scale is caused by modification in the wind profile by the topography (turbulent diffusion). Distortion in the wind profile produces snow ablation on ridges and snowdrift on hollows. Near the soil (< 10 cm) snow particles are pulled out of the snow surface and saltation is observed. Very close to the snow surface (< 1 mm), snow tends to wheel over the snow surface (Castelle 1995).

Sublimation flux during blowing flow has been estimated to return 8-50% of seasonal snowfall depending on the topography (Pomeroy and Essery 1999). In particular, the rate of sublimation, though complicated, has been found to be a function of wind speed, air temperature, humidity, particle size and solar radiation. Various studies were carried out to see how snow is redistributed at the ridge crest (see for example Pomeroy 1991). Several models were developed to simulate snow distribution in complex terrain (Liston and Sturm 1998, Hartman et al. 1999).

2.2.5. GROUNDWATER RECHARGE

Groundwater recharge takes place predominantly during snowmelt. In winter, snow inhibits any groundwater recharge. In spring the recharge is influenced mainly by (a) the presence of a permanent frost layer (permafrost or glacier), (b) the presence/absence of a seasonal soil frost, and (c) the soil/geological structure and texture.

(a) Permafrost acts generally as an impervious boundary. It is mostly over-saturated and therefore water cannot infiltrate, only lateral flow is possible (Gerber and Tenthorey 1990).Various studies were carried out to investigate the influence of permafrost on the water circulation (Speck 1994, Tenthorey 1992, Carey and Woo 2001). Kane et al. (1981) showed for example that in a subarctic area, high surface runoff was observed from a permafrost area. Nevertheless, the exact influence of permafrost on the alpine hydrogeology is little known. This is due mainly to the difficulties to accurately localise permafrost zones (Haeberli et al. 1996). Groundwater recharge is also influenced by glacier-covered areas. Usually it is assumed that the

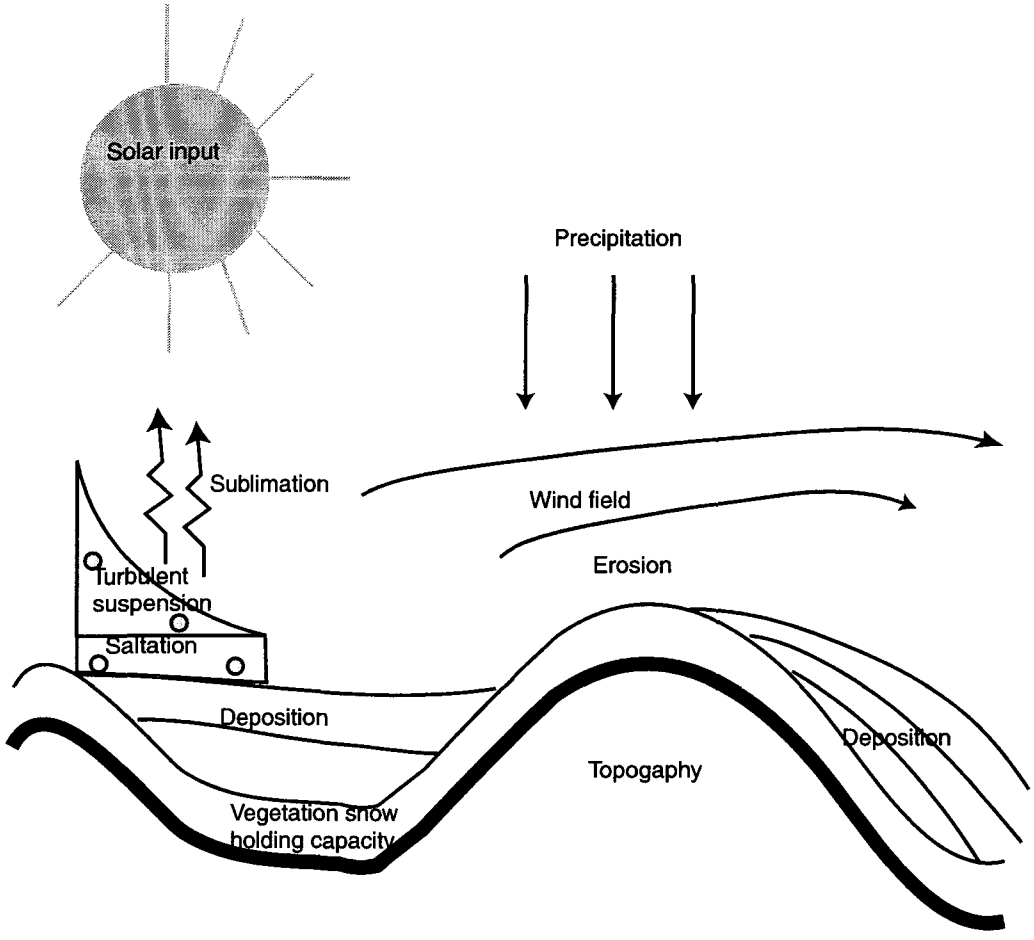

Figure 2.6: Snow transport, sublimation and deposition due to wind (Liston and Sturm 1998).

glacier will contribute to the recharge when the snow line (i.e. the line which demarcates snow free from snow covered regions) reaches the snout of the glacier and the glacier ice starts contributing to the melt runoff.

(b) Over the last years, several studies were carried out to investigate the effect of a seasonal frost on the aquifer recharge. These studies showed that this influence depends mainly on topographical aspects, and the geographical extent of the studied area. For a granitic Rock Terrain of the Canadian Shield, Thorne et al. (1998) did not find any restriction of the groundwater recharge by the frozen soils, as only shallow organic soils infield the large aperture in the rock outcrop. Cherkauer and Lettenmaier (1999) added a frozen soil and energy balance snow accumulation and ablation algorithms on an existing semi-empirical model to simulate the runoff response in two upper Mississippi sub-basins. Due to the large scale of the basins (42000 km^2 and 69 000 km^2) only a modest increase in the runoff response was observed. Over small catchments results were more contrasting. Shanley and Chalmers (1998) did not find evidence of larger surface runoff at snowmelt due to seasonal frost at the Sleeper River Watershed (111 km^2) in north-eastern Vermont. Investigation was further pursued in a smaller catchment (0.59 km^2), where soil frost had a much more pronounced effect on surface runoff. Shanley and Chalmers (1998) supposed that the effect of soil frost on a larger scale is often masked due to the variability in snowmelt timing between location at different elevations or due to aspect differences like the presence of interspersed forested land, where soil frost may be

absent.

(c) The intensity of surface runoff or overland flow depends on the soil structure and texture. Surface runoff will be more important when the soil infiltration capacity is low and vice versa. However, spatial variation of the soil types usually limits the occurrence of overland flow. In fact, rapid flow is mostly produced by subsurface flow (i.e. near surface water flow within the soil profile) (Beven 1989), which depends not only on the soil nature, but also on the underlying geological structure.

2.3. METEOROLOGICAL AND HYDROGEOLOGICAL MODELLING

In the setup of the different existing models, we distinguish the scale and the type of the model. The scale ranges from microscopic modelling of water movement in a soil up to modelling of water movement in a catchment of several 100 km^2. The type is either empirical, conceptual or physical. Model scale and type are strongly linked, as the smaller the scale is, the more detailed the model used has to describe reality.

This section is divided into two parts. Plot scale models are presented in a first part whereupon modelling of catchment is presented. The focus is on (a) presenting and describing briefly some snowpack evolution models, (b) reviewing the different models coupling water and heat flow in the soil as well as including soil frost, and (c) describing briefly different modelling approaches for catchment runoff simulation and reviewing main alpine catchment runoff studies.

2.3.1. SNOW COVER EVOLUTION AND WATER CIRCULATION AT THE PLOT SCALE

The simulation of a one-dimensional snow cover is currently mostly carried out by using energy balance models. The snow layer is either treated simply as a unique layer or is divided into a succession of layers to estimate the internal state of the snowpack, such as temperature, liquid water content, density or snow types. Multi-layers were mostly developed to forecast avalanche hazard, where knowledge on the structure of the snowpack is of critical importance. Well-known multi-layer models are SNOWPACK (Lehning et al. 1998), developed by the Swiss Avalanche Survey in Davos (FLS) and CROCUS (Brun et al. 1992) used by Meteo-France for avalanche forecasting. In such models, the processes in the soil profile are not simulated in detail. They are also computationally time consuming.

On the opposite, if interest is merely on the amount of meltwater, snow models are mostly simplified, and snow is represented as a unique layer, like the SHAW model (Flerchinger and Saxton 1989) or the COUP model (Jansson and Karlberg 2001). In fact, these two models were partially developed to simulate water flux in the unsaturated part of the soil when soil frost may occur. As pointed out by Kennedy and Sharratt (1997), results were strongly sensitive to an accurate estimation of the snow depth, as soil freezing is strongly influenced by the snow cover. To overcome this problem, improvement is currently carried out on the COUP model to integrate a multi-layer snow model in the procedure (Gustaffson et al. sub.).

Several models were developed with special attention to specific physical processes. We may quote in particular the model from Colbeck (1973 b), which investigated the influence of an impervious lower boundary on the water flux in snow; the one from Singh et al. (1997), which simulated the retention capacities of a snowpack for different rainfall events; the one from

Tseng and Illangasekare (1994), which investigated how a wetting front migrate in a layered subfreezing snowpack or the one from Coléou et al. (199), which simulated the capillary rise in a snowpack. These models are nevertheless too specific and in most cases cannot be used to simulate snow cover evolution for an entire year (Gustafsson et al. sub.).

Various models simulate water circulation in the unsaturated part of the soil. Apart from the already mentioned SHAW and COUP models, Fox (1992) and Levine and Knox (1997) incorporated freezing in their model setting to simulate water balance at plot scale. Other models are related to thermal processes only and were developed to simulate the soil frost extent under diverse climatic conditions (Benoit 1974, Cary and al. 1978, DeGaetano 1995). Soil frost and frozen ground do also have significant implication for weather forecast models. The new ETA model (Koren et al. 1999) incorporates freezing-thawing and snow accumulation-ablation processes in a coupled land-atmosphere weather prediction model. For computational rapidity, a single snow layer was assumed. Improvement of soil moisture content and temperature was appreciable, but similar to SHAW and COUP, the new ETA model was very sensitive to snow depth variation and snow cover thermal properties. An accurate simulation of the snowpack is therefore essential.

2.3.2. SNOWMELT RUNOFF MODELS (CATCHMENT SCALE)

The structure of snowmelt runoff models can be divided into two distinctive parts: snowmelt and water circulation models. Snowmelt models are further classified by the use of an energy balance approach, like those presented previously or by a temperature index approach (like the degree days approximation (Rango 1992)) to simulate snowmelt processes. Water circulation models are either lumped (i.e. the catchment is regarded as a whole) or distributed (i.e. the topography is taken into account). Simple governing laws using empirical parameters are used to describe lumped models. These empirical parameters are calibrated on measured data, but most of the time, do not have a real physical meaning. Indeed, they include several effects or properties of the system, which are too difficult to know with enough accuracy to be able to simulate the system. Distributed models are either physical or conceptual models. When using physical models, the equations have a physical, well-defined meaning, i.e. they describe a single relation independent of the other processes of the system. On the other hand, conceptual models consider physical laws in a highly simplified form. The interactions between the different components are mostly based on quantitative or semi-quantitative parameters.

Most existing snowmelt models are conceptual. The HBV MODEL (Bergström 1992) use a linear reservoir cascade routing method to compute stream flow and empirical equation, like the temperature index method or the generalized snowmelt equation to simulate snowmelt. The snowmelt Runoff Model (SRM) (Martinec 1975) also uses an empirical approach to compute average daily discharge. Importance is given to a modified depletion curve, where the snow coverage is related to the accumulated degree-days. The University of British Columbia Watershed Model (UBC) (Quick and Pipes 1977) is also based on reservoir routing and empirical snowmelt function. snowmelt runoff is divided into very slow, slow, medium and fast runoff, depending on which component the water runoff undergoes. All these models do not consider any soil frost at all.

A major problem when using a spatially distributed physical snowmelt method is the amount of available meteorological data. Extrapolation is somehow difficult especially in rugged terrain (Lang 1998). For temperatures, typically a lapse rate of 6 C°/km is assumed, but it may be less in winter or more in summer. Precipitation variations due to altitude are much more difficult to

estimate. The precipitation is extremely variable and estimation from a single gauge is hardly accurate. A second problem arises when choosing validation data of a physical distributed model. Verification of a distributed model cannot be carried out on the basis of runoff data alone (Braun 1985). Different approaches have to be used, like comparing results with the spatially distributed snow cover. A spatially distributed snowmelt model based on energy balance developed by Blöscht et al. (1991) pointed out the uncertainties introduced by extrapolating air temperature.

Some attempts have been made to create a physically-based, distributed catchment model. The SHE model (Abbott et al. 1986) combines each of the hydrological processes of water movement, i.e. interception and evapotranspiration by plants, overland and channel flow, unsaturated zone flow, saturated zone flow and snowmelt. The calibration of such a model is sophisticated and the program is time-consuming. In a same vein a simulation of the Rhone basin was carried out in France (Etchevers et al. 2001). This program combines a multi-layer snow model (CROCUS) with a macro scale hydrological model and a soil-vegetation-atmosphere transfer scheme. Validation was carried out on the major river daily discharge. But the same remarks hold true as for the SHE model and running the program necessitates a considerable amount of data and parameter calibration. Ippisch (2001) included the soil frost in a three-dimensional water and heat flow model, but the coupling between the soil and the snow cover was not integrated.

Most basin scale models do not consider the effect of frozen soil on snowmelt runoff processes. Snow cover evolution and snowmelt runoff is simulated in a similar way as rainfall runoff. As pointed out by Koren et al. (1995) this approach may not be effective in representing the snowmelt runoff as the water-absorbing properties of the soil in these regions vary considerably in response to soil freezing/thawing. Various attempts were made to incorporate soil frost in estimating water runoff at a watershed scale. Engelmark (1984) used a one-dimensional model to estimate snowmelt runoff from arable and pasture land. 80% of runoff was observed in the grass-covered land while the forest had a larger part of water, which infiltrated the soil. Stähli et al. (2001) indicated that snowmelt runoff from a moderately sloped boreal forest (8600 m^2) was little, but soil frost could, under certain special circumstances like high water saturation at the beginning of the winter, increase surface runoff markedly. A simplistic conceptual model was tested by Koren et al. (1995) coupling a snowmelt model and a water balance model. Similar to Sand and Kane (1986), results were significantly improved when soil frost was incorporated in the model to simulate runoff. Shanley and Chalmers (1998) did not find any significant correlation between maximal soil frost depth and runoff ratio (i.e. streamflow/(rain + snowmelt)). However, by analysing specific events, soil frost induced a large and quicker response to rainfall in comparison to the non-frost condition. To conclude and as pointed out by Woo et al. (2000), there is still a need to develop hydrological models taking explicitly into account the snow and frozen soil processes.

2.4. GLOBAL WARMING EFFECT ON THE ALPS

Twentieth-century climate was dominated by a universal warming. Most parts of the world recorded air temperatures, which were significantly higher at the end of the century than at its beginning (a temperature increase of 0.5°C is observed) (Easterling et al. 2000). The release through human activities of green-house gases is mainly responsible for this increase. The consequences of the green-house effect are thought to be more pronounced in the Alps than elsewhere. The Alps represent a climate barrier: their climate is Mediterranean in the south, and

rather maritime in the northern parts. This barrier has a marked influence on meteorological systems. Actual measurement indicates a warming of approximately 2°C during the winter and of approximately 1°C during the summer in Switzerland (Ohmura and al. 1998). Also temperature changes in winter are more pronounced in higher areas than in lower ones. The amount of precipitation increased by about 25% in western Switzerland and by approximately 10% in the eastern and southern part of Switzerland during the last 60 years (Widmann and Shär 1997).

To be able to predict how climates will evolve during the 21th century, various climate models were developed. The General Circulation Model (GCM) is certainly the most sophisticated tool available. The latest results predict an increase in temperature until the end of the 21 century between 2 and 5°C, as illustrated in Figure 2.7.The main drawback by using GCM models to

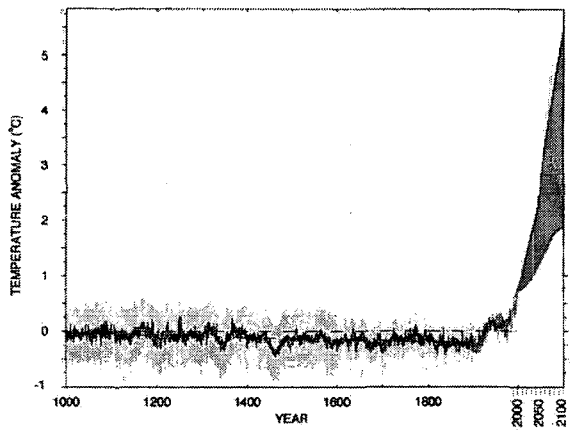

Figure 2.7: Mean annual temperature variations over the northern hemisphere compared to the estimated range of global temperature changes over the next century from a set of transient model experiments used in IPCC assessment exercises (Mann and Bradley 1999).

predict climate change over the Alps is their low spatial resolution, as grid point distances are in the order of a few 100 km. To associate possible changes between regional climate from the GCM output, «downscaling» is commonly used. Several downscaling approaches exist. A first and simple possibility is to directly interpolate climatic information from individual GCM grid points in the vicinity of the region of interest. This is not recommended, as GCM reproduces regional climate poorly. Another possibility is to rely on a high-resolution global model (Beniston et al. 1995). This is computationally time-consuming. Finally, the procedure may be based on a statistical approach using empirical relationship between variation of the large-scale and the regional weather (Gyalistras 1998). It has the advantage that it provides a very high resolution and it is computationally efficient.

Simulating water balance on a plot scale also needs a high temporal resolution. Usually, the weather variables downscaled at the resolution needed are not directly used because the temporal statistics of the large-scale model are not yet very reliable (Hulme et al. 1993). Therefore stochastics models, called weather generators, fitted on local measurements are more common. An example of such a procedure is given by Gyalistras (1998).

Stadler et al. (1997) used this approach to simulate impacts of climate warming on a sub-alpine forest (Davos and Alptal). He made the assumption that the mean air temperature would increase from the actual air temperature by either +1.5°C or +3°C. The consequences were a decrease in snow depth by about 25% and an increase in flooding risks in winter. During the winter, mean soil frost would be little affected by a warmer climate. Rainfall on a frozen ground would therefore be more likely and flooding become a major risk. If snow is not considered, various studies, (see for example Venäläinen et al. 2001) showed that frost depth would decrease significantly.

At larger scales (basins) models indicate mainly higher winter discharge as a result of intensified snowmelt, increased winter precipitation, and lower summer discharge due to the reduced winter snow storage (Rango and Martinec 1979, Bultot et al. 1988, Williams and Tarboton 1999, Bengtsson and Singh 2000, Middelkoop et al. 2001). To the author knowledge no study investigated the consequences of a changing climate on the seasonal soil frost extent over large areas and the resultant change in the hydro-geologic cycle. One of the objectives of this study will hence be to better forecast the frost sensitivity to a changing climate and the possible implication for the alpine aquifer recharge.

2.5. EARLIER STUDIES IN HYDROGEOLOGY AT THE FIELD USED IN THE PRESENT STUDY (GRÄCHEN)

Several studies have been carried out at Grächen, while no research studies on the Gd St Bernard area are known to the author. The village of Grächen is located on a large landslide stretching from 1000 m up to 3000 m and including the Hannigalp site. It is one of the major landslides in Switzerland and was thoroughly studied in the frame of the National Research Project 31 (Noverraz et al. 1998). Results showed that landslide movement was very low and did not affect human activities. A major danger comes from the Rittigraben located to the east of the village, where several debris flows occurred due to the presence of a melting permafrost (Zimmermann et al. 1997, Lugon and Monbaron 1998). This permafrost has been mapped by Gardaz et al. (1995) and, at present, is being investigated by Herz et al. (2002). This survey focuses on the importance of a coarse debris cover on the permafrost extent.

Water supply of the Grächen area has become a problem during winters with little precipitation. To resolve this shortage, a well was drilled in 1992 at Meisen. Results of the hydrogeological study of Rovina and Zuber (1997) will be given in Chapter 11.

2.6. CONCLUSION

Alpine hydrology shows to be very important for various human activities. It is therefore not surprising to find numerous research on this topic. However, most of these work did not integrate the effect of seasonal soil frost on the snow melt runoff. While numerous studies where conducted in Scandinavian or North America, there is at the moment, an obvious lack of study on this issue in alpine region, both at plot scale and at larger scales. To the author knowledge, no other study exists, except the one from Stadler et al. (1996). This research should hence enable to show how often seasonal soil frost occurs in the Alps, and to estimate it possible implication on the snowmelt runoff at both plot and large scales.

3. MODEL DESCRIPTION

3.1. INTRODUCTION

In this chapter, we set out the different numerical models, which were used in this thesis, namely the COUP model (Jansson and Karlberg 2001), the MACRO model (Jarvis and Larsson 1990) and FEFLOW (Diersch 1996). Only major features of each model needed for the general understanding are explained. The potential and possibilites of each model, in particular the COUP model, are much more sophisticated than the features presented below. For further information, please refer to the model manual.

We recall shortly for which purpose these models will be applied. To investigate the water transport behaviour at Hannigalp, we will compare results from the one domain flow model COUP with those from the two-domain flow model MACRO (Chapter 8). To simulate the features of frozen soils at local scale, we will apply the one-dimensional heat and water flux model COUP, which accounts for the phase change water/ice (Chapter 9-12). Catchment models treating snowmelt runoff do not usually include phase change in their settings (see Chapter 2: "Snowmelt runoff models (catchment scale)", page 20). Therefore, the water balance at catchment scale was simulated by coupling water flux output from COUP to the two-dimensional water transport model FEFLOW (Chapter 12).

3.2. THE COUP MODEL

COUP takes into account the connected processes in and between the atmosphere, the vegetation, the snow layer and the soil. In particular, this finite difference model considers soil surface evaporation and transpiration of plants. Input data are given hourly or daily. Minimum requirements are precipitation and temperature if no plant cover is considered, otherwise evapotranspiration data have to be added. To simulate physical processes like soil water evaporation or snowpack energy balance, additional input data like total radiation, wind speed, and relative humidity is necessary. Although the model is mainly one-dimensional, it may be applied to simulated two-dimensional processes (surface runoff and subsurface flow) (Figure 3.1). However, such processes may only be reproduced as long as the effects of the lateral runoff on the water balance are negligible. In particular COUP may not be successful in simulating surface and subsurface runoff over large areas (horizontal distance > 10-50 m); in such cases, the steady increase in the surface runoff in downslope direction affects the amount of subsurface runoff and deep percolation, when going from upper to lower areas. For such areas, the change in the surface water caused by additional water input from higher areas should be additionally taken into account in the soil water balance, and a two-dimensional model is necessary.

3.2.1. WATER FLOW

Based on Harlans concept (Harlan 1973), the model simulates a coupled atmosphere and soil processes. The two basic assumptions are the conservation of energy and mass, and the validity of Fourrier's and Darcy's law. In particular, water circulation in the unsaturated zone is governed by the Richards equation (Richards 1931):

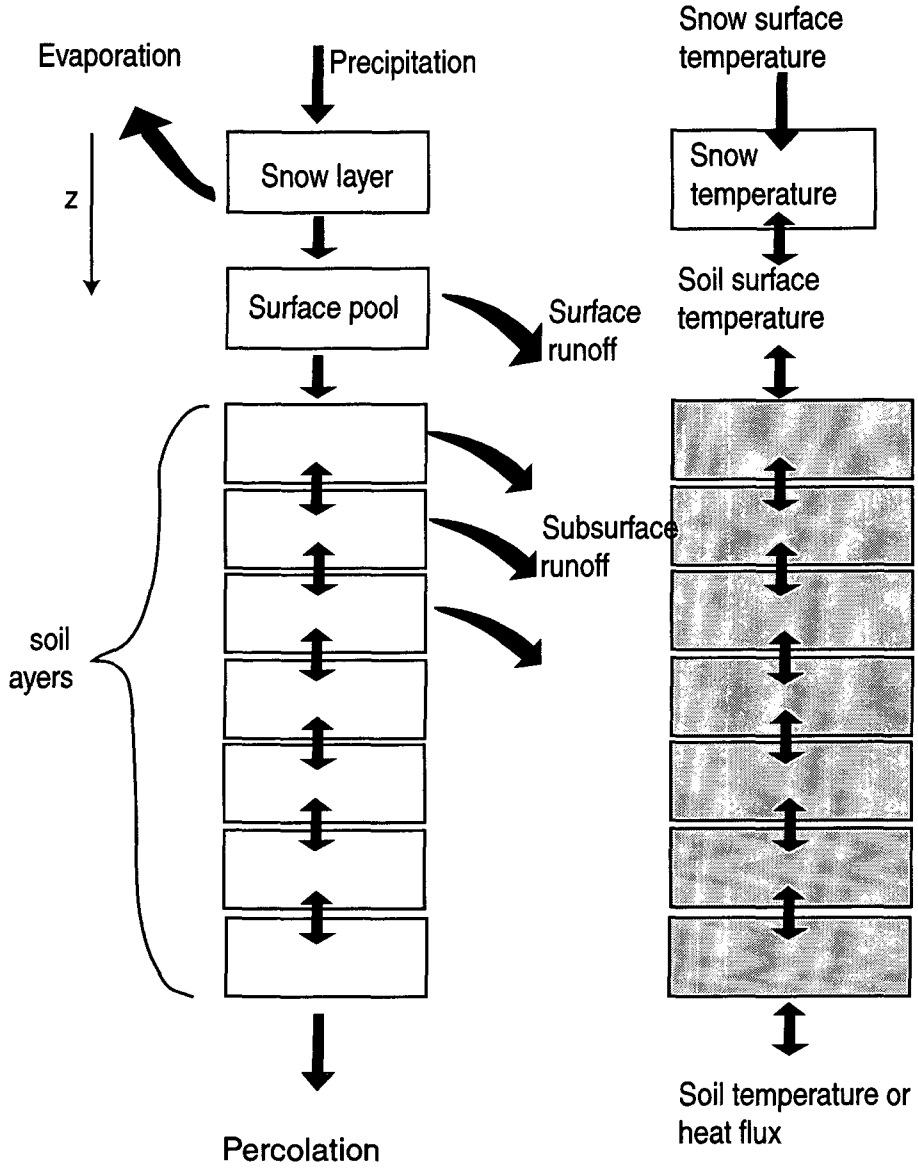

Figure 3.1: Mass balance (left) and heat flux (right) of the COUP model (Jansson and Karlberg 2001). Surface and subsurface runoff are included in the calcualtion of the mass balance.

$$\frac{\partial \theta}{\partial t} = -\frac{\partial q_w}{\partial z} + s_w \tag{3.1}$$

with: θ : liquid water content,
t : time,
q_w : water flow,
s_w : source/sink term.

The water flow $q(\psi)$ is given by Darcy's law (equ. 1.8). The source/sink term s_w may represent lateral subsurface flow q_{ssf}. This flow is assumed to be identical with the flow towards a drainage system:

$$q_{ssf} = \int_{z_p}^{z_{sat}} a_r k_{sat}(z_{sat}-z_p)/d_p \, dz \qquad (3.2)$$

with: k_{sat} : saturated hydraulic conductivity,
a_r : ratio between the layer thickness and the unit horizontal area,
z_{sat} : depth of the saturated layer,
z_p : depth of the drains,
d_p : drain spacing,

where the ratio of the two parameters d_p and z_p equals the slope inclination (Figure 3.2).

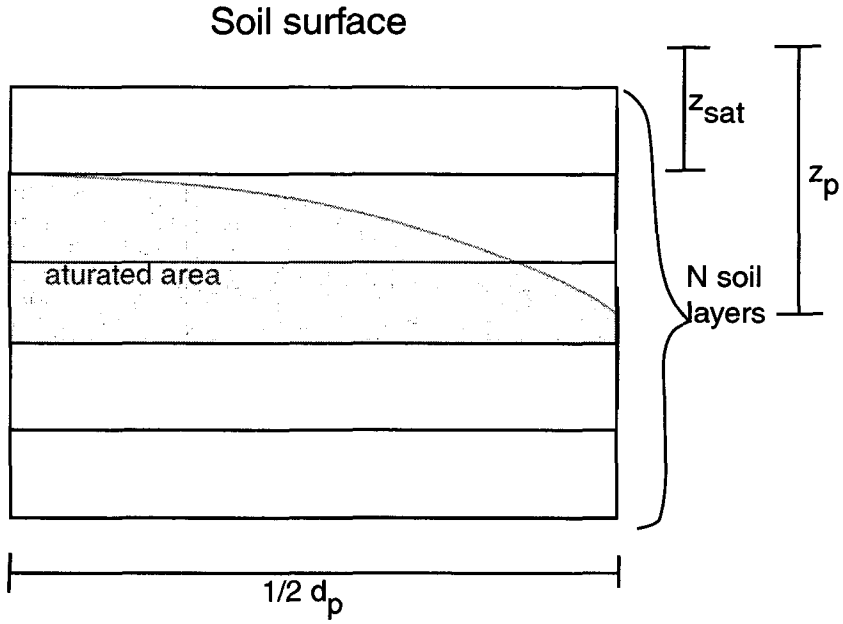

Figure 3.2: Subsurface flow may be considered equivalently to the flow towards a drainage system.

The knowledge of soil hydraulic properties is essential to solve equation eq. 3.1. When no hysteresis is assumed, these properties are expressed by using the water retention curve function $\psi(\theta)$ (Van Genuchten 1980) or (Brooks and Corey 1964):

$$\text{Van Genuchten: } s=1/(1+(\alpha\,\psi)^n)^m \qquad (3.3)$$

$$\text{Brooks and Corey: } \quad s = \left(\frac{\psi}{\psi_a}\right)^{-\lambda} \qquad (3.4)$$

where

$$s=\frac{\theta-\theta_r}{\theta_s-\theta_r} \qquad (3.5)$$

with: θ : liquid water content,
θ_r : residual liquid water content,
θ_s : liquid water content at saturation,

ψ : liquid water pressure,
α, n, m : Van Genuchten parameters,
ψ_a : air entry pressure,
λ : pore size distribution index,
k_{sat} : saturated conductivity,

and the unsaturated hydraulic conductivity function, $k_w(\theta)$ (Mualem 1976):

$$\text{Van Genuchten: } k_w = k_{sat}(1-(\alpha\psi)^{n-1}(1+(\alpha\psi)^n)^{-m})^2/(1+(\alpha\psi)^n)^{m/2} \quad (3.6)$$

$$\text{Brooks and Corey: } k_w = k_{sat}s^{\left(n_t+2+\frac{2}{\lambda}\right)} \quad (3.7)$$

with: n_t : parameter accounting for pore correlation and flow path tortuosity.

The upper boundary at the soil surface is given by separate a subroutine accounting for snowmelt (see Chapter 3.2.6., page 33). If the infiltration capacity is reached, the remaining water is stored in a pool at the soil surface. This water can either infiltrate with a delay into the ground or be drained as surface runoff. This surface runoff, q_{surf} is then calculated from:

$$q_{surf} = a_{surf}(W_{pool} - w_{pmax}) \quad (3.8)$$

with: a_{surf} : empirical coefficient,
W_{pool} : total amount of liquid water in the surface pool,
w_{pmax} : maximal amount of liquid water stored on the soil surface pool.

For unsaturated conditions, the lower boundary condition may be specified either by a time-varying pressure head of the bottom layer or by assuming a unit gradient gravitational flow. In the latest case, the water flow is calculated from the unsaturated hydraulic conductivity of the bottom layer.

3.2.2. HEAT FLOW

Soil heat processes are described by the equation of energy conservation:

$$\frac{\partial}{\partial t}(CT) - L_f\rho\frac{\partial\theta_i}{\partial t} = -\frac{\partial q_h}{\partial z} - s_h \quad (3.9)$$

with: t : time,
C : heat capacity of soil,
T : temperature,
L_f : latent heat,
ρ : water density,
θ_i : volumetric water content of ice,
q_h : heat flow, including convection and conduction heat flow,
s_h : source/sink term,

where the heat flow is:

$$q_h = -k_h\frac{\partial T}{\partial z} + C_w T q_w + L_v\rho_v q_v \quad (3.10)$$

with: k_h : heat conductivity,

T : temperature,
z : soil depth,
C_w : heat capacity of water,
q_w : water flow,
L_v : latent heat of vapour,
ρ_v : vapour density,
q_v : vapour flow.

The convective term is important especially during snowmelt, while heat transfer by conduction is important prior to snowmelt. Heat conductivity is given for a mineral soil by (Kersten 1949):

$$k_h=0.143(a_1\log\left(\frac{\theta}{\rho_s}\right)+a_2)10^{a_3\rho_s} \tag{3.11}$$

with: a_1, a_2, a_3 : empirical constants,
θ : liquid water content,
ρ_s : dry bulk density.

The logarithmic argument θ/ρ_s is equivalent to the soil liquid water content expressed on a mass basis. The three empirical constants a_1, a_2, a_3, differ depending on whether the soil is dominated by clay, by sand or by organic material. To get a more precise description of the soil thermal conductivity, additionally, the thermal conductivity $k_h(z_n)$, can be adjusted for each soil layer z_n by using a multiplicative scaling coefficient a_4:

$$k_h(z_n)=k_h 10^{a_{44}} \tag{3.12}$$

Thermal conductivity is notably different whether the soil is frozen or not, as ice is four times more conductive than liquid water. In the case of frozen soil, it is calculated by:

$$k_h(frozen) = b_1 10^{b_2\rho_s} + b_3\left(\frac{\theta}{\rho_s}\right)10^{b_4\rho_s} \tag{3.13}$$

with: θ : water content,
ρ_s : dry bulk density,
b_1 to b_4 : empirical constants.

The upper boundary condition can be given for snow free period by either assuming the air temperature equal to the soil surface temperature or by solving the heat flow equation at the soil surface. For snow cover period, the soil surface temperature is given as a weighting value between the snow surface temperature and the temperature of the top soil layer, depending on the snow and soil thermal conductivity. The snow surface temperature can be assumed to be equal to the air temperature or it can be estimated by solving the energy balance equation of the snow surface.

The lower thermal boundary condition may be specified in different ways, either as a constant heat flux or as a time-varying temperature. In this case, the temperature **T** is an analytical solution of the conduction problem and, at depth **z** and time **t**, is given by:

$$T(z,t)=T_{mean}-T_{amp}e^{-z/d}\cos(\omega(t-t_{ph})-z/d) \tag{3.14}$$

and

$$d=\sqrt{\frac{2k_h}{C\omega}} \tag{3.15}$$

with: T_{mean} : mean air temperature,
T_{amp} : amplitude of air temperature,
ω : frequency, which is given by $2\pi/365$ if annual temperature variation is of interest,
t_{ph} : time phase shift,
C : heat capacity of the soil at moisture content that equals the selected initial conditions.

3.2.3. HYSTERESIS EFFECT

Hysteresis effects on soil hydraulic properties is taken into account by the model. The calculation of the hysteresis effect R is based on three multiplicative hysteresis functions:

$$R=R_{age}R_{shift}R_{acc} \tag{3.16}$$

with: R_{age} : This function considers the time since the start of sorption loop. It expresses the fact that the hysteresis effect is reduced with increasing time.
R_{shift} : This function considers the shift point pF value. It takes into account that hysteresis is more pronounced under strong water suction.
R_{acc} : This function considers that a fast change of liquid water content will enhance the hysteresis effect.

The three hysteresis functions vary between zero and unity and are given by:

$$R_{age} = \exp(-a_A \Delta t_{shift}) \tag{3.17}$$

$$R_{shift}=\max\left(R_{age},\min\left(\frac{\log\psi - a_B}{a_C - a_B},1\right)\right) \tag{3.18}$$

$$R_{acc}=\min\left(1,\frac{\Delta\theta_{sorp}}{a_D}\right) \tag{3.19}$$

with: Δt_{shift} : time elapsed since last major shift from a desorption to a sorption,
ψ : water pressure,
$\Delta\theta_{sorp\,s}$: accumulated increase of liquid water content at a rate that exceeds a given stresshold value since the last shift form desorption to sorption,
a_A, a_B, a_C : parameters,
a_D : value of accumulated increase of liquid water content at which the hysteresis function R_{acc} reaches unity.

The hysteresis effect is then given by:

$$\psi=\psi^* 10^{R \bullet P_{phys}} \tag{3.20}$$

with: ψ : water pressure,

ψ^* : reference value of water pressure (when no hysteresis is assumed),

P_{phys} : parameter expressing the maximal hysteresis for each simulated layer.

3.2.4. TWO-DOMAIN FLOW IN A FROZEN SOIL

A two-domain approach was developed by Stähli et al. (1996), where the water moves either in a low flow domain (bounded water) or in a high flow domain (pore water) (Figure 3.3). In the

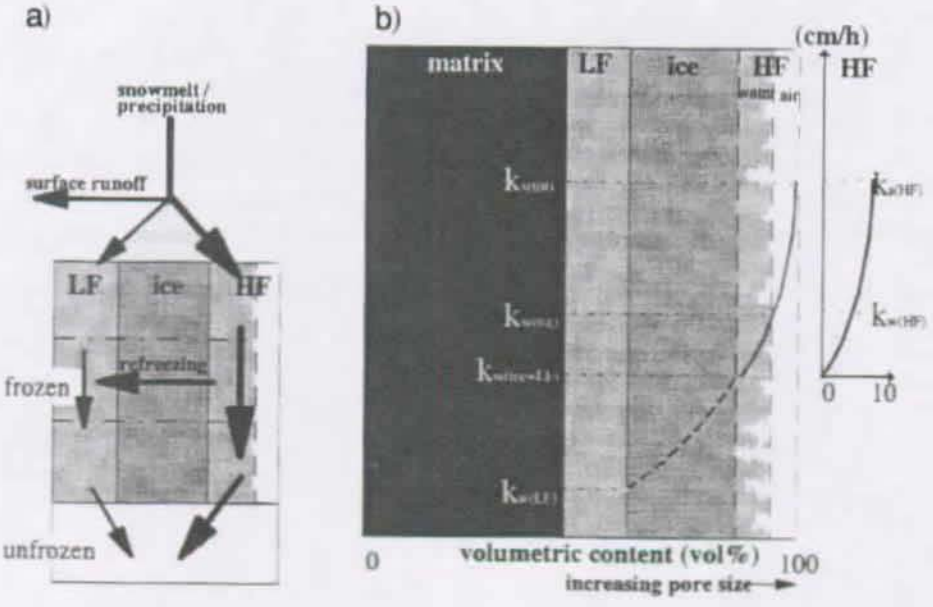

Figure 3.3: Schematic illustration of the two-domain approach. (a) Concept of the water flows in the two-domain approach. (b) Hydraulic conductivity curves for the two-flow domains. From Stähli et al. (1996).

low flow domain, the water movement is treated in the same way as in the non-frozen case. It is assumed that liquid-ice interface equals the liquid-air interface and therefore a frozen soil is equivalent to a very dry unfrozen soil, as only strongly bounded water exists at subfreezing temperature. The hydraulic conductivity is therefore very low and is proportional to the hydraulic conductivity k_w of a non-frozen soil with the same water content To reduce the often overestimate upward water flow towards the frost front, an empirical factor f_i is introduced for the calculation of the hydraulic conductivity k_{lf} in the low flow domain:

$$k_{lf}(\theta_{lf}) = 10^{f_i r_w} k_w(\theta_{lf}) \tag{3.21}$$

with: r_w : mass ratio of ice and total water or thermal quality,

θ_{lf} : liquid water content of low flow domain.

This reduction is necessary as the flow conditions at the boundary between frozen and none-frozen soil differ markedly. Ice replaces air at the boundary of the liquid phase where the flow velocity of liquid water is highest and therefore the flow depends mainly on the low flow hydraulic conductivity in the frozen soil. An identical result to reduce the upward water flow is

achieved by taking $k_{lf}(\theta_{lf})$ at the boundary as the lowest value instead of the mean one between the two adjacent layers.

In the high flow domain, water flows through the previously connected air filled pores. The flux is gravitational and is given by:

$$q_{hf} = e^{\frac{-\theta_{ice}}{f_{\theta_i}}} (k_w(\theta_{tot}) - k_w(\theta_{lf} + \theta_{ice})) \tag{3.22}$$

with: θ_{tot} : total water content corresponding to all volume occupied by water (liquid and ice),
θ_{ice} : liquid water content corresponding to the volume occupied by ice,
f_{θ_i} : damping ice content.

Water in the high flow domain may refreeze. The heat, which is released from the freezing in the high flow domain, causes melting in the finest ice filled pores. The boundaries between the low flow and the high flow are shifted, as the low flow domain gets bigger and the high flow domain smaller. The amount of water that refreezes in the low flow domain can be calculated as:

$$q_f = \alpha_f \frac{-T}{L_f} \Delta z \tag{3.23}$$

with: α_f : heat transfer coefficient,
Δz : layer thickness.

3.2.5. FREEZING POINT DEPRESSION CURVE

In a first step, the assumption is made that at a temperature T_f, all water is frozen except a residual unfrozen amount θ_{lf}, calculated as:

$$\theta_{lf} = d_f \theta_{wilt} \tag{3.24}$$

with: d_f : parameter,
θ_{wilt} : volumetric liquid water content at a soil water pressure of 4.2 pF.

Soil freezing is then based on a function for the freezing point depression curve (FPDC)[1] and the assumption of analogy between the freezing-thawing and the drying-wetting processes. The FPDC (i.e. the partitioning of the total heat content into a latent and a sensible heat portions, see Figure 2.4.) is expressed by the empiric function r:

$$r = (1 - E/E_f)^{d_2\lambda + d_3} \min\left(1, \frac{E_f - E}{E_f + L_v w_{ice}}\right) \tag{3.25}$$

with: E : heat content of soil,
E_f : soil heat content at T_f,
d_2, d_3 : parameters expressing the shape of freezing point depression

1. The amount of liquid water in a soil steadily decreases when temperature is lowered below 0°C, as the free Gipps energy depends on the absorption and capillary forces which are pore size dependent. The relation between liquid soil water content and temperature is described by the freezing point depression curve (FPDC).

curve,
w_{ice} : mass of water available for freezing.

The sensible heat content H is then given by:

$$H=E(1-f_{lat})(1-r) \tag{3.26}$$

with: f_{lat} : fraction of latent heat of ice to the total heat content of soil at -5°C,

and the soil temperature by:

$$T=H/C_f \tag{3.27}$$

with: C_f : soil heat capacity at -5°C.

3.2.6. SNOW DYNAMICS

The snowpack is assumed to be a single homogeneous layer, separated into the liquid water and the total amount of water equivalent. When the total liquid water amount in the snow layer exceeds a given retention threshold parameter value, water is released from the snowpack. Having a non-saturated soil surface layer, infiltration occurs, otherwise surface runoff takes place.

Two approaches, an empirical melting/freezing approach (**MA**) as well as a surface energy balance approach (**EA**), are possible to describe the mass balance of the snowpack.

3.2.6.1. EMPIRICAL MELTING/FREEZING APPROACH (MA)

In the **MA**, the snow temperature is set equal to the air temperature, and the empirical melting/ freezing function M is made up by three functions, accounting for the influence of temperature, global (short-wave) radiation and soil surface heat flow $q_h(0)$:

$$= M_T T_{air} + M_R R_{is} + \frac{f_{qh} q_h(0)}{L_f} \tag{3.28}$$

with: T_{air} : air temperature,
R_{is} : global radiation,
L_f : latent heat of fusion,
f_{qh} : scaling coefficient,
M_T : temperature melting-refreezing function
M_R : radiation melting-refreezing function.

M_T is given by:

$$M_T = \begin{cases} m_T & T_{air} \geq 0 \\ m_T min\left(I, \frac{m_f}{\Delta z_{snow}}\right) & T_{air} < 0 \end{cases} \tag{3.29}$$

with: m_T, m_f : parameters,
I : constant =1

The snow albedo is reduced with the age of the snow surface. As a result the snow radiation absorption is time dependent. This is expressed by making the variable M_R dependent on the age of the snow surface:

$$M_R = m_{Rmin}(1+s_1(1-e^{-s_2 t_{age}})) \tag{3.30}$$

with: m_{Rmin}, s_1, s_2: parameters,
t_{age} : age of the surface snow.

In the MA, the snow evaporation is not included in the water mass balance.

In the simulation of Chapter 9, the soil surface temperature, during snow free period, was set equal to the air temperature, and the soil evaporation calculated by the "Penman-Monteith" equation (Monteith 1965)[1] :

$$L_v E_s = \frac{\Delta(R_{ns} - q_h) + \rho_a c_p \dfrac{e_s - e_{air}}{r_{asoil}}}{\Delta + \gamma\left(I + \dfrac{r_{ss}}{r_{asoil}}\right)} \tag{3.31}$$

with: L_v : latent heat of vapour,
E_s : soil surface evaporation,
Δ : slope of the saturated vapour pressure versus temperature curve,
R_{ns} : net radiation at the soil surface (see also eq. 3.34 where *snow* has to be replaced by *soil*),
q_h : soil heat flow,
ρ_a : air density,
c_p : heat capacity of air,
e_s : vapour pressure at the snow surface,
e_{air} : vapour pressure in the air,
γ : psychrometer constant,
I : parameter =1,
r_{asoil} : soil aerodynamic resistance,
r_{ss} : surface resistance at the soil surface.

where, the soil aerodynamic resistance between the soil surface and a reference height, r_a is calculated from:

$$r_{asoil} = 1/(\kappa^2 u)\, n\left(\frac{z_{ref} - D}{z_{omsoil}}\right) \ln\left(\frac{z_{ref} - D}{z_{ohsoil}}\right) f_{stability} \tag{3.32}$$

with: κ : Karmans constant,
u : wind speed at the reference height z_{ref},
D : zero level displacement height,
z_{omsoil} : soil surface roughness length for momentum,
z_{ohsoil} : soil surface roughness length for heat,

1. Different options are given by the model

$f_{stability}$: function governing the influence of atmospheric stability;

and, the surface resistance at the soil surface, r_{ss} is estimated by two functions accounting for the soil moisutre conditions at the soil surface and the water pressure in the uppermost soil layer.

3.2.6.2. SURFACE ENERGY BALANCE APPROACH (EA)

If the **EA** is chosen, the snow temperature, the amount of snowmelt and refreezing is calculated by solving the heat conservation equation within the snowpack (same equation than eq. 2.1):

$$Q_m = R_{n,snow} + H_{snow} + L_v E_{snow} + Q_p + q_h(0) + Q_q \tag{3.33}$$

with: Q_m : melting energy,
$R_{n,snow}$: net radiation energy,
H_{snow} : sensible heat,
$L_v E_{snow}$: latent heat,
Q_p : heat input by rain,
$q_h(0)$: heat input coming from beneath,
Q_q : change of internal energy storage of snow.

$R_{n,snow}$, is given by the sum of the net short-wave radiation, R_{snet} and the net long-wave radiation, R_{lnet} (Dysli et al. 1997) (see also Figure 3.4):

$$R_{n,snow} = R_{snet} + R_{lnet} \tag{3.34}$$

where

$$R_{snet} = R_{is} - R_{\text{refl}} \tag{3.35}$$

and

$$R_{lnet} = R_{long} - R_{\text{snow}} \tag{3.36}$$

with: R_{is} : global (short-wave) radiation,
R_{refl} : reflected short-wave radiation from the snow surface,
R_{long} : incoming long-wave radiation,
R_{snow} : outgoing snow surface radiation.

While R_{is} is mostly measured, R_{refl}, R_{long}, R_{snow} are given by[1]:

$$R_{\text{refl}} = R_{is}\, a_{snow} \tag{3.37}$$

$$R_{long} = 86400\ \sigma\ \varepsilon_a\ (T_a + T_0)^4 \tag{3.38}$$

$$R_{\text{snow}} = 86400\ \sigma\ \varepsilon_s\ (T_{ssurf} + T_0)^4 \tag{3.39}$$

with: a_{snow} : snow albedo,
σ : Stefan Boltzmann constant,
ε_s : emissivity of the snow surface (which is assumed to be one),
ε_a : emissivity of the atmosphere,

1. Different options are given by the model

T_{ssurf} : snow surface temperature,
T_0 : Freezing point = 273.15°K,
T_a : air temperature.

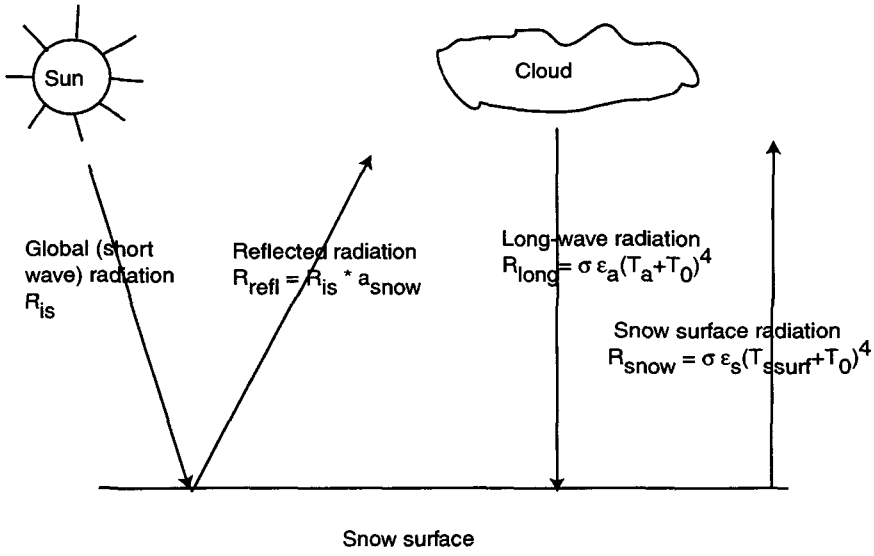

Figure 3.4: The net radiation at the snow surface is the sum of the global radiation, the reflected radiation, the long-wave radiation and the snow surface radiation.

How much global radiation is reflected depends on the snow albedo a_{snow}. This value is not constant in time, as it is influenced by the snow age and the sum of air temperature exceeding 0°C. It is given by:

$$a_{snow} = a_{smin} + a_{s1} e^{a_{s2} S_{age} + a_{s3} T_{sum}} \tag{3.40}$$

with: a_{smin} : minimum snow albedo,
a_{s1}, a_{s2}, a_{s3} : parameters,
S_{age} : age of snow since last new snow,
T_{sum} : sum of air temperature exceeding 0°C since last new snow.

The emissivity of the atmosphere, ε_a is calculated from a function given by Konzelmann et al. (1994)[1]:

$$\varepsilon_a = (r_{k1} + r_{k2} \frac{e_a}{T_a})^{1/4} (1 - n_c^3) + r_{k3} n_c^3 \tag{3.41}$$

with: r_{k1}, r_{k2}, r_{k3} : parameters,
e_a : vapour pressure in the air,
n_c : fraction of cloud covered sky.

The turbulent (H_{snow}) and latent heat exchange ($L_v E_{snow}$) between the snow surface and the atmosphere depend on the temperature and vapour pressure gradient respectively:

$$H_{snow} = \rho_a c_p \frac{T_{snow} - T_{air}}{r_{asnow}} \tag{3.42}$$

1. Different options are given by the model

$$L_v E_{snow} = \frac{\rho_a c_p}{\gamma} \frac{e_{snow} - e_{air}}{r_a} \quad (3.43)$$

with: L_v : latent heat of vapour,
E_{snow} : snow surface evaporation,
ρ_a : air density,
c_p : heat capacity of air,
T_{snow} : snow temperature,
T_{air} : air temperature,
r_{asnow} : snow aerodynamic resistance,
e_{snow} : vapour pressure at the snow surface,
e_{air} : vapour pressure in the air,
γ : psychrometer constant.

The aerodynamic resistance, r_{asnow} is calculated in the same way as in the calculation of the Penman Monteith equation (eq. 3.32, where *soil* has to be replaced by *snow*).

3.2.6.3. DENSITY AND THERMAL PROPERTIES OF SNOW

The heat flux through the snowpack and hence into the upper soil boundary depends on the thermal conductivity k_{snow}, which is time-dependent and given by:

$$k_{snow} = s_k \rho_{snow}^2 \quad (3.44)$$

with: s_k : parameter,
ρ_{snow} : snow density.

The snow density is depends on the quantity of the relative amount of free water in the snowpack and on the overburden pressure:

$$\rho_{old} = \rho_{smin} + s_{dl} \frac{S_{wl}}{S_{wlmax}} + s_{dw} S_{res} \quad (3.45)$$

with: ρ_{smin} : new snow density, assuming dry snow precipitation,
s_{dw}, s_{dl} : parameters,
S_{wl}, S_{wlmax} : free water from previous day and maximum free water of snowpack,
S_{res} : water equivalent of the snowpack from previous day.

3.3. THE MACRO MODEL

The MACRO model (Jarvis and Larsson 1990) is a one-dimensional non-steady state model of water flow and solute transport in soils. The model integrates vertical unsaturated and saturated water flow and considers the effect of the vegetation on the water balance. The model does not integrate soil frost. It can be run in two-flow domains, a high conductivity macropore domain and a low conductivity domain representing the soil matrix.

The model was mainly developed to simulate preferential flow, as such a flow allows rapid transfer of water at considerable depth in the soil profile. Preferential flow may occur in soil with macropores (Beven 1982) but also in non-structured sandy soils due to water repellency (Ritsema et al. 1993), air entrapment or hysteresis (Nieber 1996).

To take into account the rapid increase of hydraulic conductivity due to preferential flow when saturation is approached, the total porosity in each soil layer is partitioned into micropores and macropores at a given water content and potential (θ_b, ψ_b). Micropores and macropores operate then as separate flow regions. At soil surface, water will first flow into the micropores. When the maximal amount taken up by micropores is reached, the excess flows into macropores. The exchange of water between both domains, $S_w * \Delta z$, where Δz is the layer thickness, is treated as an approximated first-order process, neglecting the influence of gravity and assuming rectangular slab geometry for aggregates:

$$S_w = \left(\frac{3 D_w \gamma_w}{d^2}\right)(\theta_b - \theta_{mi}) \tag{3.46}$$

with: d : diffusion path length,
D_w : effective water diffusivity,
γ_w : scaling factor (=0.8 in average),
θ_b : liquid water content when micropores are full and macropores empty,
θ_{mi} : liquid water content in micropores.

The effective water diffusivity D_w is given by:

$$D_w = \left(\frac{D_{\theta_b} + D_{\theta_{mi}}}{2}\right)\frac{\theta_{ma}}{(\theta_s - \theta_b)} \tag{3.47}$$

with: D_{θ_b} : water diffusivity at the boundary water content θ_b,
$D_{\theta_{mi}}$: water diffusivity at the current micropore water content,
θ_{ma} : liquid water content in macropores,
θ_s : liquid water content at saturation.

Finally, in the Mualem/Brooks and Corey model, $_{\theta_{mi}}$ is given by:

$$D_{\theta_{mi}} = \frac{K_b \psi_b S_{mi}^{n_t + I/\lambda + I}}{\lambda(\theta_b - \theta_r)} \tag{3.48}$$

where

$$S_{mi} = \frac{\theta_{mi} - \theta_r}{\theta_b - \theta_r} \tag{3.49}$$

with: K_b : maximal hydraulic conductivity in the micropore,
I : parameter =1,
λ : Brooks and Corey pore size distribution index,
θ_r : residual liquid water content,
n_t : parameter accounting for pore correlation and flow path tortuosity (see eq. 3.7).

In the macropores, flow is assumed to be gravitational, i.e. soil pressure is not taken into account. The relation between soil pressure and water content is therefore not necessary. The hydraulic conductivity K_{ma} is given by (when no swelling is accounted for):

$$K_{ma} = (k_{sat} - K_b) S_{ma}^{p} \tag{3.50}$$

with: k_{sat} : saturated hydraulic conductivity,
S_{ma} : macropore saturation, varying between zero (empty) and one

(full),

p : parameter.

In the micropores, flow depends on the gravity and the soil pressure gradient. The soil water retention is calculated using the Brooks and Corey relation (eq. 3.4) and the hydraulic conductivity is given by Mualem relation, (eq. 3.7). Richards equation is used to calculate water flux (eq. 3.1).

3.4. THE FEFLOW MODEL

The FEFLOW model (Diersch 1996) was developed to simulate (a) water circulation in a saturated and unsaturated medium, (b) contaminant mass processes, and (c) heat transport processes. The model may be used in two or three dimensions and simulates the water flow for complex hydrogeological situations in an either transitory or steady state. The finite element method (FEM) is used to solve the governing balance equations.

For an unsaturated flow process, the mass conservation equation of a fluid is given by (see also eq. 3.1)[1]:

$$S_0 s(\psi)\frac{\partial}{\partial t}\psi + \varepsilon\frac{\partial}{\partial t}s(\psi) + \nabla \boldsymbol{q}_D = s_w \qquad (3.51)$$

with: S_0 : specific storage coefficient,
s : saturation (eq. 3.5),
ψ : liquid water pressure head,
ε : porosity,
$\boldsymbol{q}_D$: Darcy flux (eq. 2.6) (expressed as a vector),
s_w : Specific mass supply.

The constitutive relationships (required to solve eq. 3.51) for the saturation s as a function of the pressure ψ and for the relative hydraulic conductivity k_w (in the Darcy equation, see eq. 2.6) as a function of the pressure head ψ are given by van Genuchten, Brooks and Corey and Mualem models (eq. 3.3 to eq. 3.7).

FEFLOW does not include any phase changes. It is therefore not possible to simulate soil frost, or sub-freezing temperature. This problem may theoretically be bypassed by including a material conductivity evolution scenario, which assigns different material distribution to specified time entries. If soil frost evolution at a specific location is known, this information is integrated in the model by specifying the conductivity of the material at different times. The knowledge of heat transport processes is hence no more necessary and the problem can be treated as a flow transport problem only. However, from several tests, computing time has become very expensive, and this type of procedure was not applied.

Different types of boundary conditions may be prescribed on the outer or inner position of the domain. We find the usual Dirichlet (pressure head ψ is specified) and Neumann (water flow $\boldsymbol{q}$ is specified) conditions, as well as the Cauchy type (i.e. different transfer conditions can be put in to distinguish between inflowing and outflowing conditions) and single well-type conditions (singular point source). These boundary conditions may be constrained if they are

1. This equation is expressed in vector form. In this chapter all symbols are scalar except the water flow $\boldsymbol{q}_D$, $\boldsymbol{q}$ and the relative hydraulic conductivity k_w.

only valid as long as minimum and maximum bounds are satisfied. An application of constraint conditions refers, for example, to the case when parts of the aquifer become dry (water-table falls below the aquifer base).

Finally, the mesh generator (in two dimensions) can produce triangular or quadrilateral finite elements, allowing to reproduce thin geological elements in a satisfactory way . For a particularly complex geology, an additional mesh generator, T_Mesh, may be used (Ferrer 2000).

4. SITE CHARACTERIZATION

4.1. SITE CHOICE

The two experimental sites had to be representative for typical Alpine regions. The scientific criteria were constrained by technical criteria, as field work could only take place if safety and accessibility were guaranteed all year round and infrastructure, like electrical supply or road access in summer was available. Other aspects, such as previous research or available meteorological data were also taken into account. The different factors influencing this choice are listed below. The selected sites were Gd St Bernard (2500 m) and Hannigalp above Grächen (2090 m), both located in the southern Swiss Alps (Figure 4.1).

Regional differences

As stated above, the different sites had to be representative for typical Alpine regions. The two sites differ markedly in their meteorological characteristics. The most important discrepancies are the yearly precipitation, the air temperature, and the wind velocity. The yearly average air temperature at Hannigalp is 0.4°C (time period 1901-1960) and -1.6°C at Gd St Bernard. The Hannigalp site is located between two main alpine ranges and is protected from northern and southern meteorological influences. The annual precipitation is therefore only 512 mm per year. In contrast, at Gd St Bernard, due to its location on a pass, the precipitation is high (average 2099 mm/year). The site is also characterized by strong wind, blowing at an average of approximately 6 m/s. Wind peaks of 30 m/s are not unusual at Gd St Bernard, whereas strong winds hardly ever occur at Hannigalp (average 2 m/s).

Proximity to a meteorological station

The presence of a meteorological station was of central importance to be able to study long-term climatic effects. Unfortunately, not many stations are encountered at altitudes above 1800 m in the Alps and therefore the choice of sites was limited. A meteorological station of the Swiss Metrological Institute (SMA) measuring temperature, precipitation, wind velocity, and solar radiation every hour is located at the Gd St Bernard pass. For Hannigalp, hourly meteorological data including air temperature, precipitation, and snow depth were taken from an SMA station located at Grächen (1600 m), some 500 m below the experimental site.

Altitude

To study the effect of the snowmelt on an alpine ground water, a site location above 1800 m was required. Indeed, at such altitudes winter lasts at least for 6 months per year, i.e. from November to May, and during that period almost only snow precipitation is encountered.

Nature of the soil

The nature of the soil cover (i.e. the layer above the bedrock) was an important pre-requisite to this study. Above 2600 m hardly any soil is encountered and such regions could not be considered for this study. Also the soil had to be relatively deep (i.e. > 60 cm) to be able to measure the different snowmelt discharge flux. Finding such type of soil showed itself to be tricky especially at Gd St Bernard, where the bedrock is very close to the surface.

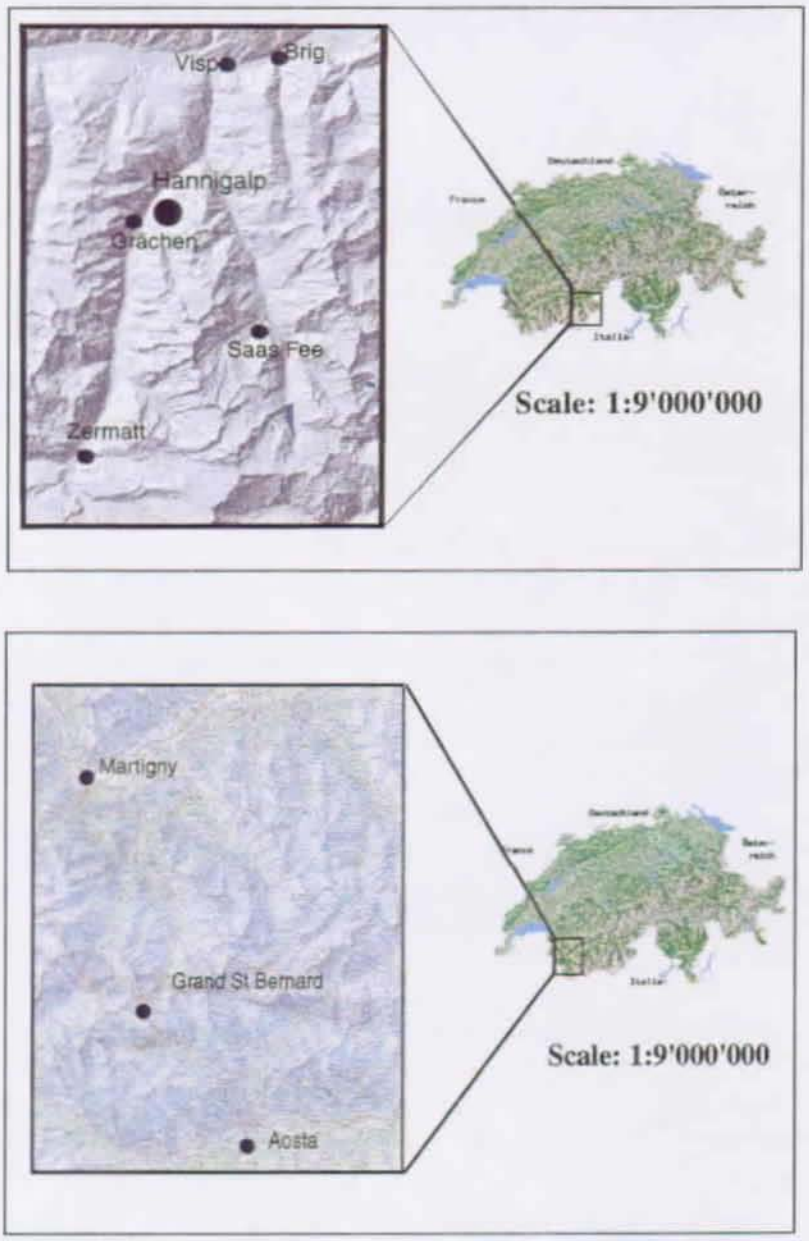

Figure 4.1: Location of the two experimental sites in the Swiss Alps.

Access

Mechanical access in winter is limited and mostly restricted to ski areas. The Hannigalp is situated next to a ski area and insofar, easy to reach under bad weather condition. The Gd St Bernard experimental site is located on the Gd St Bernard pass between Martigny (Switzerland) and Aosta (Italy). Two walking hours are necessary to reach the pass in winter. The site is close to the Gd St Bernard monastery, which is open all year around.

Avalanches (safety)

The experimental sites had to be located on slopes where avalanche danger was low. As

Hannigalp is surrounded by a forest, protection was guaranteed. In contrast, sites at Gd St Bernard were exposed to avalanches as slopes on both sides of the pass exceed 35°. It was therefore difficult to find safe experimental sites. Of the four experimental sites initially installed, two were affected by avalanches during both winters while one was definitely damaged and lost at the onset of winter 2000/2001.

Infrastructure

To run continuous measurements and to avoid frost formation in the experimental setup, the experimental plot had to be located close to an existing electrical supply. At Gd St Bernard, the electricity was taken from the monastery, while it was provided from a ski lift at Hannigalp. To install experimental apparatus in summer, road accessibility was necessary.

Previous hydrogeological studies

As our interest focused on the coupling of snowmelt processes with the groundwater recharge, previous hydrogeological studies were desirable. A listing of previous studies at Hannigalp is provided in the previous chapter, whereas no hydrological research on the Gd St Bernard is known to the author.

4.2. SITE DESCRIPTION AND PHYSICAL PROPERTIES

4.2.1. HANNIGALP

The site is located next to the Stafelwald, at an altitude of 2090 m (46°12'; 7° 52') (Swiss nat. coord. 632'500/117'100). It is surrounded by a coniferous forest, some 100 m below the tree limit, next to a ski lift and protected from external interference by a 150 m^2 wire fence. The site has an average slope of approximately 23% with east exposure. It belongs to a slope ranging from 2600 m down to 1600 m and having an average gradient of 30%. (Figure 4.2)

The soil (i.e. the layer above the substratum) is a sandy loam (Table 4.1) classified as ferric podzol. The soil is 50-70 cm thick, made up of an organic layer (5 cm), a reddish-brown horizon (20 cm) and a dark black horizon (40 cm) (Photo 4.1). An old till constitutes the substratum (approx. 5-10 m thick). From Parriaux and Nicoud (1988), the saturated conductivity is estimated between 10^{-5} m/s and 5 10^{-4} m/s. Below the till, the rock is formed by gneiss and schift from Michabel-Kristallin.

No stones (diameter $\Phi > 20$ cm) are found in the first 50 cm of soil. Roots are encountered to a depth of 50 cm, with a major fraction in the first 20 cm. The vegetation is rhododendron (*Ericaceae*) and grass (Photo 4.2). Rhododendron is inhomogeneously distributed on the experimental sites.

From Porchet infiltration tests (Audry et al. 1973, see also Appendix A), the soil hydraulic conductivity at saturation was estimated at 3 10^{-5} m/s between a depth of 20 and 50 cm. In the upper 20 cm, estimation varied between 10^{-4} m/s and10^{-3} m/s.

Measurements of the soil water characteristics were carried out in the laboratory on removed soil profiles (unaltered 10 cm deep soil columns were removed *in situ* using plastic cylinders in order to not disturb the soil strucutre), using a pressure plate device (Musy and Soutter 1991).

Figure 4.2: Location of the experimental site of Hannigalp (Swiss National Map, 1/25 000, with the authorization of the Swiss Federal Office of Topography (BA034924)).

The water retention curve obtained as well as the Van Genuchten (1980) and Brooks & Corey (1964) parameters are shown in Table 4.2 and Table 4.3

The soil freezing curve is shown in Figure 4.3 for the reddish-brown horizon (10 cm depth). A sharp decrease is noted between a soil temperature of -0.23°C and -0.5°C. At -0.7°C the volumetric liquid water content is approximately 5%. This value does not change markedly by further decreasing the soil temperature (Figure 4.3). Finally, from sorption-desorption experiments, the soil shows a strong hysteresis effect. At a depth of 5 cm, differences between the sorption and desorption curve is 50pF (Figure 4.3), while it decrease at 0.5pF at a depth of 20 cm. We may note that such type of behaviour is typical for a hydrophobic soil and will be further developed in Chapter 8.

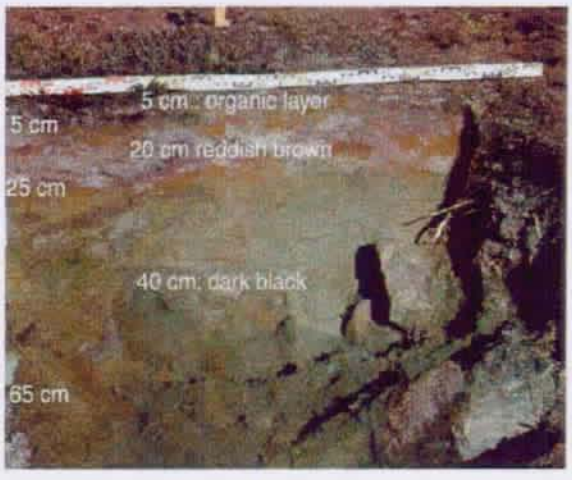

Photo 4.1: The soil profile at Hannigalp is made up of a 5 cm organic layer, followed by reddish -brown horizon (20 cm) a dark black horizon (40cm).

Horizon	*Sand content (%) 50μm<Φ<2mm*	*Loam content (%) 2μm<Φ<50μm*	*Clay content (%) Φ< 2μm*	*Saturated hydr. cond. (m/s)*	*Bulk density (g/cm3)*
5-15 cm	63.20	30.40	6.50		1.09
15-25 cm	60.55	33.65	5.85		1.12
25-35 cm	57.90	36.90	5.20	$3\ 10^{-5}$	1.12

Table 4.1: Soil physical characteristics of the ferric podzol at Hannigalp.

4.2.2. GD ST BERNARD

The main site (called south plot) at Gd St Bernard is located at 2500 m (45°52';7°10') (Swiss nat. coord. 579'250/79'800), 30 m above the Gd St Bernard monastery on the northwest. The site orientation is south and the mean slope is approx. 65%. The site is on the lower part of a slope ranging from 2600 m down to the pass at 2470 m. It is occasionally covered by avalanches. The second site (called north plot) is located 250 m southeast of the monastery, close to the Gd St Bernard lake at an altitude of 2480 m (Swiss nat. coord. 579'125/79'625). The orientation is northwest and the slope is 58%. It is located at the bottom of a steep slope (75%) and mostly covered by small avalanches in spring. The last site (called east plot) is found in Italy at 2420 m, some 100 m above the pass road on the east of the «Petite Chenalette» (Swiss. nat. coord. 79'900/578'050). The exposition is east and the mean slope is approx. 63%. It is on the top of a 100 m long slope (65%) and is not exposed to avalanches. All sites are located approx. 600 m above the tree line (Figure 4.4).

The soil physical properties were determined for the main site only (10 cm deep soil columns were removed *in situ* using plastic cylinders). Nevertheless it is feasible that the same properties are valid for the secondary sites. The soil texture is similar to the one of the Hannigalp site (sandy loam) (Table 4.4) and classified as ranker/ rhegosol. The soil, however, differs markedly from the Hannigalp soil, due to the presence of large slate stones (diameter Φ>5 cm) at all

Photo 4.2: View of Hannigalp experimental site.

Depth	m[-]	n [-]	α [-]	θ_s *(% vol.)*	θ_r *(% vol.)*	θ_{wilt} *(% vol.)*
0-10 cm	0.265	1.36	0.02	55.1	2	8
10-20 cm	0.187	1.23	0.03	54.1	2	13
20-30 cm	0.231	1.3	0.035	50.8	2	8

Table 4.2: Van Genuchten parameters for soil water characteristics at Hannigalp (eq. 3.3) and wilting point θ_{wilt}. The wilting point θ_{wilt} is given by a soil water pressure of 4.2 pF (eq. 3.24).

Depth	λ [-]	ψ_a [cm]	θ_s *(% vol.)*	θ_r *(% vol.)*	θ_{wilt} *(% vol.)*
0-10 cm	0.36	30	55.1	2	7.5
10-20 cm	0.3	25	54.1	2	7
20-30 cm	0.3	20	50.8	2	6.5

Table 4.3: Brooks & Corey parameters for soil water characteristics at Hannigalp (eq. 3.4) and wilting point θ_{wilt}. The wilting point θ_{wilt} is given by a soil water pressure of 4.2 pF (eq. 3.24).

depths in the soil. Gneiss constitutes the underground. Soil thickness varies between 40 cm and 80 cm. It is composed of 5 cm thick organic layer overlying the 50 cm deep mineral soil.

The vegetation is grass (Photo 4.3) homogeneously distributed on the experimental sites. Roots are encountered to a depth of approx. 60 cm, but mainly in the upper 30 cm.

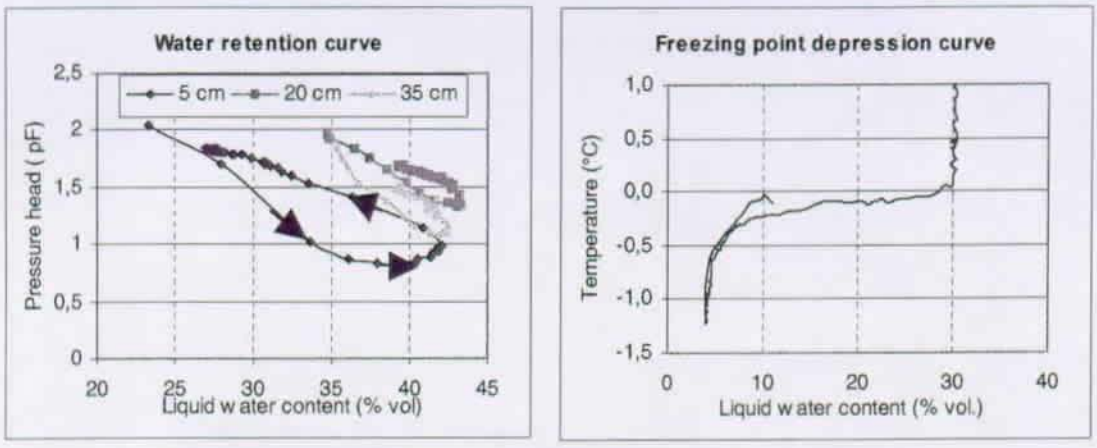

Figure 4.3: Soil water characteristics and freezing point depression curve at Hannigalp based on column measurements.

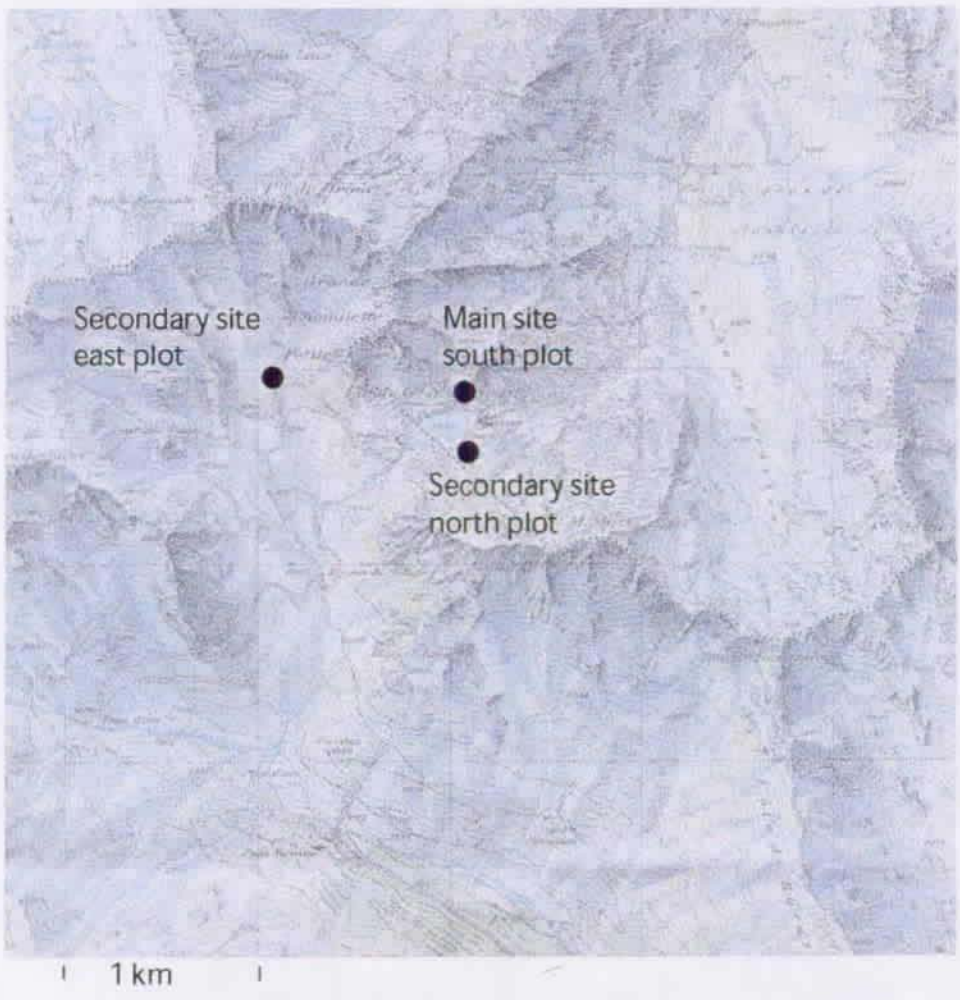

Figure 4.4: Location of the main site and the two secondary sites at Gd St Bernard (Swiss National Map, 1/25 000, with the authorization of the Swiss Federal Office of Topography (BA034924))

Horizon	Sand content (%) $50\mu m<\Phi<2mm$	Loam content (%) $2\mu m<\Phi<50\mu m$	Clay content (%) $\Phi<2\mu m$	Saturated hydr. cond. (m/s)	Bulk density (g/cm^3)
0-7 cm	53.50	38.10	8.40		0.64
7-15 cm	48.80	40.85	10.35	$5\ 10^{-5}$	0.90
15-25 cm	44.10	43.60	12.30	$5\ 10^{-5}$	0.90

Table 4.4: Soil physical characteristics of ranker/rhegosol at Gd St Bernard.

Photo 4.3: View of Gd St Bernard experimental site.

The saturated hydraulic conductivity of the soil layer 15-25 cm (approximately $5\ 10^{-5}$ m/s) was determined with the Porchet test (Appendix A).

Water retention curves were obtained similarly to the ones of Hannigalp by using a pressure plate device. Results are shown in Table 4.5 (Van Genuchten parameters) and Table 4.6

Depth	m	n	α	θ_s (% vol.)	θ_r (% vol.)	θ_{wilt} (% vol.)
0-7 cm	0.231	1.3	0.024	73	4	14
7-15 cm	0.286	1.4	0.029	59	4	8
15-25cm	0.275	1.38	0.035	57	4	8

Table 4.5: Van Genuchten parameters for soil water characteristics at Gd St Bernard and wilting point θ_{wilt}.

(Brooks and Corey parameter). We may note the high porosity value of the organic layer (73%).

No freezing curve was determined, as on the one hand, *in situ* measurements were too seldom (once per month) to be able to monitor accurately the freezing process and, on the other hand, no laboratory freezing experiments were carried out. In fact it was not possible to remove an

Depth	λ	ψ_a *(cm)*	θ_s *(% vol.)*	θ_r *(% vol.)*	θ_{wilt} *(% vol.)*
0-7 cm	0.25	25	73.5	4	14
7-15 cm	0.25	15	59.5	4	8
15-25 cm	0.22	10	57	4	8

Table 4.6: Brooks & Corey parameters for soil water characteristics at Gd St Bernard, and wilting point θ_{wilt}.

intact 50 cm deep soil column from the experimental site, as large stones were present in the soil.

4.3. INSTRUMENTATION

4.3.1. HANNIGALP

In Figure 4.5, a schematic description of the instrumental setup is shown. To measure the water flow, two different plots were installed (called lysimeter plot and lateral runoff plot in Figure 4.5). The lateral runoff plot was 2 m wide with an average downslope length of 3 m. Surface and subsurface runoff was collected at the lower end, using two gutters for each flow. The lysimeter plot had an area of 0.63 m^2 and was used to collect the deep percolation. The two plots were isolated from external water inflow by two drains, located on the top of both plots. These drains were 50 cm deep, having a plastic underground filled up with sand and gravel.

Surface runoff was collected down to a depth of 0 and 3 cm, while subsurface flow was measured between 3 and 28 cm. The collecting containers were filled up with gravel and sand to allow water to drain to the two collecting gutters. This filling allowed water to flow under unsaturated condition. It diminished the capillary barrier between the soil and the collecting device (Ross 1990). The gutters were equipped with heating wires to prevent water from freezing inside the gutters (Figure 4.6).

Deep percolation was collected using an open lysimeter (surface 0.525 m^2) (Thompson and Scharf 1994 or Haines et al. 1982). The bottom and outflow of the lysimeter was built with a metallic sheet, 70 cm wide and 90 cm long, located 40 cm under the soil. The connection between soil and lysimeter was made of gravel and sand. This filling allowed hydrological connection between soil and lysimeter and maintained the water circulation under unsaturated condition (Figure 4.7).

During winter 2000/2001, most of the measurements were carried out manually. Improvement took place during the second measurement period by collecting data automatically. The differences between both winters are listed in Table 4.7.

During winter 2000/2001, the discharge was measured using sampling containers. These containers were emptied once per day during the snowmelt period. During the second winter, the water flow was collected automatically every 10 minutes, using a 100 ml tipping bucket.

All soil physical measurements were carried out between the south and the central plot. During winter 2000/2001, the soil temperature was monitored hourly with thermistors (Grandt CT-K-W5-3) using a Grant Data logger. The unfrozen water content was measured manually using

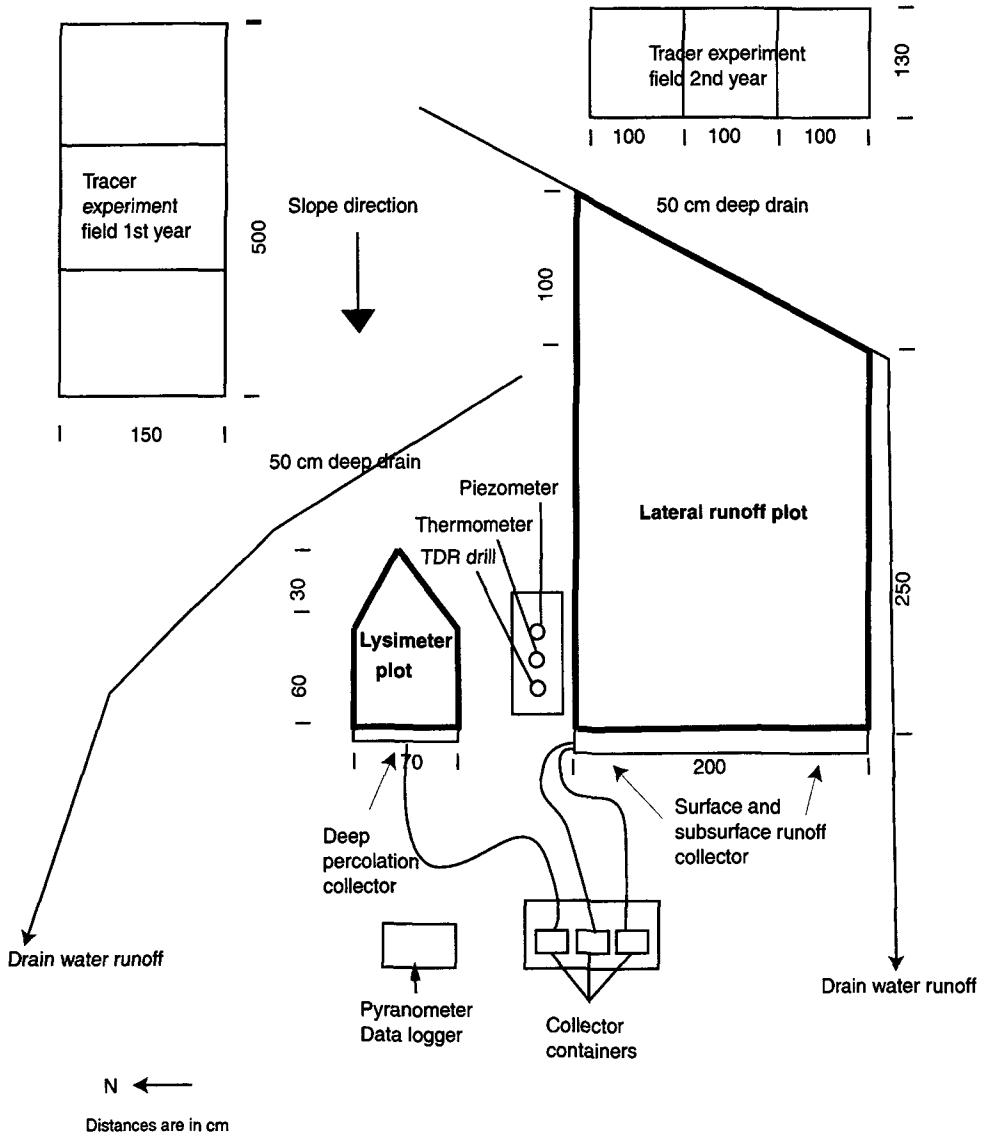

Figure 4.5: Aerial overview of the experimental site of Hannigalp.

TDR probes (time domain reflectometry) connected to a tektronix cable tester. This technique is widely used to monitor unfrozen water content in frozen and unfrozen soils (Stein and Douglas 1983). The water content was determined by applying the mixing model of Topp et al. (1980). During the snowmelt period, the manual measurements were taken daily, otherwise the measurements interval was two weeks. The thermistors and the TDR probes were installed horizontally at a depth of 5, 10, 15, 20, 30 and 40 cm. The TDR probes had a rod length of 15 cm. A piezometer was installed to detect the possible presence of a perched aquifer. The piezometer depth was 50 cm. During winter 2001/2002, the soil temperature and the water content were monitored using two sets of four probes located at 5, 10, 20 and 30 cm depths. Monitoring was hourly using multiplexers and a Campbell data logger system. The TDR signals were smoothed by making a Fourier transformation and cutting off the noise frequencies (Schneebeli et al. 1995). In addition, a third set of soil temperature was measured at the same location as the previous year.

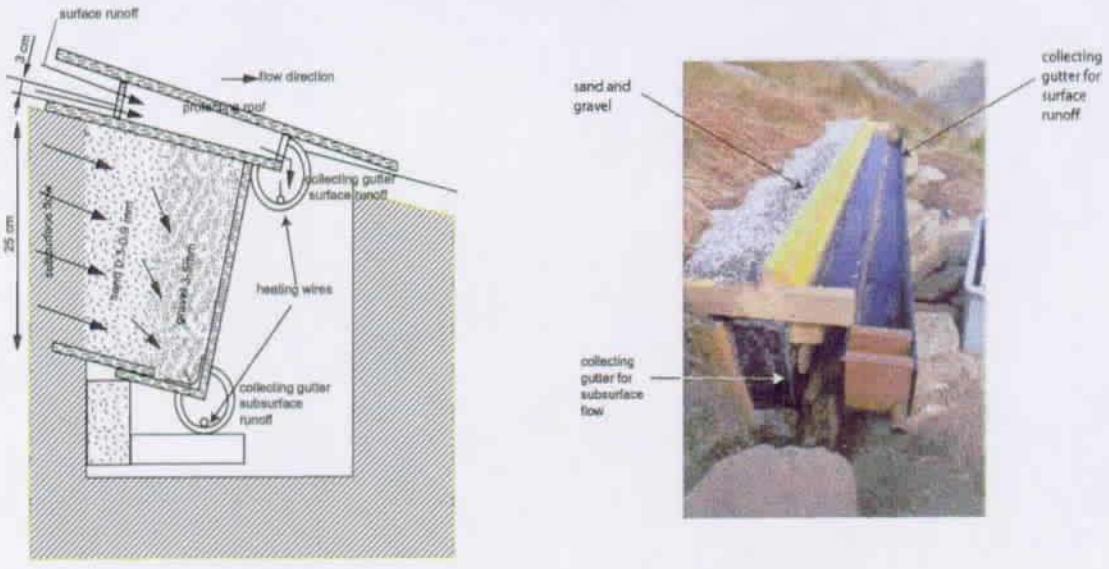

Figure 4.6: On the left, schematic instrumental setup for collecting surface and subsurface lateral runoff. On the right, picture of a collecting gutter for surface runoff. The surface water flows into the gravel, which allows excess runoff to be drained unhindered to the collecting gutter. To prevent from freezing, heating wires were installed in the collecting gutters.

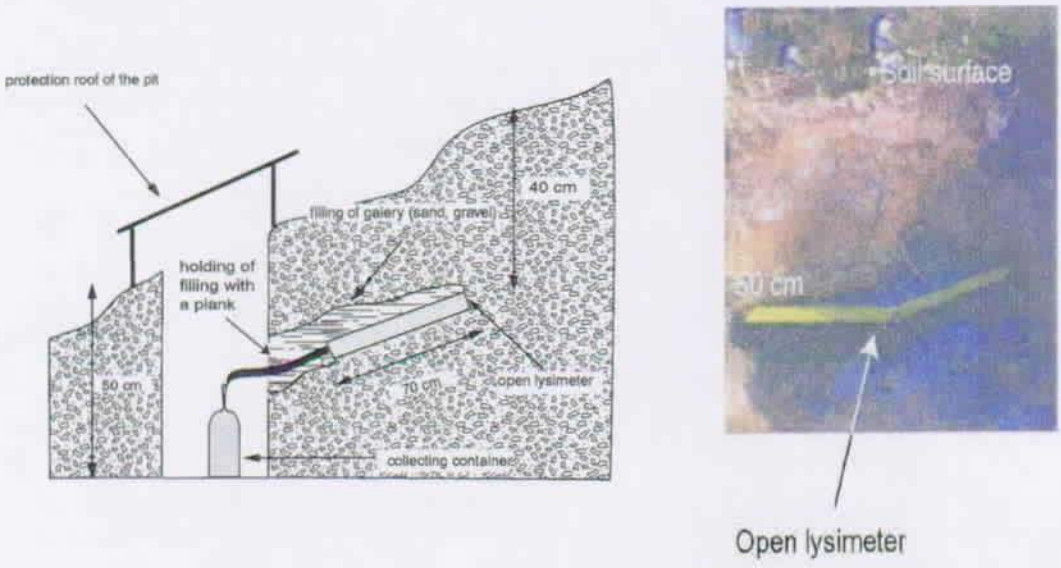

Figure 4.7: On the left, schematic setup of an open lysimeter. A plank covered with plastic sheet held back the sand and the gravel at the outlet of the lysimeter (not shown). On the right, front view of the open lysimeter.

Hourly short wave radiation was measured using a pyranometer sensor (waveband 300 nm to

Measure	*Winter*	*Depth (cm)*	*Sampling*
Surface runoff	2000/2001	0-3	Manual
	2001/2002	0-3	Automatic
Subsurface runoff	2000/2001	3-28	Manual
	2001/2002	3-28	Automatic
Percolation	2000/2001	40	Manual
	2001/2002	40	Automatic
Soil temperature	2000/2001	5,10,15,20,30,40	Automatic
	2001/2002	5,10,20,30 5,10,20,30 5,10,15,20,30,40	Automatic
Unfrozen soil water content	2000/2001	5,10,15,20, 30,40	Manual
	2001/2002	5, 10, 20, 30 5, 10, 20, 30	Automatic
Groundwater table	2000/2001	50	Manual
	2001/2002	50	Manual
Snow depth	2000/2001		Manual
	2001/2002		Manual
Global radiation	2000/2001		Automatic
	2001/2002		Automatic

Table 4.7: Instrumental setup during winter 2000/2001 and 2001/2002 at Hannigalp.

3000 nm) (SKS 110-Silicon Cell Pyranometer- Grand). Finally the snow depth was monitored manually approx. every day during snowmelt and once per week otherwise during both years.

4.3.2. GD ST BERNARD

During both years, only manual measurements were carried out at Gd St Bernard on the main and the secondary sites. On the secondary sites, instrumentation was reduced and measurements were less frequent than on the main site. Differences are listed on Table 4.8.

Measure	*Site*	*Depth (cm)*	*Sampling*
Surface runoff	Main site	0-3	Yes
	Secondary site		No
Subsurface runoff	Main site	3-28	Yes
	Secondary site		No
Deep percolation	Main site	40	Yes
	Secondary site		No
Soil temperature	Main site	5,10,20,30,40	Yes
	Secondary site	5,10,20,30	Yes
Unfrozen water content	Main site	5,15,20, 30,40	Yes
	Secondary site	5, 10, 20, 30	Yes
Groundwater table	Main site	50	Yes
	Secondary site		No
Snow depth	Main site		Yes
	Secondary site		Yes

Table 4.8: Instrumental setup at Gd St Bernard main site and secondary sites.

4.3.2.1. MAIN SITE

The experimental configuration is similar to the one at Hannigalp (Photo 4.6 and Photo 4.7). A sketch of the instrumental setup is shown in Figure 4.8. The lysimeter plot has an area of 0.63

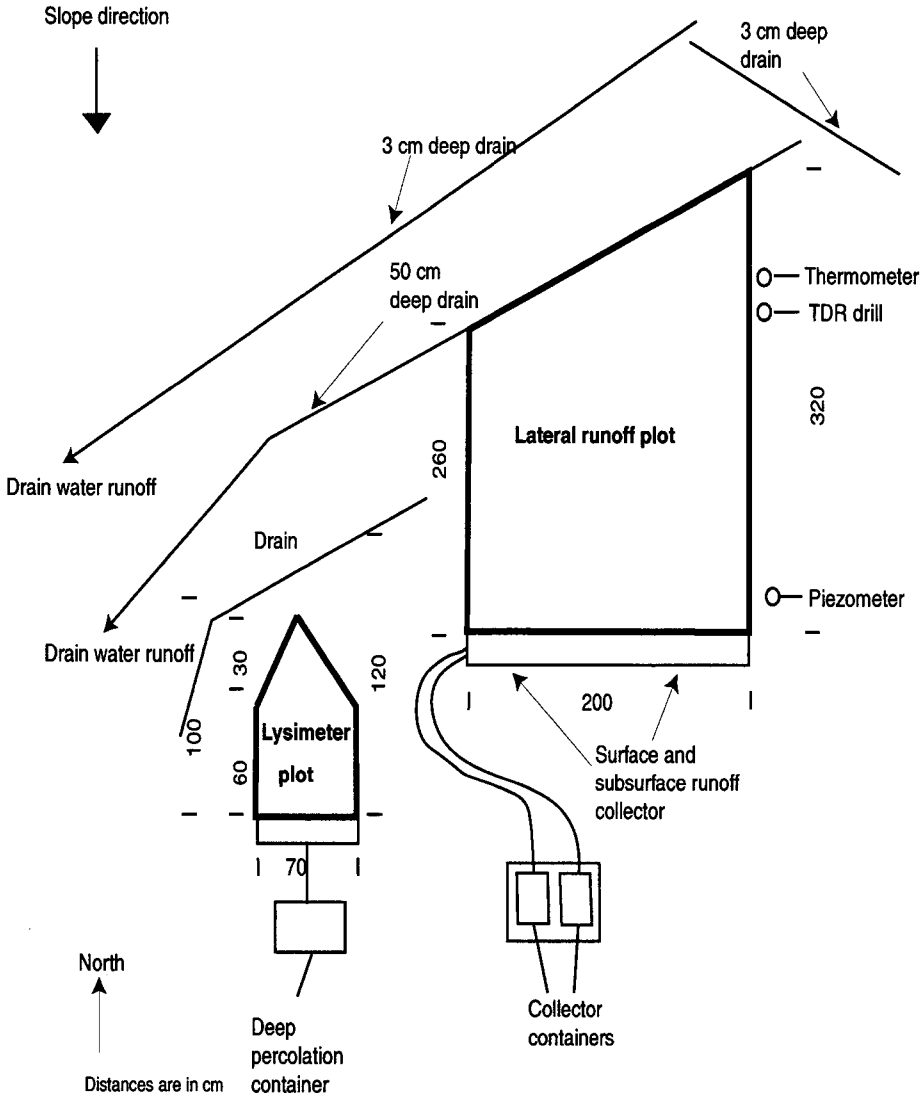

Figure 4.8: Aerial overview of the experimental site of Gd St Bernard.

m^2 and the lateral runoff plot 5.80 m^2. All measurements were manual, as providing a safe place to set up the measurements device was difficult. In particular, to avoid avalanche destruction, all devices were buried into the ground. This induced some technical problems as the electrical supply box was sometimes in contact with snow, creating short cuts. Two cables were additionally installed to hold the surface and subsurface gutter against snow movements at the soil surface (2-3 cm per month).

The soil temperature and the liquid water content were monitored at a depth of 5, 10, 20, 30 and 40 cm. During the snowmelt period, daily measurements were taken, while measurements

frequency was reduced to once every two weeks during winter 2000/2001 and once per month the next winter. Snow depth measurements were taken approx. every two days by people from the monastery.

The global radiation was measured at the Gd St Bernard SMA meteorological station.

4.3.2.2. SECONDARY SITES

As access to the sites was time-consuming, measurements were sporadic and limited to once every two days during snowmelt. Instrumentation was kept little and reduced to the snow depth, the soil temperature, and the liquid water content at four different depths, i.e. 5, 10, 20 and 30 cm. No water flow was measured.

5. METEOROLOGICAL ANALYSIS

5.1. INTRODUCTION

Although Grächen and Gd St Bernard are at a distance of only 80 km from each other, the two regions are characterized by very different microclimates. Grächen is located between two main alpine ranges (the Bernese Alps and the Pennine Alps) and is one of the driest regions in Switzerland. Gd St Bernard is situated on the Pennine Alps, southwest of Grächen. In that area, Atlantic depressions are more active and precipitation is high, approx. four times higher as in Grächen.

This chapter is divided into three parts. First, we discuss the representativeness in comparison with the Alpine climate of the two chosen sites. Then, we examine how the climate has varied during the last 30 years at Grächen and the last 60 years at Gd St Bernard. Finally, we will analyse the meteorological condition of winters 2000/2001 and 2001/2002.

All data are provided by the Swiss Meteorological Institute (SMA). The meteorological measurements have been run since 1934 at Gd St Bernard and since 1966 at Grächen. The SMA station of Gd St Bernard is located at 2469 m (Swiss nat. coordinate 579'200/79'720) and the one of Grächen at 1617 m (Swiss nat. coordinate 630'860/116'050).

5.2. REPRESENTATIVENESS OF THE CHOSEN SITES

The climate of the Swiss Alps falls into four main parts (Figure 5.1). The northern Alps are

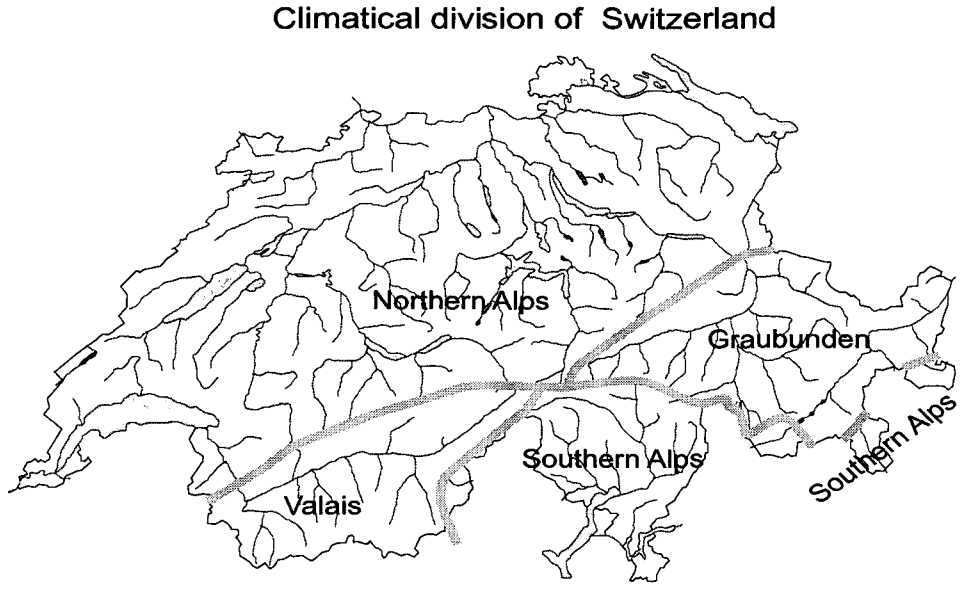

Figure 5.1: Climatic sub-division of the Swiss Alps. The Valais and the Graubünden are characterized by a similar climate.

affected mainly by Atlantic depressions, while depressions coming from the Mediterranean Sea

influence the Southern Alps. Graubünden and the Valais enjoy a similar climate due to their location between two main Alpine ranges. The Valais is protected by the Bernese and the Pennine Alps. It is less affected by depression than other parts of Switzerland and is therefore much drier.

Forty-three climate stations from the MeteoSwiss (SMA) record meteorological parameters, such as air temperature and precipitation, all over the Valais. A detailed classification into four different climatic zones was therefore possible (Figure 5.2). The western part of the Valais is

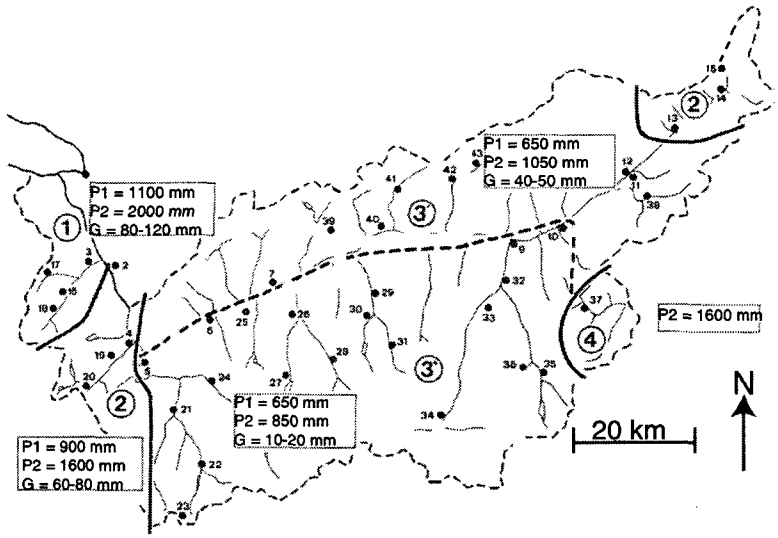

Figure 5.2: Location of the forty-three climate stations in the Valais, as well as the four different climatic zones of the Valais, characterized by the approximate precipitation at 500 m (P1) and at 1500 m (P2), by the increase in precipitation per 100 m (G) and by the annual precipitation distribution, from Werner (1994).

humid and climatically similar to the northern Alps. The climate becomes drier towards the east. The central Valais (zone three in Figure 5.2) is the driest part and may be defined as the «Valais climate» (Figure 5.1). The climate becomes wetter at the eastern end of the Valais. Zone four in Figure 5.2 is located on the southern side of the Pennine Alps and has the climate of the Southern Alps.

Precipitation increases with altitude. In the eastern part of the Valais, this increase is lower. In the valley of Zermatt, where Grächen is located, hardly any increase is measured up to an altitude of 1500 m (Figure 5.2). Above 1500 m, the increase is more pronounced in all regions.

Hannigalp is typical for the «Valais climate». Low precipitation (512 mm/year at Grächen) and low increase of humidity with higher altitude (10-20 mm/100 m). Such climates are encountered in other parts of the Alps, in particular in deep, well-protected, internal valleys, such as the Engadine valley in Switzerland or the Maurienne valley in France. Gd St Bernard is located at the edge of region two and three. The precipitation is high (2100 mm/year) and the climate very much contrasts with the one at Hannigalp. Northwest depressions influence the Gd St Bernard region, even if precipitation is lower than in regions located to the west. During winter with

strong northwest influence, the Gd St Bernard area gets large amounts of snow. Gd St Bernard weather is also influenced by the southern climate (region four) due to its location on a pass (not shown in Figure 5.2) and is representative for such a climate. Winter 2000/2001 was a typical example. Considerable snowfall was recorded from the pass down to Italy, while at Super St Bernard some 7 km north of the pass, the snow depth remained shallow throughout the whole season (< 50 cm).

5.3. CLIMATIC EVOLUTION

5.3.1. GRÄCHEN (PERIOD 1967-2000)

An analysis of the evolution of different climatic parameters at Grächen during the last 36 years is given below.

The mean annual air temperature and the precipitation from 1964 to 2000 are shown in Figure 5.3. The air temperature increased by 2 °C since 1964 at an average rate of 0.06°C/year.

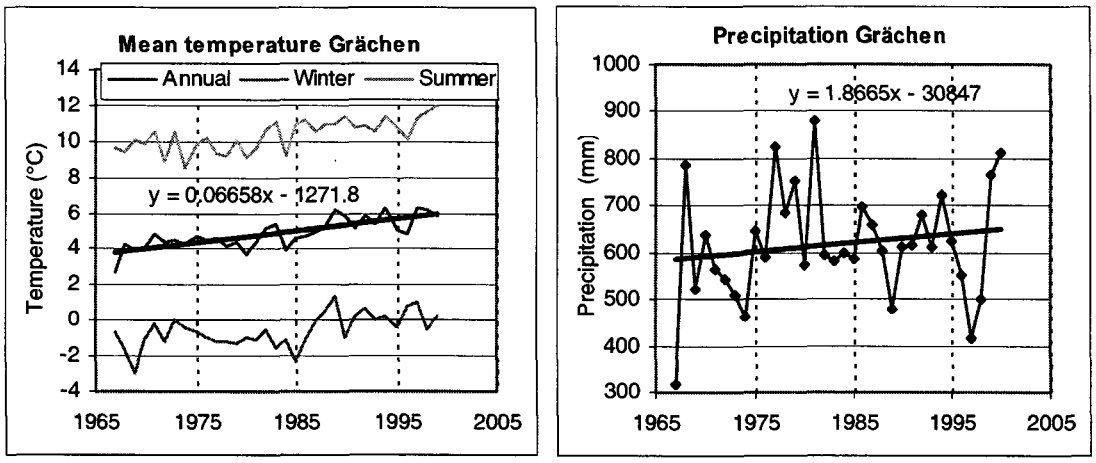

Figure 5.3: Mean annual, summer and winter temperature, and precipitation in Grächen from 1963 to 2001 including the trend line for annual values.

This is consistent with the current trends in alpine temperature change, as noted by Ohmura and al. (1998). The precipitation increased slightly at a rate of 1.8 mm/year, but this value may not be meaningful as annual precipitation variation is high. Over 36 years, it corresponds to 9% more rain, which is also coherent with current estimation (Widmann and Shär 1997). The increase in the air temperature affects in particular the annual number of snow days (i.e snow depth >10 cm) and the maximum snow depth. Winters are currently 30 days shorter than in 1967, while the maximum snow cover is 16 cm thinner. No clear trend was noted when the yearly number of snow precipitation days was analysed. The main reason was that the decrease due to a higher air temperature was balanced by the increase in the number of precipitation days. Finally, no change was observed in the wind and the relative humidity values. Heavy or stormy winds are rare at Grächen, on the average a speed of 1.5 m/s is measured, while the average relative humidity is 65%.

5.3.2. GD ST BERNARD (PERIOD 1934-2001)

The air temperature during the two observed winters was rather warm (-5.7°C and -5.1°C respectively as against -6.1°C on the average for the period of 1934-2000) and reflects the trend that has been observed over the last 65 years at the Gd St Bernard pass (Figure 5.4). Air

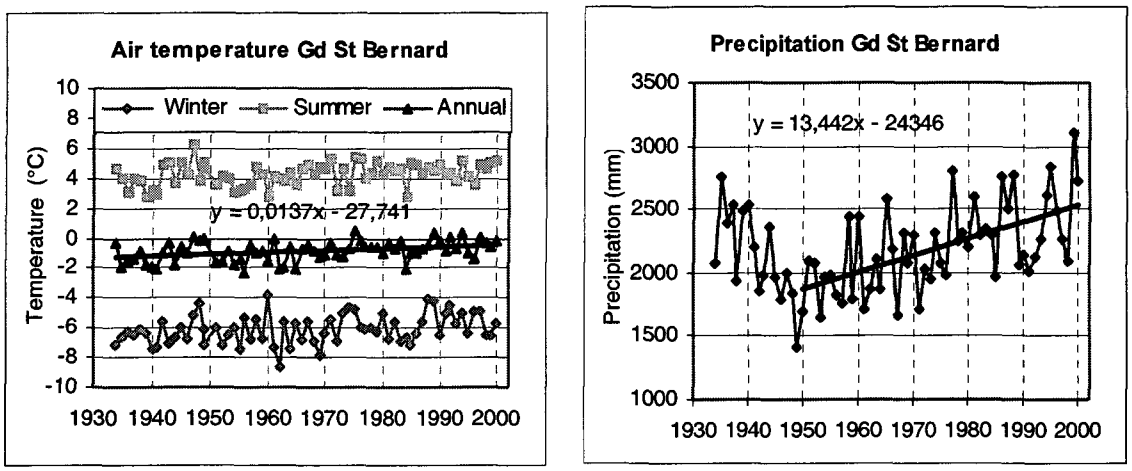

Figure 5.4: Mean annual, summer and winter temperature and precipitation at Gd St Bernard from 1934 to 2001, including the trend line for annual values.

temperature increased at a rate of 0.014°C a year during this period, which means a change of 0.9°C since 1934. This variation is four times lower than at Grächen. On the other hand, the mean annual precipitation increase is more pronounced at Gd St Bernard (approx. seven times higher) than at Grächen. Currently 35% more precipitation falls on the pass than 50 years ago, corresponding to an increase of 13 mm/year. However, this value is probably excessive. Indeed, the mean annual precipitation was more important during the years 1930 to 1945 than during the years 1950 to 1975. The low precipitation values from 1950 to 1975 may therefore be due to natural variation. No clear change could be observed in the wind speed (average 5.8 m/s) and the relative humidity values (average 75.8%). Strong winds are common at the pass and the average value is four times stronger than at Grächen. Gd St Bernard also experiences more bad weather than Grächen, which explains why the relative humidity is 10% higher at Gd St Bernard.

Due to the relative proximity to Grächen, the air temperature shows good correlation with the one observed at Grächen ($R^2 = 0.96$). The correlation with the precipitation is, however, lower (0.62), as, in contrast to Gd St Bernard, Grächen is little affected by southern depression.

5.4. METEOROLOGICAL ANALYSIS OF WINTER 2000/2001[1] AND 2001/2002

5.4.1. GRÄCHEN

A comparison between winter air temperature measurements at Hannigalp (October to June) and at Grächen SMA during winter 2000/2001 and 2001/2002 showed that the difference in air temperature between both sites was on the average 4.25°C, which corresponds to a lapse rate of 0.85°C/100m. This difference remained approx. constant during the entire measurement period. Hence, we used this lapse rate to estimate the air temperature at Hannigalp when no measurements were available.

In the following, the meteorological conditions and the snow depth evolution will be discussed for both locations at Grächen (1600 m) and at Hannigalp (2100 m).

In normal winters the daily mean air temperature in Grächen varies around 0°C in November. The coldest periods are encountered from December to February when temperatures are below 0°C. In March, the snowmelt takes place at Grächen and air temperatures are mostly above 0°C, but cold periods still exist. In April-May, cold periods become rare and temperatures are mostly above 4°C. This period corresponds to the snowmelt at Hannigalp.

Graphical displays of the air temperature evolution and the precipitation at Grächen for winter 2000/2001 and 2001/2002, as well as the snow depth at Grächen and Hannigalp during both measurement winters are shown in Figure 5.5.

5.4.1.1. WINTER 2000/2001

The heavy precipitation in October 2000 coincided with disastrous flooding in southern Switzerland and northern Italy. The air temperature was high and the snowfall limit was mostly above 2600 m. However, this event did not affect the measurements on the experimental site. No snow was recorded any more at Hannigalp a few days after the episode. But huge snow quantities fell in the region located above 2600 m, affecting the groundwater recharge at snowmelt. Heavy snow precipitation (104 mm as against 45 mm on the average) was recorded in November, resulting in a deep snowpack on both locations by the end of the month (60 cm were measured at Grächen). In January and February, the air temperature was mostly below 0°C at Grächen and the snow depth increased steadily on both sites. The final snowmelt took place in March at Grächen with variation in the daily air temperature between 3 and 10°C. At Hannigalp, the snowpack increased until mid-March. On 16th March a sharp warming in the air temperature created a first snowmelt event. At the beginning of April, a period of bad weather and low temperatures postponed the snowmelt until the end of April when the air temperature increased above 10°C and the final snowmelt started.

The snow depth at Grächen was unusually deep at the beginning of the winter. Precipitation remained above average during the entire winter with mean winter precipitation (November to April) being 6.5% higher than normal value (303.5 mm). As a result, the number of snow days, i.e. days with at least 10 cm of snow, was more than ordinary (119 instead of 105 days). In spite

1. The word "winter" followed by a specific time period (e.g. winter 2001/2002) goes from the first significant snow fall in autumn until the end of the snow cover period. This period may be much longer than the usual winter period (i.e. December- March).

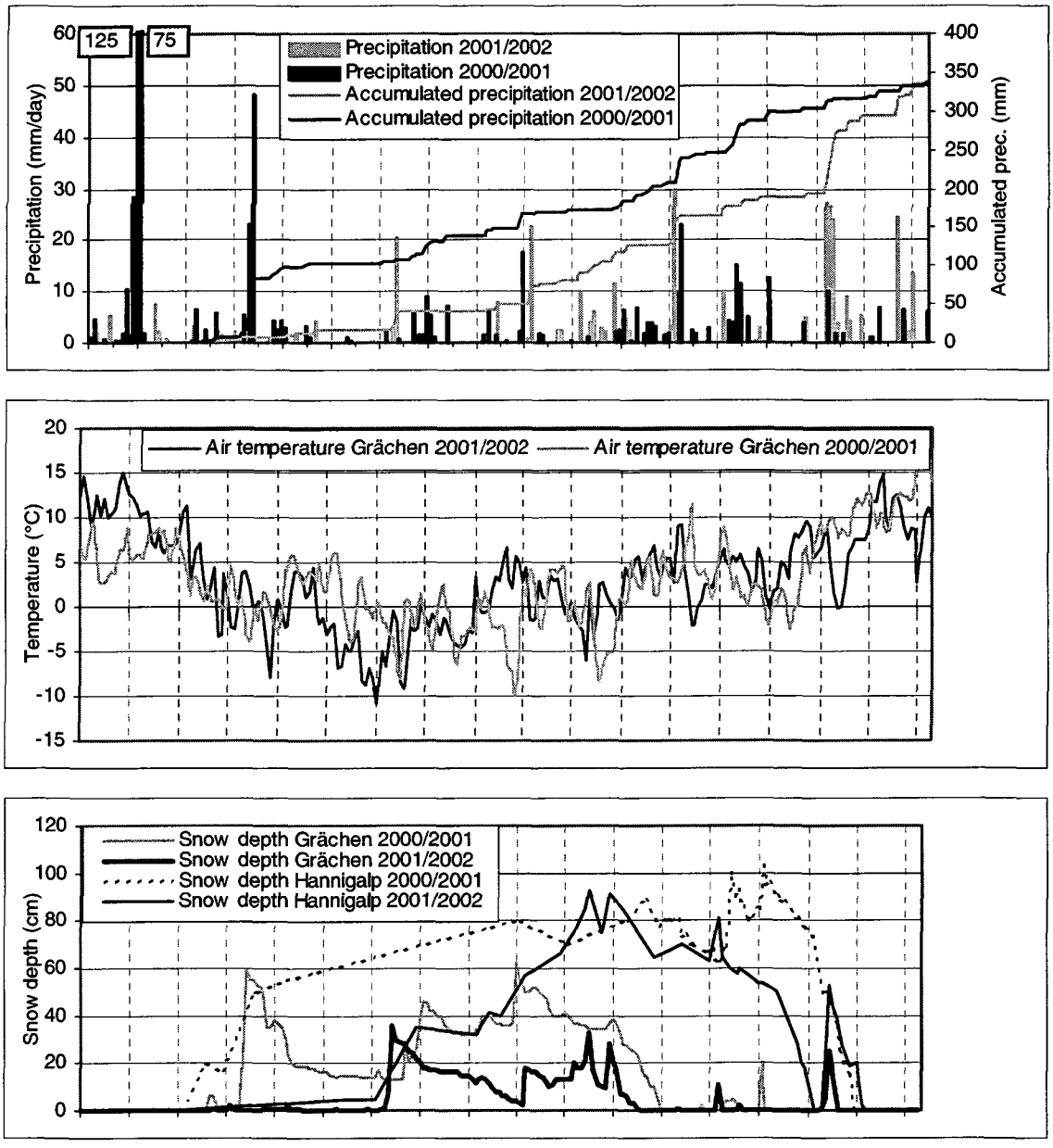

Figure 5.5: (a) Precipitation (daily fluxes and total accumulation from 1st Nov) for winter 2000/2001 and 2001/2002 at Grächen SMA. (b) Mean daily air temperature at Grächen SMA for the same period. (c) Snow depth at Grächen (1617 m) and Hannigalp (2100 m) for the same period.

of these heavy precipitations, the mean/max snow depth at Grächen was below average (mean/max snow = 29/62 cm as against 38/80 cm on the average), as particularly warm air temperatures were recorded (1.74°C warmer than average) and several snowmelt events took place in December and January. Air temperature was especially warm in March (3.1°C as against -0.7°C on the average), resulting in a fast and early snowmelt taking place.

5.4.1.2. WINTER 2001/2002

October was exceptionally warm (4.46°C above average) and relatively dry (31.9 mm as against 55 mm on the average). This warm period ended on 1st November with a sharp decrease in the

air temperature and below freezing temperatures. From then, the climate remained dry (11.4 mm in November) and cold until the end of December (-7.6°C as against -2.3°C on the average was recorded in December). Less than 5 cm of snow was lying at Grächen and Hannigalp during this period. The first significant snowfall occurred at the end of December and a maximum snow depth (36 cm) was reached at Grächen. In contrast to January, the air temperature at Grächen was mostly above freezing point (1.1°C on the average) in February and a series of rain and snow events took place (the snow depth did not exceed 33 cm). Between 5thMarch and 12thMarch, the mean daily air temperature increased to approx. 5°C at Grächen and the final snowmelt occurred. This period also coincided with the onset of the snowmelt at Hannigalp, which ended on 1stMay. However, melting was delayed in a first time between 22nd March and 1st April and, in a second time, between 14thApril and 21stApril due to an abrupt change in the air temperature.

Between 2nd May and 5th May, 83 mm of precipitation were recorded. In an initial stage, the snow limit was located above 2100 m. However, a decrease in the air temperature took place on 3rd May and the snow limit fell down below 1000 m. On 5thMay, 54 cm of snow were measured at Hannigalp, while 25 cm were reported at Grächen. This additional snow melted in 3 days at Grächen. At Hannigalp the snow lasted until 16thMay.

If compared to long-term meteorological data, precipitation remained deficient between November and January. However, the second part of the winter (February to May) was wet, resulting in above average accumulated winter precipitation (November to May) (335 mm as against 286 mm on the average). Due to warm air temperatures in February and March (2°C as against -1.8°C on the average), the snow depth at Grächen remained shallow during the entire winter (only 54 snow days were recorded as against 105 on the average). At Hannigalp the snowpack increased during these two months and, at the beginning of April, approx. the same amount of snow was measured as one year earlier. The warm temperature in March and April (3°C above average) shortened the snow cover period. Consequently, the snowpack disappeared some 12 days earlier at Hannigalp than in the previous year, while at Grächen the difference to last year made up two weeks. The abrupt temperature fall in May and the huge snowfall created a second snowmelt event, which lengthened the winter at Hannigalp to approx. the same period as the previous year, i.e. to mid-May.

5.4.2. GD ST BERNARD

An ordinary winter starts in October with a mean air temperature around freezing point. From November until the end of March, the air temperature is mostly far below 0°C and the snow cover steadily increases. Until the end of March, snowmelt is rare and limited to south exposed location. In April, the first significant melting appears and the snow depth reaches it's maximum. In May, snowmelt is at it's highest. In June, cold periods with snowfall are not uncommon and the snow cover period may be lengthened. This period usually corresponds with the end of the snow cover period. However, it is not rare that snow remains until July on northern exposed sites.

For winters studied, the precipitation, the mean air temperature, and the snow depth on the three different sites are shown in Figure 5.6.

5.4.2.1. WINTER 2000/2001

Winter 2000/2001 began early. During the period between 11th October and 16th October heavy

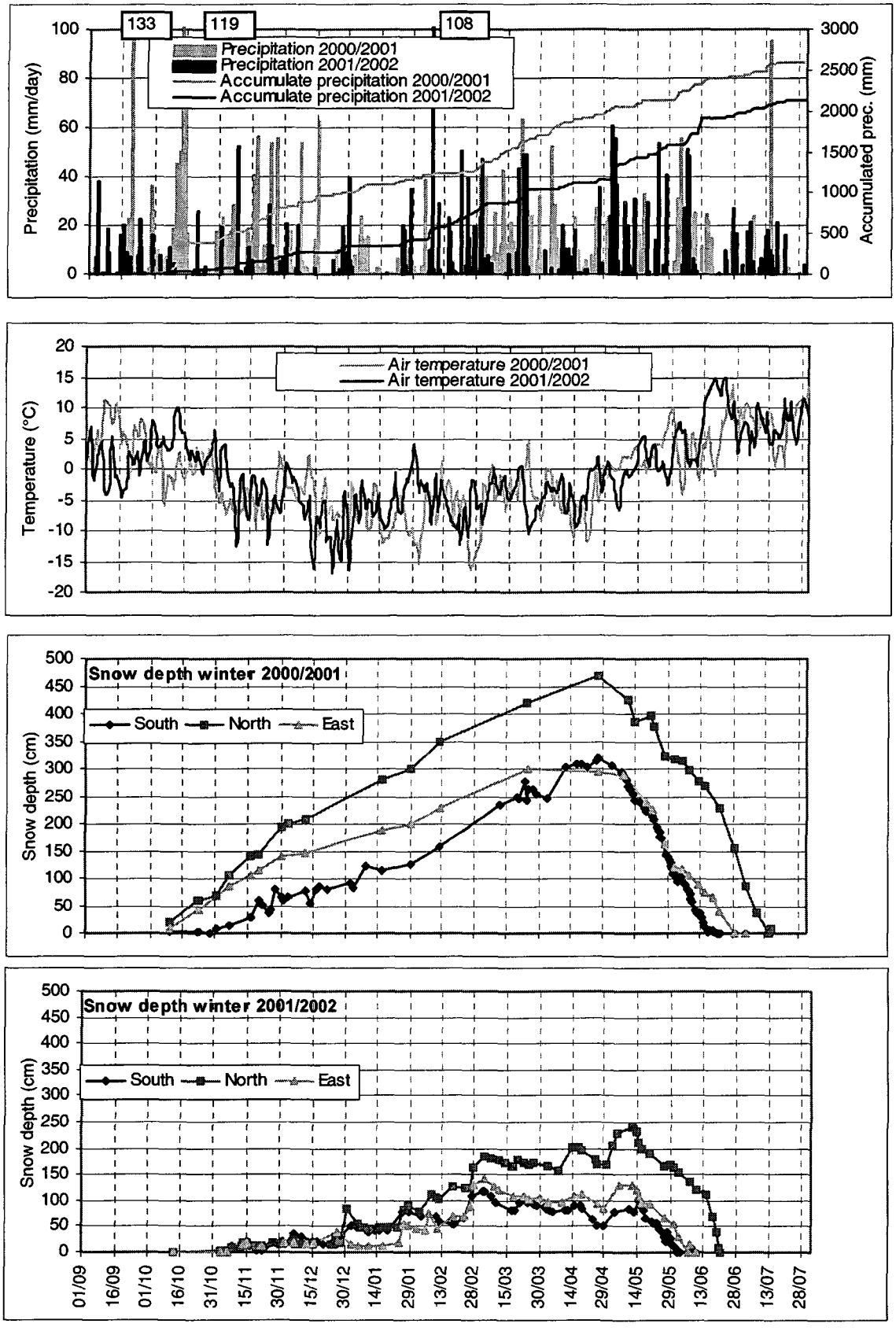

Figure 5.6: (a) Precipitation (daily fluxes and total accumulation from 1st October) and (b) mean daily air temperature for winter 2000/2001 and 2001/2002 at Gd St Bernard SMA. Snow depth evolution at the south, east and north plot during winter 2000/2001 (c) and winter 2001/2002 (d).

precipitation took place (up to 100 mm/day), sometimes rain, sometimes snow. The north- and east-facing experimental site had snow left (20 cm), lasting throughout the winter. At the beginning of November, the air temperature fell below 0°C. A steady and intense increase in snow depth took place afterwards, as heavy precipitation was present during the entire winter. At the end of the winter 3.2 m of snow were measured at the southern, wind-exposed place, whereas at the northern, wind protected site, 4.7 m of snow were lying. In March and April 2001, the weather was mostly influenced by northern depressions. The precipitation was less considerable on the southern side of the Alps. The east-facing experimental site was less affected by these perturbation than the pass and, in early May, less snow was recorded on the east site than on the south. The final snowmelt began, for all locations on 10th May. It was more rapid on the southern site than anywhere else. A delay in snow cover disappearance of one month and 14 days respectively was observed for the northern and eastern site. Finally, we noted that snowfall during the melt period melted rapidly (i.e within the day) and hardly affected the snow depth evolution.

Similar to Hannigalp, winter 2000/2001 was wet. Accumulated winter precipitation (i.e. from October to April) was 20% higher than annual precipitation and slightly warmer than average (-5.7°C as against -6.1°C on the average).

5.4.2.2. WINTER 2001/2002

Until 24th December, 190 mm of precipitation were recorded. However, the snow depth did not exceed 38 cm at all slope expositions and remained mainly below 20 cm. Strong winds were common on the pass and blew away the newly fallen snow, while on the Italian site, precipitation was probably much less significant, as all the perturbation came from the north.

Between 25th and 28thDecember, 80 mm of precipitation were measured. The snow depth increased significantly (total snow depth was 50 cm on the north and south plot on 28th December) on the pass, but remained low on the Italian side (less than 30 cm). The snow depth remained unchanged until the end of January when 78 mm fell and the snowpack increased accordingly on all expositions. A warm period early February (mean air temperature of 4°C on 30thJanuary!) created an early snowmelt episode on the south exposed plot. February was characterized by a succession of snowfall events. The snow depth increased steadily and reached its maximum at the beginning of March on the south and east exposed plot. March was warm (mean daily air temperature -4.4°C as against -6.7 on the average). Substantial snowmelt took place on the south and east exposed site (snow depth decreased by 1/3 of it's initial depth). On the north site however, the snow depth hardly varied. April was also warm (-3.1 as against -4.5 on the average) and snowmelt took place on each site. This melting period was delayed between 8th and 16th April when heavy precipitation was recorded (72 mm). At the end of April, hardly any snow remained on the south plot (52 cm on 29thApril). At the beginning of May, huge snow precipitation fell on the pass (182 mm in 4 days) and on 10th May 90 cm were measured on the south plot and 230 cm on the north plot. Between mid-May and early June, the entire snowpack melted on the south plot (i.e. some 14 days earlier than the previous year). The snow remained for some 7 days and 21 days respectively longer on the east and north exposed plot than on the south plot.

A statistical analysis of the climatic parameters shows similar trends to the one of Hannigalp. In particular, the air temperature was on the average 1°C above mean value, in spite of some very cold periods in December and January, whereas the precipitation was below average between October and January (431 mm as against 731 mm on the average) and above average

between February and May (1151 mm as against 737 mm on the average).

5.5. DISCUSSION AND CONCLUSION

The two chosen sites showed themselves to be well-adapted to represent a large diversity of climates. Protected regions located in the middle of mountain ranges experience a microclimate that is similar to the one of Hannigalp, whereas the wet climate in the Southern Alps is very close to the one encountered at Gd St Bernard. The two sites showed to be also accurate locations to study the general trend in global Alpine warming. From the climatic analyses over the last decades, the mean air temperature increases steadily, according to the current trend in alpine temperature change. The change in the yearly precipitation is more uncertain due to strong annual variations. However, we noted a slight increase over the last 30 years on both sites.

The two winters studied showed diametrically opposed patterns. Winter 2000/2001 was characterized by early snow and tremendous precipitation during the entire winter, whereas little snow fell during winter 2001/2002, except at the end of the winter. Winter 2000/2001 may be called a «standard winter» with a well-defined accumulation and ablation period. Snowmelt took place at the end of the winter only and the entire snowpack melted within a couple of weeks. Winter 2001/2002 was more complex with several short melting events and a substantial accumulation period in the ablation period. This applies to both Hannigalp and Gd St Bernard, except for the north site at Gd St Bernard, which showed a «standard» snow depth evolution.

To find relations in the snow depth evolution between both Gd St Bernard and Hannigalp is difficult, as the meteorological conditions vary heavily between both locations. However, from its exposure, the snow depth evolution at Hannigalp is in an initial stage similar to the one at Gd St Bernard north plot with a well defined accumulation period and no snowmelt events in winter. Later, in spring, changes in the snowpack are more related to those at Gd St Bernard south site, as may be viewed for winter 2001/2002 (Figure 5.7). In March and April, the

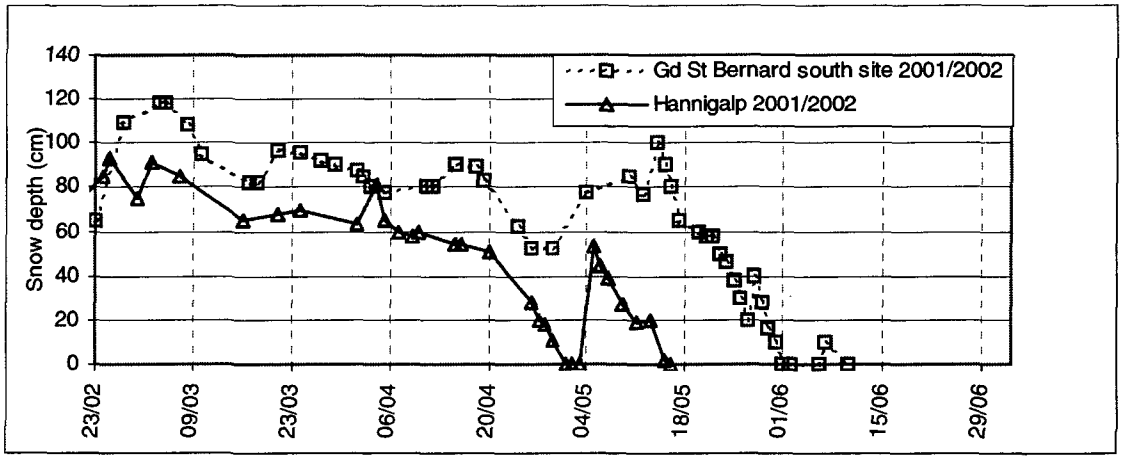

Figure 5.7: Snow depth in spring 2002 at Hannigalp and at the south-exposed plot at Gd St Bernard.

snowmelt period, as well as the melt intensity were comparable on both sites, the higher solar

radiation at Gd St Bernard south plot compensating for the warmer air temperature at Hannigalp.

As expected, the areal precipitation variation was huge even over short distances. At Gd St Bernard the snow depth was twice as high on the north as compared to the southern one. Both plots are only 200 m distant from each other. Orographic lifting, wind exposure, orientation and location are the main source of spatial variability. The variation in the snowfall with the altitude, as well as the geographical location explain the differences in the precipitation between Hannigalp and Gd St Bernard, whereas the differences in the wind speed the solar radiation and the location generates the variation in the snow depth at Gd St Bernard. As a result, determination of areal snow depth distribution over larger areas is faced with difficulties and may be questionable, especially for a complicated topography.

In the next parts, meteorological analysis will be used to (a) understand the different discharge events during the observed winters observed, (b) better comprehend the long-term effect of a climate change on the two different studied sites studied, and (c) regionalise the obtained results obtained over larger areas.

6. RESULTS AND DISCUSSION OF FIELD MEASUREMENTS

6.1. INTRODUCTION

The previous chapter showed the climatic differences between both sites examined and how these differences affected the snow depth evolution during both winters studied. In this chapter we investigate how the snowpack influences the soil frost and examine to which extent a seasonally frozen soil affects the snowmelt discharge at snowmelt.

We will begin with the description of the thermal and hydraulic soil behaviour during each winter and at each location. In a second part, the main differences between both fields are listed. Finally, we classify snowmelt events as «winter[1]», «spring», «final», and «late snowmelt events». This classification will be used to evaluate the effect of each snowmelt event on the groundwater recharge. For each type of event, we discuss the differences in the hydraulic and thermal soil behaviour and compare their water balance.

6.2. RESULTS

6.2.1. HANNIGALP

6.2.1.1. WINTER[2] 2000/2001

The soil remained unfrozen in November, as the early and rapidly growing snow cover created an insulating layer. However, some artificial soil frost was produced at the end of November when approximately 50 cm of snow were removed from the experimental site. The upper 5 cm of the soil froze and 7% vol. of residual water content was measured on 14th January at that depth (Figure 6.1.). A steady filling of the resultant snowpack gap took place in December and January and prevented the soil to freeze deeper. During this period, the soil temperatures at all depths were close to 0°C. At the beginning of February 2001, the snow depth on the experimental plot was identical to the natural undisturbed snow depth. From mid-February the soil was thawing due to the underneath heat flux. A first snowmelt event took place from 15th March to 4th April. The liquid water content increased steadily at all depths. No lateral surface was measured. A period of bad weather delayed the snowmelt for more than three weeks and, consequently, the liquid water content hardly changed. The final snowmelt began on 24th April and ended on 12th May. Similar to the first snowmelt event, the entire meltwater infiltrated into the ground and no lateral runoff was measured (Figure 6.2).

From soil digging, soil was inhomogeneously frozen in the most superficial soil layer (2-3 cm) at the end of the first snowmelt period (4th April). The meltwater infiltrated into the ground predominantly in unfrozen areas (Photo 6.1 a)). Maximal infiltration depth was approx.

1. The exact definition of "winter snow melt event" will be given later. However, we should already note that such an event is characterized mainly by the snowmelt intensity, and does not denote any time specification. A "winter snow melt event" may take place in spring.
2. The word "winter" followed by a specific time period (e.g. winter 2001/2002) goes from the first significant snow fall in autumn until the end of the snow cover period. This period may be much longer than the usual winter period (i.e. December- March).

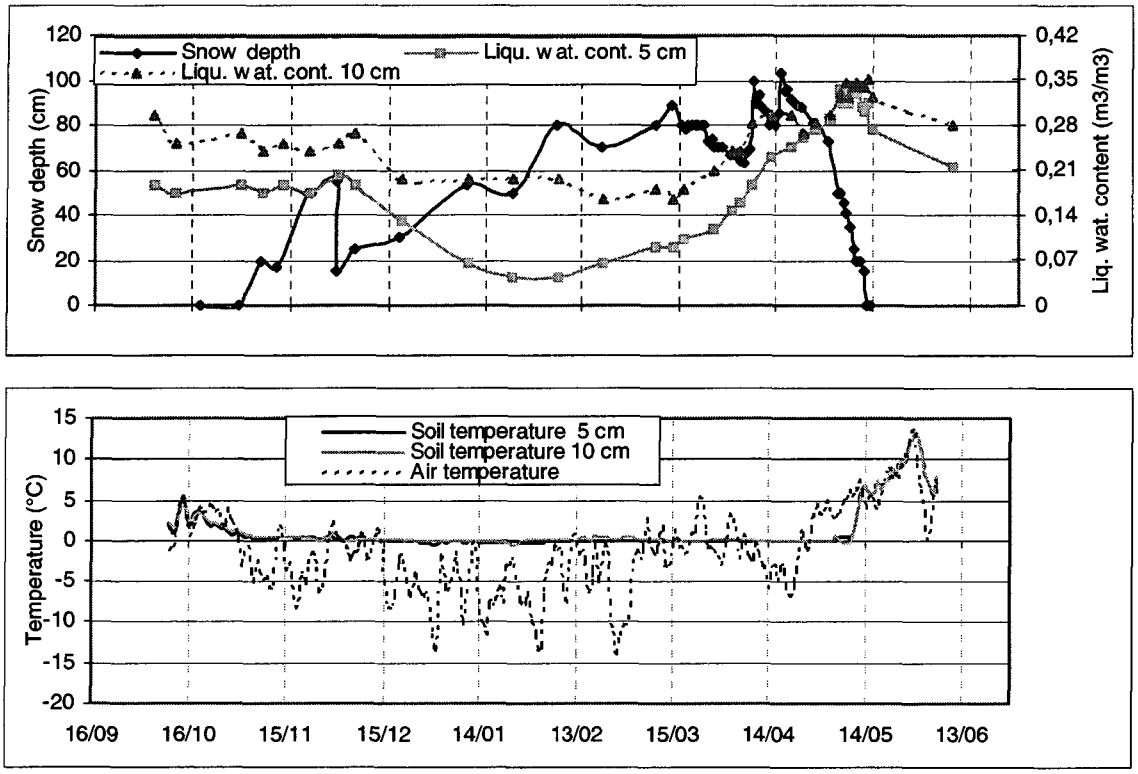

Figure 6.1: (a) Snow depth, soil liquid water content at a depth of 5 and 10 cm measured at Hannigalp during winter 2000/2001. (b) Air temperature and soil temperature at the same depths at Hannigalp.

40 cm and no water was recorded by the lysimeter. Also, no lateral flux was registered, indicating that (a) the frozen layer did not expand over large areas allowing lateral flow to take place and (b) part of the meltwater percolated through the frozen layer into the unfrozen subsoil.

During the final snowmelt, the liquid water content steadily increased and reached a maximum value on 3rd May (Figure 6.2). A temporal shift (four days) was observed between the beginning of the warm period and the first measured deep percolation. The soil was free of ice and the infiltration took place mainly through preferential pathways (Photo 6.1 b)). The intriguing infiltration picture on Photo 6.1 b) will be clarified in Chapter 8. Only slight surface runoff took place on 8th May (0.1 mm) when the maximum snowmelt intensity was reached (approximately 50 mm of SWE) due to the high soil infiltration capacity. The fact that no runoff was recorded during the rain on snow event on 2nd May indicated that there was too little precipitation (10 mm) to reach the storage capacity of the snowpack and the ground underneath.

To sum up, in an unfrozen and relatively flat soil, the meltwater entirely infiltrates into the ground due, on the one hand, to the high infiltration capacity of the soil and, on the other hand, to the low snowmelt intensity (approximately four times less than rainfall intensity). Also the underneath bedrock did not influence the soil water flux in the upper soil layer, as no perched aquifer could be measured during the entire snowmelt.

6.2.1.2. WINTER 2001/2002

Winter 2001/2002 had a much thinner snow cover, which led to deep soil frost. The soil was

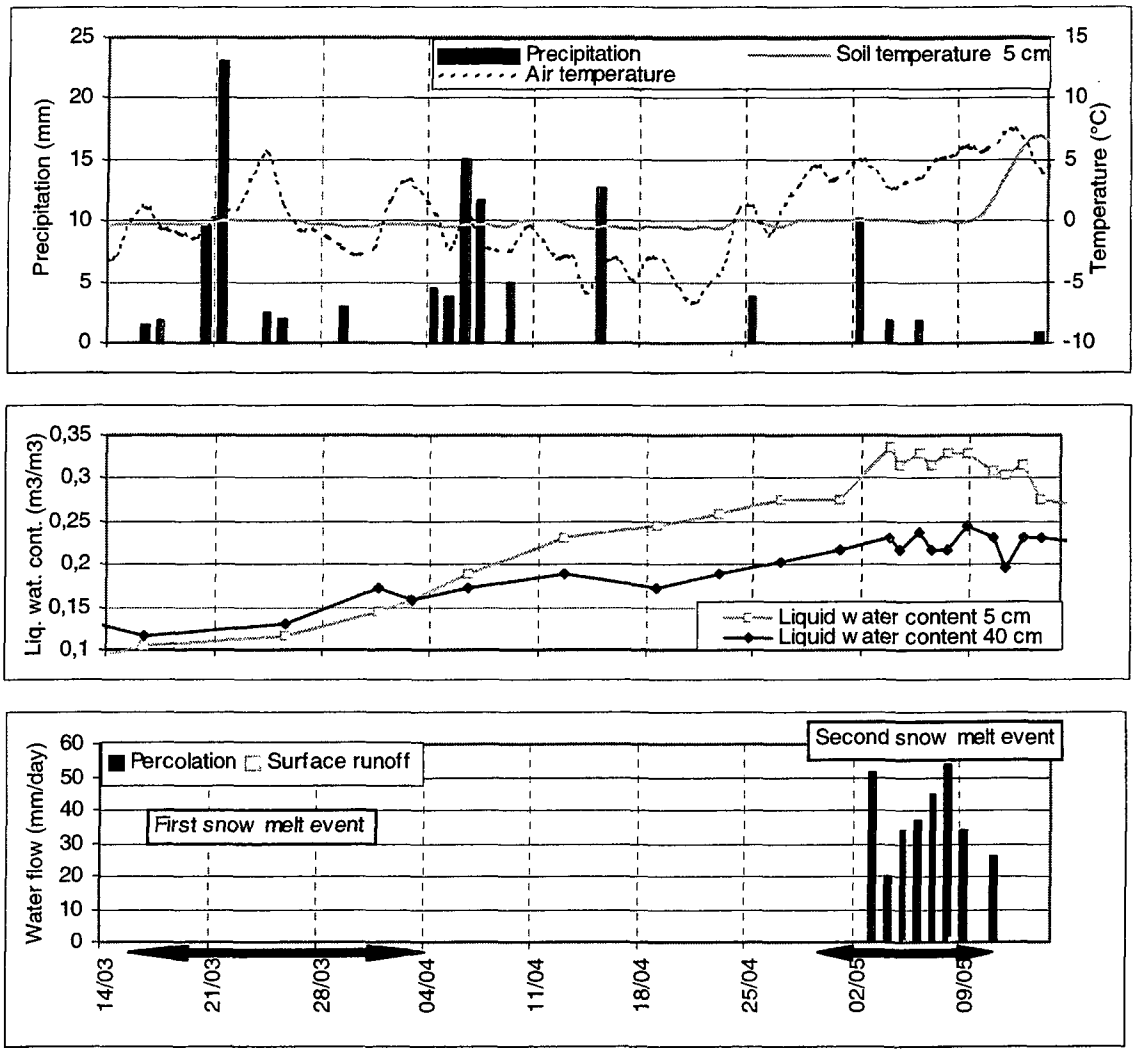

Figure 6.2: (a) Air temperature at Hannigalp, soil temperature (at a depth of 5 cm) at Hannigalp and precipitation at Grächen SMA during snowmelt 2001 (14.3-15.5). (b) Liquid soil water content at a depth of 5 cm at Hannigalp for same time period. (c) Daily discharge from the south and central plot during same time period at Hannigalp. The discharges rates are expressed per unit area of the runoff plot.

frozen over the entire studied profile, as is seen from the liquid water content measurements (Figure 6.3). The pore ice content was established from the soil moisture content prior and after freezing, as well as from the soil structure. We found that ice occupied approximately 15% vol. of the pore space, the remaining 30% vol. were filled by air. This value is rather low if compared for silt loam or silt clay, where the pore ice content may vary between 80 and 95% pore saturation (Gray and Granger 1985). The snowfall on 28th December insulated the soil from outside. Warming, due to the underneath heat flux, steadily increased the soil temperature from -5°C on 25th December up to -0.7°C on 10th March (at a depth of 5 cm). From then, the soil temperature remained close to the freezing point over the entire studied profile. A first snowmelt period began on 4th March and lasted until 21st March. Melting was not significant and consequently only the upper 15 cm of the soil showed an increase in the liquid water content (from 7.2% vol. to 9.2% vol., no change was measured below 15 cm). The still dry frozen soils did not alter drastically the infiltration rate, and no lateral runoff was measured (Figure 6.4). Between 22nd March and 3rd April, cold meteorological conditions delayed the snowmelt. On 4th

a) 4th April 2001

b)7th May 2001

Photo 6.1: Soil profile of the dye tracer experiment at Hannigalp. a) taken on 4th April 2001, b) on 7th May 2001. The distances on the white ruler are in cm. The green colour corresponds to the dye tracer. The soil surface is indicated with the upper end of the ruler.

April, the air temperature increased above 0°C and a second snowmelt event commenced. Most meltwater infiltrated into the ground. The water content increased markedly in the upper 20 cm. The dye tracer experiment (Photo 6.2) showed that the water barely infiltrated below a depth of 40 cm. During this period, 92% of the meltwater infiltrated into the soil, whereas 8% of surface runoff was measured, mainly as surface runoff (98% of the total lateral flow). Colder temperature slowed down the process between 14th and 22nd April. The liquid water content, however, increased steadily at all depths (for example from 8% vol. to 15.5% vol. at a depth of 30 cm). As no discharge had been measured, this increase was due, on the one hand, to the thawing of the pore ice (latent heat transfer between the incoming meltwater and the ice), and, on the other hand, to slightly infiltrating meltwater caused by minor snowmelt (approx. 5 cm of snow melted during this period). The final snowmelt began on 21st April and ended on 1st May. Although most of the water infiltrated into the ground, lateral runoff was more important than during the previous snowmelts (approx. 25% of total meltwater).

A consequence of the rather dry climatic conditions in October 2001 was that a small amount of ice filled the soil pores. The soil had a high soil infiltration capacity (30% vol. was filled by air), and one would expect that all meltwater infiltrates into the ground during small snowmelt events. During the second snowmelt event, meltwater from the snowpack was low and, TDR

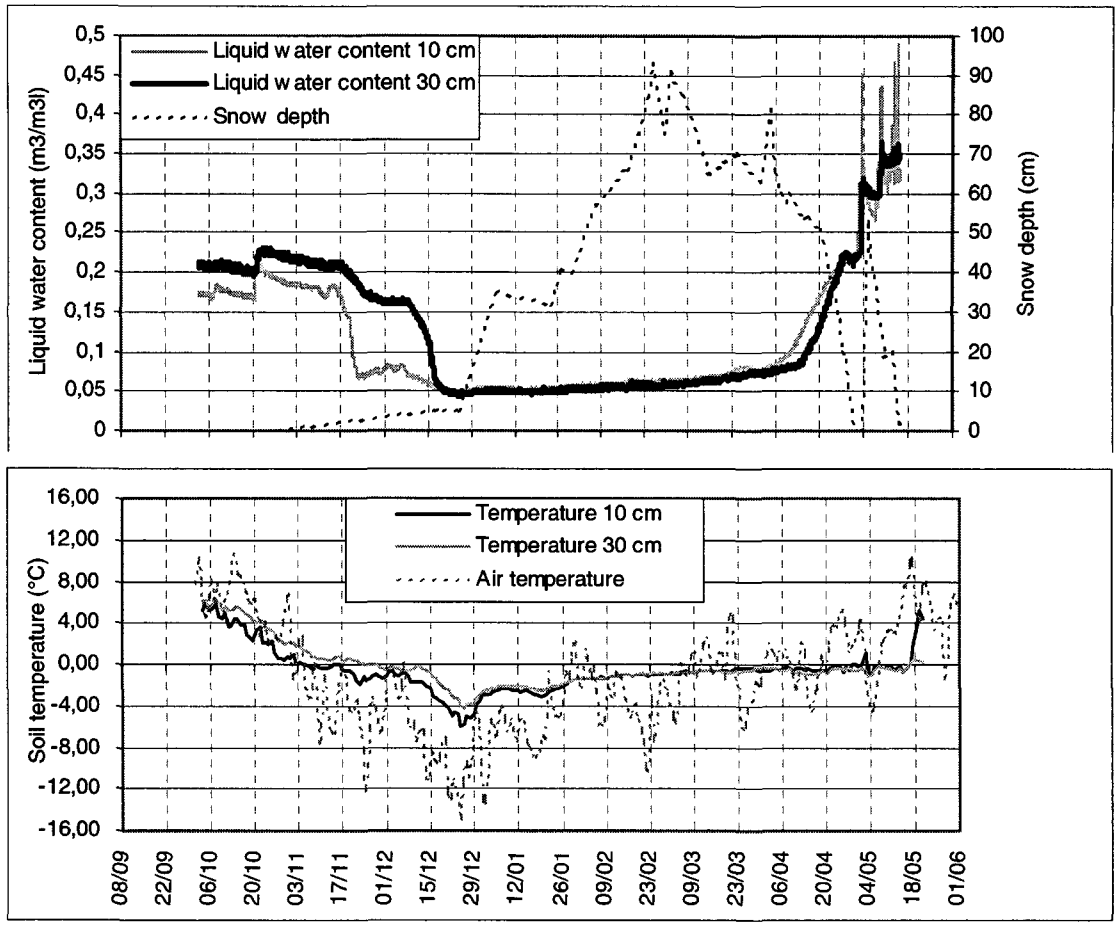

Figure 6.3: (a) Snow depth, soil liquid water content at a depth of 10 and 30 cm, (b) soil temperature at a depth of 10 and 30 cm measured at Hannigalp during winter 2001/2002.

measurements showed that the soil was not saturated. However, we noted slight surface runoff. This lateral flow was caused by the presence of a basal ice sheet, which was formed by the latent heat transfer between the liquid water at the bottom of the snowpack and the ice at the soil surface. This ice sheet reduced dramatically the infiltration capacity of the soil, and produced early surface runoff. No subsurface flow was recorded as the uppermost soil layer remained unsaturated.

During the first stage of the final snowmelt (between 21st to 24th April), the measurement apparatus did not work and no data were available. Between 25th April and 1st May, most of the meltwater infiltrated into the soil (Figure 6.4). 87% of the meltwater was collected by the lysimeter, and 13% ran off as lateral flow. However, this percentage fluctuated with time. The relative percentage of the lateral discharge made up 31% of the total discharge on 26thMay, and diminished to less than 2% on 1st May, due to a steady increase of snow-free areas between these two dates. On bare areas, the upper soil frost melted, increasing the soil infiltration capacity. As more water was able to circulate in the upper unfrozen soil, subsurface flow constituted approximately 25% of the total amount of lateral flow on 26thApril, and 100% on 1stMay. An estimation of the water balance between 21st and 26th April shows that at least 37% of the meltwater ran off as lateral flow (see note page 85).

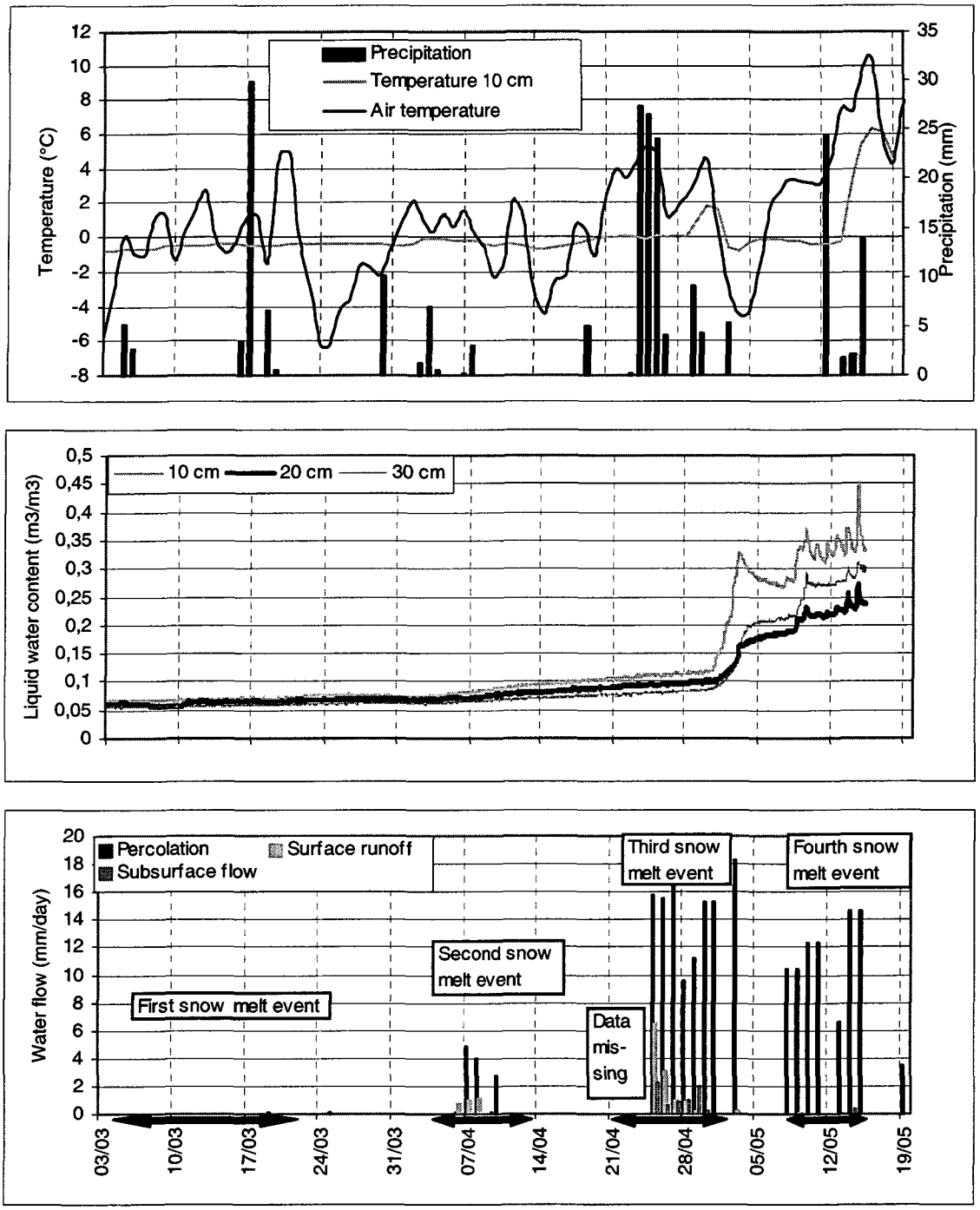

Figure 6.4: (a) Soil temperature (10 cm), air temperature and precipitation at Hannigalp in spring 2002. (b) Soil liquid water content at a depth of 10, 20 and 30 cm. (c) Daily discharge (surface runoff, subsurface runoff and percolation).

The soil infiltration capacity increased steadily between each snowmelt event (Figure 6.4). We believe that the main reason was the alteration of the basal ice by the incoming meltwater (Woo et al. 1982), and the biological activity beneath snowpack (Richardson and Salisbury 1977, Jones et al. 2001). Indeed, meltwater contributes to ice destruction through thermal and mechanical erosion. This alteration of the ice sheet becomes more important with increasing snowmelt, explaining why the basal ice sheet lost its blocking capacity with time. On the other

a) 16th Mars 2002

b) 2nd April 2002

c) 2nd May 2002

d) 13th May 2002

Photo 6.2: Soil profile of the dye tracer experiment at Hannigalp. a) taken on 16th Mars 2002, b) on 2nd April 2002, c) on 2nd May 2002 and d) on 13thMay 2002. The distances on the white ruler are in cm. The green colour corresponds to the dye tracer. The soil surface is indicated with the upper end of the ruler.

hand, the penetration of visible light through the snowpack affects many plant processes, in particular germination and emergence. Plants are able to melt the surrounding snow or ice, in particular when the snowpack is shallow (< 20 cm), increasing markedly the soil infiltration capacity, and partly explaining why lateral runoff decreased greatly between 26th and 29th May.

Between 1st May and 3rd May, the ground was bare and the soil thawed to a depth of 10 cm approximately, but remained frozen below that. The huge precipitation between 3rd and 5th May enabled to monitoring of two distinctive events: (a) rain precipitation over a frozen ground, and (b) snowmelt over a partly frozen soil. During the rainfall on 3rd May, the liquid water content increased significantly throughout the entire profile (Figure 6.5). Due to the higher rainfall

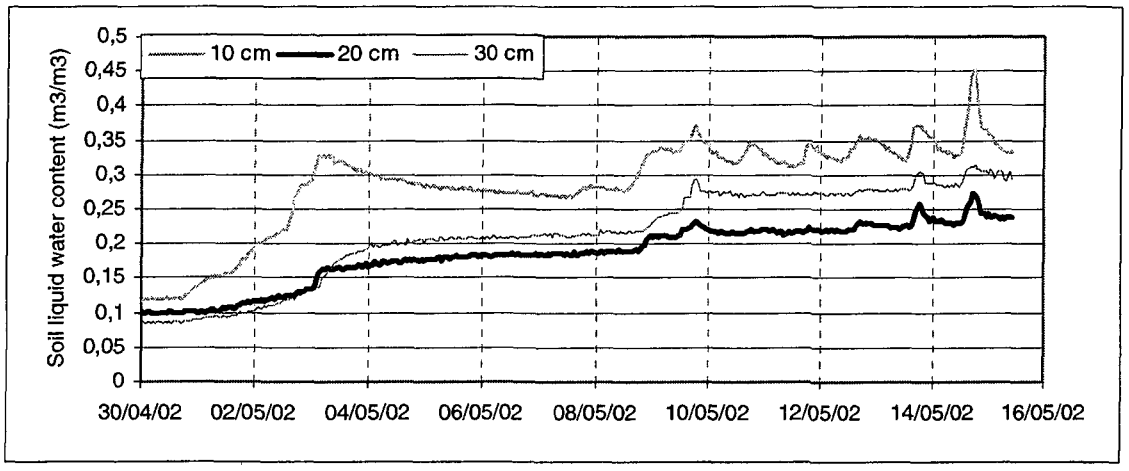

Figure 6.5: Soil liquid water content at a depth of 10, 20 and 30 cm between 2nd May and 16th May at Hannigalp. The sharp increase at all depth on 3rd May is due to a rain event. The daily variation of the liquid water content between the 10th May and the 16thMay are caused by the daily variation in the snowmelt release, which takes place between 13:00 and 20:00.

intensity, the infiltration capacity at the soil surface was reached, and 0.2 mm of meltwater ran off as surface flow (no subsurface flow was recorded). After this initial stage the rain turned into snow. The soil liquid water content decreased steadily from 45% vol. to 26% vol. at a depth of 10 cm until 7th May, when the snowpack began to melt. The melting period lasted 10 days and showed a similar pattern every day. The soil liquid water content increased between 13:00 and 20:00, and a steady decrease took place afterwards. All the water infiltrated into the ground, except on 9th May and on 14th May, when slight lateral discharge was recorded (0.17 mm and 0.35 mm). On the two dates mentioned, the mean air temperature was extremely warm (7°C) and high snowmelt was recorded (50 mm of SWE). These two events showed that the soil infiltration capacity was hardly reduced by the pore ice below 10 cm. The absence of a basal ice sheet may partly explain this behaviour. Another reason have arisen from the fact that the upper organic soil, with a high water retention capacity and hence a great blocking effect was already unfrozen, in contrast to the mineral soil, where only a little pore ice was present, and the ice blocking effect reduced.

To sum up, soil frost influences notably the meltwater discharge at Hannigalp. During the two winters examined, lateral runoff increased from 0 to 25%. This increase is mainly caused by the presence of a basal ice sheet, which builds up after the first snowmelt event. Mechanical erosion

and biological activity alter this ice sheet, resulting in an increase in the soil infiltration capacity with time. No lateral runoff is recorded, when the basal ice sheet is absent. In particular the infiltration capacity of the soil is only slightly reduced by the pore ice.

6.2.1.3. SPATIAL VARIABILITY OF FIELD MEASUREMENTS AT HANNIGALP

The dye tracer infiltration patterns were shown to vary greatly during both winters. For example, on 2nd May 2002 no dye tracer was seen on the left-hand side of Photo 6.2 c) below a depth of 50 cm, despite the fact that the entire snowpack melted and mainly infiltrated into the ground, whereas, on the left-hand side, the entire profile (i.e. 80 cm) was spotted with the tracer.

During the frozen winter, this variability was a probable consequence of the considerable horizontal variation of organic material along the profile. A high proportion of organic material causes an increase in the water retention capacity. As a result, more ice fills the pores, which reduces the infiltration capacity. The liquid water content at two locations 50 cm apart was measured during winter 2001/2002 (Figure 6.6). The soil moisture content at a depth of 10 cm

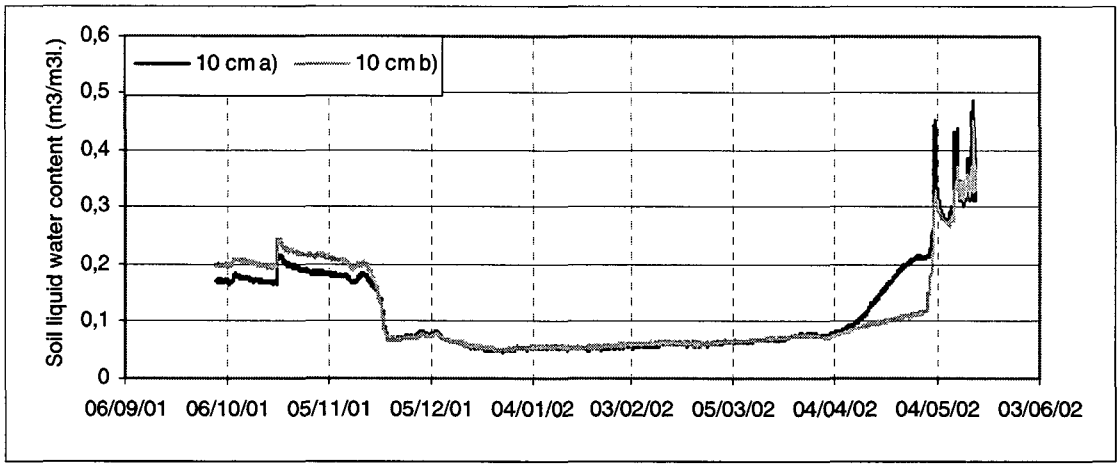

Figure 6.6: Soil liquid water content at a depth of 10 cm at Hannigalp during winter 2001/2002 at two locations 50 cm apart. Between 4th April and 1st May the liquid water content between both locations shows a different evolution pattern.

was similar at both locations, except during the final snowmelt in April. During this period, the liquid water content increased significantly at location (a) (from 7% vol. to 23% vol.), whereas little change was measured at location (b) (from 7% vol. to 13% vol.), indicating little meltwater infiltration. Ice blocking was probably more effective at location (b) than at location (a), as at a depth of 5 cm, 10% more pore ice was measured at location (b) than at location (a) (the ice was estimated from the difference between the measured liquid water content before and after freezing).

We should hence keep in mind that some snowmelt events might not have been recorded by the TDR probes, as meltwater did not necessarily infiltrate at the location of the probes. We hardly measured any change in the liquid water content during the first snowmelt event in spring 2002 (March 4 to March 22), whereas from the dye tracer experiment it was obvious that meltwater infiltrated to a depth of 10 cm.

6.2.2. GD ST BERNARD

6.2.2.1. WINTER 2000/2001

Heavy and early snowfall in November prevented the soil from freezing at all slope orientations, as shown by the liquid soil water content measurements (Figure 6.7). On 1st December, the dye

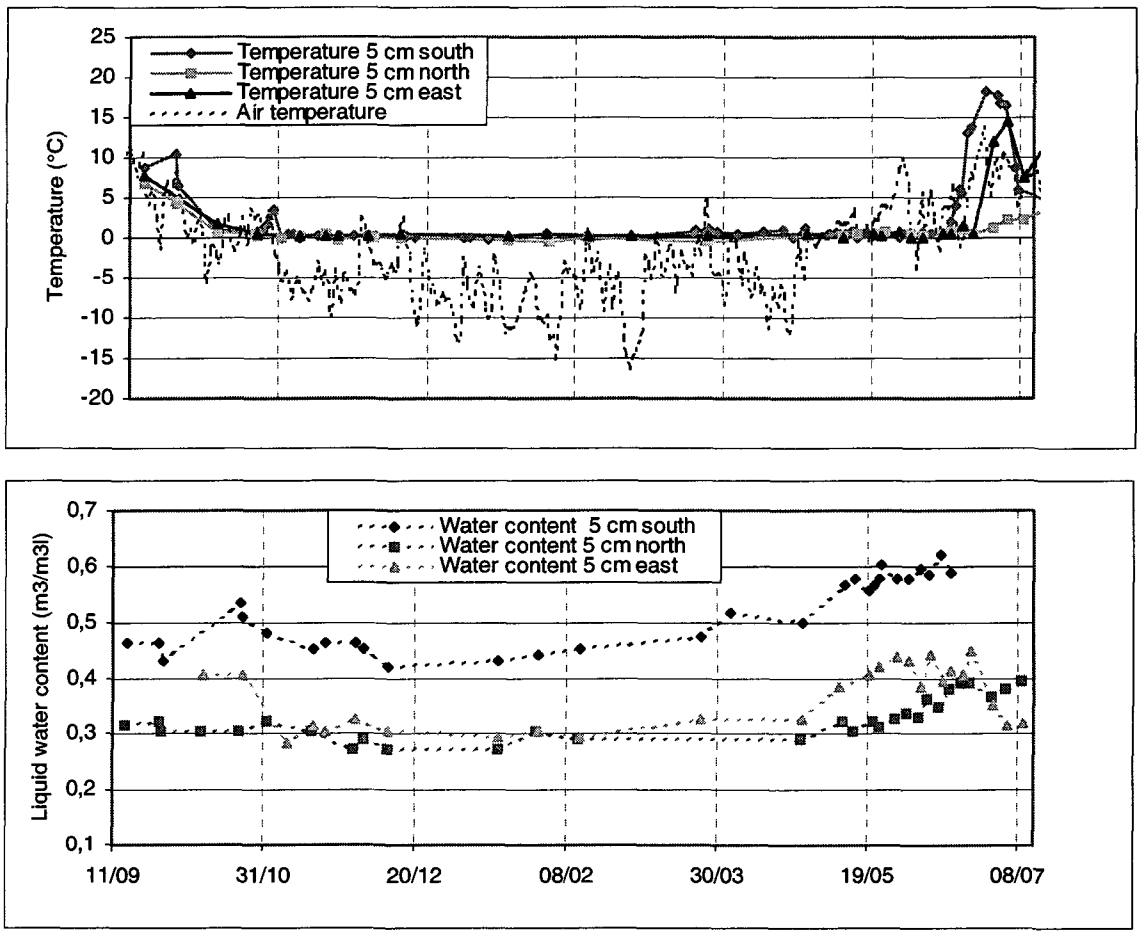

Figure 6.7: (a) Air temperature and soil temperature at a depth of 5 cm for the southerly, easterly and northerly exposed site at Gd St Bernard during winter 2000/2001 at snowmelt. (b) Soil liquid water content evolution at a depth of 5 cm.

tracer was applied in a similar way to Hannigalp. However, the thinning of the snow cover did not affect the soil frost, as strong winds allowed a fast filling of the resultant hole. From December to April, air temperatures were below freezing point and no significant snowmelt was recorded. The soil liquid water content did not change. The first snowmelt event took place between 23rd March and 3rd April, affecting mainly the south plot, and meltwater infiltrated to a depth of 50 cm (Photo 6.3 a)).

The final snowmelt began on 6th May and lasted until 17th June for the southerly exposed site, until 29th June for the easterly exposed site and until 1st July for the northerly exposed site. The soil was close to saturation during the entire melt period. The rather low soil moisture content (Figure 6.9) on the east and north plots, was due to the presence of large slate stones between the TDR rods, which were particularly abundant on both sites. On the south plot, where the

a) 09.04.01

b) 01.06.01

Photo 6.3: Soil profile of the dye tracer experiment at Gd St Bernard south plot. a) taken on 9th April 2001, b) on 1st June 2001. The distances on the white ruler are in cm. The green colour corresponds to the dye tracer. The soil surface is indicated with the upper end of the ruler.

snowmelt discharge was quantified, the lateral flow was approximately 10% of the total snowmelt, despite the unfrozen soil. However, a higher proportion (16%) was measured during the initial stage of the final snowmelt (until 1st June). From 2nd June, the surface and subsurface flow diminished, as initially less snow melted (cold weather conditions), and afterwards, soil infiltration was favoured, as from 10th June part of the surface plot was free of snow.

No water was measured in the piezometer, indicating that the lateral runoff was not caused by a rise of the groundwater table. We believe that this flow was favoured by the steepness of the experimental plot and by the important snowmelt taking place in May and June. The diurnal variation in the air temperature reduced the snowmelt to approximately 10 hours, with maximum snowmelt intensity between 14:00 and 16:00. Hence considerable meltwater may have reached the surface over a short time period, especially as water flow through snow is not stable and is strongly affected by flow instabilities such as flow fingers (Schneebeli 1995, Waldner et al. sub.). We may therefore expect that, *locally*, a significant amount of snowmelt reached the ground, which saturated the soil and created lateral flow. The soil steepness further accelerated the surface runoff. The subsurface flow was probably caused by lateral flow through the relatively porous organic upper soil layer, and lateral deviation of infiltrating water by large stones close to the collecting gutter. The occurrence of such type of saturated lateral flow at the bottom of the snowpack has been shown by Waldner et al. (2000).

In conclusion, 10% of total meltwater ran off as lateral flow on the south exposed plot at Gd St Bernard, despite the fact that the soil remained unfrozen. Steepness and melt intensity were the major causes of this lateral runoff. On the east and north exposed plot, we may assume a reduced

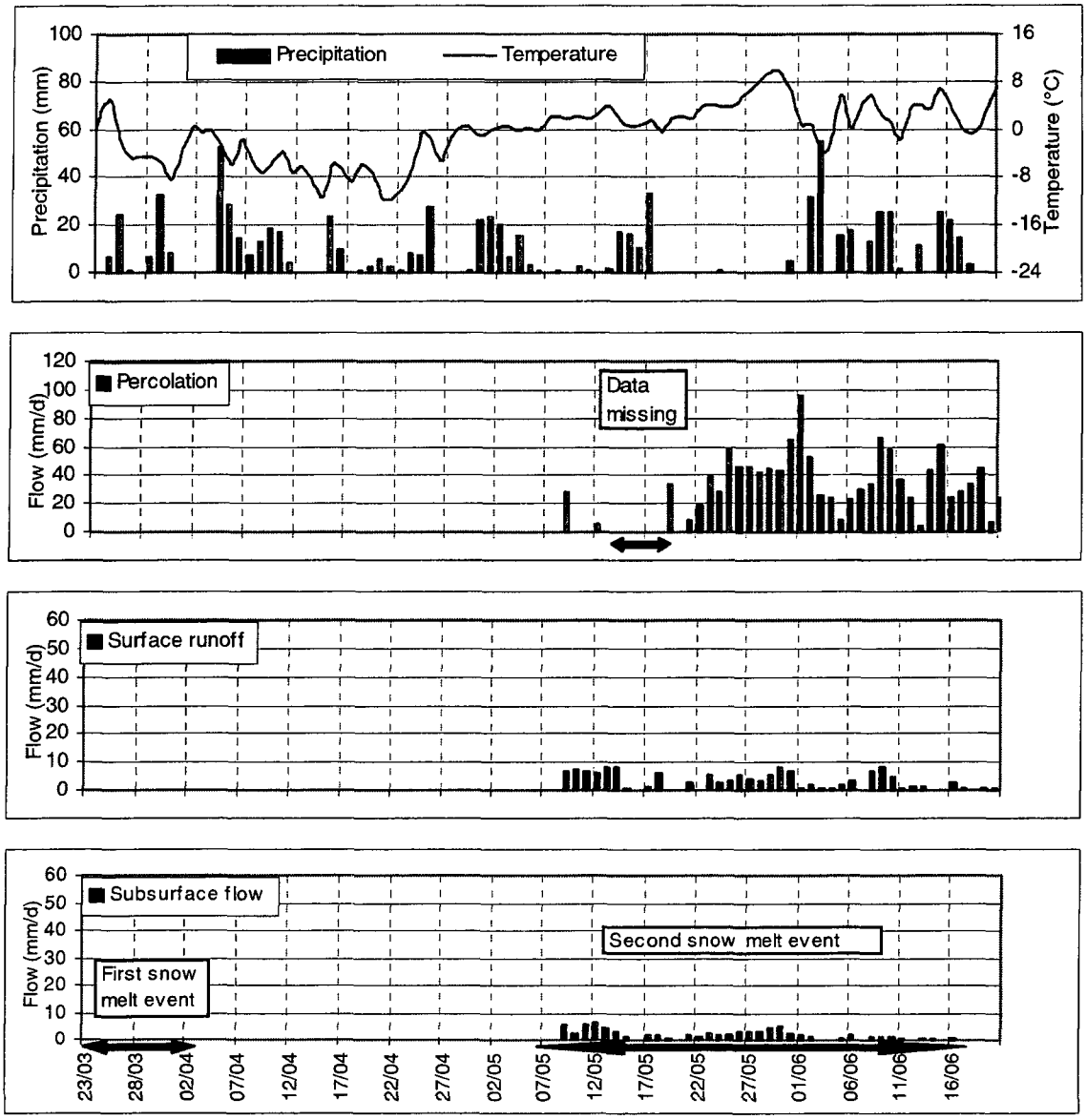

Figure 6.8: (a) Air temperature and precipitation measured at Gd St Bernard during snowmelt 2000/2001. Daily discharge: percolation (b), surface flow (c) and subsurface flow (d) at the south plot. Discharge rates are expressed per unit area of the runoff plot.

proportion of lateral flow, as snowmelt intensity was lower.

6.2.2.2. WINTER 2001/2002

The snow cover remained shallow between November and December, and the soil froze deeply at all locations. The soil liquid water content for all profiles (except at 40 cm on the south plot) decreased to approx. 8% vol., which corresponds to an ice content between 20% and 35% vol., depending on the depth and exposure (Figure 6.9).

From the soil temperature measurements (Figure 6.10), the frost was deepest on the east plot (a soil temperature of -1.8°C was measured at a depth of 30 cm on 26th January), and shallowest

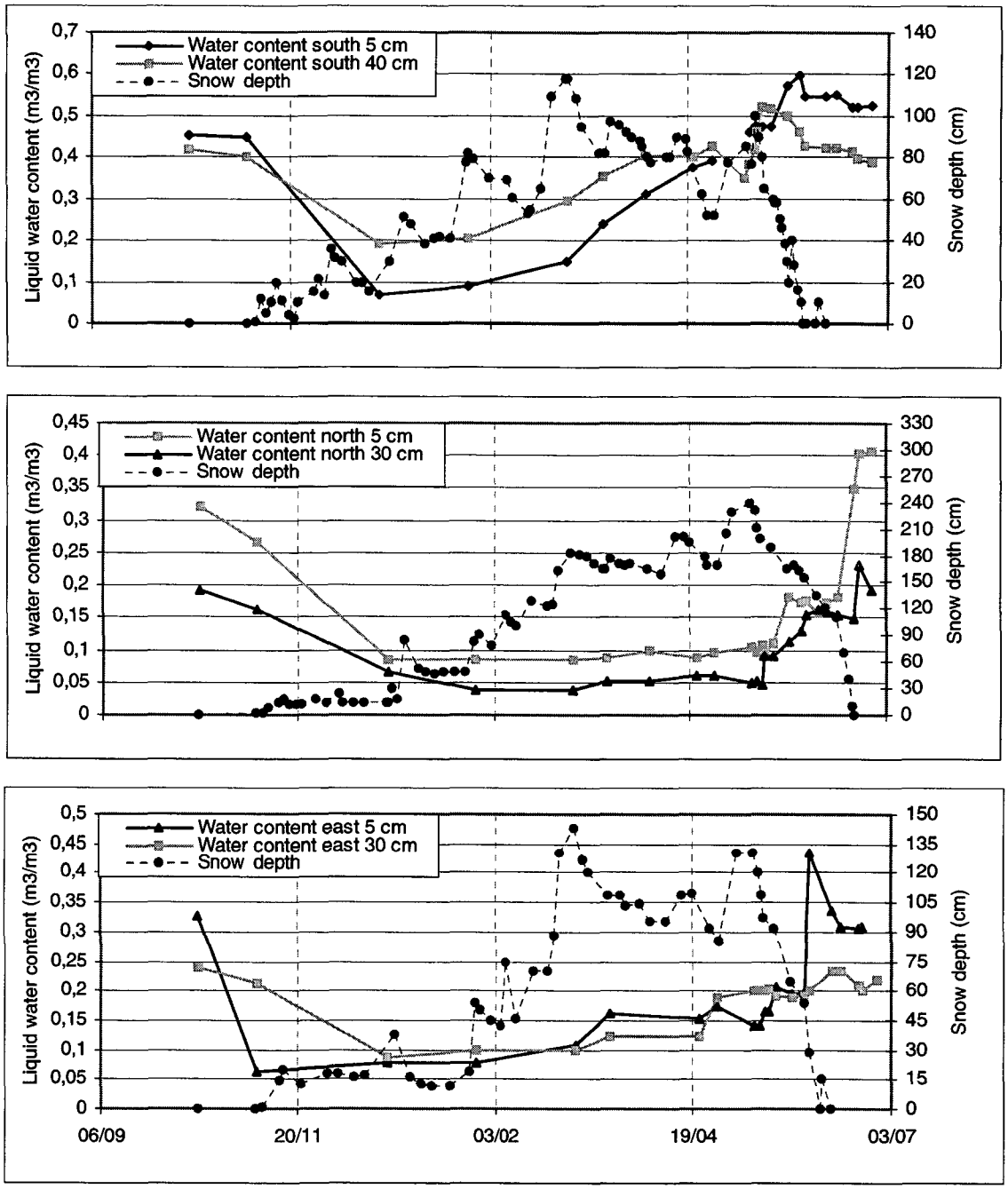

Figure 6.9: Liquid water content at a depth of 5 and 30 cm and snow depth for the south (a), north (b) and east site (c) at Gd St Bernard during winter 2001/2002.

on the south site. This extremely deep soil frost at the east plot was a consequence of the very thin snowpack, which remained until the end of January (<30 cm). At the south plot the max. frost depth was approximately 40 cm (the liquid water content was approx. 20% vol. in January (Figure 6.11) indicating that the soil did not freeze entirely at that depth).

Between February and March, the soil temperature increased at all depths and the soil profile became isothermal at the beginning of April. This temperature increase was accentuated in the south profile, as a light snowmelt took place between 28th January and 21st February. On the

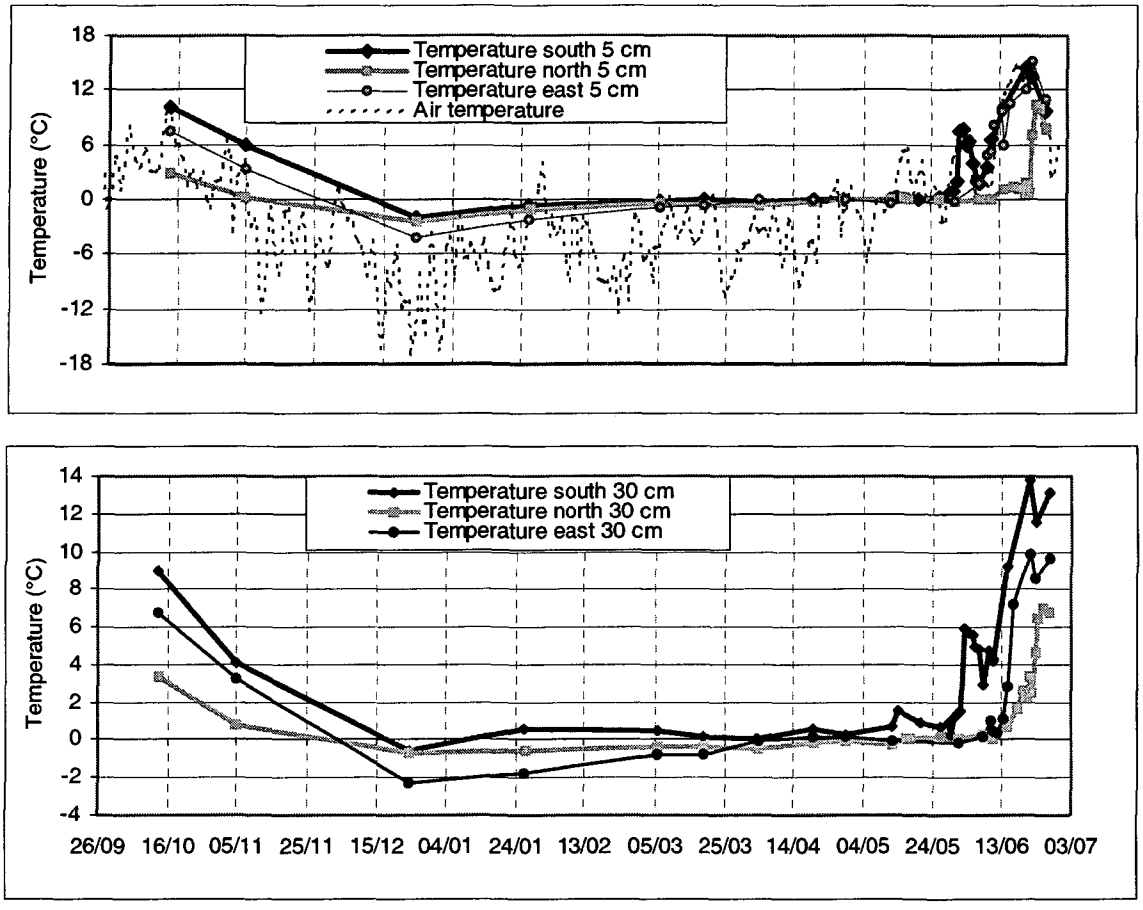

Figure 6.10: (a) Soil temperature at a depth of 5 cm and air temperature for the south, north and east plots at Gd St Bernard in 2001/2002. (b) Soil temperature at a depth of 30 cm.

south and east plots, four main snowmelt periods were recorded, one in March (8th to 21st), two in April (1st to 7th and 21st to 30th) and one in May (14th to 30th) (Figure 6.12), increasing the liquid water content continuously at each depth. Saturation was reached in May. On the north plot, however, the meltwater did not reach the soil surface before mid-May (Figure 6.9), due on the one hand to the larger retention capacity of the snowpack (the snow cover was three times deeper on the north site than on the south site), and on the other hand to reduced snowmelt. On the south plot, lateral runoff made up to 46% of total runoff during the melt periods, 2% was stored in the soil, and 52% of meltwater was collected by the lysimeter (Figure 6.12).

The first snowmelt event between 28th January and 12th February was exceptional, as usually at this period air temperatures are always below 0°C. A mean daily air temperature of 4°C was measured on 30th January, and due to the shallow snowpack (75 cm), meltwater reached the soil surface. Similar to Hannigalp, a basal ice sheet was formed caused by the latent heat transfer between the wet snowpack and the frozen soil. No discharge was measured. We note that the mean daily air temperature has to be far above freezing point to create any significant melting in January, as the solar radiation is low due to the relatively low position of the sun in the sky at that time of the year.

During the second snowmelt event in March, soil infiltration was strongly reduced by the combined effect of the basal ice sheet and the still significant pore ice content at that time, and

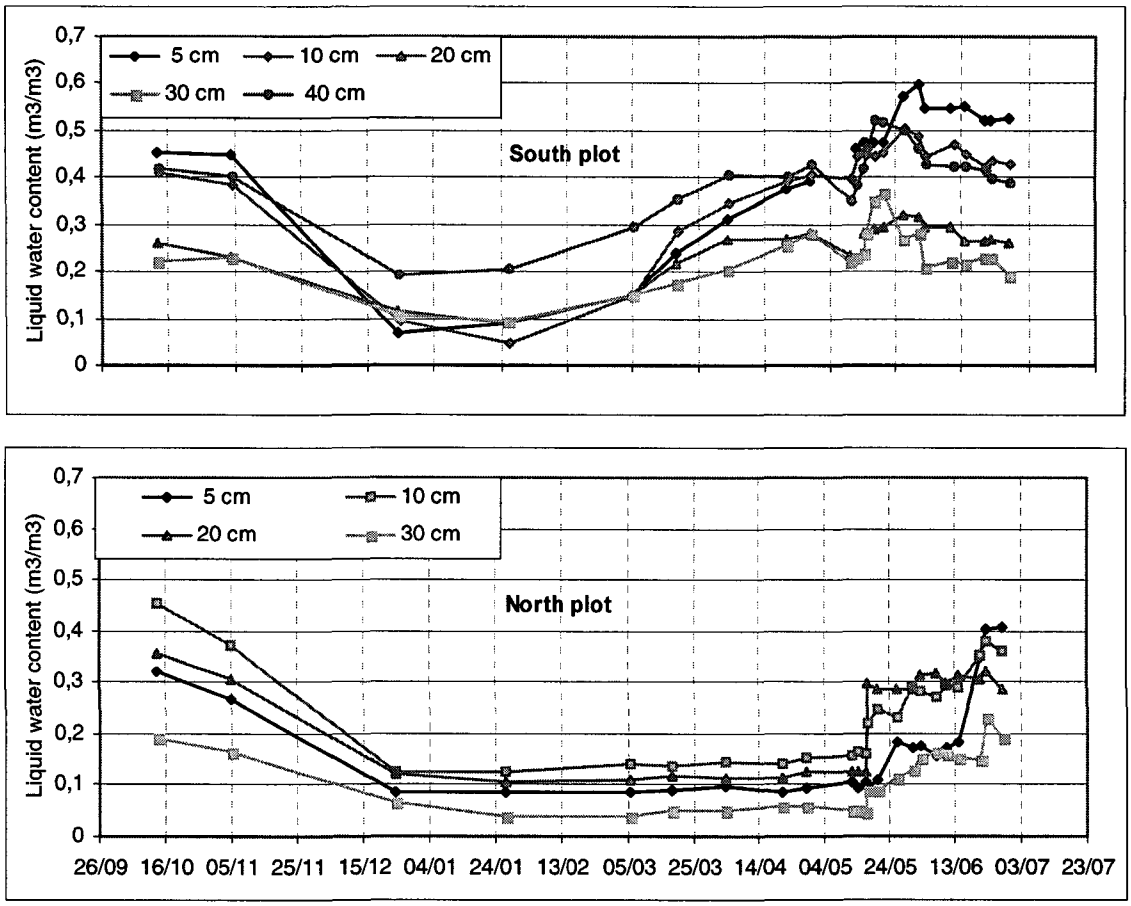

Figure 6.11: Soil liquid water content for the south (a) and north plot (b) at Gd St Bernard during winter 2001/ 2002.

considerable lateral runoff took place (41% of total snow water discharge).

The third snowmelt took place in early April, when 50 mm SWE melted in one week. Surprisingly, lateral runoff made up only 30% of the melted snow, denoting a probable early alteration to the basal ice sheet. The next snowmelt event at the end of April was more intense (100 mm of SWE in 9 days). The additional meltwater ran off mainly as lateral flow, which made up 57% of total discharge. During the final snowmelt, the basal ice was spoiled, and, between the 15th and the 30th April, lateral runoff was reduced to 40% of total discharge, despite the intense melting due to warm weather (average daily air temperature 2.1°C).

In contrast to the north and east plots, hardly any pore ice remained on the south plot at snowmelt. This statement is based on the change of the liquid water content during the final snowmelt between both years examined (Figure 6.7 and Figure 6.11). It shows that the upper 5 cm were still frozen at snowmelt (15% vol. of pore ice), whereas most pore ice thawed below that depth. At the south plot, enough heat was stored in the ground during the summer to enable considerable underneath heat flux towards the frozen layer in winter. The strong ice melting may also have been caused by soil warming from adjacent rock formations. These rocks covered an area of 10 m^2 and were free of snow at the end of February. In spring they were heated during the day, melting the surrounding snow, and possibly affecting the underneath pore ice. This supposition was strengthened by the fact that the entire frozen profile melted at the same time,

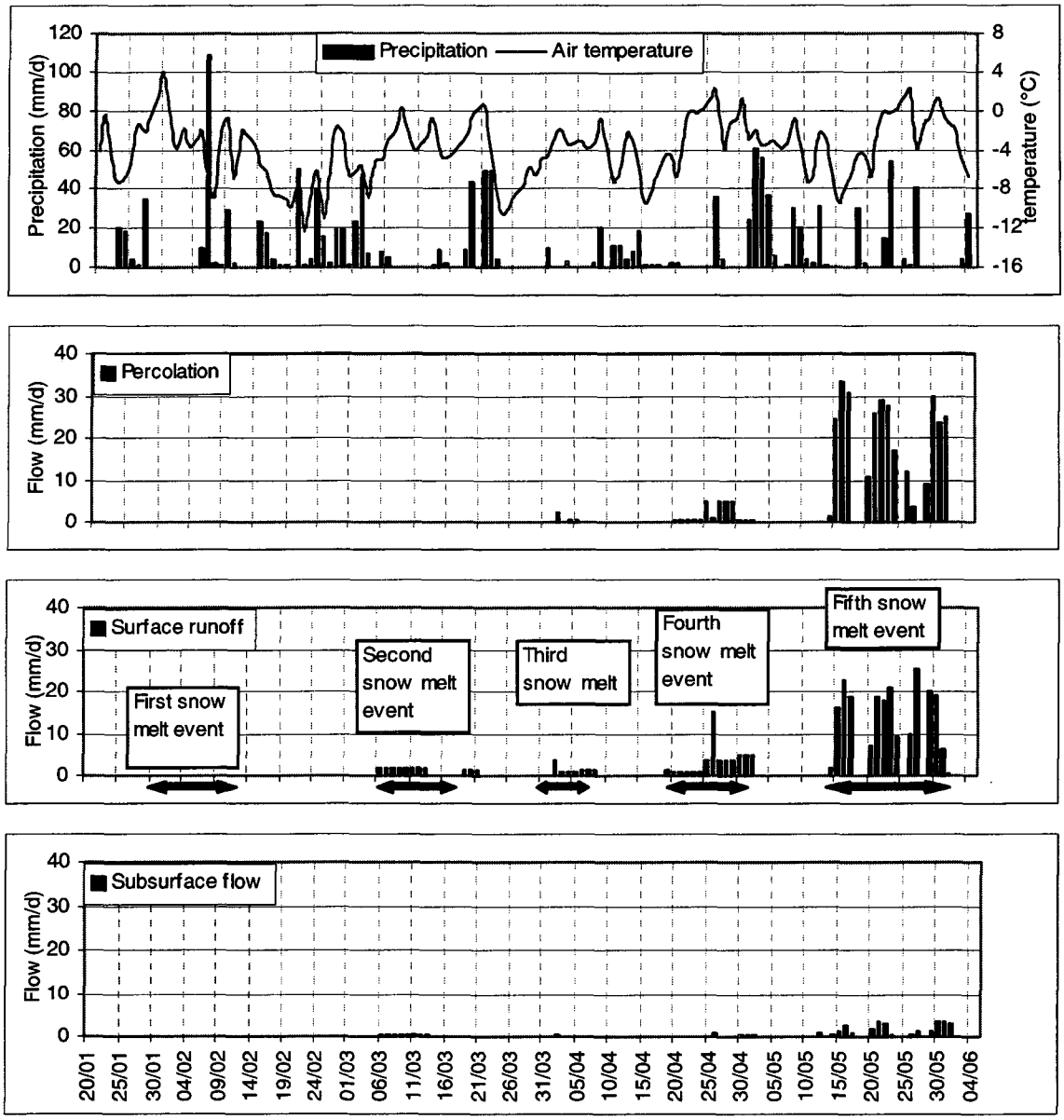

Figure 6.12: (a) Air temperature and precipitation measured at Gd St Bernard during snowmelt 2001/2002. Daily measured discharge at the south plot: percolation (b), surface flow (c) and subsurface flow (d). Discharge rates are expressed per unit area of the runoff plot.

indicating probable lateral soil heating. On the north and east plots the ice content hardly changed until the end of the melt period. We may hence assume that a higher proportion of melt water runoff was lateral flow on the east and north plots than on the south plot.

If we compare these results to those from Hannigalp, we see that the main differences in the hydrological behaviour was due to differences in steepness and snowmelt intensity, rather than textural changes, as at both sites the infiltration capacity was approx. similar. However, the texture had a dominant influence on the thermal processes. The thermal properties of the soil control the heat diffusion in the soil. At Gd St Bernard, we would expect a fast soil freezing, due to the presence of conductive slate stones. At the other site, the soil retention capacity, and hence the amount of latent heat, depends on the texture. The soil retention capacity was particularly

important at Gd St Bernard south site (approx. 40% vol.) and freezing was slowed down by the high water content. In contrast at Hannigalp, the dry sandy soil enabled a fast freezing.

To sum up, the soil frost influenced markedly the water balance at Gd St Bernard. The lateral runoff increased by 35% on the south plot between both winters examined. The spatial frost extent was controlled by the snow depth at the onset of the winter and the exposure. Depending on the snow depth, the frozen layer was more or less deep. In winter, the part of the frozen layer thawed due to underneath heating. Thawing was more pronounced at the south plot, as more heat was stored by the soil.

6.3. CLASSIFICATION OF SNOWMELT EVENTS

In the next part, we will discuss quantitatively, by means of water balance, the hydrological response of the different snowmelt events during each winter. We classify into winter, spring, final, and late snowmelt events and examine the influence of soil frost on the meltwater circulation for each case. We illustrate the different melt events with examples from Hannigalp and Gd St Bernard.

An estimation of the water balance for both locations was carried out to assess the significance of the various pathways of the meltwater and to compare the estimated percolation flux with the measured discharge. The following equation was used, with q_{input} given by eq. 6.2 side and q_{output} by eq. 6.3 (see also Figure 6.13):

$$q_{input} = q_{output} \tag{6.1}$$

$$q_{input} = q_{prec} + \Delta V_{snow} \tag{6.2}$$

$$q_{output} = q_{sub} + q_{perc} + q_{surf} + q_{ssf} + \Delta V_{soil} \tag{6.3}$$

with: q_{input} : water input,
q_{output} : water output,
q_{prec} : precipitation,
ΔV_{snow} : change in snowpack water storage,
q_{sub} : sublimation from the snowpack,
q_{perc} : percolation flux,
q_{surf} : surface runoff,
q_{ssf} : subsurface flow,
ΔV_{soil} : change in soil water storage.

The flux q_{prec} was measured with an accuracy of approximately 10% at Hannigalp. At Gd St Bernard the error on the precipitation measurements is large (estimated error 40%), as new snow was often blown away by the wind and serious discrepancies between measured precipitation and newly fallen snow were not uncommon. The change in the snow water storage ΔV_{snow} was calculated from snow depth and snow density measurements (error in the order of 20%). The sublimation, q_{sub} was calculated using the numerical model COUP (Jansson and Karlberg 2001), with an estimated error of 10%. ΔV_{soil} was estimated using soil water content measurements between 5 and 40 cm (estimated error 10%). Error on q_{surf} and q_{ssf} was low (1%), as the experimental field was isolated by a 5 cm thick soil edge (on both sides), and by a 50 cm deep trench (on the upper part of the field). The remaining percolation flux q_{perc} was treated as an unknown during the first winter, as the measurements from the lysimeter did not stand for

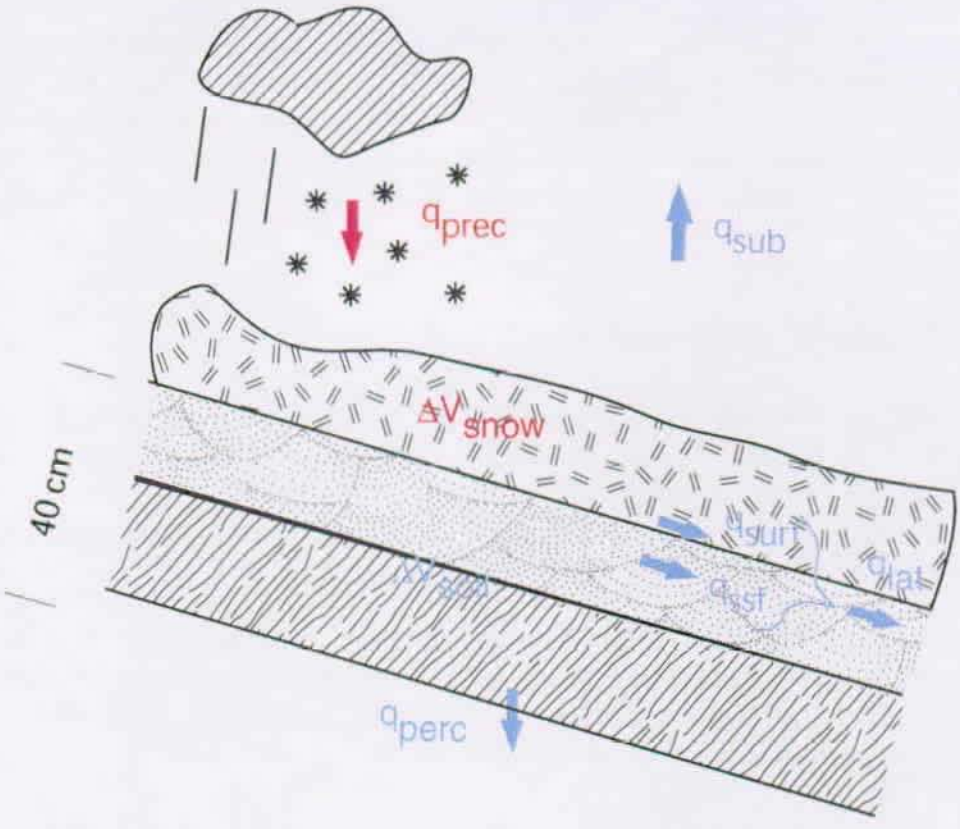

Figure 6.13: Water balance of the soil -snow system during a snowmelt event. Input flux are in red, output flux in blue.

the absolute discharge, but only for a fraction of it (open lysimeter)[1].

All water balance were within measurement errors. Results[2] are shown for each year in Figure 6.14 toFigure 6.17. In order to keep these graphics legible, surface and subsurface runoff are given as a single value, i.e. the lateral runoff: $\mathbf{q_{lat}=q_{surf}+q_{ssf}}$

1. Comparison between the calculated and measured deep percolation flux indicated that, at Hannigalp for winter 2000/2001, only 5% of the percolated water was collected by the lysimeter, due to the poor connection between the gravel and the sand. This value became higher when the profile was saturated, and lower under unsaturated condition, as under dry conditions the capillary barriers inhibit the melt-water from infiltrating into the artificial sand-gravel soil above the lysimeter (none-linear response of an open lysimeter (Ross 1990)). To establish the daily discharge graph in Figure 6.2, the restitution ratio was increased during warm days, when a restitution proportion calculated daily was used. The percentage of water collected by the lysimeter rose up to 20% during such days. The following winter, the seepage values were not readjusted as the lysimeter setup was improved in summer 2001 by filling the gap between the lysimeter and the soil and hence suppressing the capillary barrier. At Gd St Bernard, approximately 30% of the total meltwater was collected by the lysimeter.

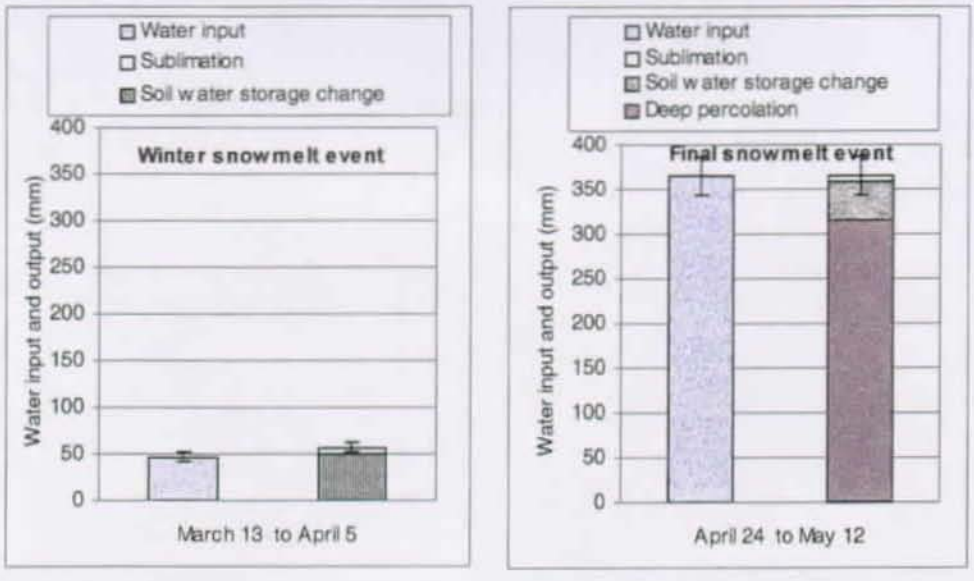

Figure 6.14: Water balance at Hannigalp during the two snowmelt events in winter 2000/2001. In left-hand columns the sum of the water input, $\mathbf{q}_{input}$ (snowpack water storage change + precipitation) is shown, while in right-hand columns the sum of the outputs (sublimation ($\mathbf{q}_{sub}$)+ percolation ($\mathbf{q}_{perc}$)+ lateral runoff ($\mathbf{q}_{lat}$) + soil water storage change ($\Delta \mathbf{V}_{soil}$)) is given.

Winter snowmelt events

Such snowmelt events were characterized by reduced snowmelt (less than 60 mm of SWE), and none-negligible water lost through sublimation (more than 10% of total input). The snowpack was still thick enough to inhibit refreezing of (soil-) infiltrated meltwater, even during very cold periods. The first snowmelt events at each location during winter 2000/2001 and the two first events for the next winter were typical winter snowmelt events.

During these melt periods, the water remained in the upper part of the soil (first snowmelt event 2001 and 2002 at both locations). Under frozen conditions, surface runoff was recorded after the first snowmelt event, as the soil infiltration capacity was reduced by refreezing of melt water in the frozen soil, and on the soil surface (second snowmelt 2002 at both locations).

The timing depended on the exposure and the altitude. In January 2002, no snowmelt was recorded at the protected site of Hannigalp, in spite of a very warm air temperature (2°C for several days). In contrast, on the south plot at Gd St Bernard, melting took place as early as January (first snowmelt event at Gd St Bernard winter 2001/2002), due to the strong solar radiation. On the north site at Gd St Bernard, a unique «winter snowmelt event» was reported for the two winters examined in April 2002. Melting was reduced and the meltwater was retained within the thick snowpack. It did not reach the soil surface.

2. An estimation of the water balance between 21st and 26th April at Hannigalp was carried out. We supposed the soil infiltration capacity to be constant and we used the measured deep percolation value between 26th and 30thMarch to estimate the amount of deep seepage water. We were hence able to estimate the lateral flux, which made up 37% of total meltwater runoff. This proportion should, however, be more important, as the soil water infiltration capacity increased with time.

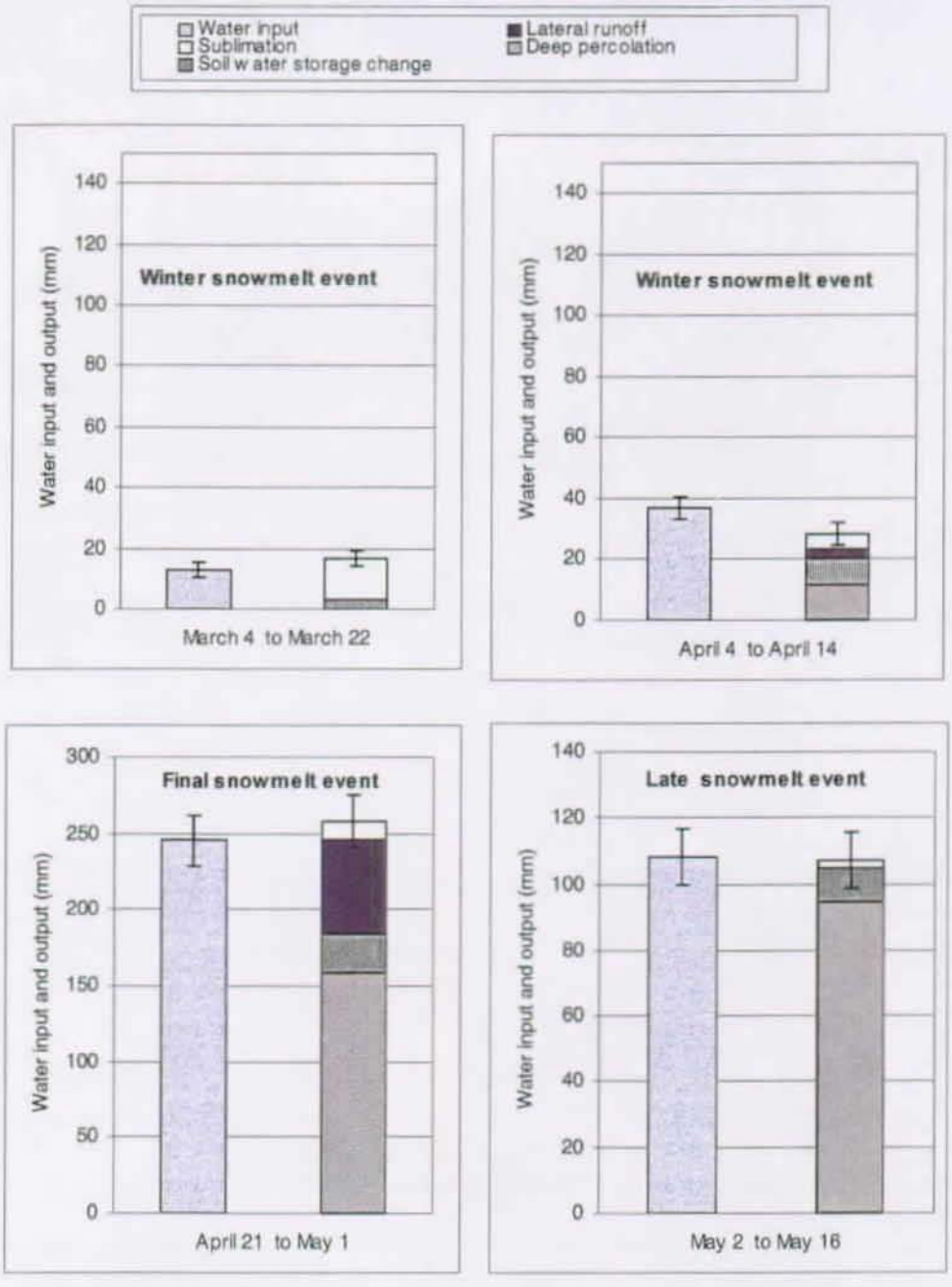

Figure 6.15: Water balance at Hannigalp during the four snowmelt events in winter 2001/2002. Note the differences in the abscissa scale.

Spring snowmelt events

Intense melting over a short period may reduce significantly the snow depth. If the soil is frozen, meltwater runs off mainly as lateral flow, as the pore-/basal ice is little altered. Such events were reported in April 2002 at the southerly and easterly exposed sites at Gd St Bernard. Melting intensity was approximately 9 mm/day for 10 days (third and fourth snowmelt event 2002), and 60% of total meltwater ran off as lateral flow during the fourth snowmelt event. In 2000/2001, no «spring snowmelt event» was recorded, due to poor weather conditions (cold and wet) in

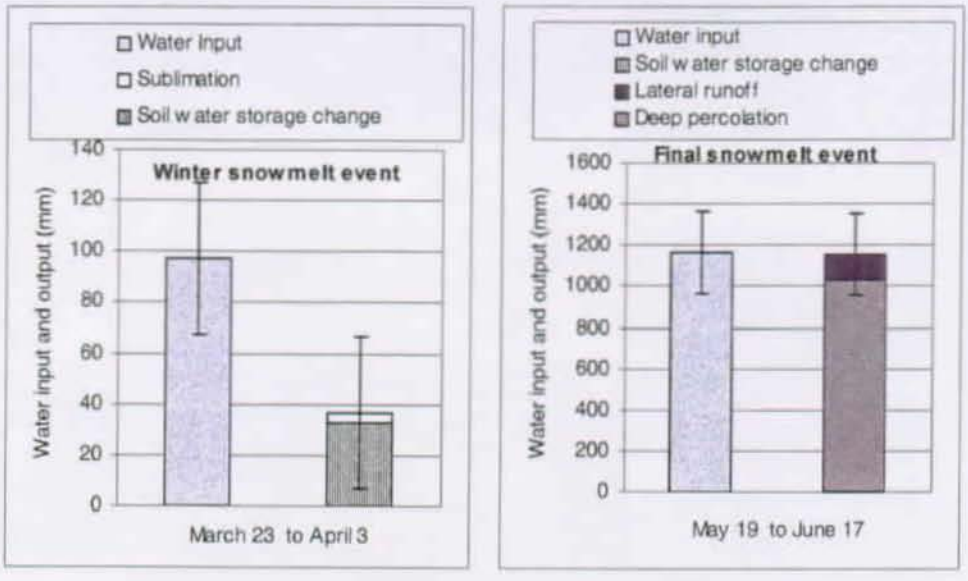

Figure 6.16: Water balance at Gd St Bernard during the two snowmelt events in winter 2000/2001. For the second snowmelt event, no sublimation is shown as it was negligible. Note the differences in the abscissa scale.

April 2001.

At Hannigalp and at the north site at Gd St Bernard such events are rare, as in March and May, the still low air temperature and the reduced solar radiation inhibited intense snowmelt. In May and June, continuous melting starts, as the air temperature remains mostly above freezing point, matching the onset of the final snowmelt.

Final snowmelt events

The final snowmelt takes place between end of April and early May at Hannigalp, and mid-May to July at Gd St Bernard. Duration depends on the snowpack thickness and the exposition. Whereas most of the winter snow precipitation melts in two to three weeks at Hannigalp, it takes between two to eight weeks at Gd St Bernard.

The high melting intensity creates surface runoff even under unsaturated conditions (second snowmelt event 2001). If the soil is still frozen, the lateral runoff increases sharply (fourth and fifth snowmelt event 2002 at Hannigalp and Gd St Bernard respectively). However, the melting of the pore/basal ice increases the soil infiltration capacity with time.

Late snowmelt events

Such an event was recorded at Hannigalp in May 2002, when huge snowfall occurred after the end of the snowmelt. In this case, the discharge was little affected by the remaining pore ice, as most ice melted when the ground was bare. However, we would expect that a higher percentage of pore ice (caused by wet conditions prior to freezing in autumn) would induce some non-negligible lateral runoff. Indeed, in May 2002, in spite of the low ice content, some slight subsurface runoff was measured during the melt period.

At Gd St Bernard, we would expect a significant increase of the lateral runoff on steep areas, as

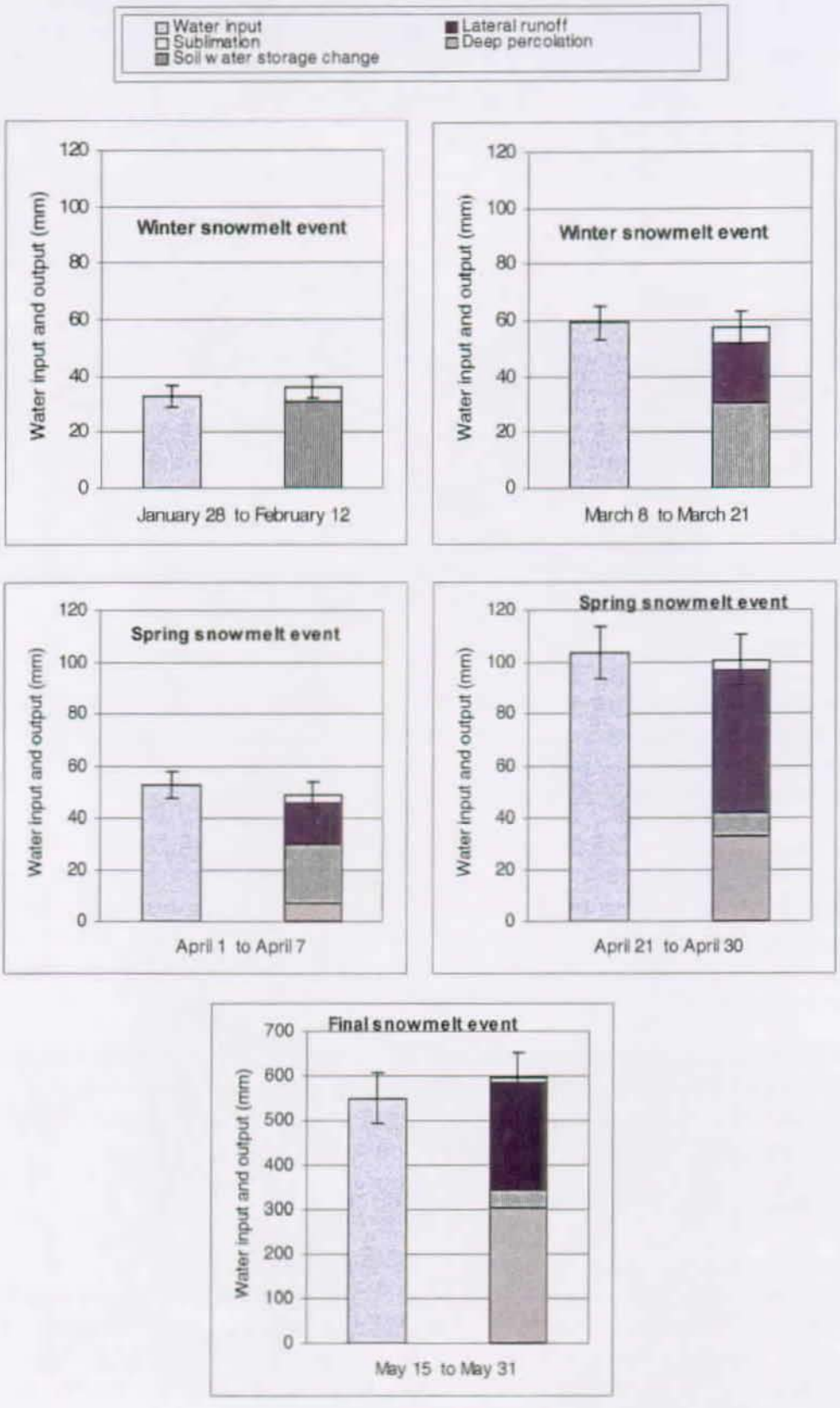

Figure 6.17: Water balance at Gd St Bernard during the five snowmelt events in winter 2001/2002.

the remaining pore ice would further reduce the already saturated unfrozen infiltration capacity.

We summarize the different snowmelt events' characteristics and timing in Table 6.1 and Table 6.2. From this classification we conclude that: (i) seasonal soil frost has hardly any effect on the melt water infiltration pathways during winter and late snowmelt events; (ii) seasonal soil frost affects the snowmelt runoff mainly during spring and final snowmelt events; (iii) because of the high and intensive snowmelt, the final snowmelt is essential for the groundwater recharge. The critical period for groundwater recharge lasts from April to July. This lengthy period is caused by the strong spatial and altitudinal variability in the snowmelt process.

Exposure and altitude	*Winter snowmelt event*	*Spring snowmelt event*	*Final snowmelt event*	*Snowmelt event after final snowmelt*
South / 2500 m	January-April	April	May-June	June
East / 2500 m	March to April	April	May-June	June
North/ 2500 m	April	-	May-July	-
Northeast /2100 m	March to April	-	April-May	May
Discharge frozen soil	Infiltration into the upper 40 cm	Significant lateral runoff due to the presence of an unaltered basal ice sheet	Reduced lateral runoff. Basal ice sheet is altered	Little lateral run-off, as basal ice sheet is inexistent
Discharge unfrozen soil	Infiltration into the upper 40 cm	Infiltration into the soil	Slight surface run-off if snowmelt intensity is high and slope steep	Slight surface run-off if snowmelt intensity is high and slope steep

Table 6.1: Timing of the different types of snowmelt events for four locations differing in their altitude and exposure. Discharge runoff characteristics for the four snowmelt events, under frozen and unfrozen soil conditions.

	Winter snowmelt event	*Spring snowmelt event*	*Final snowmelt event*	*Snowmelt event after final snowmelt*
Sublimation (% of total water loss of the snow-pack)	> 10	5-10	< 5	< 5
Water snowpack run-off (% of total water loss of the snowpack)	< 90	90 -95	> 95	> 95
Water snowpack run-off (mm/day)	< 5	5 -15	15-40	15-40
Soil infiltration frozen soil (% water snow-pack runoff)	60-100	40-70	60-75	80-100
Lateral runoff frozen soil(% water snow-pack runoff)	0-40	30-60	25-40	0-20
Soil infiltration frozen soil (% water snow-pack runoff)	100	100	90-100	90-100
Lateral runoff frozen soil(% water snow-pack runoff)	0	0	0-10	0-10

Table 6.2: Water balance characteristics for the four snowmelt events, under frozen and unfrozen soil conditions.

6.4. CONCLUSION

During two consecutive years we studied the different processes affecting the snowmelt in an alpine region at four sites, differing in their altitude, exposure and textural composition. The frost depth was inversely related to the snow depth in late autumn (November and December). Whereas the soil remained unfrozen during the snow-rich winter 2000/2001, the soil froze deeply at each location the following winter.

Variation in the pore ice content controlled the different parameters of the water balance. The surface runoff and subsurface flow increased by up to 30% under frozen conditions. The presence of a basal ice sheet was mainly responsible for this change. It acted as a barrier, inhibiting the melt water from infiltrating into the ground. During early snowmelt events, this barrier was particularly effective, as in spite of the low melt intensity, surface flow was recorded.

The snowmelt dynamic was closely related to the exposure and the altitude. In particular high solar radiation enabled snow melting even in January at high altitude locations like Gd St Bernard. Variations in the altitude and in the exposure also affected the physical state of the profile studied in winter. In particular, the underneath heating proved to be a dominant mechanism. At the southerly exposed plot at Gd St Bernard, in contrast to the other locations, most pore ice thawed during the frozen winter 2001/2002.

In conclusion, we summarize the main results of this study:

- despite the significant amount of precipitation in alpine regions, soil frost is present during specific winters. This soil frost may remain until the end of the winter and, when it does, influence the snowmelt runoff pathways (the lateral runoff increased by approx. 30% for the two investigated sites).
- for the development or absence of soil frost, the late autumnal and early winter meteorological weather conditions are decisive, as they affect the timing and thickness of the snow cover. In mid-winter, the snowpack is mostly thick enough to insulate the soil from outside and the weather conditions do not influence the soil frost depth extent any more.
- a frozen soil is not impervious; the amount of surface runoff depends on the building of a basal ice sheet and on the amount of soil moisture at the onset of the winter. Basal ice sheets are mostly encountered in Alaska or Antarctica. This study emphasized that this was also the case in alpine areas.
- hydraulic soil properties and steepness of the slope are the governing factors regulating the amount of lateral runoff under both frozen and unfrozen conditions. In particular, we measured approx. 10% lateral runoff during the unfrozen winter at the steep location of Gd St Bernard.
- seasonal soil frost affects the groundwater recharge mainly during spring and final snowmelt events. In particular, hardly any surface runoff was measured during winter snow melt events.
- differences in the altitude and the exposure determine the snowmelt and frost depth dynamic. While the soil frost depth remained almost unchanged on northerly exposed locations, most of the pore ice melted in spring at the south plot of Gd St Bernard.

7. DYE TRACER EXPERIMENT

7.1. INTRODUCTION

As reported by numerous studies, meltwater penetrates the soil using various paths, which are influenced by local factors, like the soil texture or the plant cover (Kane and Stein 1983, Engelmark 1984 and 1987, Baker and Spaans 1997). This spatial variability is particularly difficult to describe with local measurements (like TDR or neutron probe measurements). For this purpose, several studies were conducted, which demonstrated the potential of dye tracers to visualize water flow in different types of non-frozen agricultural soils (Flury et al. 1994, Forrer et al. 2000).

An additional governing factor affecting the infiltration capacity is the soil ice content. In the previous chapter, we demonstrated that ice affects the infiltration capacity of frozen soils. Pore ice has a blocking effect on the infiltration meltwater by reducing the available pore space. The residual liquid water between pore ice and particles contributes only marginally to the total flux and the meltwater infiltrates the soil mainly through larger, initially air-filled pores, separated from the solid matrix by the pore ice. To the author's knowledge no investigation has been reported to visualize and quantify *in situ* the different infiltration pathways in frozen soils. A dye tracer experiment was hence used as an investigation tool to survey these various infiltration pathways. As until now infiltration tests in frozen soils were only carried out in the laboratory (Stadler et al. 2000, Schlachter 2000), we compared the *in situ* results to those obtained from similar infiltration experiments in the laboratory.

The two main purposes of the tracer experiment were:

1. to observe the different flow pathways at snowmelt under frozen and unfrozen conditions,
2. to test a dye tracer method *in situ* in an alpine environment.

The image analysis procedure is explained in detail by Stähli et al. (sub.) This chapter summarizes the main results and discusses the different flow patterns observed under frozen and unfrozen conditions.

7.2. SOIL VISUALIZATION USING A DYE TRACER TECHNIQUE

7.2.1. IMAGE ANALYSIS

Two analysing methods exist depending on the type of tracer and the information needed. The Fluorescence Imaging Technique (a) results in concentration maps with a high spatial resolution and is used with fluorescence tracers. The stained method (b) is used with dye tracers and provides information on the spatial dye tracer distribution. The two methods are briefly explained below. For more information, see Stadler et al. (2000) and Stähli et al. (sub.).

(a) The method of Fluorescence Imaging consists in emitting light in the excitation spectrum of the fluorescent dye and by choosing the emission filter of the dye's emission spectrum. The thus resulting well-defined fluorescent signal is detected by a charge coupled device (CCD) camera. An advantage of the fluorescence imaging technique is that a good restitution of the tracer's

spatial concentration is achieved, which makes it possible to quantify the water infiltration. This method is used mainly in the laboratory, as this approach makes use of a specifically designed camera, which is difficult to install *in situ*, in particular when no motorised access is possible.

(b) A stained method may be used, where each pixel is either considered as stained or not stained. To be able to compare each picture, the average level of the colour channels is, in a first step, standardized to a reference brightness common for all profiles. A supervised classification procedure is used to separate the pixels stained with dye tracer from unstained profile pixels. In a last step, erroneously classified single pixels are eliminated and small gaps in connected stained areas are filled, by using the image analysis operations *erosion* and *dilation*. All these operations provide the depth distribution of the fraction of stained areas. However, the tracer concentration cannot be determined.

7.2.2. LABORATORY EXPERIMENTS

The laboratory tests were conducted for the Hannigalp soil only, on two soil columns of 25 cm in diameter and 60 cm in height. These soil columns were removed some 20 m south of the *in situ* tracer plot using steel cylinders. The cylinders were brought to the laboratory, where a number of measurements probes were inserted at different levels to monitor the water and heat balance inside the soil column (Figure 8.1). Physical soil properties, as well as boundary conditions and measurements set up during the irrigation are given in Table 7.1. Four

	Unfrozen column	*Frozen column*
Initial water content (% vol.)	10	35
Room temperature (°C)	+4	-4
Irrigation temperature (°C)	+4	+2
Irrigation intensity 1 (mm/hour)	5	7
Irrigation intensity 2 (mm/hour)	5	7
Irrigation time (hour)	6	6
Tracer	Brilliant Blue/ Sulfa-flavine	Brilliant Blue/ Sulfa-flavine
Solution concentration of Brilliant Blue FCF and Brilliant Sulfaflavine (g /l)	2	2
Thermistors/TDR depths	5, 20, 35, 45	5, 20, 35, 45

Table 7.1: Physical soil properties and initial boundary conditions of the laboratory dye tracer infiltration experiment.

infiltrations tests were carried out in the laboratory, on either a totally frozen (two irrigation tests) or an unfrozen (two irrigation tests) soil column. For the frozen soil column, the room temperature was set to -4°C. As soon as the soil was frozen, a sprinkler device was placed on the top of the column and the soil was irrigated during 6 hours. During the irrigation, the room temperature was set to 2°C. The soil was relatively wet at the onset of the freezing with an average liquid water content of 35% vol. For the unfrozen soil column, the soil was rather dry with a liquid water content of 10% vol. Irrigation intensity was similar for unfrozen and frozen columns and varied between 5 mm/hour and 7 mm/hour respectively for each irrigation test. Thermistors and TDR probes were inserted at four depths in each column and the soil column insulated by a box filled with cork crumbs. The tracers were the dye tracer Brilliant Blue CFC (colour index 42090, adsorption maximum 630 nm), which has been used in numerous soil physical studies before (see for example Forrer et al. 2000) and the fluorescent tracer Brilliant

Sulfaflavine (Aebi et al. 2001). Both tracers are quasi-conservative, none toxic and mobile in soil. At the end of the experiment, the room temperature was set to -8°C and all columns were frozen. Finally, they were sawed with a diamond slitting wheel, in an initial step horizontally at a depth of 30 cm and then 4 vertical cuts were produced. Pictures were taken from each sectioned column with a digital camera (Nikon Coolpix 990) and with a cooled CCD camera, and analysed using the stained method and the Fluorescence Imaging.

7.2.3. FIELD EXPERIMENTS

7.2.3.1. HANNIGALP

To complement these measurements, a tracer test was undertaken. Brilliant Blue was applied at the beginning of the winter. In the first winter non-dissolved Brilliant Blue was applied on 10 cm snow by manually scattering the tracer over the snowpack. The amount of applied tracer is given in Appendix B. To prevent loss of the non-dissolved tracer, a further 10 cm of snow were used to cover the tracer. During the snowmelt, several soil profiles were excavated and the infiltration pattern was determined by means of image analysis. To be able to compare results, the tracer application had to be as close as possible to the experimental setup and was set two metres to the north of it. The tracer application plot (or tracer plot) was divided into three sub-areas, each of it having a surface of 2.4 m^2. Infiltration patterns were investigated at the onset, during and after the snowmelt.

In the second winter, non-dissolved Brilliant Blue was scattered on the soil surface prior to the first snowfall. A more homogeneous distribution of the tracer could therefore be achieved, as all parts of the plot were easily accessible (no snow). To protect the tracer from possible rain, the tracer plot was covered with a plastic sheet. The sheet was removed in mid-December when the soil was frozen and the tracer was covered with 5 cm snow. During snowmelt, the same procedure was carried out as in the previous year. The tracer plot was divided into three sub-areas, each of it having a surface of 1.3 m^2.

During the spring snowmelt, we returned to the sites and excavated several vertical profiles on the tracer plots, starting at the onset of the snowmelt and finishing shortly after the complete melt of the snow. For each date, we excavated 2 to 4 profiles. Finally, each profile was photographed using a digital camera (Nikon Coolpix 990) at a pixel resolution of less than 1.5 mm and the pictures were analysed using the stained method.

7.2.3.2. GD ST BERNARD

The tracer application site was located forty metres to the west of the main site. The field had a width of 180 cm and a length of 480 cm and was divided into three sub-areas to be able to make measurements during three different time periods. To measure the effect of lateral diffusion, tracer application was not made on the entire width but only on a 50 cm strip. At Gd St Bernard, the tracer experiment was carried out during the first winter only.

7.3. RESULTS

7.3.1. HANNIGALP

7.3.1.1. COLD CHAMBER EXPERIMENT

The depth profiles of the four infiltration tests are shown in Figure 7.1. When the soil stayed unfrozen, the water infiltrated to a depth of approximately 25 cm during both irrigations. For the frozen soil, only the upper 5 cm were stained with dye tracer. However, caution has to be used in the interpretation, as water probably infiltrated the soil column along the inner side of the columns and entered the soil horizontally at the location where the TDR probe were inserted. It explains for example why a single dye tracer spot was visualized at a depth of 18 cm for the frozen experiment.

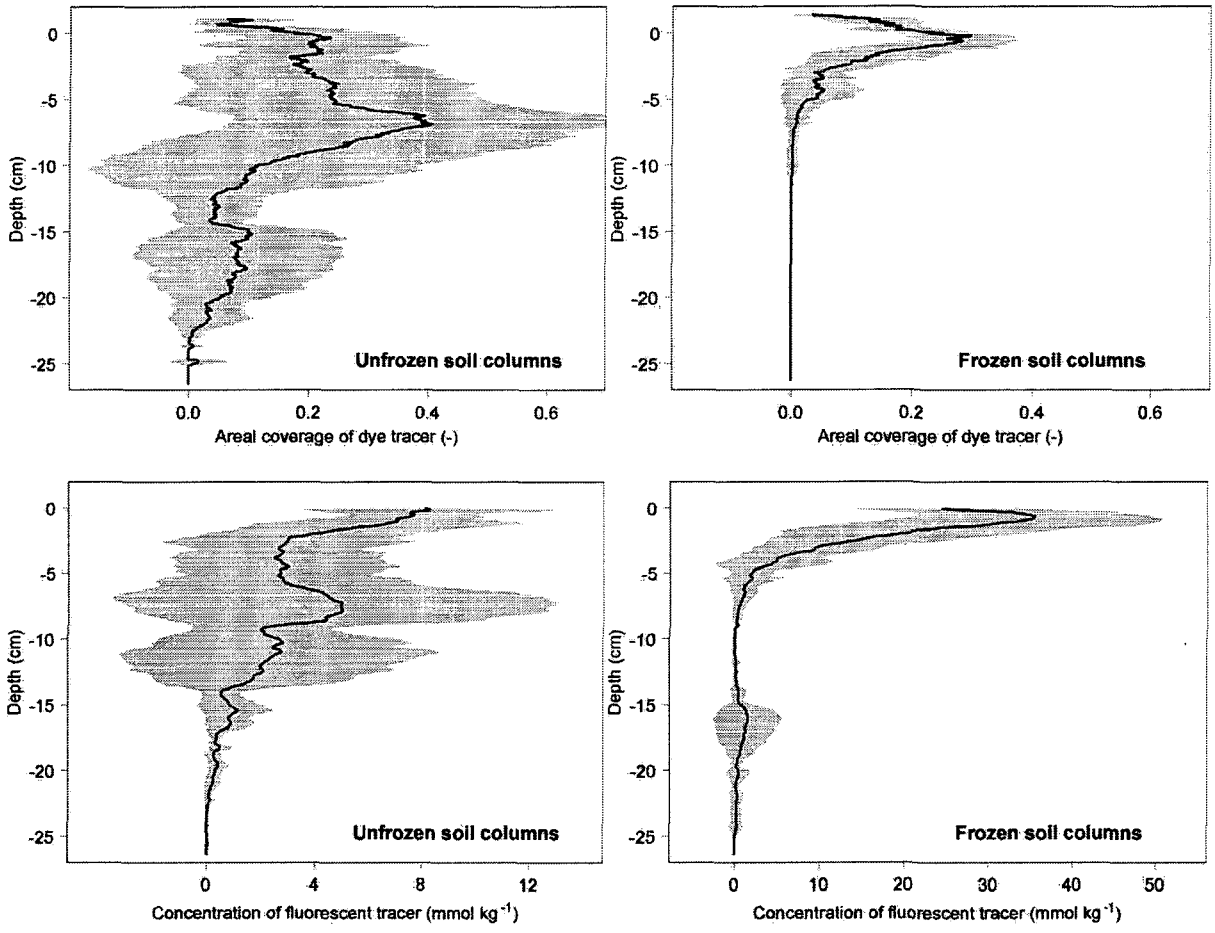

Figure 7.1: Depth profile of areal coverage of pixel stained with the dye tracer Brilliant Blue on top. Depth profile of concentration of the fluorescent tracer Brilliant Sulfaflavine on bottom. Mean and standard deviation for unfrozen (left) and frozen (right) soil columns.

The stained water flow paths observed in the unfrozen column showed a pronounced heterogeneous pattern. To illustrate this variability between the different cross sections, mean depth and standard deviations is shown in Figure 7.1. For the most part, the standard deviation was large. As noted from *in situ* observations, the presence of macropores (roots, ants channel)

(Photo 7.1) and the soil water repellency (see next chapter) were the probable causes for this variability. We believe that the dye tracer infiltrated the upper 10 cm of soil using mainly preferential flow paths (Photo 6.1 b)). It explains why the dye tracer areal coverage increased with greater depth in the upper 10 cm (values varied between 0.2 at a depth of 5 cm to 0.4 at a depth of 9 cm), whereas below that, the tracer was dispersed, as the root density diminished and the hydrophobicity of the soil disappeared. The concentration profile from the fluorescent tracer showed a different picture. Most of the tracer remained in the uppermost 5 cm and the concentration steadily decreased with greater depth.

Photo 7.1: Preferential flow along ants channel at Hannigalp in spring 2001.

For the frozen case, the infiltration patterns were very uniform. All cuts showed an accumulation of the stained water between 5 and 10 cm, and from the concentration profile, the stained water remained mainly at the soil surface. The water did not go beyond a depth of 10 cm. The high soil ice content reduced markedly the soil infiltration capacity. As a consequence, the dye tracer was not able to infiltrate deeply into the soil. In contrast to the unfrozen irrigation, the areal coverage was highest at the soil surface and steadily decreased with greater depth. This may be a result of reduced soil water repellency, as the soil matrix was surrounded by pore ice.

7.3.1.2. FIELD EXPERIMENT

Results for both winters are shown in Figure 7.2. No more than 50% of the uppermost soil layers were pervaded in the winter 2000/2001. During that first winter (without soil frost), we did not notice any indication for impeded water flow at any depth. Towards the end of the snowmelt the stained infiltration front penetrated further down in the profile. Distinct preferential flow fingers were formed at the soil surface and led down to the coarser soil layer at 40-80 cm, just above the bedrock, where the water was able to spread (Photo 6.1).

In the second winter (with massive soil frost down to a depth of 50 cm), the first snowmelt produced a slightly different infiltration pattern: the stained water concentrated in the top 25 cm, impeded by the underlying frozen soil layer (Photo 6.2 a)). However, in the course of the spring, the stained water percolated downwards although the soil frost persisted at the end of the snowmelt (Photo 6.2 b) to d)). The areal coverage of the stained water was close to unity in the

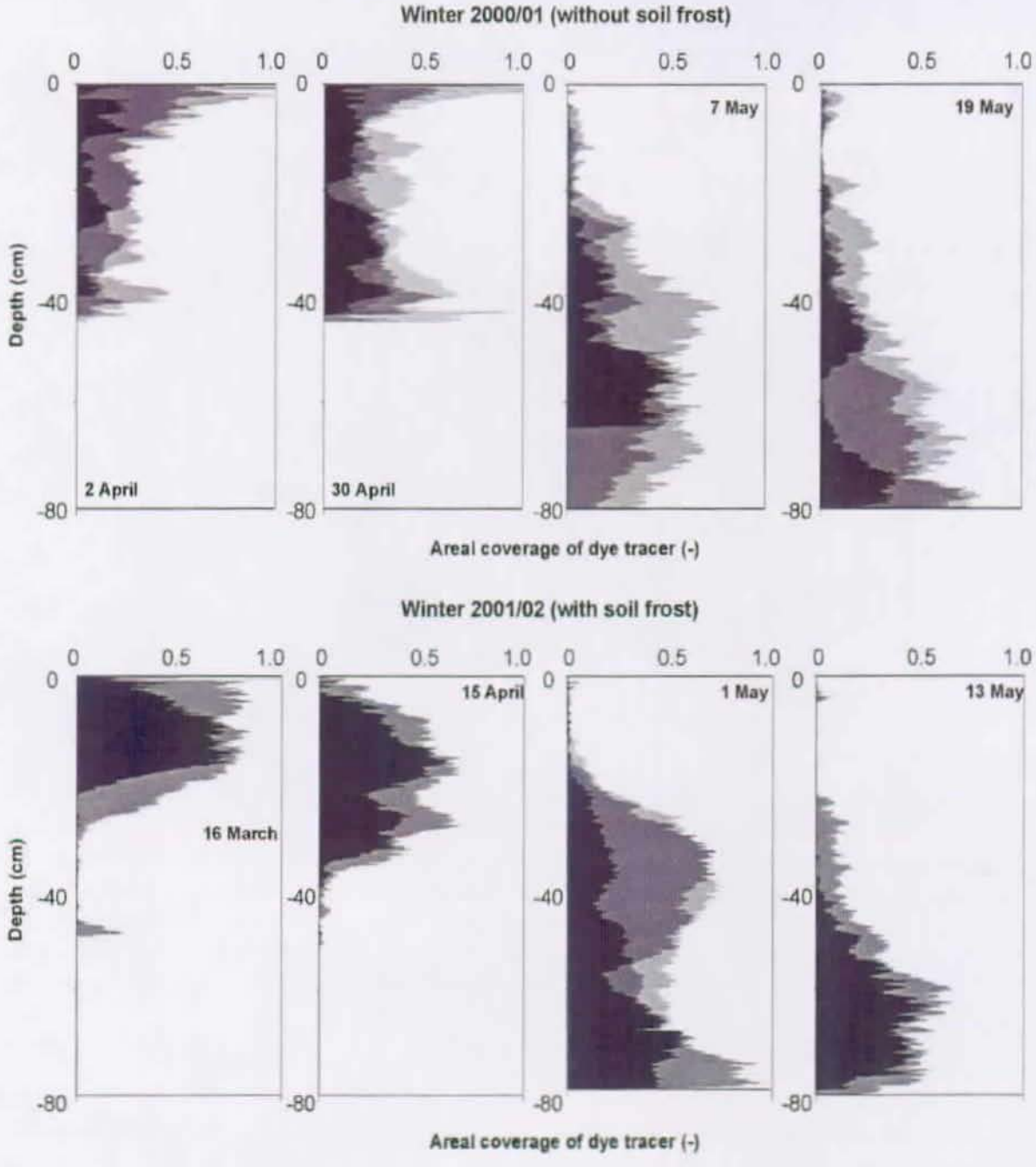

Figure 7.2: Eight depth profiles of areal coverage of dye tracer excavated during snowmelt 2001 and 2002 at Hannigalp. On each graphic, different profiles for the same date are stacked.

top soil, due to the fact that the hydrophobicity was probably restrained by the pore ice. Nevertheless, we observed some preferential flow paths formed in the upper part of the profile, in areas where excessive pore ice was present, inhibiting the infiltrating water to further penetrate (Photo 6.2 b)).

Although the stained profiles clearly showed considerable infiltration and percolation through the frozen soil, we also discovered considerable amounts of stained water 10 to 20 m downslope

of the experimental site originating from lateral surface runoff. A closer examination confirmed that the thin ice layer on the soil surface had triggered that surface runoff. With our tracer experiment we were able to visualize this layer in spite of its relatively thin (< 5cm) extent (Photo 7.2).

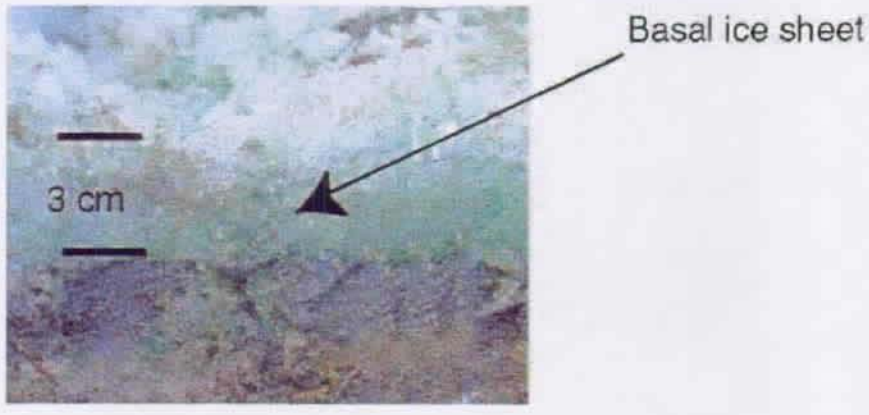

Photo 7.2: In spring 2002, a thin ice sheet formed on the soil surface.

A close comparison between the first melt event of each winter examined and the laboratory irrigation tests revealed that the infiltration profiles were very similar for both experiments. Relevant heterogeneity in the infiltration flow pathways was observed in the laboratory and *in situ*. The only difference was noted in the maximum dye tracer infiltration depth when the soil was frozen. Meltwater infiltrated much more deeply *in situ* than in the laboratory. The main reason is to be found in the differences in the pore ice content. At Hannigalp this value was approximately 20% vol., whereas it increased to 35% vol. in the soil column experiment.

7.3.2. GD ST BERNARD

Excavating soil profiles at the Gd St Bernard sit was problematic. The snowpack of nearly 3 m and the harsh winter climate provided unsuitable working conditions. A first attempt in early April remained unsuccessful due to the prevailing weather conditions. However, we succeeded in photographing several profiles on 14th May and on 1st June 2001, which are shown in Photo 6.3. In Figure 7.3 the depth profile of areal coverage of dye tracer is given.

In contrast to Hannigalp, the meltwater infiltrated over the entire profile into the ground (the areal coverage was closed to unity). The soil was not hydrophobic and the infiltration at the soil surface was not affected by the soil constitution. During the first snowmelt event, approximately 60 mm of water infiltrated into the ground. Preferential flow along the plant roots enabled the water to infiltrate rapidly into deeper regions and dye tracer was found down to a depth of 80 cm. The areal coverage of the dye tracer steadily diminished due to the decrease in the root density. On 1st June, the tracer plot was already free of snow (in contrast to the experimental site). The infiltration areal coverage profile showed an identical pattern with the previous one. Dye tracer was mainly encountered in the upper 20 cm, while a steep decrease in the surface coverage was noted below. This decrease was more pronounced than the decrease at the onset of the snowmelt In particular at a depth of 60 cm, no more stained water was detected. A

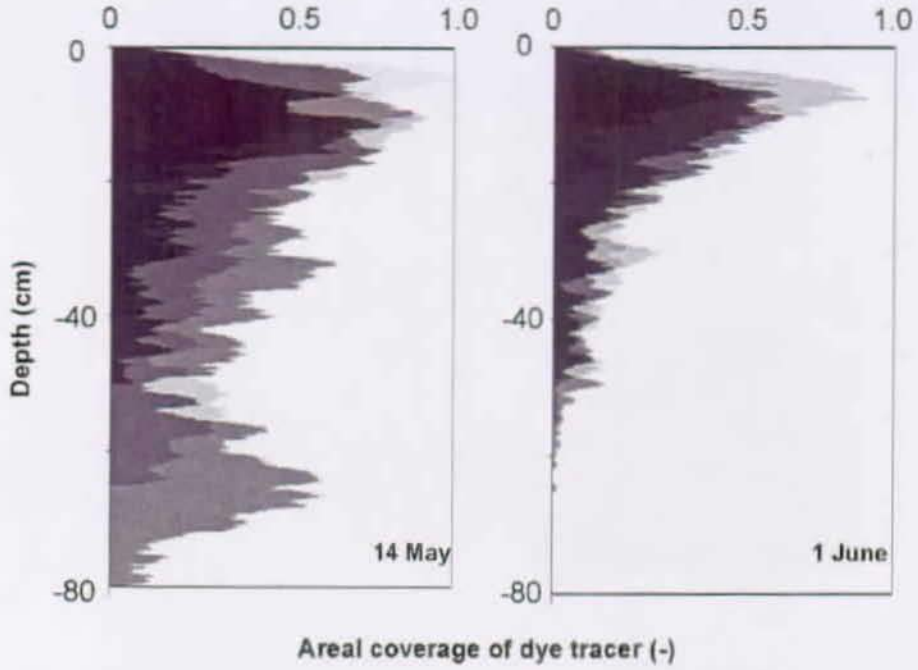

Figure 7.3: Depth profile of areal coverage of pixel stained with the dye tracer for two profiles excavated on 14th May (left) and 1st June (right) at Gd St Bernard.

possible explanation for this behaviour arises from the fact that the dye tracer plot was not isolated by a drain. Water was able to infiltrated into the tracer plot from above and the dye tracer may have been washed away by a possible subsurface flow.

7.4. DISCUSSION AND CONCLUDING REMARKS

The method developed was successful to show *in situ* the spatial patterns of water infiltration. The tracer method proved its reliability when used in extreme situations. It was possible to visualize infiltration pattern, regardless of the snow depth or the snowmelt period length. The dye tracer Brilliant Blue showed to be a good conservative tracer and was little affected by the daylight in spite of its being applied some six months before the onset of the snowmelt.

Nevertheless some critical points must be paid attention to:

- The timing of the tracer application is crucial. It should take place late enough to avoid a pre-winter rain or melt event, but not too late to minimize the disturbance of the snow cover. The amount of applied tracer should be large enough with respect to the expected snow water equivalent to ensure visibility in the soil throughout the melt season.
- The timing of the excavating date is also essential. Weather is variable in alpine regions, where sunny periods may alternate with snow precipitation and strong winds. Photographing becomes extremely difficult under such conditions. At Gd St Bernard, during snowfall or when strong winds were blowing, it was not possible to take photograph profiles without restriction.
- At Gd St Bernard, subsurface flow probably washed out the dye tracer below a depth of 20

cm. For a future *in situ* application of the dye tracer method, a complete isolation of the experimental plot is hence desirable, in particular when huge amounts of meltwater are present or if the experimental field is steep.

The method also showed that laboratory results are suitable to quantify infiltration, despite some disadvantage caused by boundary effects of the sidewalls, as well as measurements apparatus influencing the flow paths and the resulting concentration profiles.

Finally, the areal coverage depth profile resulting from this experience allowed us to differentiate the infiltration processes between Gd St Bernard and Hannigalp. In particular we found out that the water infiltrated over the entire soil profile at Gd St Bernard, whereas it flowed along preferential pathways at Hannigalp. It also confirmed the current hypothesis concerning infiltration into frozen and unfrozen soils: (i) a frozen soil layer does not totally prevent water infiltration, (ii) a basal ice sheet reduces the soil infiltration capacity, (iii) water infiltration in a water repellent soil occurs mainly trough preferential pathways, passing the active topsoil and dispersing below in areas where the hydrophobicity disappears.

8. SOIL HYDRAULIC PROPERTIES AT HANNIGALP

8.1. INTRODUCTION

After the first winter, we noted intriguing infiltration pathways at Hannigalp. The meltwater did not infiltrate as a planar front, but showed flow finger patterns. This was the starting point to discuss more in detail the soil hydraulic behaviour at Hannigalp. In this chapter we aim to give evidence of the soil hydrophobicity and to clarify which type of numerical model is best fitted to simulate the water flow processes at Hannigalp, with respect to the timing of the infiltrating waterfront. To this extent, we tested and compared two one-dimensional models differing in their flow domain, the first one, COUP (Jansson and Karlberg 2001), using the Richards equation to calculate the water flow, the second one, MACRO (Jarvis and Larsson 1990), using additionally gravitational flow in the macro flow domain.

8.2. MATERIALS AND METHODS

The definition of soil hydrophobicity, as well as the physical reasons behind the preferential flow patterns in water repellent soils were given in Chapter 2 ("Soil water repellency", page 15).

8.2.1. FIELD EXPERIMENT

Apart from the dye tracer experiment already described in Chapter 7 to visualize the water infiltration pathways, we carried out the commonly used water drop penetration time procedure (WDPT). The procedure involves placing a drop on the soil surface and measuring the infiltration time into the soil. If the infiltration time exceeds five seconds, the soil is water repellent. WDPT indicates the stability of the repellency. It measures the time required for liquid-solid angle contact Θ to change from a value greater than 90° to a value close to 90°. If the latter, the capillary rise $\boldsymbol{h}$ in eq. 2.7 becomes positive and water is no more rejected by the soil.

8.2.2. LABORATORY EXPERIMENT

In addition to the field experiment, we conducted two infiltration tests in the laboratory to measure the soil water characteristics curve (Figure 4.3) and to compare it to typical hydrophobic pF curves (Figure 2.4). Soil was removed from the Hannigalp site using steel cylinders, which were driven into the ground and dug out afterwards. The experimental setup is shown in Figure 8.1. The soil was set into a plexiglas cylinder with an inner diameter of 250 mm and a height of 600 mm. Eight TDR probes with a length of 120 mm were inserted horizontally, measuring automatically the unfrozen water content at 5, 20, 35 and 45 cm from the top. Additionally, four thermistors and three tensiometers were inserted to measured soil temperature and liquid water pressure at different depths (Table 8.1). The top of the column was uncovered and the bottom consisted of a copper plate. A Tectronix 1502B cable tester was used to perform measurements. Data were stored in a data logger. The time resolution was 10 minutes.

The irrigation intensity was 4.2 mm/h for both experiments and irrigation time was 12 and 3

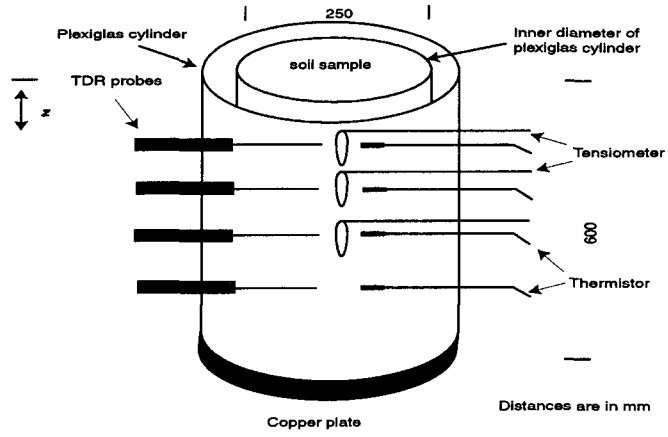

Figure 8.1: Sketch of the soil columns. The instrumental setup consisted of four thermistors, eight TDR probes and three tensiometers. Lengths are given in millimetre.

Profile depth z (cm)	*TDR probe*	*Thermometer*	*Tensiometer*
5	two	one	one
20	two	one	one
35	two	one	one
45	two	one	none

Table 8.1: Number of instrumental probes at different depths of the soil column.

hours respectively. During the irrigation the room temperature was set to 4°C and the soil column was unfrozen. Prior to both irrigations, the soil was dried out during 30 hours by using a dryer. Neither surface runoff nor drainage at the bottom of the soil profile was observed during both experiments.

8.2.3. MODEL DESCRIPTION

We simulate these irrigation experiments with the two numerical models COUP (Jansson and Karlberg 2001) and MACRO (Jarvis and Larsson 1990), which were described in Chapter 3.

8.3. RESULTS

8.3.1. FIELD EXPERIMENT

WDPT was carried out on several samples in the laboratory and *in situ*. The infiltration time varied between 10 and 30 seconds. Consequently, the soil may be considered as strongly water repellent (Bisdom et al. 1993).

8.3.2. MODEL SIMULATIONS

In this part, we tested two models differring in their flow domain. The main objective was to see which one best describes the water flux and, in particular, to see which type of flow (macro/ micro flow) is predominant. Hence, for both models, we carried out curve fitting on the conducted laboratory infiltration tests and compared the results obtained by both models one to the other. As interest was focused on the hydraulic properties of the soil, the soil temperatures were not simulated. The general procedure carried out in the calibration of the models is shown in Figure 8.2.

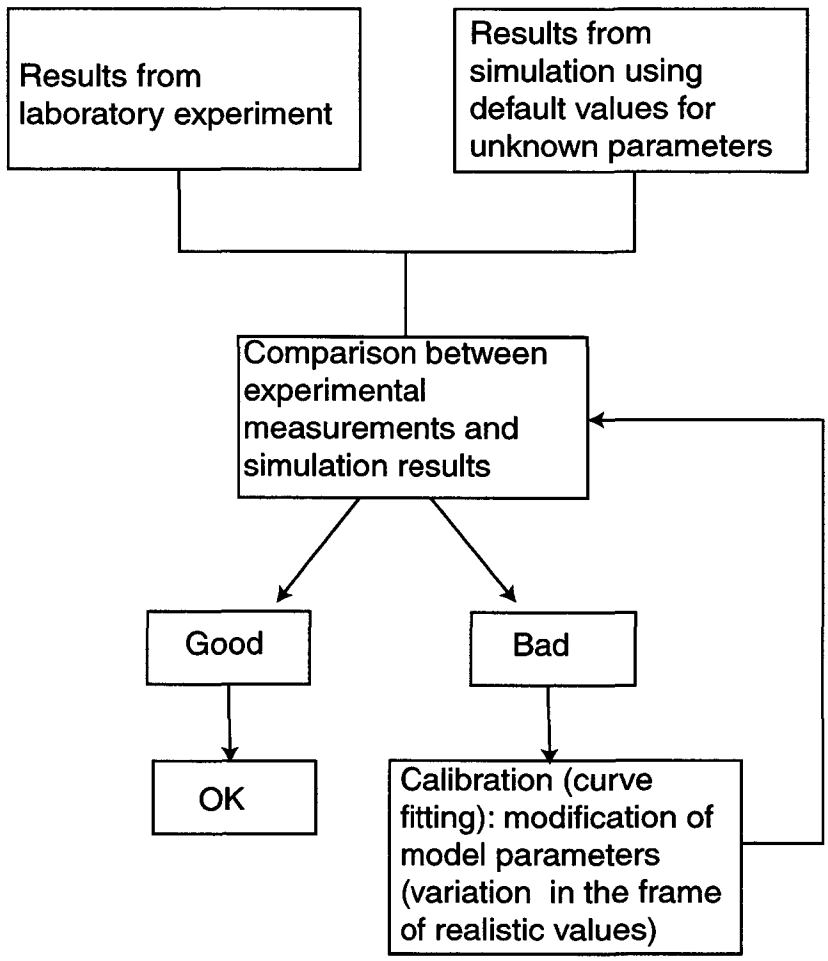

Figure 8.2: General procedure for the calibration of numerical models.

8.3.2.1. COUP MODEL

The soil water characteristics (Van Genuchten 1980) were determined in the laboratory (Table 4.3) and are shown in Table 8.2. The upper boundary is given by the irrigation flow, while, at the lower boundary, the liquid water pressure ψ was set to the atmospheric pressure.

The fitted parameters (i.e. the saturated conductivity k_{sat}, the maximum hysteresis parameter P_{phys} and the 4 hysteresis parameters a_A, a_B, a_C, a_C) are given in Table 8.3. The calibration of the hydraulic conductivity, k_{sat}, was constrained by *in situ* infiltration tests (see "Site description and physical properties", page 43). These tests showed that k_{sat} decreases with greater depth,

having a value ranging between 10^{-4} m/s and 10^{-5} m/s. The fitting of the hysteresis was more difficult. Indeed, the difference in the drainage and wetting function of a water repellent soil may be viewed as a strong hysteresis in the sorption-desorption curve. We integrated this hysteresis by adapting, in a first step, the three functions R_{age}, R_{shift}, R_{acc} (i.e the hysteresis parameters a_A, a_B, a_C, a_C) as well as the parameter expressing the maximal hysteresis effect P_{phy} (eq. 3.16 to eq. 3.20). However, despite numerous tests, we were not able to reproduce the strong hysteresis of Figure 4.3. The best results were achieved when a small hysteresis effect was included in the simulation (P_{phys}=0.1 in eq. 3.20, while other parameters were set to the default values). If higher values were introduced, simulation results were only marginally improved, but computing time became expensive. For example, by setting P_{phys} to 1 (which creates a lower hysteresis effect than the one measured) the model did not reach stability.

Soil layer	*Soil layer thickness (cm)*	m	n	α	θ_s *(% vol.)*	θ_r *(% vol.)*
1	7.5	0.265	1.36	0.02	55.1	2
2	5	0.226	1.30	0.025	54.55	2
3	5	0.187	1.23	0.03	54.1	2
4	5	0.209	1.27	0.03	52.45	2
5	5	0.231	1.3	0.035	50.8	2
6	5	0.231	1.3	0.035	50.8	2
7	5	0.231	1.3	0.035	50.8	2
8	5	0.231	1.3	0.035	50.8	2
9	5	0.231	1.3	0.035	50.8	2
10	5	0.231	1.3	0.035	50.8	2
11	5	0.231	1.3	0.035	50.8	2
12	2.5	0.231	1.3	0.035	50.8	2

Table 8.2: Soil water characteristics (van Genuchten 1980) used in the simulation (with COUP) of the unfrozen laboratory soil column irrigation.

Soil layer	*Sat. hydr. cond.* k_{sat} *(m/s)*	*Max. hyst. param.* P_{phys} *(-)*	a_A *(s^{-1})*	a_B *(pF-value)*	a_C *(pF-value)*	a_D *(-)*
1	4.5E-4	0.1	0.5	1.5	4	0.2
2	1.5E-4	0.1	0.5	1.5	4	0.2

Table 8.3: Calibration parameters in COUP used in the simulation of the unfrozen laboratory soil column irrigation.

3	1.2E-4	0.1	0.5	1.5	4	0.2
4	1.2E-4	0.1	0.5	1.5	4	0.2
5	9.6E-5	0.1	0.5	1.5	4	0.2
6	6.8E-5	0.1	0.5	1.5	4	0.2
7	5.8E-5	0.1	0.5	1.5	4	0.2
8	3.7E-5	0.1	0.5	1.5	4	0.2
9	1.26E-5	0.1	0.5	1.5	4	0.2
10	1.0E-5	0.1	0.5	1.5	4	0.2
11	1.0E-5	0.1	0.5	1.5	4	0.2
12	1.0E-5	0.1	0.5	1.5	4	0.2

Table 8.3: Calibration parameters in COUP used in the simulation of the unfrozen laboratory soil column irrigation.

Results for the second irrigation (soil moisture content and matric potential at a depth of 5 and 35 cm) are shown in Figure 8.3. Results at a depth of 20 and 45 cm and for the first simulation are similar and are given in Appendix C.

Measured soil water tensions were satisfactorily well reproduced by the model as long as the drying curve was considered. However, the model was unable to reproduce the fast, sharp and early increase in pressure. No improvement was achieved when the saturated conductivity was increased, as the better results in the wetting curve were compensated by bad results in the drying curve. This result suggests that the early change in the water pressure was due to preferential infiltration pathways, which cannot be reproduced by the COUP model. The fact that the drying curve of a water repellent soil is similar to that of a hydrophilic soil (see "Soil water repellency", page 15) may explain why the drying curve was well simulated by the model.

Calibration was made on the available pressure measurements. As a result, matching between measured and simulated soil moisture was less accurate. In particular, significant differences were registered when both initial water contents were compared. Nevertheless, the evolution between both curves, the simulated and the measured one, was similar and, by recovering the initial water content, the agreement was acceptable with differences of approx. 5% vol. between both drying curves.

8.3.2.2. MACRO MODEL

Boundary conditions are identical to those used for COUP. The parameterization of the soil's hydraulic properties in the micropore domain is given by Brooks and Corey (1964) (Table 4.3). The boundary soil water tension ψ_b was set equal to the Brooks and Corey air entry pressure. The hydraulic conductivity of the micropores, K_b (eq. 3.48), was estimated by using the ROSETTA model (Schaap et al. 2001). For the tortuosity n_t, the value suggested by Jarvis and Larsson (1990) was used.

The saturated hydraulic conductivity k_{sat}, the volumetric water content at the boundary between

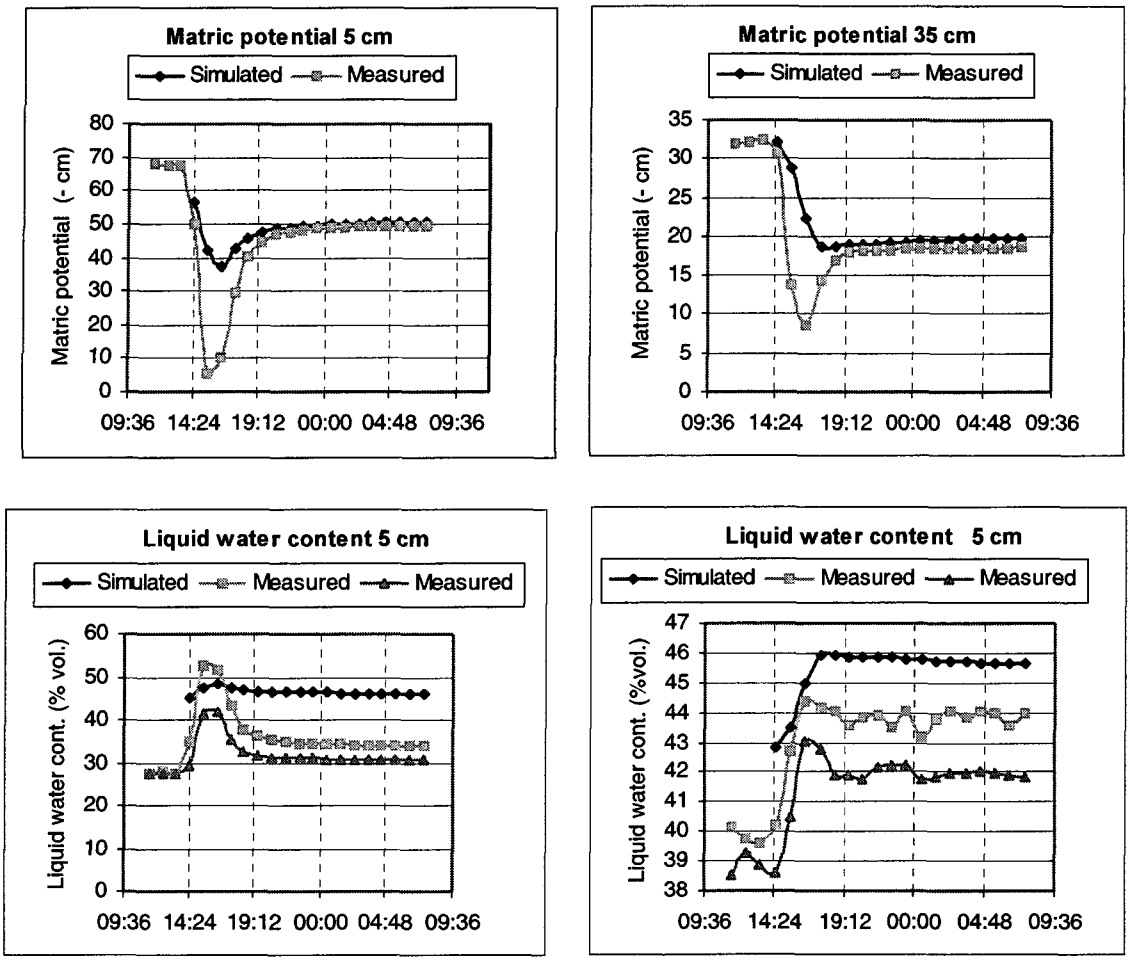

Figure 8.3: Comparison between simulated and measured matric potential and liquid water content at a depth of 5 and 35 cm. Simulation was carried out with COUP.

the two-flow domains, θ_b in eq. 3.46, and the effective diffusion path length, d in eq. 3.46, were taken as calibration parameters. In a first step, we estimated these three calibration parameters: the saturated hydraulic conductivity was taken similar to the one set for COUP (Table 8.3); θ_b was set 10% above the value of the water content at the end of the drying curve (Figure 8.3) in the upper 45 cm of the soil and closed to saturation beneath 45 cm, as no macropore flow was noted below this depth; and the diffusion path length, d was set equal to the default value given by Jarvis and Larsson (1990). Curve fitting was then carried out, by modifying initally d, then θ_b, and finally k_{sat}.

The different parameters are summarised in Table 8.5 and Table 8.5.

Soil layer	λ [-]	ψ_a [cm]	*Sat. water content* θ_s *(%vol.)*	θ_r *(% vol.)*	*Tortuosity parameter* n_t (-)	*Boundary soil water pressure,* ψ_b *(cm)*	*Boundary hydr. cond.* K_b *(m/s)*

Table 8.4: Soil water characteristics used in the simulation (with MACRO) of the unfrozen laboratory soil column irrigation. Brooks and Corey parameters were obtained from laboratory measurements (Table 4.3), the boundary hydraulic conductivity K_b was obtained by using the ROSETTA model (Shaap et al. 2001).

1	0.36	30	55.1	2	1	30	1.25 E-5
2	0.33	27.5	54.55	2	1	27.5	1.28 E-5
3	0.3	25	54.1	2	1	25	3.1 E-6
4	0.3	22.5	52.45	2	1	22.5	3.1 E-6
5	0.3	20	50.8	2	1	20	3.3 E-6
6	0.3	20	50.8	2	1	20	3.9 E-6
7	0.3	20	50.8	2	1	20	3.9 E-6
8	0.3	20	50.8	2	1	20	3.9 E-6
9	0.3	20	50.8	2	1	20	3.9 E-6
10	0.3	20	50.8	2	1	20	3.9 E-6
11	0.3	20	50.8	2	1	20	3.9 E-6
12	0.3	20	50.8	2	1	20	3.9 E-6

Table 8.4: Soil water characteristics used in the simulation (with MACRO) of the unfrozen laboratory soil column irrigation. Brooks and Corey parameters were obtained from laboratory measurements (Table 4.3), the boundary hydraulic conductivity K_b was obtained by using the ROSETTA model (Shaap et al. 2001).

Soil layer	*Soil layer thickness (cm)*	*Sat. hydr. cond.* k_{sat} *(m/s)*	*Sat. micropore wat. content* θ_b *(% vol.)*	*Diffusion path length,* d *(mm)*
1	7.5	4.7 E-4	47	5
2	5	3.9 E-4	46.55	5
3	5	3.3 E-4	44.1	5
4	5	2.8 E-4	42.45	5
5	5	2.2 E-4	40	5
6	5	1.7 E-4	40	5
7	5	1.1 E-4	43	5
8	5	1.0 E-4	46	5
9	5	1.0 E-4	49	5
10	5	1.0 E-4	50	5

Table 8.5: Calibration parameters in MACRO used in the simulation of the unfrozen laboratory soil column irrigation.

11	5	1.0 E-4	50	5
12	2.5	1.0 E-4	50	5

Table 8.5: Calibration parameters in MACRO used in the simulation of the unfrozen laboratory soil column irrigation.

Results at a depth of 5 and 35 cm are shown in Figure 8.4. Measurements at a depth of 20 and 45 cm are comparable and can be viewed in Appendix D.

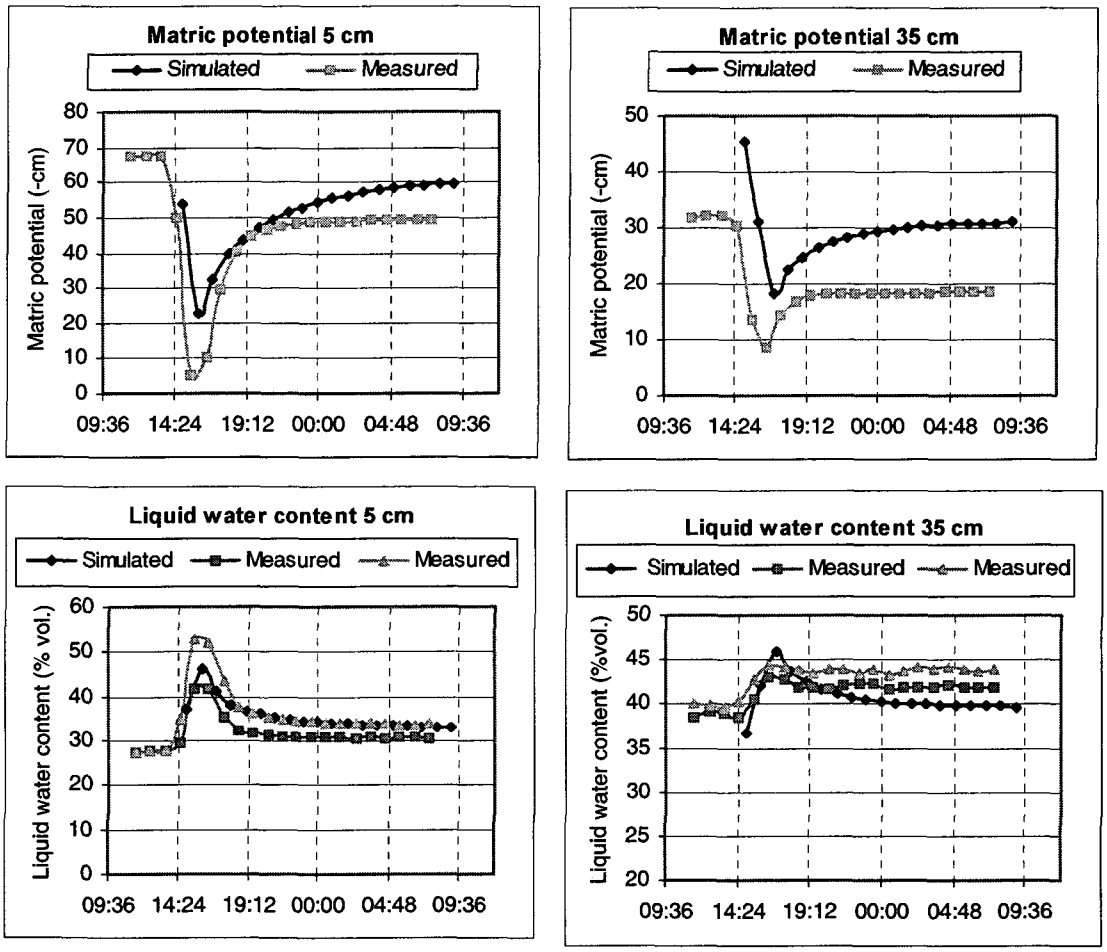

Figure 8.4: Comparison between simulated and measured matric potential (up) and liquid water content (down) at a depth of 5 and 35 cm. Simulation was carried out with MACRO.

In contrast to COUP, the model calibration for the liquid water content and the matric potential resulted in good agreement between simulation and measurements. The simulated dynamic of the infiltrating water was well reproduced, especially the timing and amplitude of the wetting curve. In particular, no shift was observed in the simulated imbibing front. The slight overprediction in the simulated matric potential is due to the fact that the calibration was mainly made on the liquid water content measurements.

As a result, the simulation results were markedly improved by using the MACRO model. It confirms that (a) the flow occurs mainly through preferential flow, and (b) the necessity to use

a two-flow domain model to adequately simulated the hydraulic process at Hannigalp.

8.4. DISCUSSION AND CONCLUSION

Water repellent soils are characterized by (i) a high WPDT, (ii) a specific sorption-desorption curve, and (iii) a high acidity and organic content (Miller and Wilkinson 1977). These different attributes were all recognized at Hannigalp. In particular the typical wetting and drying function for hydrophobic soils could well be reproduced by laboratory infiltration experiments, where at the imbibing front, matric potential was close to the atmospheric pressure.

A major consequence of hydrophobic soils is the ability to influence the water infiltration pathways (Hendrickx et al. 1993). Water is rejected by the organic upper soil layer, creating large variations in the soil water content, which induce preferential flow patterns, as water does not infiltrate as a planar wetting front. This could be verified *in situ* by the dye tracer experiment, but also in the laboratory, where adequate simulation results were obtained when a numerical model integrating preferential flow in his settings was used.

These results showed the difficulty to incorporate a hysteresis function in the water retention function of a one-dimensional model to simulate preferential flow. Models need to be further adapted (Nieber 1996). Ritsema and Dekker (2000) introduced a hysteresis function in a two-dimensional Richards flow model. They indicated which assumptions should be made on a two-flow domain model to be able to simulate hydrophobic soils. These assumptions, including stable flow above a critical water content value or a zero flux condition when the water contents drop below a critical level to allow the formation of perched water-table above the dry water repellent zone, were, however, mostly not taken into account by MACRO.

MACRO was not developed to simulate flux in water repellent soils, but predominantly to reproduce macropore flow along large apertures like roots or ants channels. Conceptually, the flow dynamic differs markedly in a macro-type soil and in a water repellent soil. In hydrophobic soils, preferential flow takes place under dry conditions and a critical water content has to be defined above which preferential flow disappears. In MACRO opposing assumptions are made. Water fills up, in a first stage, the micropore domain. In a second step, when the micropore domain is full, water penetrates into the macropores domain and initiates preferential flow. These conceptual differences may lead to errors, especially when low precipitation takes place, as, in that case, MACRO does not simulate any preferential flow. Also, MACRO does not incorporate the physical and chemical characteristics of the soil causing hydrophobicity. Such an omission may be problematic, especially when frozen soils are studied. Soil frost may affect the hydrophobic soil characteristics, which depend mainly on the soil structure and the soil organic matter (plant fragments, roots) (Bisdom et al. 1993). Possibly, under frozen conditions, the organic aggregates may be partly influenced by ice reducing the repulsive effect on water and we may hence expect a different behaviour.

To sum up, modelling accurately the hydraulic and thermal processes at Hannigalp would necessitate to developed a two-dimensional model, incorporating hysteresis effects as well as soil structure components and simulating phase change. As, to our knowledge, such a model has not been developed, the following simulations will be carried out with COUP, which, in contrast to MACRO, simulates soil freezing. It may result in errors in the simulated water dynamic during unfrozen winters, as the infiltrating waterfront may be underestimated. However, under frozen conditions, this error is probably smaller, as the pore ice may reduce hydrophobicity.

9. NUMERICAL SIMULATION OF SNOWPACK EVOLUTION AND SNOWMELT RUNOFF

9.1. INTRODUCTION

The main objective of this chapter is to calibrate and validate the numerical model COUP. We have to differentiate the snowpack calibration from the soil profile calibration, as both entities are considered separately by the model. Two different approaches were applied to describe the mass balance of the snowpack: an energy balance approach (Jansson et al. 2002) was tested against an empirical melting/freezing approach. For the calibration of the soil hydraulic and thermal parameters, we proceeded in a slightly different way at Hannigalp than at Gd St Bernard. At Hannigalp, most physical parameters were calibrated in the laboratory and validated against *in situ* measurements. At Gd St Bernard, we were not able to bring soil columns into the laboratory, and thus we concentrated our calibration and validation simulations on field measurements only.

The COUP model simulates a homogeneous single-layer snow layer, which proved to be an adequate approximation of shallow snowpacks (Stadler et al. 1997, Stähli and Jansson 1998, Gustafsson et al. 2001). However, it was not tested for wet and cold condition with huge snowfall. Therefore, an other objective will be to evaluate the ability of this one-dimensional model to reproduce heat fluxes and snow cover dynamics for thick snowpacks. In a final step, we discuss the parameters describing the freezing and thawing behaviour, as these parameters determine the degree of soil ice, and accordingly also the amount of infiltrating meltwater.

9.2. SNOWPACK

9.2.1. MODEL APPLICATION

The snow depth was extensively calibrated and validated against measurements for both experimental winters at Gd St Bernard and Hannigalp. In particular, we compared two different ways to simulate the snowmelt. Melting was either calculated by using an empirically based function (**MA**) or by solving the surface energy balance (**EA**) (Chapter 3: "Snow dynamics", page 33). For both approaches, the snow depth, the temperature at the snow surface as well as the water outflow from the snowpack were the decisive outputs. As the two models differ markedly in their structure, we calibrated both snow modules separately and compared the outputs given by each model.

The meteorological inputs were taken from the SMA at Grächen and Gd St Bernard (Chapter 5). To take into account the increase in the precipitation with the altitude, we assumed (from adjacent meteorological stations) the precipitation at Hannigalp to be 10% higher than at Grächen SMA. Missing observations of long-wave radiation, $\boldsymbol{R}_{lnet}$ were simulated using eq. 3.36. The emissivity of the atmosphere was calculated from a function given by Konzelmann et al. (1994) (eq. 3.41), which takes into account air temperature, vapour pressure and cloudiness. At Hannigalp the global radiation was only measured *in situ* during the winter (October to May). Outside this period, the global radiation was estimated from the potential global radiation and the relative duration of sunshine.

9.2.2. HANNIGALP

9.2.2.1. MODEL CALIBRATION: WINTER 2000/2001

The parameters were set according to the default values suggested by Jansson and Karlberg (2001), unless they were calibrated (Table 9.1and Table 9.2). In the **MA**, the site specific parameter related to the radiation-induced snowmelt m_{Rmin} was set to 1.5 E-7 kg J^{-1}(eq. 3.30) and the density of new snow, ρ_{smin} to 120 kg/m^3. Also for the **EA**, a value of 120 kg/m^3 was taken for the new snow density. The site specific parameter z_{omsnow} (snow surface roughness length for momentum) was set to 0.004 m (eq. 3.32). We supposed the snow surface roughness length for heat to be identical (z_{omsnow}= z_{ohsnow}).

Symbol	*Parameter*	*Value*	*Reference*	*Equation*
	Correction in the precipitation (prec. = measured prec. * correct.)	1.1	Estimation	
m_T	Temperature melting parameter	2 Kg m^{-2} day^{-1} $°C^{-1}$	Jansson and Karlberg (2001)	eq. 3.29
m_f	Refreeze parameter	0.1 m	Jansson and Karlberg (2001)	eq. 3.29
m_{Rmin}	Global radiation melting parameter	1.5 E-7 kg J^{-1}	Calibration	eq. 3.30
s_1	Surface age parameters for melt 1	2	Jansson and Karlberg (2001)	eq. 3.30
s_2	Surface age parameters for melt 2	0.1 day^{-1}	Jansson and Karlberg (2001)	eq. 3.30
ρ_{smin}	New snow density	120 kg/m^3	Calibration	eq. 3.45
s_{dw}	Snow density parameter 1	0.5 m^{-1}	Jansson and Karlberg (2001)	eq. 3.45
s_{dl}	Snow density parameter 2	200 kg/m^3	Jansson and Karlberg (2001)	eq. 3.45

Table 9.1: Some snow related parameters used in the **MA** simulations. The site specific parameter is m_{Rmin}

Symbol	*Parameter*	*Value*	*Reference*	*Equation*
	Correction in the precipitation	1.1	Estimation	
z_{omsnow}	Surface roughness length for momentum	0.004 m	Calibration	eq. 3.32
z_{ohsnow}	Surface roughness length for heat	0.004 m	Calibration	eq. 3.32
a_{smin}	Minimum albedo parameter	0.4	Plüss (1997)	eq. 3.40
a_{s1}	Parameter 1 in albedo function	0.5	Plüss (1997)	eq. 3.40
a_{s2}	Parameter 2 in albedo function	-0.05 day^{-1}	Plüss (1997)	eq. 3.40
a_{s3}	Parameter 3 in albedo function	-0.1 $°C^{-1}$	Plüss (1997)	eq. 3.40
ρ_{smin}	New snow density	120 kg/m^3	Calibration	eq. 3.45
s_{dw}	Snow density parameter	0.5 m^{-1}	Jansson and Karlberg (2001)	eq. 3.45
s_{dl}	Snow density parameter 2	200 kg/m^3	Jansson and Karlberg (2001)	eq. 3.45

Table 9.2: Some snow related parameters used in the **EA** simulations. The site specific parameters are the surface roughness length for heat and momentum.

Both models reproduced in a generally satisfactory way the measured snow depth (Figure 9.1).

However, excessive snow was simulated by both approaches at the onset of the winter in November after the large snowfall on 17th November. This difference may be a consequence of an error in the precipitation input data, as measurements were taken at Grächen some 3 km south-east of the experimental site. It probably also arises from the fact that the model uses a too simple snow densification function (eq. 3.45), which does not account for the destructive metamorphism of the snow, caused by the vertical temperature gradient across the snow cover (the vapour flux induced by the temperature gradient destroys warm crystals and reforms them on the cold site of the snowpack), and by sublimation and condensation processes. Recently, we were able to test an improved COUP version (Jansson et al. 2002), taking into account such a relation. Results were better over short periods, when important snowfall was recorded, but did not change markedly over the whole winter.

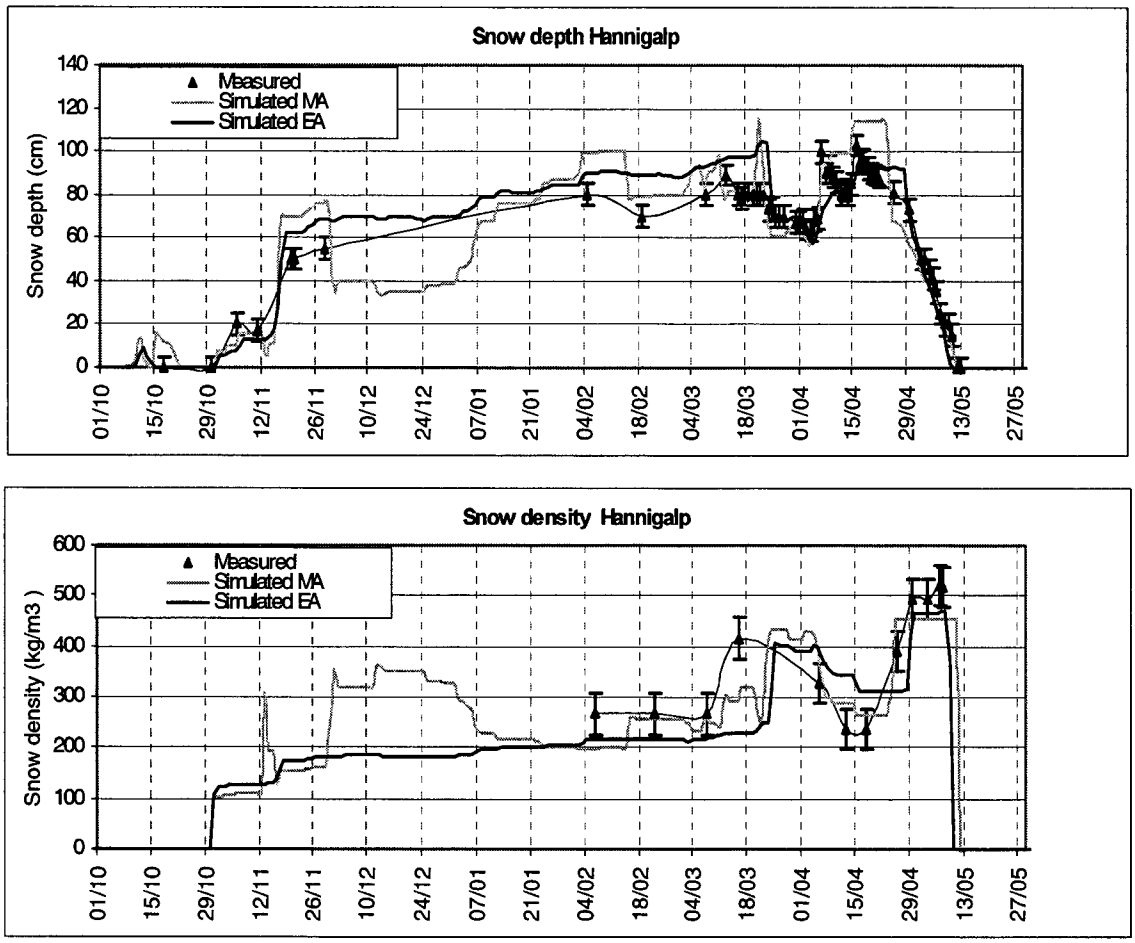

Figure 9.1: Comparison between measured and simulated snow depth and snow density at Hannigalp, using either the **MA**, or the **EA**. The error in the snow depth/density measurements was estimated to be 5 cm and 40 kg/m^3 respectively.

At the end of November, the mean daily air temperature remained above 0°C for a few days, and the **MA** simulated erroneous snowmelt (the snow depth decreased from 75 to 35 cm). This error in the predicted snow dynamics was a result of the wrong model assumption, which considers air and snow surface temperature to be identical. In winter, the snow surface temperature is mostly colder than the air temperature, as the outgoing long-wave radiation is not compensated for by the incoming global (short-wave) radiation and by sensible heat flux

(Waldner et al. 2000). This error did not occur using the **EA**, where the calculated snow surface temperature was well below freezing point.

A correct simulation of the snow density is an essential condition for being able to simulate the heat exchange between soil and snowpack, and, especially, to reproduce soil freezing. Due to the square dependence between the thermal snowpack conductivity and the snow density (eq. 3.44) an inadequate value for the simulated snow density modifies markedly the soil frost depth. Both approaches were able to simulate accurately the density dynamic, in particular at the end of the winter (Figure 9.1). The error in the measured density was large (estimated error 40 kg/m^3), as large variations in the density throughout the snowpack were noted, in particular in spring, when, after snowfall periods, a density of 500 kg/m^3 was measured at the bottom of the snowpack, as against 160 kg/m^3 at the top.

9.2.2.2. MODEL VALIDATION: WINTER 2001/2002

Results simulated with the calibrated model for winter 2001/2002 are shown in Figure 9.1.

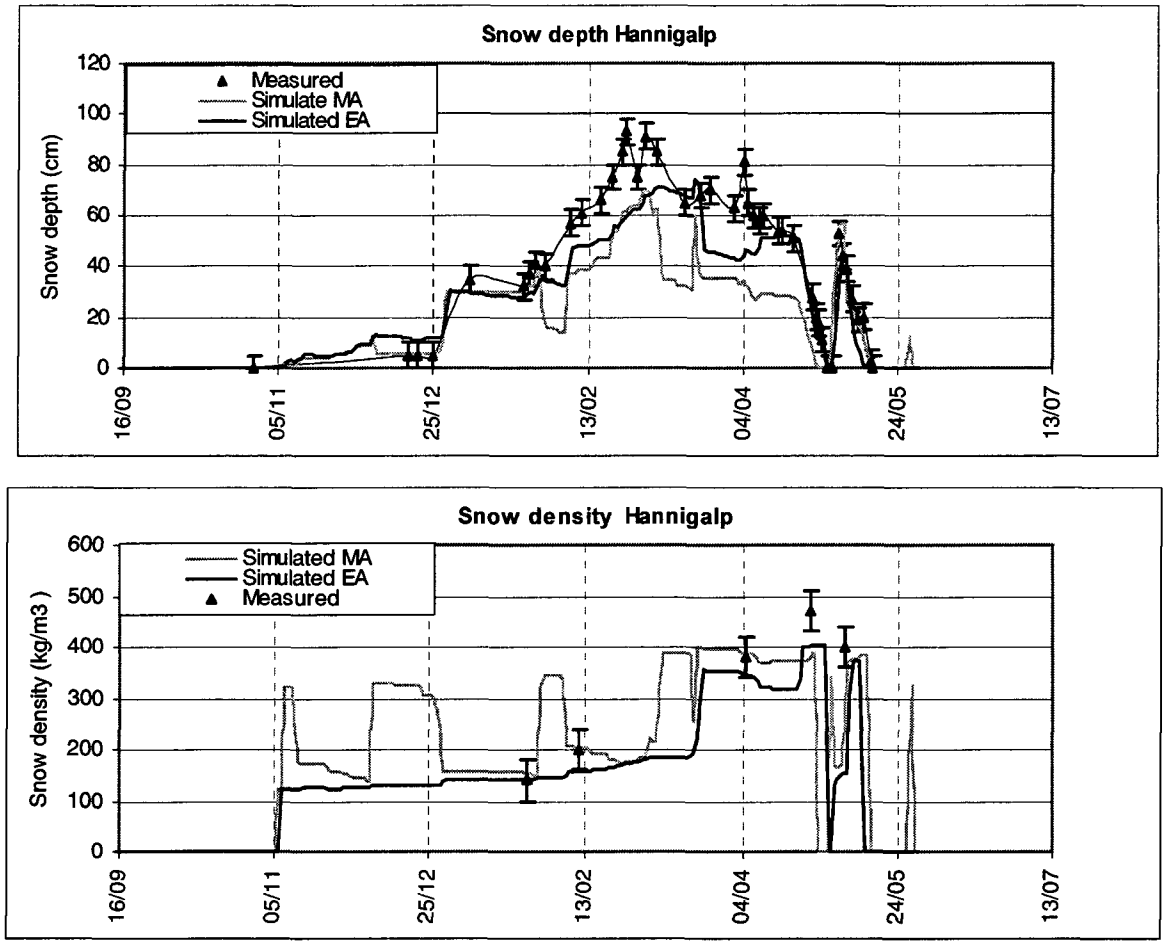

Figure 9.2: Comparison between measured and simulated snow depth and snow density at Hannigalp, using either the **MA** or the **EA** during winter 2001/2002.

During this winter, the precipitation as well as the air temperature differed markedly from the

previous winter (Chapter 5: "Meteorological analysis of winter 2000/2001 and 2001/2002", page 59), which enabled a good testing of the calibrated parameters. Simulated snow depths were closer to those measured when we applied the **EA**. The **MA** produced poor results, especially in February and March, when the snow depth was underestimated by more than 20 cm. Similarly to the calibration, the **MA** simulated significant unrealistic melting in early winter when the air temperature was above 0°C. In particular excessive melting took place during the first two melt events in March and April. Only the final snowmelt intensity was well reproduced.

The **EA** simulated excessive snow depth at the onset of the winter in December (12 cm as against 5 cm). Later on, the snow depth was underestimated mainly in January and February. As no snowmelt was simulated before March, this underestimation was probably caused by an error in the precipitation input. The timing of the snowpack depletion during the final snowmelt was well predicted. This is an important result when interest is focused on the water runoff.

Better agreements were achieved when the simulated and measured snow density were compared. However, there was a systematic underestimation of the density by the **EA**, because, as with the calibration winter, the **EA** underestimates snowmelt events in winter.

9.2.2.3. SNOWMELT DISCHARGE

Another essential prerequisite for an accurate simulation of the soil water dynamic is a correct quantitative simulation of the snowpack discharge. In Chapter 6 ("Classification of snowmelt events", page 73), we estimated the water input at the soil surface during each snowmelt event by adding the precipitation to the snowpack water storage change. In Figure 9.3 we compare these estimations with the snowpack discharge simulated by both approaches.

Both approaches showed contrasting behaviour. The **EA** underestimated the snowmelt in early winter, whereas the **MA** overestimated it. In 2000/2001, the best results were given by the **MA**, which simulated quantitatively and qualitatively both snowmelt events. Results were less good with the **EA**, as no discharge was simulated during the first snowmelt. During the second measurement winter, the **MA** simulated excessive discharge during the two first snowmelt events, and not enough discharge during the final snowmelt, as most of the snowpack had already melted at that time. The **MA** was closer to reality, but similar to the first winter, all meltwater was caught inside the snowpack until the final snowmelt at the end of April, when all water was released by the snowpack.

In conclusion, at Hannigalp a better agreement with the measurements was achieved by using the **EA** to simulate the snow depth, in particular during winter months. However, during the snowmelt period, melting tended to be underestimated by the **EA**, in contrast to the **MA**, which was able to reproduce each measured snowmelt event.

9.2.3. GD ST BERNARD

9.2.3.1. MODEL CALIBRATION: WINTER 2000/2001

Snow depth measurements from winter 2000/2001 were used to calibrate the snow depth model at each location. To be able to simulate the spatial variability in the snowpack evolution, following adjustments had to be carried out:

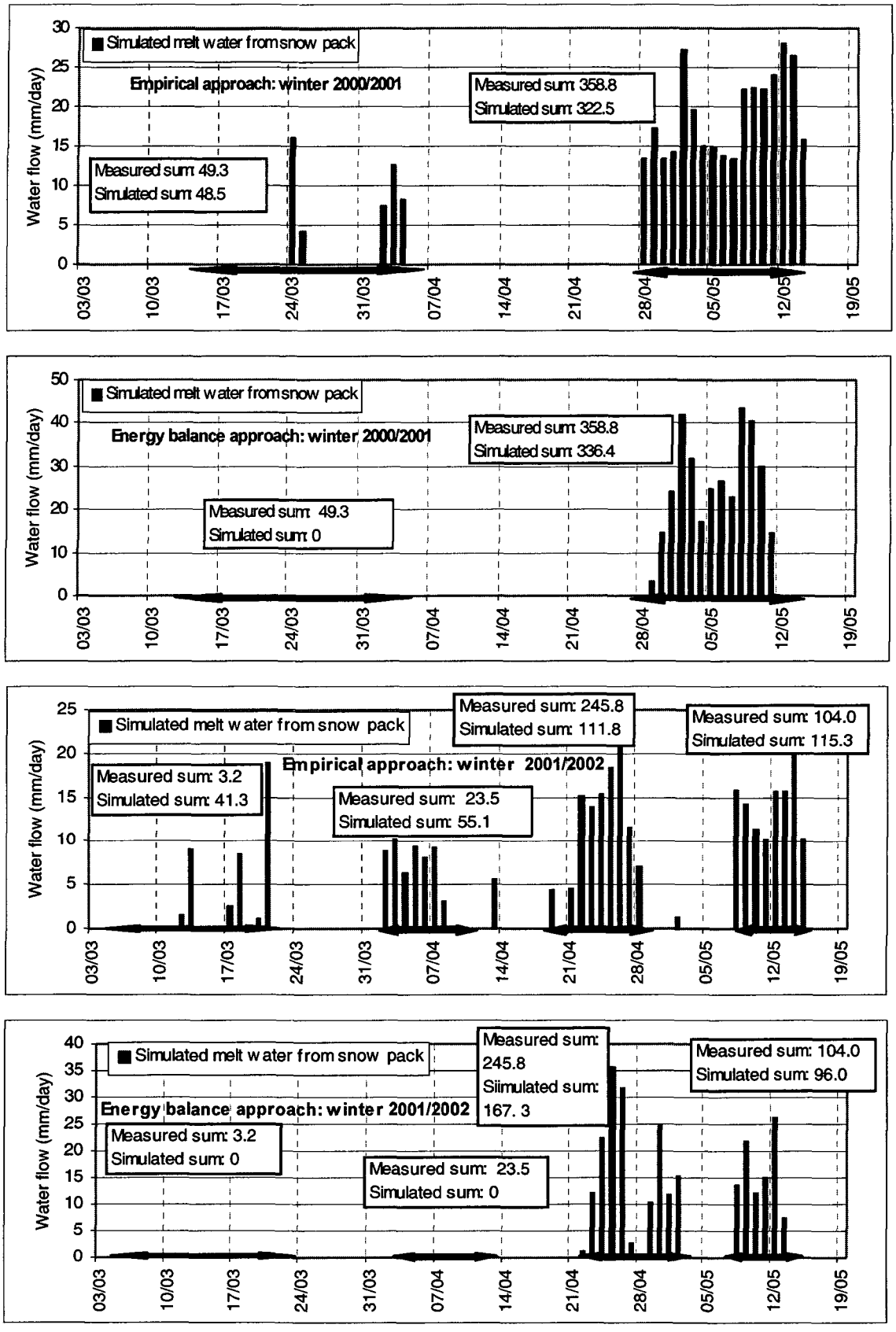

Figure 9.3: Simulated and measured snowmelt discharge at Hannigalp during spring 2001 ((a) and (b)) and 2002 ((c) and (d)), using either the **MA** or the **EA** to simulate the snow depth. For each snowmelt event, the total sum (in mm) of measured and simulated discharge is shown. Error in the estimated discharge is approx. 15%.

Meteorological data

The differences in the global (short-wave) radiation was mainly responsible for disparities in the snow depth. Adjustment of the measured radiation was carried out for each site. To calculate the new global radiation we assumed an exposure of 35°, 0° and -25° for the south, east and north site respectively.

Model settings

Using a single snow layer model becomes problematic when the snowpack is thick (i.e. >150 cm). In winter 2000/2001, the snow density was greatly overestimated when the default model parameters were used (a snow density of approx. 1 kg/m^3 was simulated in spring 2001 at the south site), which resulted in a crass underestimation of the snow depth. The snow density is governed by the compacting rate function (eq. 3.45) that expresses the increase in the snow density caused by the overburden snow and the amount of liquid water in the snow. To obtain realistic simulation results, the density coefficient mass value, s_{dw} in eq. 3.45, had to be reduced from 0.5 to 0.1, and the new snow density increased from 100 to 200 kg/m^3. A low value for s_{dw} was used to reduce the compacting effect of the overburden snow, especially when the snow pack was very thick. A high value for the new snow density was used to compensate the underestimated snow compacting effect at the onset of the winter.

For both approaches, the differences in the model settings from those at Hannigalp (Table 9.1 and Table 9.2) (site specific parameters) are listed in Table 9.3. In the **MA**, the global melting coefficient (m_{Rmin} in eq. 3.30) is consistent with the common value used for open fields.

Location	*New snow density* ρ_{smin} *(kg/m3)*	*Density coeff. mass* s_{dw} (m^{-1})	*Melt coeff. global rad.* m_{Rmin} $(kg\ J^{-1})$	*Surface roughness* z_{omsnow}, z_{ohsnow} *(m)*	*Prec. corrected MA*	*Prec corrected EA*
South site	200	0.1	6.5E-7	0.001	0.8	0.6
North site	200	0.1	6.5E-7	0.0001	1	1
East site	200	0.1	6.5E-7	0.0005	0.8	0.7

Table 9.3: Some snow related parameters used in the **MA** and the **EA** simulations at the south, north and east sites.

The precipitation input had to be modified to consider snow lost due to wind displacement. The diminution was subject to the chosen snowmelt approach as well as to the site orientation. No correction was necessary for the northern more protected site. In contrast, the southerly exposed site was located close to a ridge and wind erosion was high. Up to 40% of the precipitation was removed when the **EA** was used. This percentage was lower with the **MA** (-20%), due to the fact that several snowmelt events were simulated in winter, allowing a better matching between simulation and measurements. At the east site the reduction varied between 20% (**MA**) and 30% (**EA**).

Results

The comparison between simulated and measured snow depth for the three orientation is shown in Figure 9.4. The model calibration results are generally in good agreement with the

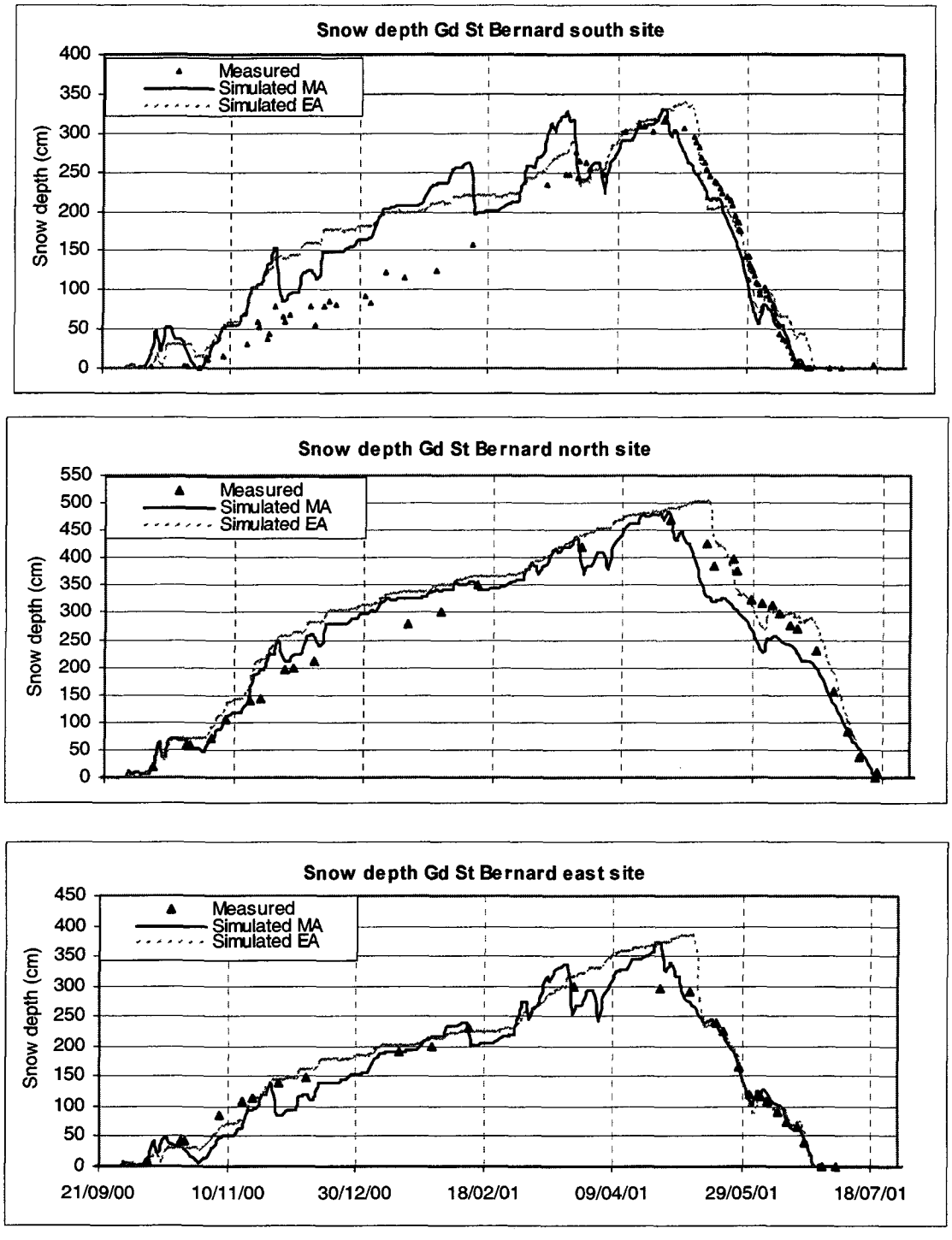

Figure 9.4: Simulated snow depth after calibration using either the **MA** and the **EA** compared with measured snow depth at the south, north and east sites at Gd St Bernard during winter 2000/2001.

measurements. However, the simulated snow depth at the south plot was markedly overestimated during the initial stage of the winter. For the **EA**, this error arises partly from the previously mentioned underestimated snow surface temperature, which resulted in excessive

snow in early winter. In the **MA**, matching between measurement and simulation was better at the onset of winter, as the simulated snowmelt induced a strong decrease in the snow depth. Nevertheless, these melt events were excessive, and could not be identified on the site. At the north and east sites, where winter snowmelt events were rare, matching between simulation and measurement was much better for both approaches.

The depletion curve at snowmelt was well predicted by all models. During the ablation periods, the new-fallen snow melted fast, mostly within a few hours after the end of the precipitation event. Due to the daily temporal input of the model, the model was not able to simulate accurately this increase in the snow depth, which was usually slightly overestimated, in particular at the south site (for example the 2nd June 2001).

Difficulties in simulating the snowpack evolution on the south plot also arose from the wide variation in the snow depth due to the complicated topography. Typically, at the end of the final snowmelt, some parts of the experimental site were already snow free, whereas at other locations, there was still 20 cm of snow. Spatial measurements of the snow cover were carried out during both winters at randomly distributed points. The standard deviation of the 8 snow measurements was 38 cm. Taking into account this spatial variability, we conclude that the simulated snow depth fits accurately with the observed snow evolution.

9.2.3.2. MODEL VALIDATION: WINTER 2001/2002

When using the previously calibrated model, matching between simulation and measurement

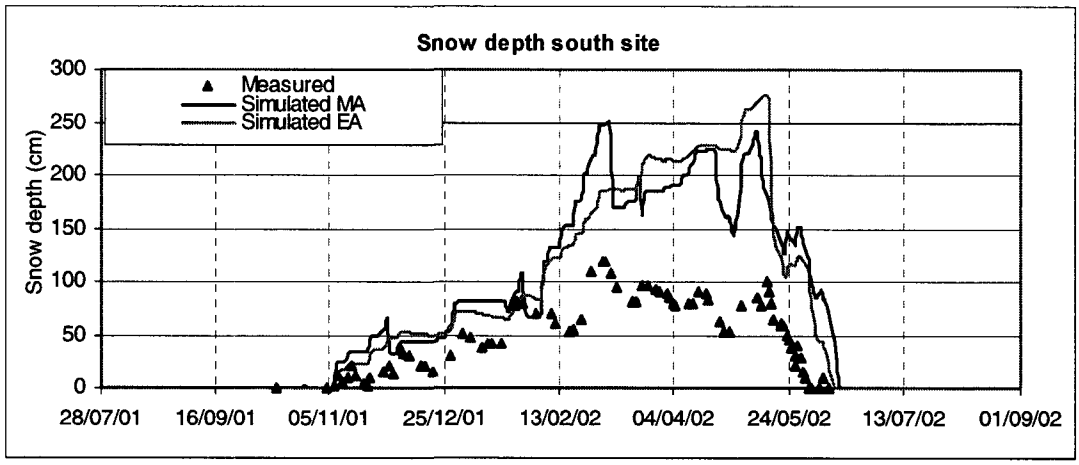

Figure 9.5: Simulated snow depth for validation compared with measured snow depth during winter 2001/2002 for the south plot at Gd St Bernard, using either the **MA** or the **EA**.

was poor for winter 2001/2002. The snow depth was largely overestimated (by twice as much) at each location (results for the south plot are shown in Figure 9.5). This considerable discrepancy was probably caused by errors in the precipitation measurements at the SMA station and by snow relocation due to wind. Indeed, to obtain optimal precipitation measurements, one should select gauge locations in relatively flat areas some 1.5 m above the snow surface that are sheltered from the wind (Tabler, Berg et al. 1990). At Gd St Bernard, the gauge location was next to the monastery roof, approximately 10 m above the soil surface, and was exposed to strong winds. Hence, the potential error in measuring snow precipitation was

high, as the surrounding wall may have acted as a deposition area of relocated snow, which would have been mistaken for precipitation: also, the strong winds on the pass may have created distortion in the wind field around the gauge, which possibly reduced the number of snow particles caught. Other sources of error were the effects of the topography on the spatial distribution of precipitation and the snow surface properties, which inhibited the new fallen snow from remaining on the surface. From observations, most of the new snow was blown away by the wind when the underneath snow surface hardened and densified. This may explain why, at the onset of winter 2001/2002, 190 mm of precipitation were measured by the gauge, whereas only 20 cm of snow remained on the south plot.

9.2.3.3. CORRECTED PARAMETERIZATION

To obtain a better fitting between simulations and measurements, a new parameterization was carried out. The main errors arose from the uncertainty in the precipitation inputs. Therefore the only modification made was to decrease the precipitation, so as to minimize the differences between simulation and measurement *for both winters*. The adjustments used are given in Table 9.4, and the results shown in Figure 9.6. At the north and east sites, an identical decrease in the precipitation input was used for the whole winter. At the south site, the diminution was higher between November and December, where 40% (**MA**) and 60% (**EA**) of the precipitation were removed as against 20% (**MA**) and 40% (**EA**) between January and June. These modifications are arbitrary and hence questionable, but they allowed best fitting between measurement and simulation for both winters, especially at the onset of winter.

	South	*North*	*East*
Precipitation corrected empirical approach	0.8 (0.6)	0.85	0.6
Precipitation corrected energetic approach	0.6 (0.4)	0.75	0.4

Table 9.4: Correction in the precipitation input for each site. On the south site, the correction in the precipitation was more important (0.6 and 0.4) at the onset (October to December) of the winter.

Best fitting was obtained with the **MA** for the south and east plots, and with the **EA** for the north plot (Table 9.5). Fitting for the east site was poor ($r^2<0.6$ for both approaches). This was mainly a consequence of the bad simulation results in winter 2000/2001, when the model recreated the end of the snowmelt period some three weeks earlier than in reality.

	South	*North*	*East*
Determination coefficient r^2 empirical approach	0.73	0.69	0.55
Determination coefficient r^2 energetic approach	0.65	0.76	0.51
Number of measurements points	139	105	76

Table 9.5: Determination coefficient r^2 between modelled data and measurements for both winters examined at the south, north and east sites at Gd St Bernard.

To sum up, the simulation of the snow depth proved to be particularly tricky at Gd St Bernard. The main problem arose from the uncertainty in the precipitation data, which influenced the accuracy of the simulation results. In spite of this imprecision in the input data, the dynamic in the snow cover could be reproduced accurately by both single layer models, the **EA** giving better results for the south and east sites, and the **MA** showing good simulations for the north site.

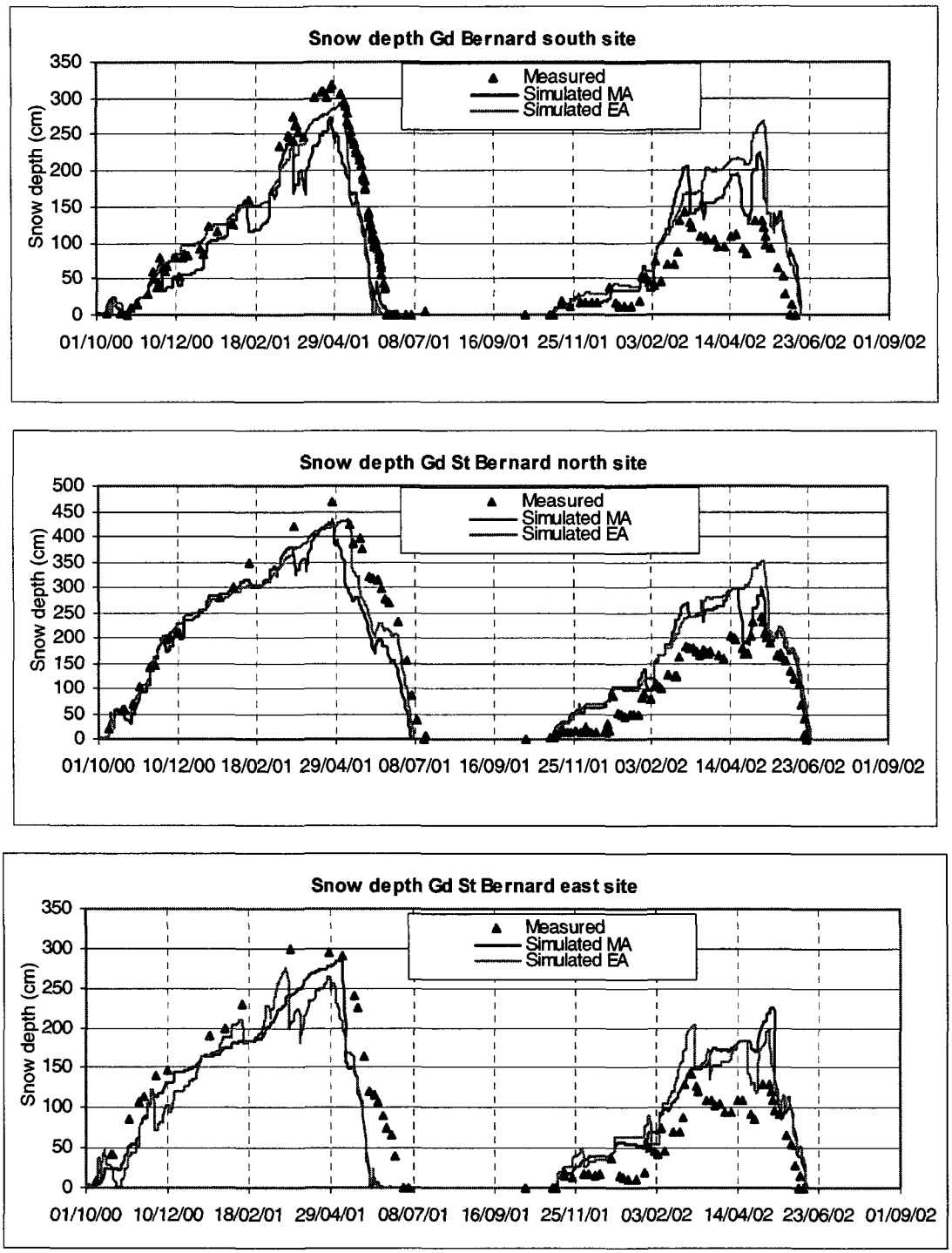

Figure 9.6: Simulated and measured snow depth at Gd St Bernard on the south, east and north plots, with new corrected precipitation input values using either the **MA** or the **EA**.

9.2.4. DISCUSSION

By using two different snow models, we were able to understand better the snow-atmosphere processes for various Alpine meteorological conditions. Both models differ markedly in their formulation but were able reproducing the snow depth for specific locations. Comparison

between the model settings at Hannigalp and Gd St Bernard leads to the following comments:

Single layer

Using a single layer model to simulate a snowpack allows the snow depth to be to reproduced correctly, as long as the snowpack is not too thick, as at Hannigalp. Otherwise, the assumption of linear relationship between snow density and overburden pressure is not valid for deep snow depth, as noted by several studies (see for example Tabler, Pomeroy et al. 1990). At Gd St Bernard, we obtained apparently satisfying results by modifying the snow density function. However, the great uncertainty in the input data makes it difficult to give a useful interpretation of the outputs results.

An improvement was recently made to obtain a layered numerical snow model (Gustafsson et al. sub.). This model simulated the snow depth reliably, but was not able to reproduce satisfactorily the formation of the snow layers, in particular because it does not take into account the effect of the snow microstructure on the water redistribution in the snow, which may produce lateral water flow and preferential flow. Also the model proved to be numerically unstable for snow depth deeper than 100 cm.

Empirical approach

Correct prediction of the snow density requires specification of the heat exchange between the soil surface and the atmosphere. In early winter, the **MA** overestimated the air temperature at the snow surface, in particular for northerly exposed locations. It resulted in early, unrecorded snowmelt episodes, and in artificial increases of the snow density. In spring however, this assumption was mostly satisfied and modelling results reflected the measured snow depth evolution. At well-exposed locations, the strong global radiation allowed relevant snowmelt events even early in winter. At such locations, the **MA** gave reliable results throughout the winter.

Energetic approach

On the north plot at Gd St Bernard and at Hannigalp, this approach enabled best simulation. On the south and east plots the snow depth was mainly overestimated. What caused this overestimation is not quite clear, but it probably arose from the daily temporal time step used in the simulations. This time step does not integrate the variation in the daily radiation that causes snowmelt during a few hours of the day; although globally (i.e. over one day) not enough energy is available to cause melting. By using hourly input data, Gustafsson et al. (2001) did not encounter the same problem. The only discrepancies occurred during the snowmelt when the net radiation was underestimated due to a systematic overestimation of the albedo.

We were not able to test the error in the calculated latent and sensible heat. Such a calculation would involve sophisticated measuring apparatus like eddy-correlation systems. However, Gustafsson et al. (2001) compared in their study the simulated turbulent heat flux with the measured one, using the same model procedure to calculate the snow surface temperature. Their simulation results fitted well with measurements, and we may hence expect that the turbulent heat flux was appropriate in our simulation.

In alpine areas, the snowmelt is mainly dominated by the net radiation (Plüss 1994). This could

be verified at Gd St Bernard, where the differences in the snowmelt onset between the three sites investigated was mainly caused by the change in the radiation. In the simulations, the beginning of the snowmelt coincided with the beginning of positive net radiation values. As shown by the calibration of the surface roughness parameter, the turbulent flux only slightly affected the snowmelt intensity, whereas the net radiation was the dominant factor during the whole snowmelt.

Meteorological input

At the Gd St Bernard pass, the contrasting topography combined with the strong winds and the huge snow precipitation induced massive spatial snow depth variation. Hollows were filled up with snow, whereas snow was blown away on ridges. A doubling of the snow depth between locations two metres apart was not uncommon. Simulating the snow depth was hence much more difficult at Gd St Bernard than at the calm location of Hannigalp. A major unknown arose from the snow remove by the wind, which depended among other things on the wind speed, the air temperature, the sow surface hardness, and the snow structure. Another uncertainty was caused by the inaccurate snow gauge measurements. These errors explain the difficulties in obtaining a reliable model calibration of the snowpack at Gd St Bernard. As it is not evident how much quality snow precipitation data will be available in the future, one possibility would be to use radar data to obtain the areal variability: but such a model would not be able to reproduce topographical-induced variation in the snowpack over short distances. Another promising method would be to apply snow depth measurements instead of precipitation measurements Apart from automatic point measurements, which are already available and applied over large areas (for example the ENET network, which provides automatic snow depth measurements in Switzerland), remote sensing combined with GIS-based modelling may offer a reliable method to obtain areal snow depth estimation (Stähli et al. 2002). Tappeiner et al. (2001) were for example able to model the spatial differences in the days covered by snow on an alpine hill slope using easily available data, like elevation, slope angle and aspect, potential radiation and number of days with temperature below freezing point.

9.3. SOIL WATER AND HEAT FLUX

9.3.1. MODEL APPLICATION

At Hannigalp, we calibrated most soil physical parameters in the laboratory from infiltration experiments, whereas at the Gd St Bernard south plot, where only *in situ* measurements were available, we used the field experiments to calibrate the different hydraulic and thermal parameters. At both sites, the parameters describing the thermal behaviour, especially the freezing and thawing processes were estimated from the soil liquid water content measurement and the soil temperature measurements from both winters.

Validation was carried out on the measured discharge runoff for the two winters. As hydraulic and thermal processes in the soil depend to a large extend on the processes in the overlaying snowpack, both snow model (the **EA** and the **MA**) were tested and compared with each other. On the north and east plot at Gd St Bernard, no discharge measurements were available. Hence we used the identical validated model to that for the south plot to simulate the snowmelt dynamic, and changed only the soil temperature at the lower boundary of the model.

9.3.2. HANNIGALP

9.3.2.1. MODEL CALIBRATION

9.3.2.1.1. CALIBRATION WITH LABORATORY MEASUREMENTS

Two laboratory experiments were used to calibrate the hydraulic conductivity, the thermic conductivity and the freezing point depression curve (FPDC). The first experiment was made up of two artificial irrigations of an unfrozen soil column, whereas the second consisted in monitoring the soil freezing. Results for the first experiment were already presented and discussed in Chapter 8, and will not be further developed.

In the second experiment, the room temperature was set to -5°C, and the soil column began to freeze. No irrigation was carried out. As the empty space between the two cylinders create and quasi isolating layer (Figure 8.1), freezing could only take place from above. The experiment ended when the soil frost reached a depth of 40 cm.

Following comments are done on the changed model settings:

- A very fast decrease of soil temperature over the entire profile took place during the experiment. To be able to adjust the simulation to the measurements, the soil thermal conductivity was abnormally increased ($a_3 = 1$ m^3 kg^{-1} in eq. 3.11, the default value is 0.64 m^3 kg^{-1}).
- Using the model default values, the heat transfer under frozen condition was too fast. Hence, the thermal conductivity was reduced ($b_2 = 0.1$ m^3 kg^{-1} and $b_4 = 0.05$ m^3 kg^{-1}, in eq. 3.13, instead of 1.33 m^3 kg^{-1} and 0.9 m^3 kg^{-1} respectively).
- The thermal conductivity was adjusted for each simulated layer. It was lowest at the upper part of the soil column due to presence of organic material, and increased with depth.
- From the experimental results, the temperature T_f (eq. 3.24) where all water is frozen except a remaining unfrozen amount θ_{lf} was set to -5°C. In the calculation of θ_{lf} (eq. 3.24), d_f was set to 0.5 and θ_{wilt} given by Table 4.2.
- The soil texture was approximately homogeneous in the upper 60 cm. We supposed therefore that the FPDC was independent of the soil constituent (d_2=18, d_3=0, in eq. 3.25) (Figure 9.7).

The results for the soil temperature and the liquid water content at a depth of 5 cm are shown in Figure 9.7 . The results at 20 and 35 cm, are given in Appendix E.

We used the laboratory experiment to calibrated the FPDC. However, we had to reject the calibration of the thermal conductivity, as the calibrated unfrozen conductivity was equivalent to the quartz's conductivity (approximately 9 W m^{-1} C^{-1} for a water content of 30%). We believe that this error arise from an inadequate lateral column insulation creating a fast cooling of the soil column.

9.3.2.1.2. CALIBRATION WITH *IN SITU* MEASUREMENTS

To accurately simulate the thermal behaviour *in situ*, we began to adjust the simulated snow depth with the measurements. The model setting are discussed before proceeding to the simulation results.

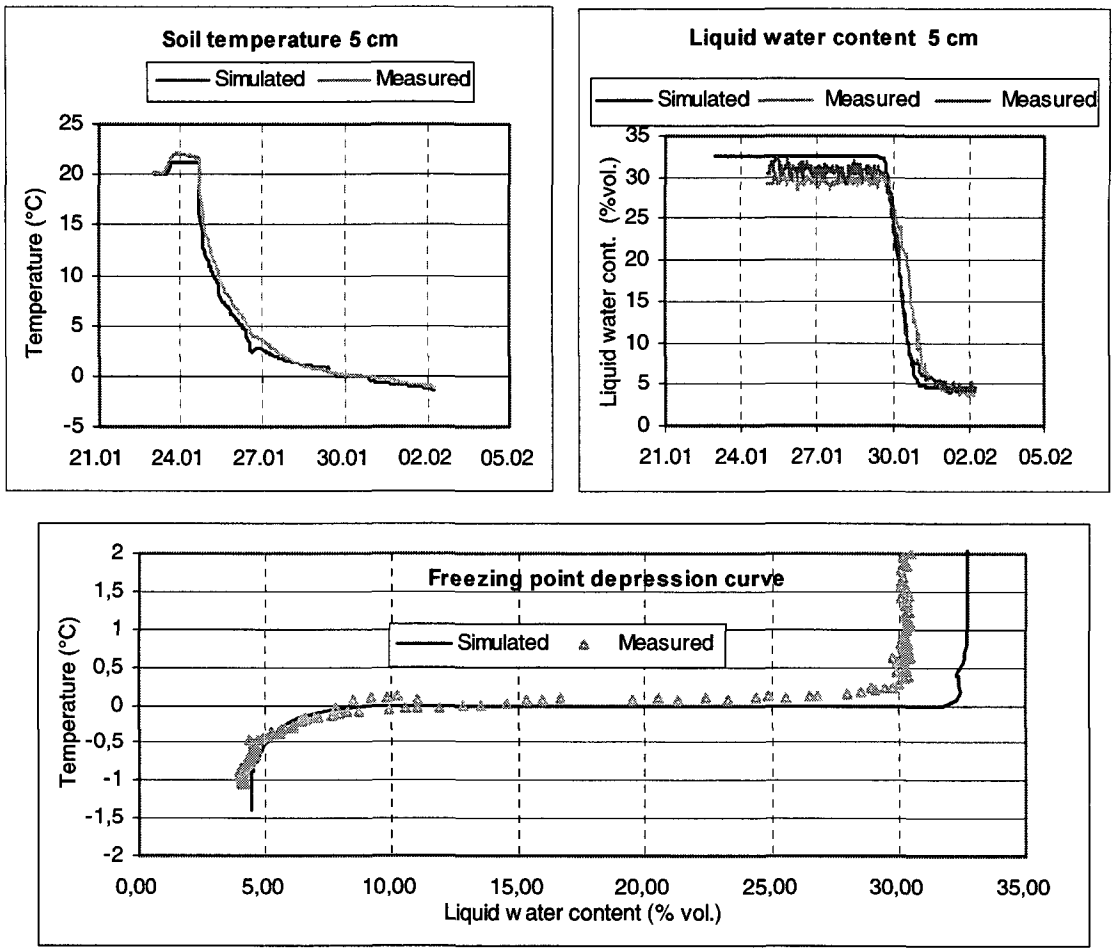

Figure 9.7: Simulated soil temperature and liquid water content at a depth of 5 cm compared with measurements (up). Simulated and measured Freezing Point Depression Curve (down).

Model settings

To consider possible underneath warming, the profile was made 9 m deep with lower boundary conditions given by a soil temperature varying over the time (Figure 9.4). Mean soil temperature was set to 3°C.

The soil profile was composed of a one-metre-deep layer of fine material overlaying an eight-metre-deep bedrock. As the soil characteristics of the old till were unknown, we approximated, from *in situ* calibration, the bedrock thermal conductivity to 3.5 J/msK (for a liquid soil moisture of 20%), which is more than three time as much as the conductivity in the fine material layer. Also, because no perched water-table was measured during the snowmelt, the hydraulic properties of the bedrock were set to the lowest soil layer. Indeed, by setting soil hydraulic properties identical to the interface bedrock soil cover, the substratum did not influence water circulation markedly in the upper soil during the snowmelt. But it is clear that this lack in our knowledge of the physical properties may have introduced an uncertainty in the final results. The newly calibrated thermal conductivity is summarized in Appendix F. The amount of evaporation from the soil surface during snow free periods depends on the soil surface roughness for heat and momentum, z_{ohsoil} and z_{omsoil}. These two values were calibrated against the liquid water content and set to 0.003 m. Surface runoff was expected to take place as soon

as the soil infiltration capacity was reached. Consequently no damping in the outflow of the surface pool was assumed (a_{surf}= 1) and no water was allowed to remain on the soil surface (w_{pmax}= 0). All other parameters were unchanged.

We used the second measurement winter to set the frozen hydraulic parameters, f_i (impedance factor governing the upwards flow to the frozen front), α_f (heat transfer coefficient, which gives the rate of refreezing between low and high flow domain) and f_{θ_i} (damping of the ice content in the high flow domain) of the two domain flow in a frozen soil (see eq. 3.21 and eq. 3.23). As the infiltration rate is very sensitive to these parameters (Stähli et al. 1999), we first made an attempt to find an appropriate description of hydraulic conductivity in the high flow domain, using a scaling factor for the high flow domain (f_{θ_i} =5.5% vol. (**MA**), 5.8% vol. (**EA**)). As no reduction in the soil infiltration capacity took place during the snowmelt, refreezing of meltwater during snowmelt was kept low. This was achieved by increasing the impedance factor f_i (=10), as less liquid water flowed towards the ice body causing less ice content, and by lowering the value of α_f (=50), so as to allow water to infiltrate deeply into the frozen soil, without refreezing. The different parameters are summarized in Table 9.6.

Symbol	*Parameter*	*Value*	*Reference*	*Equation*
z_p	Depth of the drains	0.28 m	measurement	eq. 3.2
d_p	Drain spacing	1.21 m	measurement	eq. 3.2
a_1	Heat conductivity parameter 1 for unfrozen soil	0.1	Jansson and Karlberg (2001)	eq. 3.11
a_{sur}	Empirical coefficient for surface runoff	1 s^{-1}	estimation	eq. 3.8
w_{pmax}	Maximal amount of liquid water stored on the soil surface pool	0 $m^3 m^{-2}$	estimation	eq. 3.8
a_2	Heat conductivity parameter 2 for unfrozen soil	0.058	Jansson and Karlberg (2001)	eq. 3.11
a_3	Heat conductivity parameter 3 for unfrozen soil	0.6245 $m^3 kg^{-1}$	Jansson and Karlberg (2001)	eq. 3.11
a_4	Multiplicative scaling coefficient	see Appendix F	Calibration	eq. 3.12
b_1	Heat conductivity parameter 1 for frozen soil	0.00158 J m^{-1} °$C^{-1}s^{-1}$	Jansson and Karlberg (2001)	eq. 3.13
b_2	Heat conductivity parameter 2 for frozen soil	1.336 $m^3 kg^{-1}$	Jansson and Karlberg (2001)	eq. 3.13
b_3	Heat conductivity parameter 3 for frozen soil	0.00375 J m^{-1} °$C^{-1}s^{-1}$	Jansson and Karlberg (2001)	eq. 3.13
b_4	Heat conductivity parameter 4 for frozen soil	0.9118 $m^3 kg^{-1}$	Jansson and Karlberg (2001)	eq. 3.13
f_i	Impedance factor	10	Calibration	eq. 3.21
f_{θ_i}	Damping coefficient	5.5% vol. (**MA**) 5.8% vol. (**EA**)	Calibration	eq. 3.22
α_f	Heat transfer coefficient	50 W m^{-1} °C^{-1}	Calibration	eq. 3.23
d_2	FPDC parameter 1	18	Calibration	eq. 3.25
d_3	FPDC parameter 2	0	Calibration	eq. 3.25
z_{omsoil}	Soil surface roughness length for momentum	0.003 m	Calibration	eq. 3.32
z_{ohsoil}	Soil surface roughness length for heat	0.003 m	Calibration	eq. 3.32

Table 9.6: Some hydraulic and thermal parameters used in the **MA** and the **EA** simulations at Hannigalp.

Results

In order to keep the number of figures low, simulation results for the soil temperature and the liquid water content will only been shown at a depth of 5 and 30 cm. At other depths, results may be viewed in Appendix G.

During the first winter soil temperatures and liquid water contents were fairly constant. This is in contrast to the following winter when a sharp decrease in the liquid water content and soil temperature was noted in December, resulting in persistent soil frost. For both winters, the soil temperature was slightly better simulated with the **EA** (r^2= 0.95 at 5 cm) than with the **MA** (r^2 = 0.93) (Figure 9.8 and Figure 9.9). At the onset of winter the **MA** slightly overestimated the

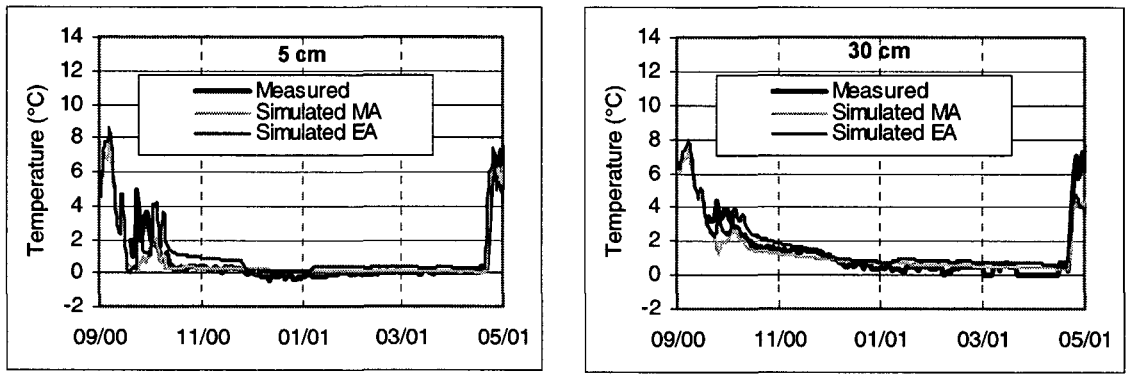

Figure 9.8: Simulated and measured soil temperature (°C) at a depth of 5 and 30 cm at Hannigalp from September 2000 to June 2001 using either the **EA** or the **MA**.

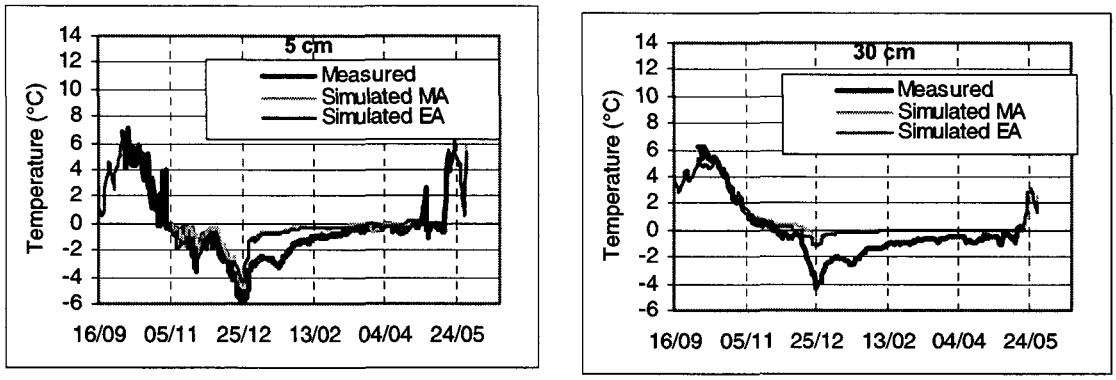

Figure 9.9: Simulated and measured soil temperature (°C) at a depth of 5 and 30 cm at Hannigalp from September 2001 to June 2002 using either the **EA** or the **MA**.

snow surface temperature. For this reason, the simulated soil frost depth was underestimated in winter 2001/2002, which was expressed in the liquid water content measurement (Figure 9.11). Better results were obtained when the thermal snow conductivity was increased by a factor of two, or by setting a higher value for the new snow density. However, both changes produced erroneous soil freezing in spring 2002 and, therefore, had to be rejected. The shallow freezing in winter 2000/2001 was not simulated, because the artificial snow removal was not reproduced by the model.

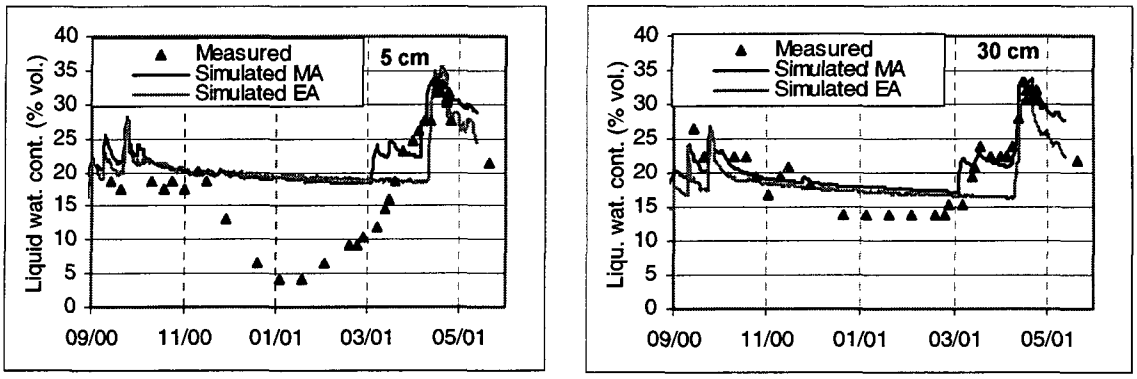

Figure 9.10: Simulated and measured soil liquid water content (% vol.) at a depth of 5 and 30 cm at Hannigalp from September 2000 to June 2001 using either the **EA** or the **MA**.

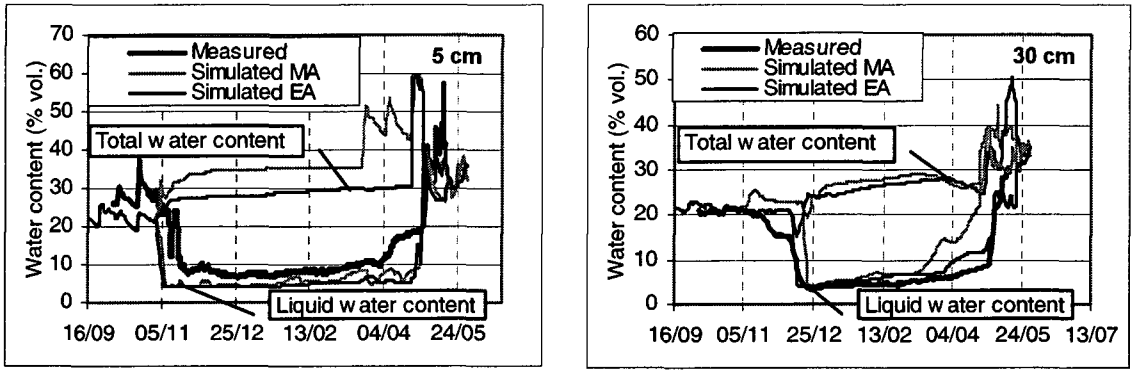

Figure 9.11: Simulated and measured soil liquid water content (% vol.) at a depth of 5 and 30 cm at Hannigalp from September 2001 to June 2002 using either the **EA** or the **MA**.

The soil temperature and the moisture content were satisfactorily reproduced by the **EA**. In 2001/2002 however, freezing was too fast in the upper part of the soil (0-15 cm), due to the fact that the simulated water content was underestimated between 0-10 cm (Figure 9.12), which in turns resulted in fast freezing of this layer.

9.3.2.2. MODEL VALIDATION WITH *IN SITU* MEASUREMENTS

The model was validated against the measured discharge (surface runoff, subsurface flow and percolation) of both winters. The **MA** did not simulate any deep percolation during the first snowmelt event of winter 2000/2001. All water was kept in the upper 40 cm of soil, which was consistent with the measurements (Figure 6.2) (in the **EA** no meltwater discharge was simulated). The timing of deep percolation was correctly simulated by both models during the final snowmelt. However, the intensity was too low, due to the underestimated snowmelt discharge (Figure 9.3). As a result, the accumulated simulated deep percolation was 19% (**EA**) and 8% (**MA**) lower than that measured.

In spring 2002, the soil was frozen and the discharge pattern changed. The presence of pore ice in the uppermost 10 cm blocked the pores and reduced the soil infiltration capacity. This reduction was intensified by the presence of a basal ice sheet, resulting in a sharp increase of the

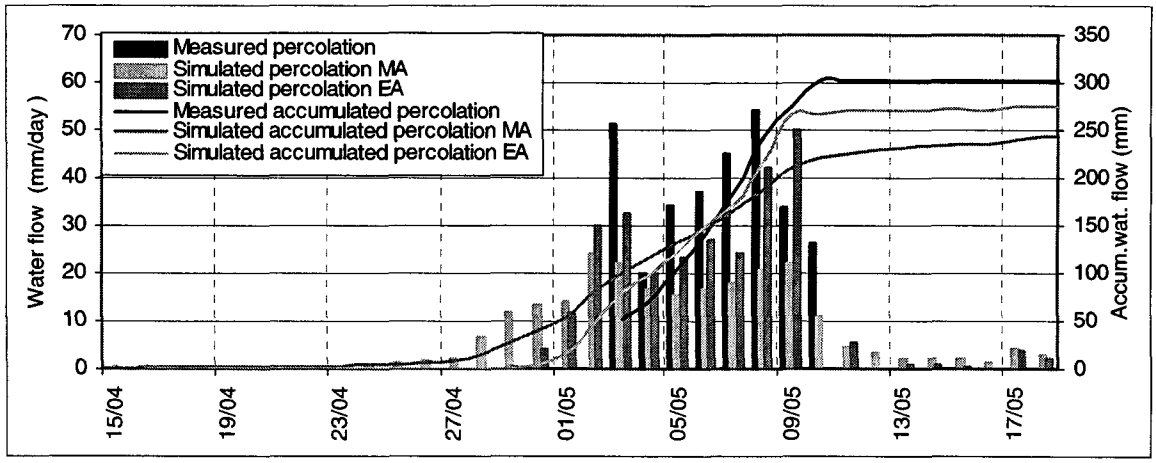

Figure 9.12: Simulated and measured deep percolation (daily flux and total accumulation) during main snowmelt event in spring 2001 at Hannigalp, using either the **EA** or the **MA**.

surface runoff. The surface runoff was well reproduced by the **MA** (Figure 9.13). However, the excessive snowmelt prior to the final snowmelt (first two events) resulted in too much simulated subsurface runoff. The infiltrating water saturated the upper 20 cm of the soil, creating subsurface flow already in May. In reality however, the upper part of the soil remained unsaturated until the onset of the final snowmelt. The accumulated sum of lateral runoff (surface + subsurface) was hence greatly overestimated (+36%).

The **EA** did not simulate any snowmelt discharge for the two first snowmelt events. During the final snowmelt, the amount of simulated surface and subsurface flow was in agreement with the measurements (the total simulated lateral flow was 64 mm, whereas 67 mm were measured). We observed, however, a delay at the onset and the end between measured and simulated lateral runoff. As no measurement were available between 21st and 25th May, the shape of the lateral runoff curve may vary from the one indicated[1], and hence, no comments will be made on the initial stage. During the final stage, the main differences between measurements and simulations arose from the fact that the snow cover did not melt uniformly over the entire plot, but was more intense in the lower part of the plot, close to the collecting gutters. Some parts of the plot were already free of snow on 28th May, reducing the amount of collected meltwater.

To sum up, the discharge and soil frost depth simulation at Hannigalp was more accurate when the **EA** was applied to simulate the snow depth, especially the accumulated sums of lateral runoff were well reproduced. The drawback was that the **EA** did not simulate any discharge during early snowmelt events.

1. To estimate the temporal evolution of the discharge between 21st and 24th May, we supposed that the daily discharge showed a similar pattern each day, except for the 21st when the snowmelt started and less water melted. The amount of lateral runoff during this period had already been calculated in Chapter 6 (Figure 6.14). We estimated the relative percentage between surface and subsurface runoff to be the identical to that between 25th and 26th May.

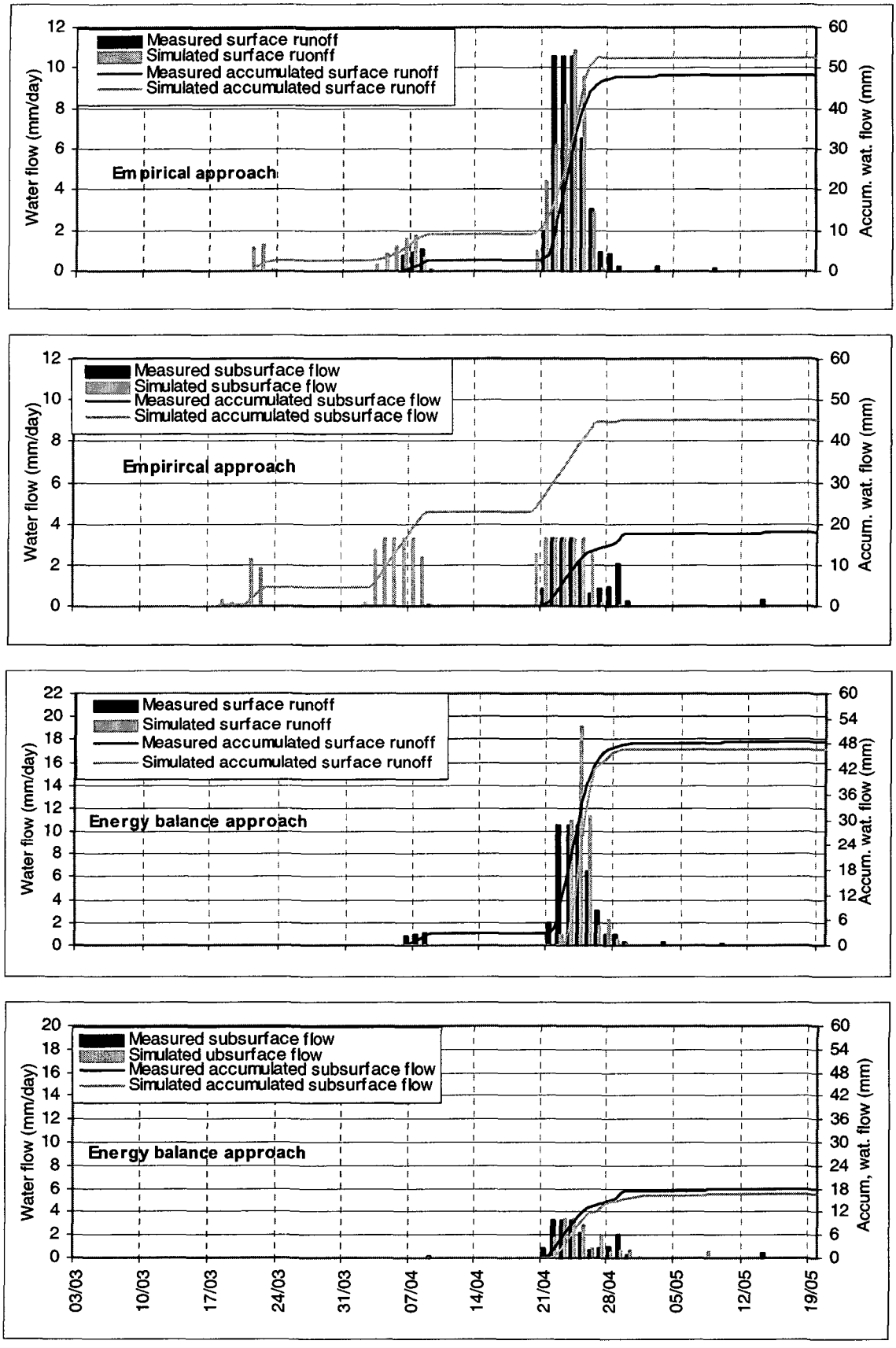

Figure 9.13: Simulated and measured surface ((a) and (c)) and subsurface ((b) and (d)) runoff (daily fluxes and total accumulation) at Hannigalp during snowmelt 2002, using either the **EA** or the **MA** to simulate the snow depth.

9.3.3. GD ST BERNARD

9.3.3.1. MODEL CALIBRATION WITH *IN SITU* MEASUREMENTS (SOUTH SITE)

As shown above, both calibrated snow depth models (especially the **EA**) showed poor results, especially at the end of the winter during the snowmelt period. Therefore, to obtain an accurate simulation of the water and heat processes in the soil, we chose to use the snow model providing the most accurate results (i.e. **MA**), and, additionally, forced the simulated snow depth to match measurements.

Model settings

Similar to Hannigalp, the soil was divided into 24 layers for a total depth of 9 m. Van Genuchten's parameterization was used to characterize the pedotransfer functions (Table 4.5). Lower thermal boundaries were given by a time-varying temperature. To take into account the substantial warming during the snowmelt period, the mean soil temperature at the lower boundary was set, after calibration, to 7°C. To simulate the fast and substantial soil frost in December 2001, the soil thermal conductivity was increased. For the fine material, the calibrated value for the thermal conductivity was set to approx. 3 $Jm^{-1}s^{-1}K^{-1}$ (for a liquid soil moisture of 20%). This high value was due to the presence of large slate stones in the fine material that had a high thermal conductivity. The thermal bedrock hydraulic conductivity was set to 4 $Jm^{-1}s^{-1}K^{-1}$ (for a water content of 20% vol.). A constant value of $5*10^{-5}$m/s over the entire soil profile was used for the hydraulic conductivity (Table 4.4). The soil surface roughness for heat and momentum, z_{ohsoil} and z_{omsoil} were set to 0.001 m No change was made to the default ice blocking parameter value α_f (=100 W m^{-1} K^{-1}). The damping ice content f_{θ_i} and the impedance factor f_i were used as calibration factors. A rather high value was found for f_{θ_i}=10.5% vol. Similar to Hannigalp, f_i was set to 10, as no reduction in the soil infiltration capacity took place during the snowmelt. The differences in the model settings from Table 9.6 are listed in Table 9.7.

Symbol	*Parameter*	*Value*	*Reference*	*Equation*
z_p	Depth of the drains	0.28 m	Measurement	eq. 3.2
d_p	Drain spacing	0.43 m	Measurement	eq. 3.2
a_4	Multiplicative scaling coefficient	See Appendix F	Calibration	eq. 3.12
f_i	Impedance factor	10	Calibration	eq. 3.21
f_{θ_i}	Damping coefficient	10.5% vol.	Calibration	eq. 3.22
α_f	Heat transfer coefficient	100 W m^{-1} $°C^{-1}$	Jansson and Karlberg (2001)	eq. 3.23
d_2	FPDC parameter 1	10	Jansson and Karlberg (2001)	eq. 3.25
d_3	FPDC parameter 2	0	Jansson and Karlberg (2001)	eq. 3.25
z_{omsoil}	Soil surface roughness length for momentum	0.001 m	Calibration	eq. 3.32
z_{ohsoil}	Soil surface roughness length for heat	0.001 m	Calibration	eq. 3.32

Table 9.7: Some hydraulic and thermal parameters used in the simulations at Gd St Bernard.

Results

In order to keep the number of figures low, simulation results for the soil temperature and the liquid water content will only been shown at a depth of 5 and 30 cm. At other depths, results may be viewed in Appendix G.

The model calibration resulted in a generally satisfactory agreement between simulation and measurements (Figure 9.14 to Figure 9.17). In particular the temperature variation at the end of

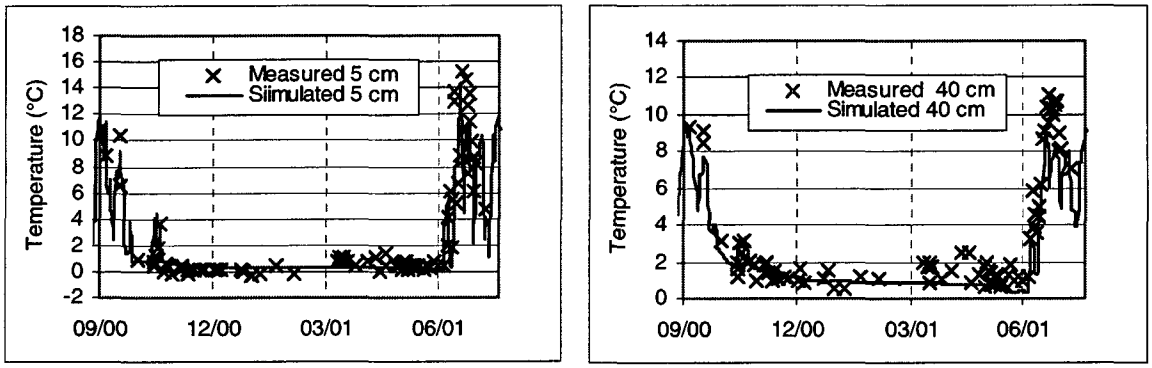

Figure 9.14: Simulated and measured soil temperature at a depth of 5 and 40 cm during winter 2000/2001 at Gd St Bernard south plot using the **MA**.

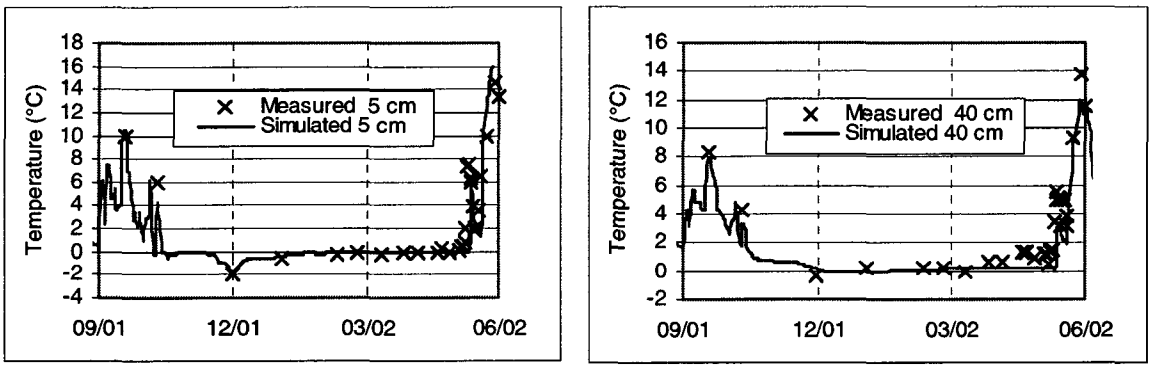

Figure 9.15: Simulated and measured soil temperature at a depth of 5and 40 cm during winter 2001/2002 at Gd St Bernard south plot using the **MA**.

the snowmelt was accurately reproduced, indicating that the model correctly simulated the melting of the soil frost. Measurements during the first winter indicated at 40 cm a soil temperature of approx. 1.2°C, which strengthened the hypothesis that, despite the high location of Gd St Bernard, the mean soil temperature is relatively warm at a south exposed location.

The simulated liquid soil water is a key value for both thermal and hydraulic soil processes, as, on the one hand, the soil frost penetration depends on the amount of liquid water content, and, on the other hand, the amount of surface runoff is mainly determined by the soil ice content at snowmelt. A correct simulation hence requires a precise estimation of the FPDC, and a successful estimation of the liquid water content prior to the onset of the winter. In contrast to Hannigalp, the calibration of these parameters was less precise, as no laboratory tests were carried out. However, during both winters, results were in good agreement with the

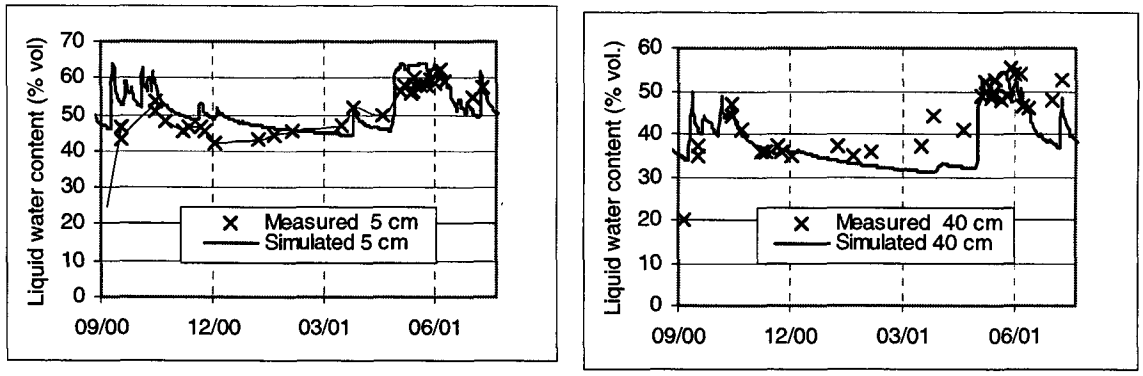

Figure 9.16: Simulated and measured liquid water content at a depth of 5 and 40 cm during winter 2000/2001 at Gd St Bernard south plot using the **MA**.

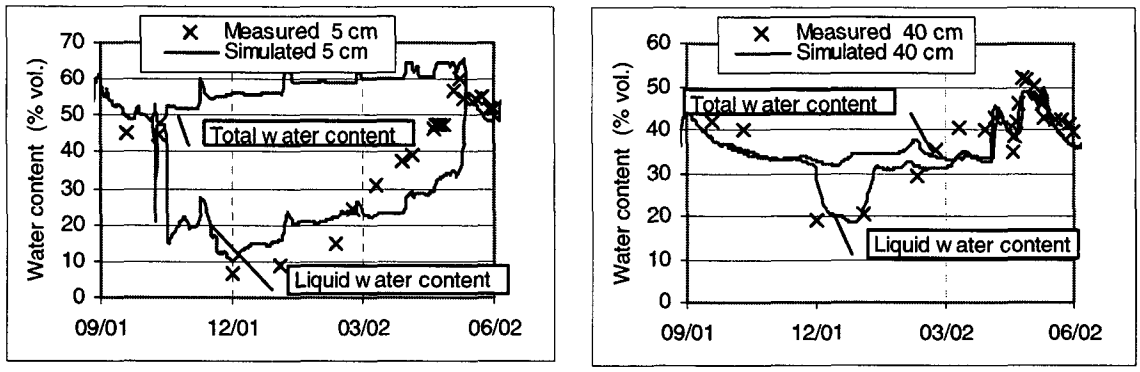

Figure 9.17: Simulated liquid/total water content compared with measured liquid water content at a depth of 5 and 40 cm during winter 2001/2002 at Gd St Bernard south plot using the **MA**.

measurements (except at 20 cm). In 2001/2002 the timing of freezing as well as maximal soil frost depth fitted well with measurements. At the end of the winter, the model underestimated the liquid water content at 5 and 10 cm. As already mentioned, this error probably arose from a fast melting of the pore ice due to heating from adjacent rocks.

No direct measurements were available of the volumetric content of ice. This value could not be directly derived from TDR measurements, but only deduced from the initial soil moisture content prior to freezing. It was not possible to carry out a direct measurement (for example with neutron probe) due to access constraints. This resulted in a major uncertainty about the amount of pore ice (and hence degree of ice blocking) during the different melt period, as, due to underneath heat flux, part of the ice thawed during the winter. The simulation indicated that most soil ice melted during winter 2001/2002 and only the upper 10 cm were still frozen before the final snowmelt.

9.3.3.2. MODEL VALIDATION WITH DISCHARGE MEASUREMENTS

The calibrated hydraulic conductivity had to be rejected. Indeed, the model was unable to simulate any surface runoff in spring 2001 (10% of the total meltwater runoff as lateral flow). This omission was due to the fact that the slope was not introduced in the calculation of the

surface runoff by the model. We had hence to change the soil conductivity, so as to be able to saturate the upper soil layer during the snowmelt. The hydraulic conductivity, k_{sat} was modified from 5 10^{-5} m/s to 10^{-5} m/s for the whole soil profile, which reduced the soil infiltration capacity and increased the lateral runoff.

By introducing this modification, the model was able to simulate a perched aquifer, resulting in both surface and subsurface flow (Figure 9.18.). While timing was in good agreement with

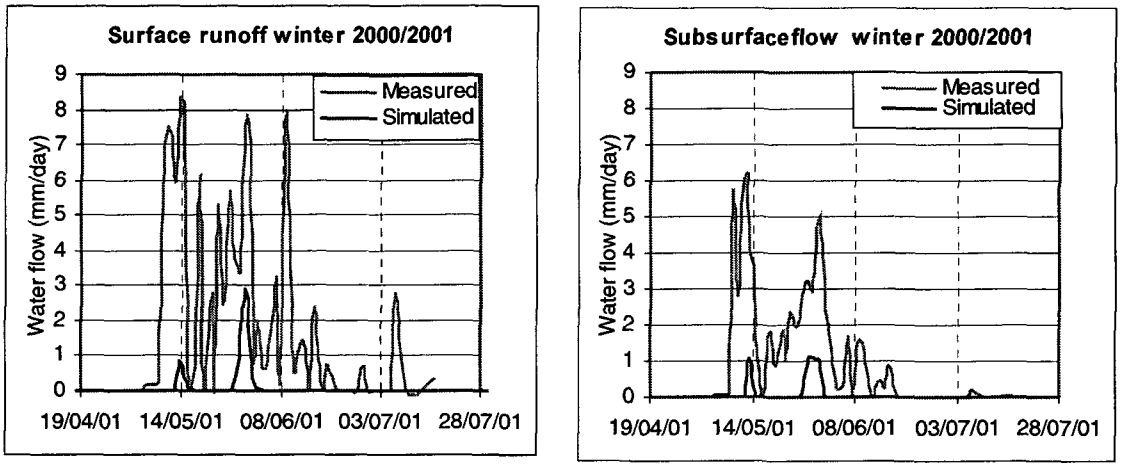

Figure 9.18: Simulated and measured surface and subsurface runoff during winter 2000/2001 at Gd St Bernard south plot using the **MA**. The hydraulic conductivity was set constant (k_{sat}=10^{-5}m/s) over the entire profile

measurements, the total accumulated lateral flow was largely under-predicted (8.7% of measured lateral flux). The model proved to be very sensitive to the hydraulic conductivity, and a further decrease created a notable overestimation of the surface runoff. This sensitivity of the model is questionable, and may have arisen from an underestimation in the vertical flow under specific saturated conditions. From several tests, the model appeared not to simulate any vertical water flow through the soil profile when a perched aquifer was present. Only lateral drainage took place.

In 2001/2002, the temporal evolution of the percolation was well represented by the model (Figure 9.19). In particular the total accumulation from 19th May to 25th June was well recreated. Previously, between 10th and 18th May, the collecting gutter was out of order and no data were collected. The fact that the model hardly simulated any lateral flux between 18th and 31st May affected the deep percolation, which was overestimated during that period. Later, between 1st and 18th June, simulation and measurements results were very close. From 18th June, the model did not simulate any deep percolation, as the simulated snow depth vanished.

At the onset of the melt period in March 2002, most meltwater ran off as lateral flow. As stated previously, we believe that the unaltered basal ice layer was mainly responsible for the high percentage of lateral runoff. Similar to Hannigalp, the model was not able to simulate this early surface runoff, as the basal ice sheet was not represented in the model, and no lateral flow was simulated during the minor snowmelt events until mid-April. (Figure 9.20). The total accumulated simulated runoff during both main snowmelt events (April and May) was in good agreement with the runoff recorded at the outlet of the plot field. However, we noticed that some

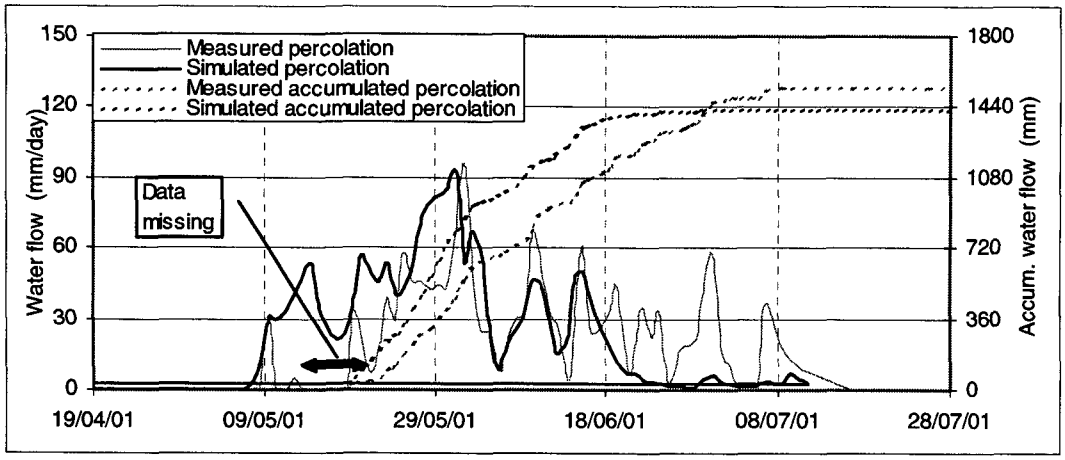

Figure 9.19: Simulated and measured deep percolation (daily flux and total accumulation from 18th May) during winter 2000/2001 at Gd St Bernard south plot using the **MA**.

specific snowmelt events were poorly reproduced. In particular, the model did not simulate any surface runoff during the cold period between 25th and 28th May (daily mean air temperature below 0°C), whereas we measured significant amounts of surface runoff, due to the intense global radiation during the day. This error may have resulted in an underestimation of the snowmelt by the **MA** under sub-zero temperatures (m_f in eq. 9.15), but may also have been the consequence of wrongly simulated temporal snowmelt water discharge, as the simplistic one layer snow model does not account for the movement of meltwater in the snowpack.

In May 2002, the upper part of the soil was mostly saturated, and subsurface flow was measured. In the simulation, this flux was constrained by (a) the amount of pore ice, (b) the number of drains in the model (i.e. the slope), and (c) the number of saturated layers. As during the final snowmelt, the simulated pore ice content hardly changed in the upper 10 cm (where the drainage flow originated), the maximal subsurface flow did not change with time. This explains why this flow was underestimated, in particular at the end of the snowmelt period (Figure 9.19).

To sum up, the water runoff was accurately simulated during the frozen winter by the **MA**. The thawing of the pore ice was, however, underestimated during the final snowmelt, as the model does not consider multi-dimensional features like the lateral heating, which are essential at that period. During the first winter, the model was unable to adequately reproduce the surface runoff.

9.3.3.3. APPLICATION TO THE NORTH SITE

No change was carried out in the model settings, except for the soil temperature at the lower boundary (9 m), where a mean soil temperature of 2°C was set. In an initial step, we tested both snow models, and chose the one reproducing the measurements best.

Due to the reduced available solar energy, the snow surface temperature was probably much colder at the north site than the measured air temperature at the monastery. This may explain why the **MA** was not able to reproduce accurately the soil freezing (simulated max. soil frost depth = 25 cm, measured soil frost depth > 40 cm). Results were improved by using the **EA** and simulation results will be discussed below.

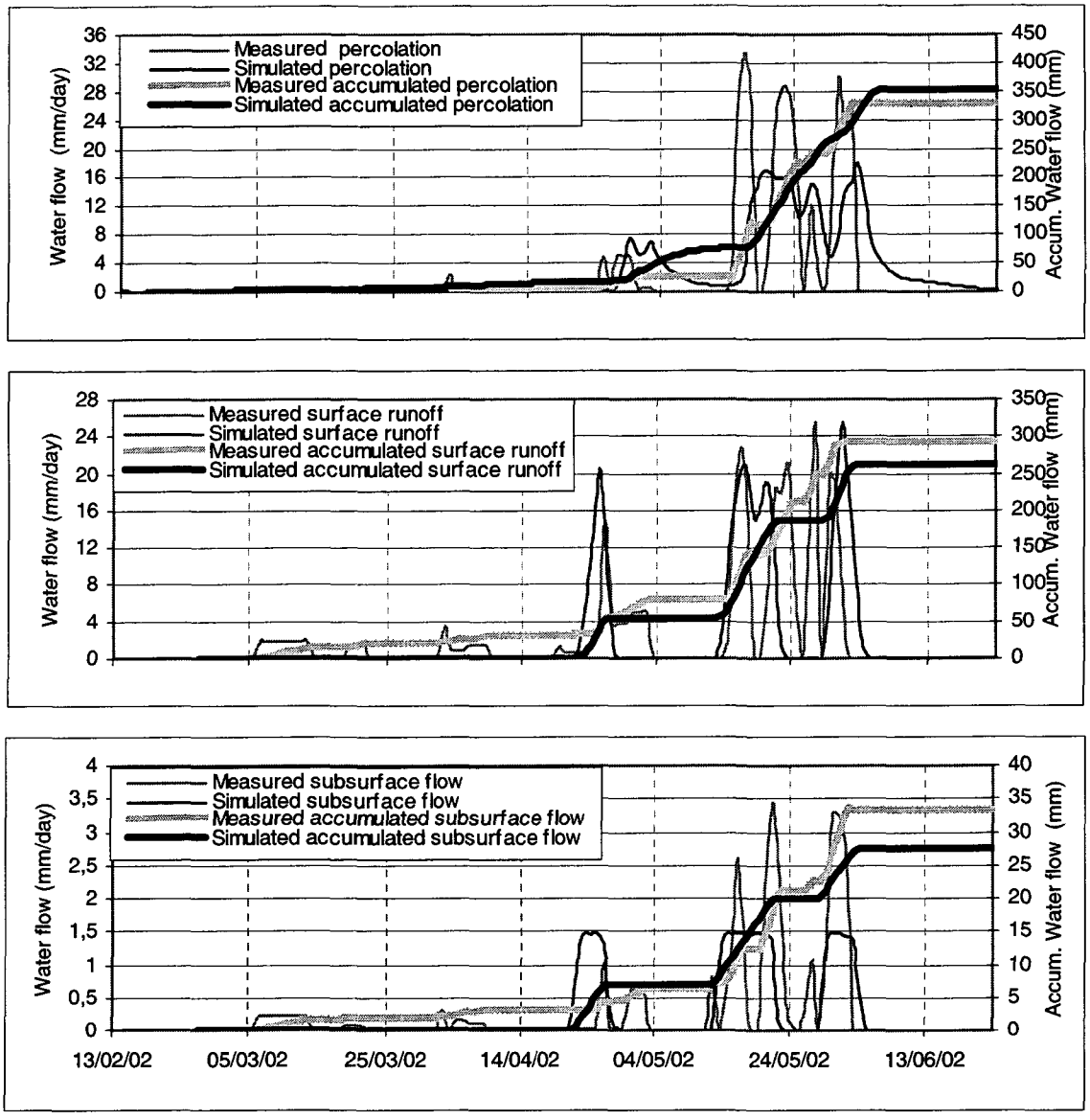

Figure 9.20: Simulated and measured deep percolation (a), surface flow (b), and subsurface runoff (c), during winter 2001/2002 at Gd St Bernard south plot using the **MA**.

The soil temperature was satisfactorily well reproduced by the model, especially at the onset of the winter, as illustrated in Figure 9.21. Similar to the south site, a fast soil temperature rise at the end of the winter indicated that most soil frost disappeared rapidly. The model did not reproduce as distinctively this change in June 2002, indicating a probable overestimation of the soil frost content at that time. From observations, the snow distribution was very inhomogeneous. At the end of June some parts close to the experimental plot were already free of snow, while there was still 20-30 cm of snow covering the site. We may hence expect a fast thawing of the soil ice due to heating from adjacent unfrozen areas. This may explain why, in July 2000, despite the presence of snow, a soil temperature of 1.9°C was measured at a depth of 30 cm, one week before the end of snowmelt, as against 0.5 on the average during the winter. .

Apart from the successful simulation of the soil temperatures, the time series of the liquid water content in the uppermost 30 cm were well reproduced by the model (Figure 9.22). In particular,

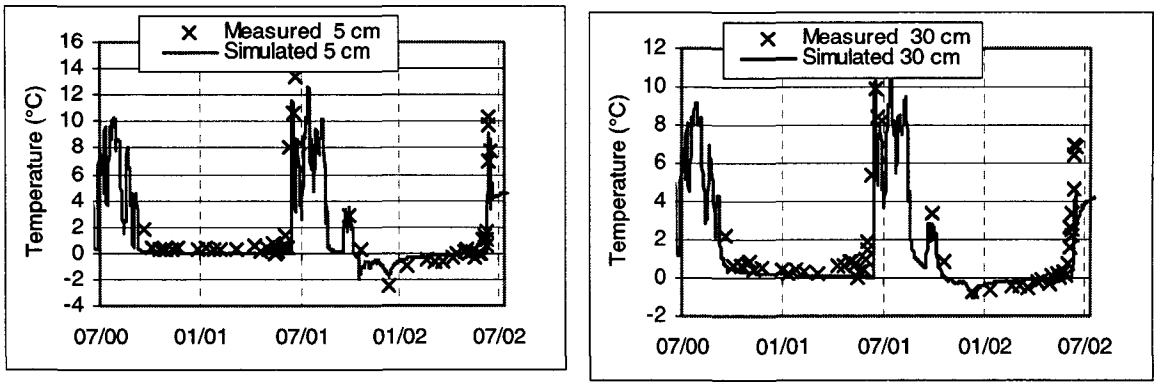

Figure 9.21: Simulated and measured soil temperature (°C) at a depth of 5 and 30 cm at Gd St Bernard north plot from October 2000 to July 2002 using the **EA**.

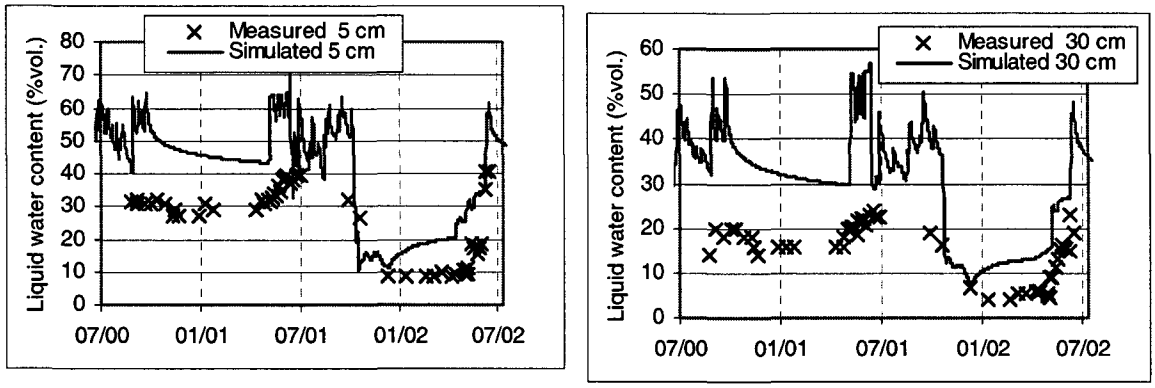

Figure 9.22: Simulated and measured liquid water content (% vol.) at a depth of 5 and 30 cm at Gd St Bernard north plot from October 2000 to July 2002 using the **EA**.

the marked increase in the water content during the onset of the final snowmelt in spring 2002 was well recreated. Nevertheless, the model tended to overestimate the soil liquid water content, due to the heterogeneous soil structure. The large slate stones reduced the available pore space, affecting the liquid water content measurements when located between the rods of the TDR probes.

The underneath soil heat flux was kept low by setting the mean soil temperature close to the freezing point (2°C). As a result, the heat flux hardly affected the soil frost depth (in spring 2002 the simulated soil frost depth remained at 70 cm). This result could only be partly verified, as, from measurements, we know that only the upper 30 cm of soil remained frozen until the end of the snowmelt period.

Finally, large amounts of meltwater were able to infiltrate into the soil. The simulation results showed that during the second winter, 64% of the total meltwater ran off as lateral flow.

9.3.3.4. APPLICATION TO THE EAST SITE

By setting the soil temperature at the lower boundary to 4 °C, the **EA** was unable to accurately simulate the soil temperature (in autumn 2001 soil freezing was excessive and too early). Simulation results were improved by using the **MA**, but the frost depth was underestimated

(maximal simulated frost depth 30 cm). Finally, the best fit was obtained by further decreasing the soil temperature at the lower boundary from 4°C to 2°C, so as to allow a deeper frost penetration. With this procedure, the soil liquid water content and the soil temperatures were satisfactorily well reproduced (Figure 9.23 and Figure 9.24). Similar to the two other sites, we note an overestimation in the frozen soil temperature and liquid water content.

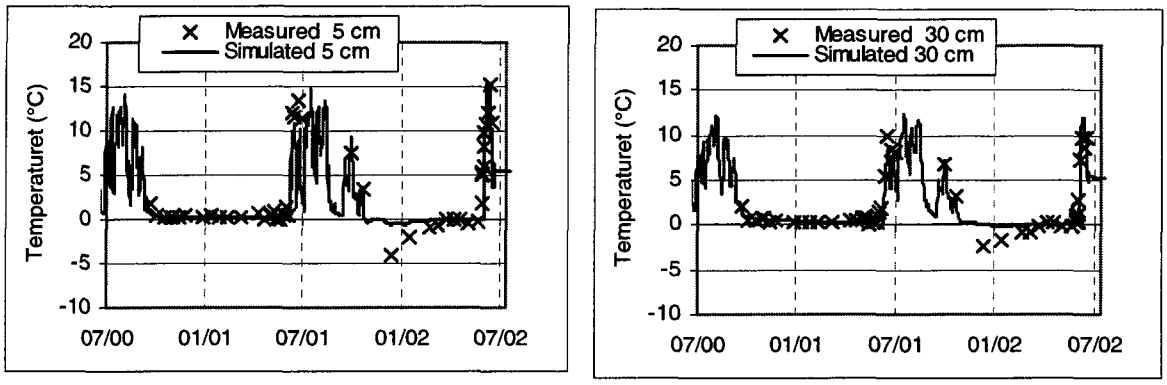

Figure 9.23: Simulated and measured soil temperature (°C) at a depth of 5 and 30 cm at Gd St Bernard east plot from October 2000 to July 2002 using the MA.

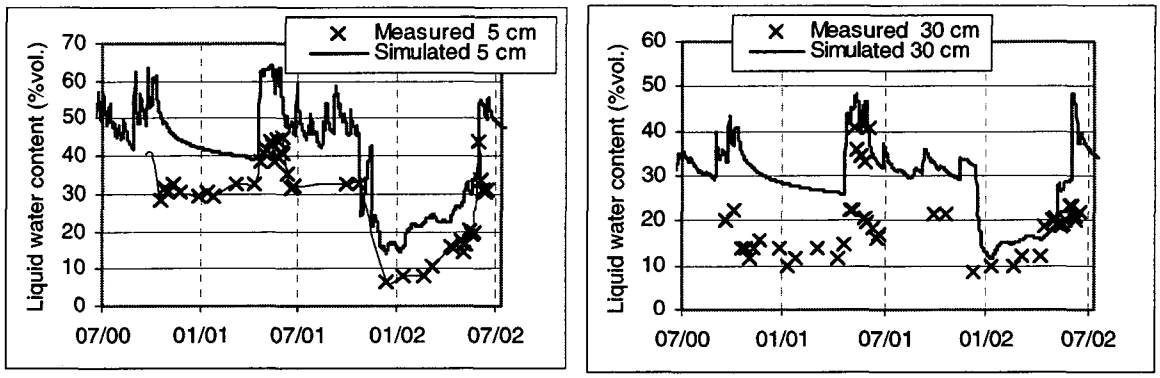

Figure 9.24: Simulated and measured liquid water content (% vol.) at a depth of 5 and 30 cm at Gd St Bernard east plot from October 2000 to July 2002 using the MA.

The soil was hardly ever saturated in spring 2001 and less than 1% of total meltwater runoff as lateral flow. During the next winter, the upper 40 cm of soil remained frozen until the end of the winter. The pore ice only marginally thawed, inhibiting most meltwater to infiltrate into the soil (58% of total meltwater ran off as lateral flow). To sum up, we found that the percentage of lateral flow was highest on the deeply frozen north plot, and lowest on the shallowly frozen south plot.

9.3.4. DISCUSSION

The horizontal component of the water balance (surface and subsurface runoff) showed to be particularly important during the frozen winter 2001/2002 at both experimental sites. The model was able to reproduce both lateral components in a satisfactory way. The presence of deep drains at the upper end of the experimental plots was essential (Figure 4.5 and Figure 4.8). It

allowed a complete insulation and a reduced horizontal extent of the experimental plots (approx. 3 m). As a result, we were able to use COUP, as the error resulting from the approximation in the pseudo-simulation of the lateral runoff was negligible. However, it would be desirable in future to further develop the model, in order to be able to simulate multi-dimensional processes. Indeed, significant differences in the soil water balance exist between areas close to the drains and areas next to the collecting gutter. At the upper end of the experimental plot, water input is mainly vertical, while at the lower end, horizontal input from adjacent areas has to be considered in the soil water balance.

A major difficulty arose from the fact that the basal ice layer was not simulated by COUP. At Gd St Bernard, the water discharge from early snowmelt events refroze in the upper soil layers, diminishing the soil infiltration capacity. This process of refreezing may be considered to be similar to the blocking effect of a basal ice sheet. At Hannnigalp, however, the model did not simulate any snowmelt until the onset of the final snowmelt. The calibration of the parameter f_{θ_i} is questionable, as at the onset of the melting period, the physical state of the simulated and real soil were different, the simulated one having a very low ice content in the upper soil layers and a high infiltration capacity. A different value for f_{θ_i} may be expected at Hannigalp, during winters with soil frost, but no basal ice.

Numerous models exist that simulate meltwater infiltration pathways in the snowpack (Colbeck 1972, Colbeck 1973, Marsh and Woo 1985) and the influence of ice layer on the meltwater pathways (Furbish 1988). These models are mostly process oriented and it seems difficult to incorporate such detailed calculations in long-term models, as is the case with COUP. We may, however, make a simple improvement to the model, by adding a «basal ice» layer between the soil surface and the snowpack. The basal ice would be formed when enough sensible energy is available to freeze the liquid water stored in the snowpack. This procedure would nevertheless involve determining appropriate values for the empirical factor describing the intensity of the blocking effect (the basal ice sheet is not impervious), and using a multi-layer snow model, so as to simulate the water content at the base of the snowpack.

The surface runoff depends on the pore ice content, which is related to amount of water refreezing in the soil α_f, as well as to frost-induced water flux f_i. As only few investigations were carried out to evaluate these two parameters, their values are very uncertain. α_f was found to vary between 100 to 1000 W m^{-1} $°C^{-1}$ (Stadler et al. 1997) (Stähli et al. 1999) (Stähli, Nyberg et al. 2001). In particular Stähli (2001) found that the value might vary considerably for similar soils. In our simulations, the prediction were not sensitive to this parameter, and the lateral runoff increased only marginally when high value were set for α_f. The impedance factor f_i is related to the ice content in the deepest soil layer and a low value induces significant lateral water flux towards the frozen fringe, increasing the amount of lateral runoff. It seems difficult to connect this factor to the soil type. Stähli (1999) noted for example that it might differ between years for the same soil. In our calibration, the value for f_i was much higher than values reported by earlier studies (Lunding 1990), (Stadler et al. 1997) (Stähli 1999). However, this value should be regarded with great caution, as a unique winter was available to set this value. Also, we did note have direct measurements of the rate of the frost-induced water flux, and we used a unique snowmelt discharge event to calibrate all three frost parameters f_i, f_{θ_i} and α_f.

A well known consequence of soil frost is frost heaving (i.e. a volume displacement when a soil freezes). Frost heaving has often been investigated over the last decades and is caused by the presence of excess ice (which is defined as "ice present in excess of the volume of the soil pores had the soil been unfrozen" (Williams and Smith 1989)). The origin of excess ice is mainly ice

segregation (i.e. water migration caused by the gradient in the liquid water pressure). Most of this ice is found in the form of ice lenses. When these lenses melt, the soil porosity, and hence the soil permeability, is affected (Miller and Lee 1999). In our simulations, we did not integrate the effect of ice building on the soil permeability, as on the one hand no ice lenses were observed, and on the other hand, the soil liquid water content previous to freezing was far below the total porosity. For such types of soils (i.e. sandy-loam), soil frost marginally affects the hydraulic properties of the unfrozen soil (Dysli 1991).

9.4. CONCLUSION

Modelling the snow depth evolution in Alpine regions appeared to be a delicate undertaking due to the multiple meteorological driving factors. Although it was possible to simulate the evolution accurately for the protected location of Hannigalp, the simulation of the snow depth at Gd St Bernard was less successful. The main reasons for the deviation were twofold: (i) the precipitation inputs were imprecise, and (ii) the one-layer snow model was limited to simulating a thick snowpack. To obtain accurate results some physical parameters expressing the influence of the overburden weight of the snow on the density had to be adapted, which could have caused erroneous simulation results, especially at the onset of the winter. Nevertheless using a single layer to simulate the snow depth should be sufficient, as long as interest is focused on the snowmelt discharge. It may be very limited when internal processes are of interest (like avalanches).

The two snow models tested differed in the formulation of the upper snow boundary, which is essential to simulate accurately mass and heat flux processes in the snowpack. The detailed **EA** was able to describe complex phenomena at the boundary, but errors in the outputs were probably a result of the inadequate daily temporal resolution of the weather data. A high temporal resolution, as well as a high number of parameters values, and consequently also a high number of measurements would result in a reliable calibration. The **MA** simulated snowmelt events as soon as the temperature arose above freezing point, and hence gave better results at an exposed location.

Much effort was put into calibrating the soil physical properties at Hannigalp. In addition to the *in situ* experiment, we used laboratory experiments to fix most soil physical parameters. This fairly precise model characterization gave good confidence in the resulting outputs, which was confirmed by the validation results of the modelled discharge runoff. In particular, the subdivision of the lateral flow into surface and subsurface flow was well reproduced by the model. At Gd St Bernard, the soil structure prevented any laboratory experiments being carried out. Hence the soil physical properties could not be described as precisely as at Hannigalp. The numerical model was only calibrated from *in situ* measurements, and the outputs are very uncertain. During unfrozen soil conditions, the model was unable to adequately reproduce the lateral flow (surface and subsurface flow), mainly because the slope is not considered explicitly in the calculation of the surface runoff. Interestingly, this was not the case when the soil was frozen, as the total amount of lateral runoff was well reproduced by the model. However, significant differences were noted in the discharge time evolution between measurements and simulation. The frost depth dynamic was well reproduced at both locations, especially the thawing of the pore ice at Gd St Bernard south plot was simulated fairly well. However, the model overestimated the liquid water content at Gd St Bernard. This excess pore ice may have partly caused the observed delay in the soil thawing at the end of the winter.

The sensitivity of the model response to several frost-related parameters showed the importance of finding appropriate values for these parameters. They controlled the pore ice content and consequently the soil infiltration capacity. The calibration and validation of these parameters were difficult, as only results from a single winter were available to set the values. In addition, the soil infiltration process was controlled by a basal ice sheet, which is not explicitly taken into account by the model. Despite these limitations, the accurately modelled results imply that the model is valid to represent at least the trend in the soil frost and snow depth evolution as well as the meltwater pathways for different climatic situations.

10. FREQUENCY OF SEASONAL SOIL FROST IN MOUNTAINS AND ITS SPATIAL EXTENSION

10.1. INTRODUCTION

The problem of describing the spatial soil frost distribution is made complex because of its strong correlation with the snow depth. The highly variable snow cover produces a variable soil frost distribution, which in turn has an impact on the snowmelt discharge. Water infiltrates predominantly in unfrozen or shallow frozen areas, whereas frozen areas prevent infiltration. Knowledge of the temporal evolution and spatial distribution of the pore ice content is hence essential to understanding the complex alpine hydrology.

In this section we discuss the influence of the altitude and the orientation on the soil frost extent, duration, and occurrence. We used the COUP model that had previously been calibrated for Hannigalp and Gd St Bernard to simulate the snow and soil frost dynamics under various climatic conditions. The main objective was to characterize the heterogeneous infiltration patterns in a mountain area and to outline the main climatic and topographical factors that favours the building of soil frost.

10.2. METHOD

The simulations were run for the period June 1967 to July 2002 at Hannigalp and between June 1982 and July 2002 at Gd St Bernard. The snow depth was simulated with the approach (empirical or energy balance) that yielded the most consistent results for each site.

10.3. HANNIGALP

10.3.1. COMPARISON OF THE TWO WINTERS EXAMINED WITH THE WHOLE SIMULATED PERIOD

Table 10.1 and Table 10.2 summarizes the main results obtained from the simulation between the period 1967-1968. We start by comparing these average values with the simulated results for the two winters examined.

	Winter air temperature (°C) (Nov-April)	*Winter precipitation (mm) (Nov-April)*	*Max. snow depth (cm)*	*Mean snow depth (cm)*	*# days with more than 70 cm of snow*	*# days with more than 10 cm of snow*
Mean value 1967-2001	-4.79	304.5	108 (25)	73.6 (19.8)	163 (38)	191.2 (20.3)
Winter 2000/ 2001	-3.49	333.9	108	78	157	190
Winter 2001/ 2002	-3.36	212	74	31	5	159

Table 10.1: Mean values for selected snow variables at Hannigalp, from a simulation based on daily data from 1968 to 2001 (with standard deviation), compared with simulated values for winter 2000/2001 and 2001/2002. The mean snow depth was taken between the beginning of November and the end of March.

	Max. soil frost depth (cm)	*Mean soil frost depth (cm)*	*# days with more than 8 cm of frost*	*Deep percolation (%)*	*Surface runoff (%)*	*Subsurface runoff*
Mean value 1967-2001	17.29 (18.4)	11.98 (12.4)	76.3 (89.3)	78.2 (21.4)	14.4 (16.9)	7.2 (5.36)
Winter 2000/ 2001	0	0	0	100	0	0
Winter 2001/ 2002	45	36	196	77.0	16.9	6.1

Table 10.2: Max/mean soil frost depth and mean percentage of deep percolation, surface runoff and subsurface runoff from a simulation based on daily data between 1968 and 2001 (with standard deviation), compared with simulated values for winter 2000/2001 and 2001/2002 at Hannigalp. The mean soil frost depth was taken between the beginning of November and the end of March.

Interestingly, winter length (i.e. number of days with more than 10 cm of snow), maximum and mean snow depth as well as well as the number of days with a thick snowpack (>70 cm) were all approximately within an average range for the warm and wet winter 2001/2002, in spite of the extremely high winter precipitation. This was a consequence of the rather warm air temperature throughout the winter, which caused increased snowmelt especially in spring, shortening the snow cover period. However, the reduction in the snow cover was not as drastic as at the village of Grächen, where the maximum and mean snow depths were far below average (Chapter 5: "Winter 2001/2002", page 60.). Results are consistent with the common assumption that a warmer temperature affects the snow cover mainly at lower altitudes, in locations where the mean winter temperature is close to the freezing point (Bultot, 1994).

Simulated snow depth was under-predicted (Figure 9.2) and it should be interpreted with caution. Nevertheless, results showed that the winter was particularly snow poor with a mean snow depth twice as low as the average value. The snowpack remained shallow throughout the winter, and rarely exceeded 70 cm. The reduction in the winter length (-16%) was not as sharp due to the late snowfall in May 2002. The simulated maximum soil frost depth was the second deepest over the whole period. As a result, all frost-associated parameters (maximum and mean soil frost depth, number of days with a soil frost depth > 8 cm) were far above average. Surprisingly and despite the deeply frozen soil, the percentage of deep percolation was within an average range. This was partly because the soil was already thawed to a depth of 10 cm in May 2002, and all melt water (106 mm) from the late snowmelt was able to infiltrate into the ground.

10.3.2. SNOW AND SOIL FROST DEPTH

The effectiveness of the snow cover in inhibiting the frost penetration in the soil is shown in Figure 10.1. During frozen winters, the soil frost is built up during the brief period prior to the arrival of a thick snowpack. An exception was winter 1968/1969, where in spite of an early thick snow cover, a soil frost of 13 cm was simulated at the end of the winter. This was a result of extremely cold air temperatures recorded during that winter (mean air temperature between December and April of -7.25°C as against -4.79°C on the average), which was the coldest winter in the last 50 years. One should nevertheless be suspicious of this simulation result, as 1.20 m of snow were simulated prior to any frost. Using a single snow layer may lead to excessive heat flow towards the soil surface, especially in spring when the snow density is at its highest. Indeed, the simulated thermal conductivity is overestimated by a single layer model[1], and the model overestimates the heat flux when the snowpack is thick, which may result in an erroneous

increase of the soil frost depth at the end of the winter.

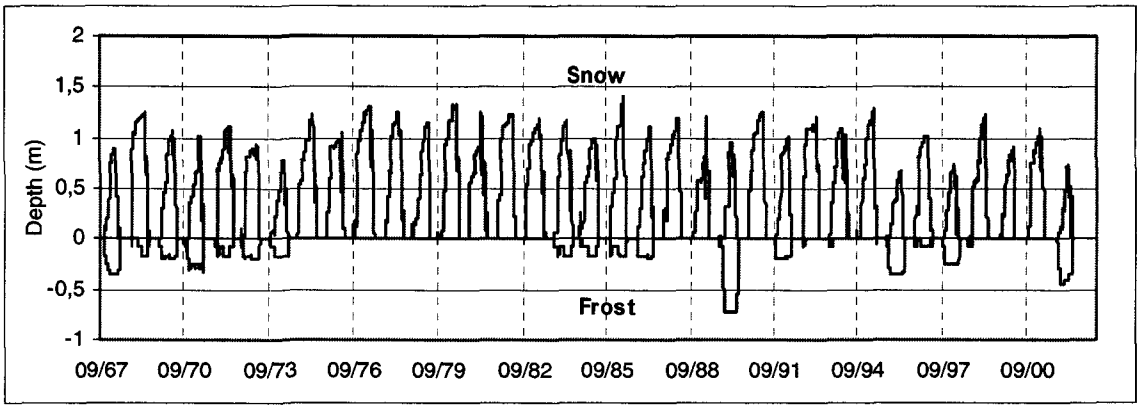

Figure 10.1: Simulated snow/frost depth between 1967 and 2002 at Hannigalp.

From the simulation results, we were able to classify the 35 winters as either deeply frozen (frost depth > 20 cm at the onset of the final snowmelt), frozen (8 cm < soil frost < 20 cm), shallow frozen (soil frost < 8 cm), and unfrozen (Table 10.3) The common assumption that is that there is in general sufficient snow as well as flow of ground heat to keep the soil unfrozen in alpine regions was generally verified. Indeed 67% of the simulated winters stayed unfrozen or shallowly frozen. Nevertheless, the soil was frozen below a depth of 8 cm for 33% of all simulated frozen winters, and this frozen layer had a significant influence on the flow pathways.

	# winters	*Winter*	*Mean percolation (%)*
Deep soil frost (> 20 cm)	5	68, 71, 96, 98, 02	46
20 < soil frost < 8	6	70, 73, 74, 87, 90, 92	53
Shallow soil frost (< 8 cm)	6	72, 84-86, 88, 00	86.7
No soil frost	17	75-83, 88, 89, 91, 93-95, 97, 99 01	100
Particular winter	1	69	-

Table 10.3: Deeply frozen, shallowly frozen or unfrozen winters at Hannigalp, with average mean percolation for each category of winter. Winter 68 stands for 1967/1968

10.3.3. DISCHARGE

From Table 10.3 we note that the amount of meltwater that runs off as lateral flow increases with soil frost depth. This increase is particularly significant, and varies between 13% vol. for a shallowly frozen soil to 54% for a deep soil frost. The fact that the soil frost depth influences the amount of infiltration water has long been recognized (Granger 1984), as part of the infiltrating water refreezes when it comes into contact with the frozen soil. In our case, we nevertheless expected a slighter reduction of the soil infiltration capacity with soil frost depth, as the (simulated) proportion of lateral flow made up 35% of total snowmelt during the main

1. The thermal conductivity in the model is proportional to the square of the average density of each snow layer, which is higher than the average of the square densities of different layers.

snowmelt event in the deeply frozen winter 2001/2002. Reasons for these differences are the following. On the one hand, the soil was very dry prior to freezing in 2001/2002 (approx. 22% vol. of moisture content), and a higher value would have significantly increased the amount of surface runoff. This could be verified in 1971, when a high ice content (30% vol. of moisture content) prevented most water from infiltrating (57% of the melt water runoff as lateral flow). On the other hand, soil infiltration capacity was reduced when refreezing of melted snow in the soil occurred after an early snowmelt due to the cold air temperature. In 1968 the snowpack was reduced to 40 cm after an early snowmelt event. This shallow snowpack no longer insulated the ground and a sharp increase in the ice content of the upper soil layers took place after the weather changed to very cold conditions. Additionally, infiltration of snowmelt into frozen soils is also dependent on different factors like the melt rate or the storage capacity of the snowpack, factors that affect the snowmelt runoff curves. Typically, high melting intensity increases the amount of surface and subsurface flow, as the soil amount of infiltrating water is limited by the soil infiltration capacity.

10.4. GD ST BERNARD

10.4.1. COMPARISON OF THE TWO WINTERS EXAMINED WITH THE WHOLE SIMULATED PERIOD

Similarly to at Hannigalp, we compared the *simulated* rather than the measured results for both winter examined with those for the whole simulation period. Due to the significant differences between simulated and measured snow depth (Figure 9.6), it was the only way to obtain a reasonable comparison.

At the north site, in contrast to Hannigalp, all snow related parameters were far above the average values (Table 10.8). In particular, the rather warm air temperature during that winter apparently, rarely affected the max and mean snow depths. If elevation had an impact on the snow-related parameters, orientation also greatly influenced the snow cover evolution. The warm air temperature affected the snow cover, predominantly on the south plot, but also partly on the east plot. As a result the maximum snow depth at those locations were approx. within the average value (Table 10.4 and Table 10.6), whereas the mean snow depth showed average values at the south plot only. The number of days with a snow depth exceeding 70 and 150 cm (ND) provides a sensitive index of the snow cover length. The higher the ND, the longer the snow cover period. These numbers showed a similar evolution for all orientations with higher than average values. This is a result of the high precipitation recorded during that winter, which enabled a long snow cover period. The warm temperature did little to alter the ND, as the increased melt water on the south and east plots was retained in the snowpack.

For winter 2001/2002, results were similar to those at Hannigalp. The snow depth was greatly affected by the warm air temperature and the reduced winter precipitation, regardless of the orientation. The soil-frost-depth related parameters were also far below average for each simulated site. By not adjusting the simulated snow depth to the measured values, some differences in the output were noted between the results shown and those from the calibrated and validate simulations (Figure 9.6). Especially the soil frost depth was underestimated for the east site (25 cm). At the south site, a slight underestimation of the soil frost depth in January enabled the soil to thaw almost entirely in May, which explains why only 20% of the total melt water runoff was lateral flow. At the two other sites, the percentage of lateral runoff was far

above average, as the soil remained frozen until the end of the snow cover period.

SOUTH	*Winter air temperature (°C) (Nov-April)*	*Winter precipitation (mm)[a] (Nov.-April)*	*Max. snow depth (cm)*	*Mean snow depth (cm) November to March*	*# days with more that 150 cm of snow*	*# days with more that 70cm of snow*
Mean value 1981-2002	-6.1	1208.0	220 (0.43)	76 (15)	50 (10)	118 (8.6)
Winter 2000/ 2001	-5.7	1544.8	222 (+1%)	82 (+8%)	53 + 6%)	139 (+18%)
Winter 2001/ 2002	-5.1	1084.2	182 (-17%)	54 (-27%)	25 (-50%)	111 (-6%)

Table 10.4: Mean values from the simulation based on daily data from 1982 to 2002 (with standard deviation) for selected snow variables at the south plot at Gd St Bernard, compared with simulated values for winters 2000/2001 and 2001/2002 (with change from mean value as percentage). The mean snow depth was taken between the beginning of November and end of March.

a. *The precipitation shown is that measured by the SMA, and not the modified precipitation used for the simulation.*

SOUTH	*Max. soil frost depth (cm)*	*Mean soil frost depth (cm)*	*# days with more than 8 cm of frost*	*Deep percolation (%)*	*Surface runoff (%)*	*Subsurface runoff*
Mean value 1967-2001	30.7 (28.4)	19.1 (15.7)	136 (99.1)	74.9 (24.8)	23.1 (22.3)	2.0 (1.8)
Winter 2000/ 2001	0	0	0	98.9	0.6	0.4
Winter 2001/ 2002	38	24	186	81.4	15.6	2.8

Table 10.5: Max/mean soil frost depth and mean percentage of deep percolation, surface runoff and subsurface runoff from the simulation based on daily data from 1968 to 2001 (with standard deviation), compared with simulated values for winters 2000/2001 and 2001/2002 at Gd St Bernard south plot. The mean soil frost depth was taken between the beginning of November and end of March.

EAST	*Winter (Nov-April) air temperature (°C)*	*Winter (Nov-April) precipitation (mm)[a]*	*Max. snow depth (cm)*	*Mean snow depth (cm) November to March*	*# days with more that 150 cm of snow*	*# days with more that 70cm of snow*
Mean value 1981-2002	-6.1	1208.0	284 (13.4)	137 (8.5)	111 (11.3)	177 (5.7)
Winter 2000/ 2001	-5.7	1544.8	279 (-1%)	156 (+14%)	137 (+23%)	194 (+9%)
Winter 2001/ 2002	-5.1	1084.2	217 (-24%)	83 (-39%)	73 (-40%)	131 (-13%)

Table 10.6: Mean values from the simulation based on daily data from 1982 to 2002 (with standard deviation) for selected snow and soil frost variables at the east plot at Hannigalp, compared with simulated values for winters 2000/2001 and 2001/2002 (with change from mean value as percentage). The mean snow depth and mean soil frost depth were taken between the beginning of November and end of March.

a. *see note a above*

10.4.2. SNOW AND SOIL FROST DEPTH

Figure 10.2 shows the snow and soil frost depth for each site between 1982 and 2002. The simulation results reflect the strong variability due to the differences in the exposure. As

EAST	Max. soil frost depth (cm)	Mean frost depth (cm)	# days with more than 8 cm of frost	Deep percolation (%)	Surface runoff (%)	Subsurface runoff
Mean value 1967-2001	16.2 (15.4)	11.7 (9.9)	80.3 (75.2)	77.1 (22.6)	21.2 (19.2)	1.7 (1.2)
Winter 2000/ 2001	0	0	0	98.8	0.7	0.4
Winter 2001/ 2002	25	19	137	56.9	39.6	3.5

Table 10.7: Max/mean soil frost depth and mean percentage of deep percolation, surface runoff and subsurface runoff from the simulation based on daily data from 1968 to 2001 (with standard deviation), compared with simulated values for winters 2000/2001 and 2001/2002 at Gd St Bernard east plot. The mean soil frost depth was taken between the beginning of November and end of March.

NORTH	Winter (Nov-April) air temperature (°C)	Winter (Nov.- April) precipitation (mm)[a]	Max. snow depth (cm)	Mean snow depth (cm) November to March	# days with more that 150 cm of snow	# days with more that 70cm of snow
Mean value 1981-2002	-6.1	1208.0	396 (13.7)	215 (12.6)	178 (9)	220 (5.3)
Winter 2000/ 2001	-5.7	1544.8	434 (+10%)	264 (+23%)	220 (+24%)	242 (+10%)
Winter 2001/ 2002	-5.1	1084.2	351 (-11%)	131 (-39%)	127 (-29%)	195 (-11%)

Table 10.8: Mean values from the simulation based on daily data from 1982 to 2001 (with standard deviation) for selected snow and soil frost variables at the north plot at Hannigalp, compared with simulated values for winters 2000/2001 and 2001/2002 (with change from mean value as percentage). The mean snow depth and mean soil frost depth were taken between the beginning of November and end of March.

a. see note a previous page.

NORTH	Max. soil frost depth (cm)	Mean soil frost depth (cm)	# days with more than 8 cm of frost	Deep percolation (%)	Surface runoff (%)	Subsurface runoff
Mean value 1967-2001	19.4 (17.4)	15.8 (13.1)	55.7 (48.8)	86.3 (25.7)	13.0 (12.3)	0.7 (1.3)
Winter 2000/ 2001	0	0	0	100	0	0
Winter 2001/ 2002	77	71	151	52.8	44.2	3.0

Table 10.9: Max/mean soil frost depth and mean percentage of deep percolation, surface runoff and subsurface runoff from the simulation based on daily data from 1968 to 2001 (with standard deviation), compared with simulated values for winters 2000/2001 and 2001/2002 at Gd St Bernard north plot. The mean soil frost depth was taken between the beginning of November and end of March.

expected, the snow depth was deepest on the north plot (average max snow depth 396 cm) and lowest on the south plot (267 cm).

The soil frost distribution showed a contrasting picture. Although it was deepest at the north site, only 5 out of 19 winters were deeply frozen (Table 10.12), as an early snowpack created a mostly insulating layer. On the south plot, soil frost was simulated at the onset of hardly every winter (Table 10.10). But due to the relevant underneath heat flux, the soil was mostly unfrozen in May/June (only 9 winters remained frozen at snowmelt). On the east plot, soil frost was shallowest and no soil frost occurred below 50 cm. During the 10 winters with soil frost, the

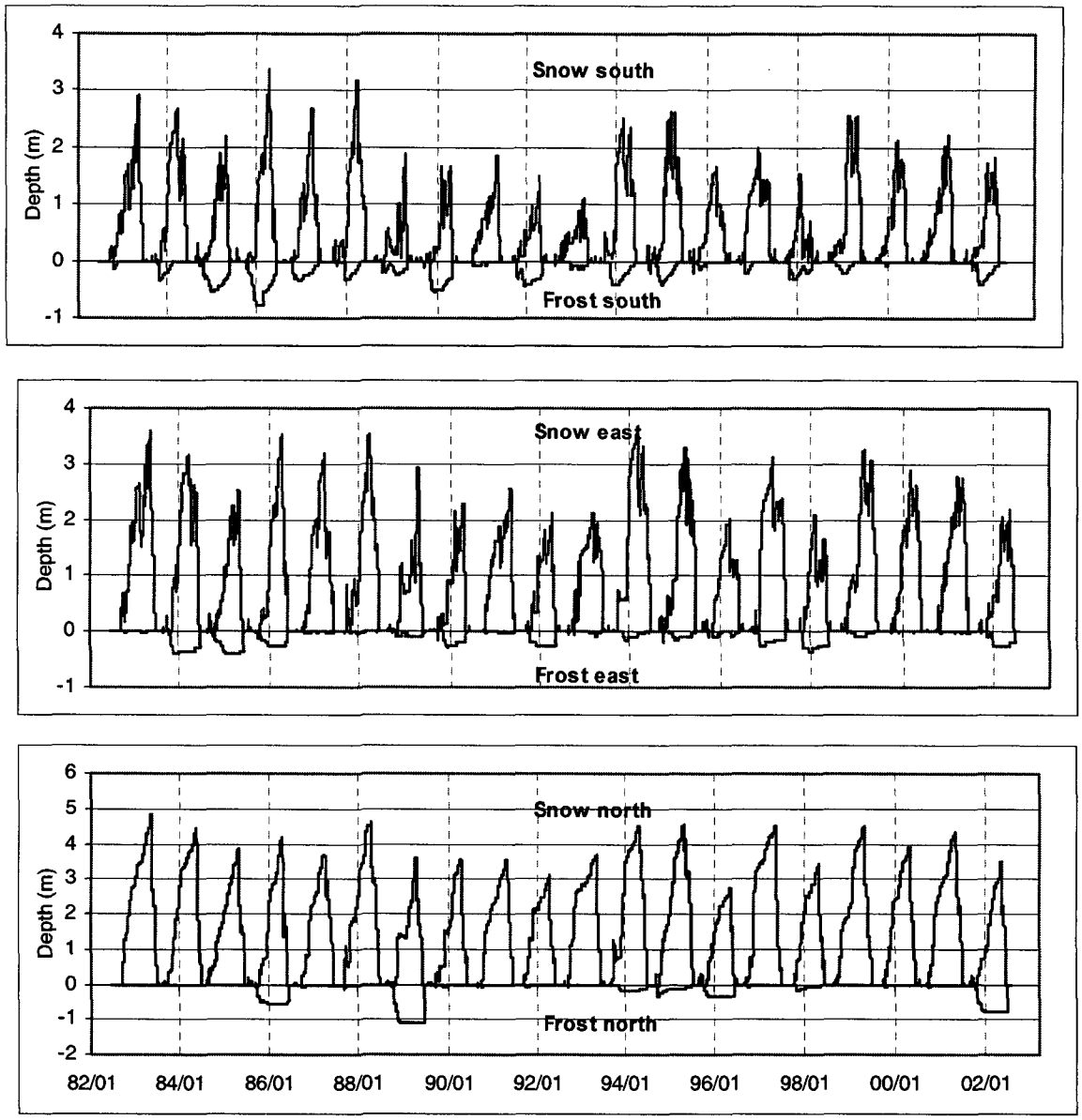

Figure 10.2: Simulated snow and soil frost depth at Gd St Bernard south, east and north plots between 1982 and 2002.

rather low underneath soil heat enabled the soil frost to remain until the end of the snow (Table 10.11).

SOUTH	*# winters*	*Winters*	*Mean percolation (%)*
Deep soil frost (> 20 cm)	5	85, 86, 90, 92, 98	32
20 < soil frost < 8	4	87, 89, 94, 02	69
Shallow soil frost (< 8 cm)	1	93	81
No soil frost	9	83, 84, 88, 91, 95-97, 99-01	98

Table 10.10: Deeply frozen, shallowly frozen or unfrozen winters at Gd St Bernard south site, with average mean percolation for each category of winter. Winter 68 stands for 1967/1968

EAST	*# winters*	*Winters*	*Mean percolation (%)*
Deep soil frost (> 20 cm)	8	84-86, 90, 92, 97, 98, 02	47
20 < soil frost < 8	2	89,95	84
Shallow soil frost (< 8 cm)	1	94, 99	98
No soil frost	8	83, 87, 88, 91, 93, 96, 00, 01	99

Table 10.11: Deeply frozen, shallowly frozen or unfrozen winters at Gd St Bernard east site, with average mean percolation for each category of winter. Winter 68 stands for 1967/1968.

NORTH	*# winters*	*Winters*	*Mean percolation (%)*
Deep soil frost (>20 cm)	4	86, 89, 96, 02	48
20 < soil frost < 8	1	94	73
Shallow soil frost (< 8 cm)	2	95, 98	92
No soil frost	12	83-85, 87, 88, 90-93, 97, 99-01	98

Table 10.12: Deeply frozen, shallowly frozen or unfrozen winters at Gd St Bernard north site, with average mean percolation for each category of winter. Winter 68 stands for 1967/1968.

In contrast to other studies (see for example Hardy et al. 2001) we did not find any specific relationship between the maximum snow and soil frost depth (R^2<0.1 for each orientation). This result was not surprising, because the soil frost depth was not influenced by the snow depth as soon as the snow was deeper than approx. 50 cm.

Warming by underneath heat flux may also affect the soil frost at the north site. This could be verified in winter 1994/1995, when a rather warm autumn was followed by a cold, snow-poor period, resulting in soil freezing (25 cm). By mid-November, a thick insulating snow had recovered the soil. The still warm ground thawed most of the accumulated soil pore ice, and at the end of the winter, only the upper 8 cm were still frozen.

The comparison of the soil frost extent for each site examined highlights the strong spatial variation in the soil frost distribution. From the 19 winters simulated, only 9 showed a similar soil frost extent for each site (i.e. soil was frozen (unfrozen) everywhere at snowmelt). Almost all possible combinations were found, even the most surprising. For example, soil was frozen on the north plot in 1995/1996, whereas it remained unfrozen on the south and east plots. In 1989/1990 however, the soil remained frozen on the south and east plots, but stayed unfrozen on the north plot.

Elevation also had a relevant impact on the soil frost distribution. While the total number of frozen and deeply frozen winters are approximately similar at Gd St Bernard north plot (5) and Hannigalp 6) between the period 1982-2002, a closer investigation revealed that most frozen winters at one place were unfrozen at the other (67% of all winters).

Finally, we note also the effect of the soil texture on the soil frost depth. The fact that highly conductive large slate stones were found at Gd St Bernard allowed a fast and deep freezing. As a result, the simulated soil frost depth was much deeper at Gd St Bernard north plot, than at Hannigalp, as for example in 2001/2002, when 70 cm were simulated at Gd St Bernard as against 45 at Hannigalp

10.4.3. SOIL TEMPERATURE AND SOIL MOISTURE

The differences in the exposure between each site resulted in deviation in the soil temperatures. Soil temperatures shown in Figure 10.3 stand for the temperature differences between the combined north and east plots and the south plot from 1982 to 2002. A value above 0°C indicates that the temperature on the south plot was warmer. The soil temperature was mostly highest on the south plot, due to the increased solar radiation and the lower snow cover period. Differences are particularly marked for the north plot (up to 15°C) in June, as the snow remained between 2 and 4 weeks longer on the north plot. In winter, the soil temperature was mostly very close to 0°C at each site, and therefore little difference was found between each orientation.

The liquid water content (Figure 10.3) was lowest in summer on the north plot. However, one would have expected the opposite, as evaporation is lowest for that exposure. These differences

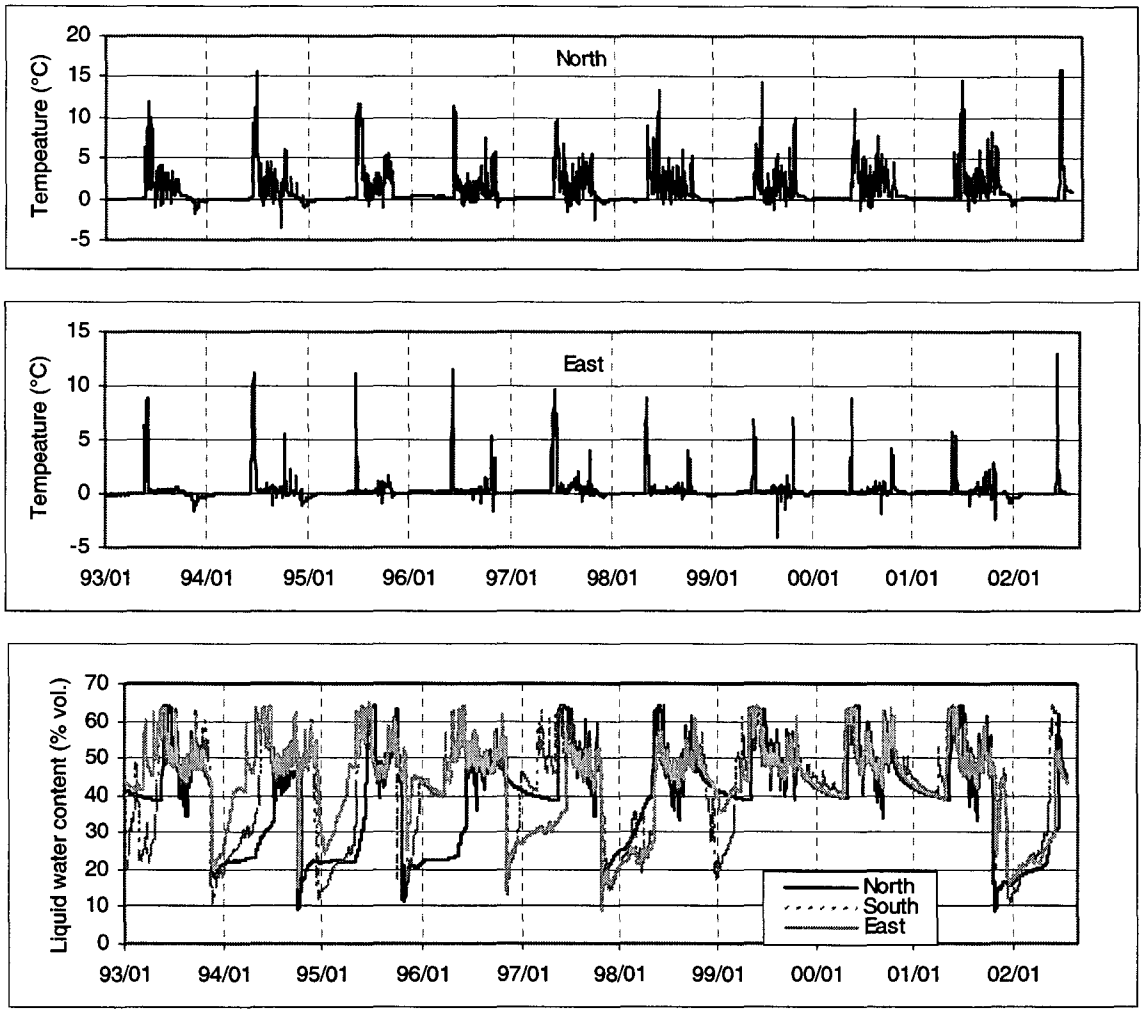

Figure 10.3: Differences between the soil temperature at the north/east plots and the south plot at a depth of 5 cm from 1993 to 2002, as well as liquid water content at a depth of 5 cm at the south, east and north plots for same period.

arise from the fact that two different methods were used to simulate evaporation (energy balance

and empirical). At the onset of the freezing period, the simulated water content was mostly very similar for all orientations, due to the reduced evaporation in late autumn, as well as to the frequent precipitation at that time of the year.

10.4.4. SNOWMELT DISCHARGE

Similar to Hannigalp, the soil infiltration capacity was considerably reduced by the soil frost. Between 32% and 48% of the total meltwater infiltrated into a deeply frozen soil. When soil frost was less pronounced (between 8 and 20 cm), most meltwater was able to infiltrate into the ground (between 69% and 84%). Finally, a shallow soil frost (< 8 cm) hardly affected the soil infiltration capacity. The higher intensity in the snowmelt on the south plot may explain why more surface runoff was simulated for that location. The fact that snowmelt mostly takes place three to four weeks later at the north plot than elsewhere may explain why hardly any differences were noted between the discharge results for the east and north plots, as, at that time, snowmelt was intensive due to the warm air temperature.

10.5. CONCLUSION

We used the COUP model to simulate the snow/soil frost depth and the snowmelt discharge for a wide range of climatic conditions at Hannigalp and Gd St Bernard. Whereas in winter 2001/ 2002, soil was deeply frozen at each location examined, the simulations results showed a contrasting picture of the spatial soil frost distribution. Soil frost varied extensively depending on the altitude and the orientation. The complex energetic interactions between soil, snow and atmosphere accounted for these large variations. During specific winters, the soil could freeze on the south and north plots, but remain unfrozen on the east plot at Gd St Bernard. Also, the south plot was frequently subject to soil frost at the onset of the winter: however, this frost rarely remained until the end of the snowmelt period. On northerly exposed plots, soil frost was very deep but not very frequent and lasted mostly until the end of the melt period. Altitudinal variation of soil frost between Hannigalp and Gd St Bernard north site indicated that heat and water fluxes are very sensitive to the altitude. This last point will be further developed in Chapters 11 and 12.

As expected, the soil frost depth had a strong impact on the snowmelt discharge. On a southerly exposed plot, this led to extremely high amounts of surface runoff as the snowmelt intensity was higher than elsewhere.

11. GROUNDWATER RECHARGE AT SNOWMELT: THE EXAMPLE OF GRÄCHEN

11.1. INTRODUCTION

Quantifying the influence of the soil frost on the aquifer recharge remains difficult due to its spatial variability (see previous chapter). Also, the groundwater recharge depends upon several conditions like the rate of snow ablation, the soil moisture conditions, and the thickness and composition of the soil over the bedrock (Kane and Chacho 1990). Main objective of this chapter is hence to relate the local effect of soil frost on the snowmelt runoff with its influence on an alpine aquifer recharge. For this purpose, we investigate the water table rise of a small aquifer in the area of Grächen.

11.2. METHOD

The influence of seasonal soil frost on the water balance of large areas involves a complete hydrogeological analysis. It requires in particular a surface, geophysical and hydraulic cartography, as well as a long-term water balance study of the entire catchment investigated. Such a research would go far beyond the scope of this study and could not be undertaken. As a result, we limited ourselves to making the best possible use of the available data. These were given by the snow depth and water table fluctuation at Grächen, as well as by the frost and snow depth at Hannigalp. For Hannigalp, we used the calibrated COUP model to simulate the snow and frost depth at different altitudes over the entire catchment, using altitudinal corrected input data. Snow depth measurements at Grächen were used to better adjust the model (Figure 11.1). Each winter was then classified as «frozen», «partially frozen» or «unfrozen», depending on the spatial frost depth extent. Finally, we compared the water table rise at Grächen at snowmelt with the precipitation between early November and the end of the snow melt period. If seasonal soil frost influences the alpine aquifer recharge, we may expect a reduction in the water table rise at snowmelt period during «frozen» winters.

11.2.1. DESCRIPTION OF THE AREA STUDIED

The rather small catchment (approx. 10 km^2) stretches between the village of Grächen (1600 m) and the Wannehorn (2600 m) (Figure 11.2). The village of Grächen is located on a terrace, built up by an interglacial subsidence. The region located above the village is mainly constituted by a quaternary deposit (till and slope deposit). The thickness of these rocks is estimated to be 100 to150 m. Single-well response tests were performed in wells and yield high hydraulic conductivity values of 10^{-4} m/s (Rovina and Zuber 1997). Due to the high infiltration capacity of the soil surface, most of the precipitation infiltrates into the soil and little surface runoff (river) takes place.

The vegetation map of Grächen may be related to that of the Turtmanntal valley, a valley some 20 km to the west with similar climatic conditions. Hoersch et al. (2001) produced different scale vegetation maps for that valley by dividing the altitude into five zones between 1000 and 3000 m and by classifying the elevation distribution of the vegetation using remote sensing (Figure 11.3). From this study, we note that forest is predominantly present between

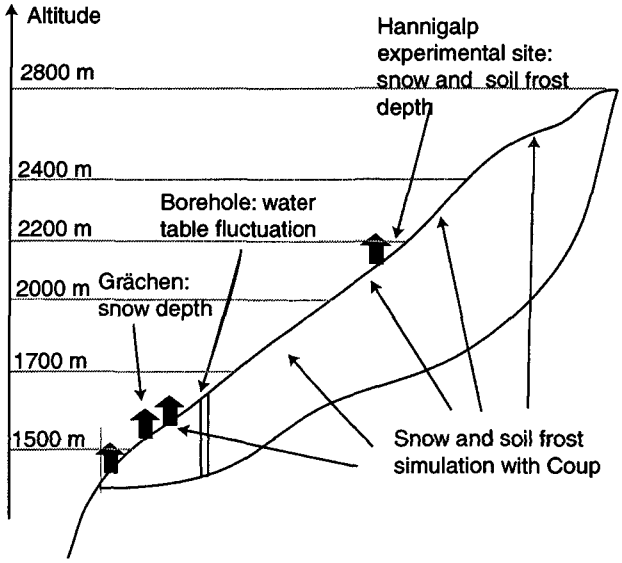

Figure 11.1: Schematic profile of the aquifer of Grächen. Available data at the studied area, as well as division of the hydrogeological catchment into five sections differing in their altitude. For each section, the snow and frost depth was simulated with COUP between 1992 and 2002.

1000-2200 m. Alpine grassland varies between 17% (1000-2200 m) and 40% (2200-2700 m). Above 2500 m, alpine grassland becomes rare and none vegetated area increases. No more grassland is found above approx. 2700 m, and landscape is composed of glacier or rocks. The Hannigalp experimental site may be accounted for alpine grassland, i.e. for a region located mainly between 2000 and 2300 m. In lower areas, the vegetation cover differs markedly between 1600 and 2000 m, as most part of this area is covered with larch forest. Above 2300 m the vegetation disappears entirely and fallen rocks build up the soil surface; the soil structure differs markedly from the one at Hannigalp. Above approximately 2500-2600 m, permafrost is encountered.

The orientation (North-West) and the slope (40%) of the catchment are approximately constant between the Wannehorn and the village of Grächen.

Measurements of the aquifer water-table began in 1992, when a 50 m deep well was completed at Meisen (1650 m) on the upper end of the village of Grächen. Continuous water-table depth monitoring, using a paper roll, has been maintained since then.

11.2.2. SNOW AND SOIL FROST DEPTH SIMULATION

To incorporate the spatial and temporal variations due to the elevation, we divided the catchment into five sections differing in their altitude (Table 11.1) For each section, we simulated the snow and soil frost depth between 1992 and 2002 using the previously calibrated model of Hannigalp. By using this procedure, we hence supposed identical soil texture and aspects over the entire catchment. This assumption is of course a strong simplification of the reality, but enabled to obtain an estimated soil frost and snow depth dynamic over the whole catchment.

As all meteorological data were measured at a single observation station, the model inputs had

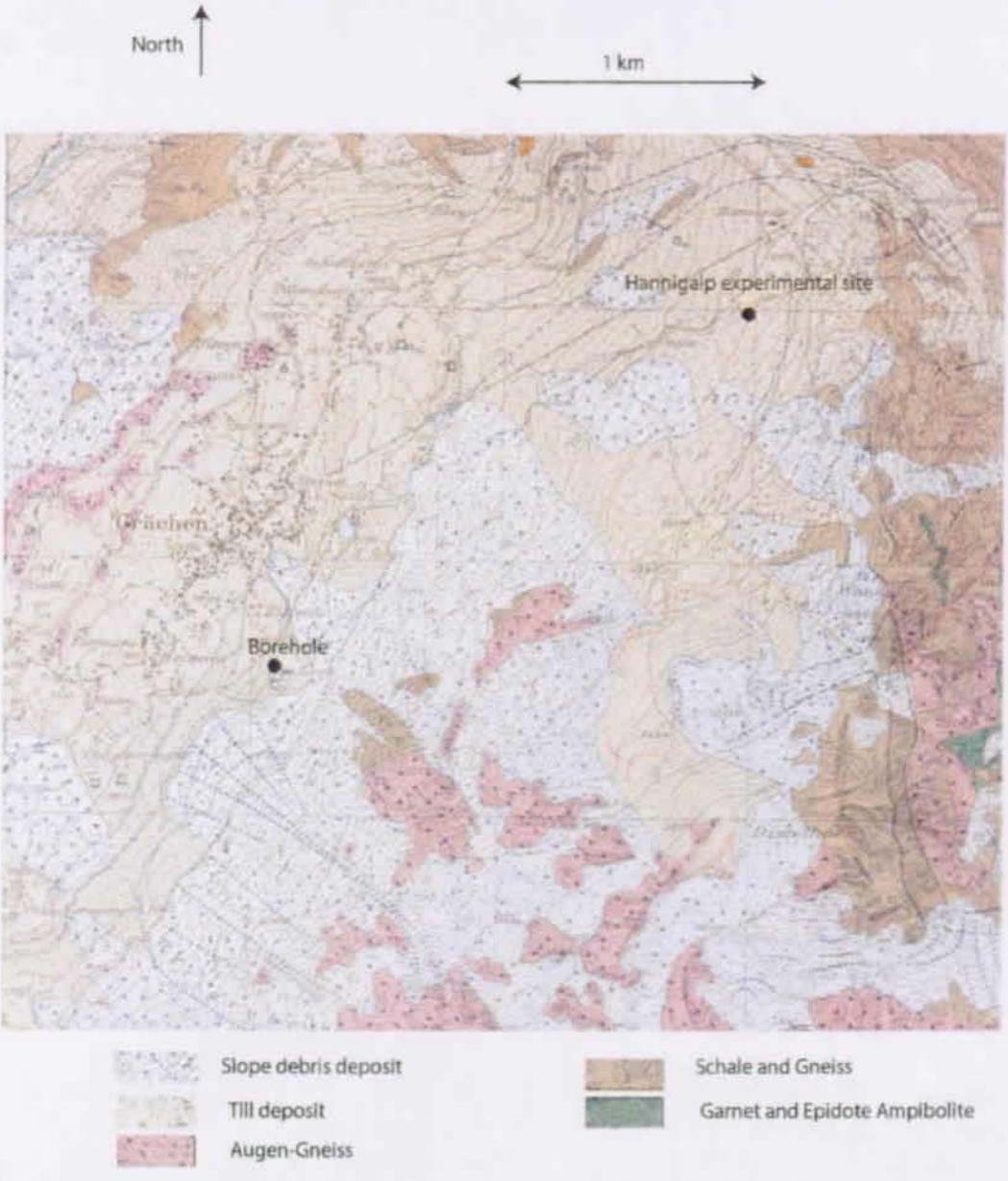

Figure 11.2: Geological map of the Grächen region (Swiss Geologic National Map, 1/25 000, with the authorization of the Swiss Federal Office of Topography (BA034924))

to be extrapolated for each band and were set variable with the altitude. In addition some model settings were modified according to the altitude. The following part briefly describes the adjustment and physical reason behind these adjustments.

Meteorological data

To accurately represent the air temperature at the different elevations, we applied between 1600 and 2100 m the mean winter lapse rate between Grächen SMA and Hannigalp (-0.88°C/100 m), which was found during the two studied winters. Above 2100 m, the standard value of -0.55°/ 100 m was used.

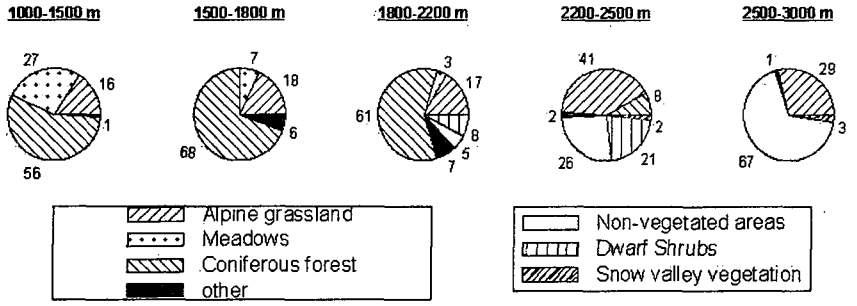

Figure 11.3: Elevation distribution of vegetation classes in the Turtmanntal, from Hoersch et al. (2001)

Input parameter	Value
Elevation bands	1500-1700 m
	1700-2000 m
	2000-2200 m
	2200-2400 m
	2400-2800 m
Air temperature lapse rate (dT/dZ)	-0.88°C/100 m
Lower boundary temperature lapse rate (dT/dZ)	-0.5°C/100 m
Precipitation lapse rate (dP/dZ)	10 mm/100 m
New snow density at the elev. band 2200-2400	130
New snow density at the elev. band 2400-2800	130
Overburden pressure param. band 2200-2400	0.3
Overburden pressure param. band 2400-2800	0.2

Table 11.1: Input parameters used for simulation.

The altitude induced solar radiation lapse rate was fixed at 1.1 Wm^2/100m. This value takes into account the reduction of the radiation due to covered sky and was established for the winter season (November to May) in Switzerland between an altitude of 500 m and 3000 m (Marty 2001). As the SMA station does not directly measure the solar radiation, this value was estimated by diminishing the potential solar radiation depending on the cloud cover. We then adjusted this value to the radiation measured at Hannigalp during the two years studied and extrapolated it for other altitudes by using the fixed lapse rate.

From adjacent meteorological stations (Chapter 5: "Representativeness of the chosen sites", page 55), the precipitation was only slightly increased with the altitude, using a gradient of 10 mm/100 m. By using such an approach, the spatially heterogeneous precipitation regime is of course poorly represented and errors may arise from this assumption. Also, we note that such a linear relationship of increasing precipitation with the elevation occurs mainly in winter, when advective influences are more relevant, in contrast to summer, when a poor relationship to elevation exists due to convective precipitation (Hanson 1982).

Finally, we assumed identical relative humidity as the model showed to be little sensitive to this meteorological parameters and identical wind speed at each altitude. This last assumption is

mainly based on the experience that Hannigalp is a wind still place. However, at higher altitudes (above 2600 m), this assumption has to be corrected, as the wind gradient heavily increases with the altitude.

Model settings

The annual soil temperature in the upper part of the soil cover is similar to the one at the soil surface. In snow rich regions however, due to the isolating effect of the snowpack, the mean upper soil temperature is higher than the mean air temperature. As a result, in alpine areas, we may expect a lower soil temperature lapse rate than the air temperature lapse rate. At 2600 m, the soil temperature was set to 1°C at the lower boundary of the model, as this region is on the lower edge of the permafrost zone. At 1600 m, the soil temperature was set equal to the mean air temperature at that altitude (6°C), and the resultant lapse rate was used to determine the soil temperature at the other elevation bands.

The surface roughness had to be adjusted for each elevation band. Indeed, to simulate accurately the snow depth at Grächen, the snow surface roughness was slightly increased from 0.004 m to 0.006 m (Figure 11.4). The SMA station is located close to the village of Grächen and surrounded by houses and trees, creating locally this increase in the aerodynamic resistance above the snow surface. From topographical similarities, the surface roughness for locations between 1600 and 2000 m was set equal to the one at Grächen SMA, whereas above 2000 m, it was taken identical to the one at Hannigalp.

Finally, the parameter in the snow density function had to be adapted for the two upper bands. By considering the snowpack as a single layer, the snow density (and hence also the soil frost depth) is overestimated as soon as the snowpack becomes thick (i.e. more than 150 cm) (see also Chapter 9: "Model calibration: winter 2000/2001", page 115). Therefore, to obtain an accurate and realistic snow density simulation at high elevations (above 2200 m), we decreased the parameter expressing the influence of the overburden pressure on the snow density in eq. 3.45, and increased the new snow density (Table 11.1). As shown by numerous simulation tests, this last modification enabled to obtain a correct snow density value at the onset of the winter.

11.3. SIMULATION RESULTS

We started by comparing the simulated snow depth at 1600 m to the measured one at Grächen (Figure 11.4). The snow depth was mostly satisfactorily reproduced by the model (coefficient of determination $R^2 = 0.84$). In particular, onset and end of the snow period were well timed. The main differences were observed in January and February, when the snow depth was mostly overestimated by the model. Reasons for this error are similar to those creating the errors in the snow depth simulation at 2100 m (Chapter 9: "Discussion", page 121). The applied daily resolution in the meteorological inputs underestimates the snowmelt, due to the smoothing of the temperature gradient between the atmosphere and the snow during daytime. Also the solar radiation at Grächen, which was not directly measured but estimated from the cloud cover, may have been underestimated in winter, due to the complex mountain topography, and the relatively low position of the sun in the sky at that latitude.

To investigate the general behaviour of similar winters, we classified each winter as «frozen» (considerable soil frost during the snowmelt in > 80% of the area), «partially frozen» or «unfrozen» (no soil frost during the snowmelt in > 80% of the area). Since the beginning of the aquifer elevation measurements in 1992, three winters were «frozen» (1996 = winter 1995/

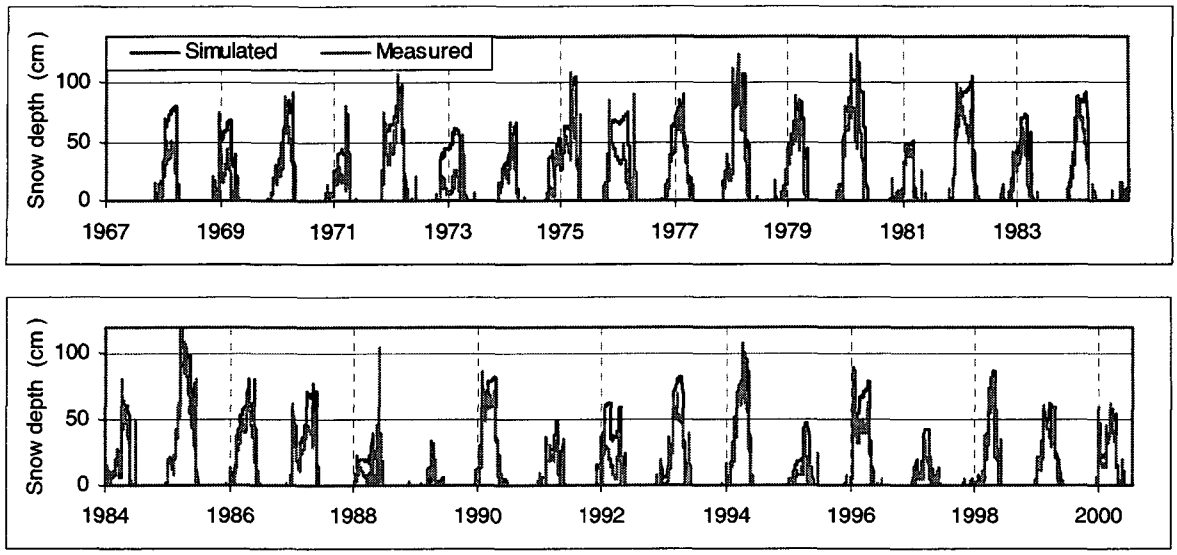

Figure 11.4: Simulated and measured snow depth between 1967 and 2001 at Grächen SMA (1600 m).

1996, 1998 and 2002), five winters «unfrozen» (1993, 1995, 1997, 2000, 2001) and two winters «partially frozen» (1994, 1999). Results for each band is given in Table 11.2.

Winter	*Soil frost 1600*	*Soil frost 1950*	*Soil frost 2100*	*Soil frost 2300*	*Soil frost 2600*
1993	no	no	no	no	no
1994	yes (11 cm)	yes (15 cm)	no	no	no
1995	no	no	no	no	no
1996	yes (31 cm)	yes (17cm)	yes (34 cm)	yes (45 cm)	yes (70 cm)
1997	no	no	no	no	yes (20 cm)
1998	yes (15 cm)	no	yes (25 cm)	yes (35 cm)	yes (30 cm)
1999	yes (24 cm)	yes (16 cm)	no	no	no
2000	no	no	no	no	yes (12 cm)
2001	no	no	no	no	no
2002	yes (35 cm)	yes (20 cm)	yes (40 cm)	yes(45 cm)	yes (70 cm)

Table 11.2: Classification of each elevation band as either frozen or unfrozen. Soil frost depth at snowmelt for frozen winters. If the simulated soil frost depth is less than 8 cm at snowmelt, the winter is classified as unfrozen for the given band.

During the three frozen winter, the snow depth remained very shallow in each band, inducing a deep soil frost at each altitude. Exception was the region located between 1800 m and 2100 m, where the simulated soil frost was always lower than at other altitudes. For example no soil frost was simulated at that altitude in 1994. Reasons for this behaviour are twofold. Unlike at higher altitudes, the soil is warm enough in winter to inhibit any deep soil frost, whereas the snow cover is still thick enough to isolate the ground in winter in contrast to areas located below 1800m.

During the two partially frozen winters 1994 and 1997, the two lowest bands (between 1500 and 2000 m) were frozen, whereas the higher areas remained unfrozen. At high altitude, a significant snow cover isolated the soil from the atmosphere in November. At lower areas the soil was still free of snow during this period. In December, little precipitation was recorded, allowing the soil

to freeze deeply in lower areas.

11.4. AQUIFER RECHARGE

In Figure 11.5, we show the water-table elevation between 1993 and 2002 at Grächen/Meisen. The large water table rise in April-May (approx. 10 m) may be viewed as an indicator of the aquifer recharge, neglecting any effect induced by the geology or the topography on the recharge and considering the piezometer to be representative of the system. The high conductivity of the aquifer layer, large differences between aquifer expansion and recharge area, as well as a possible confinement of the aquifer in the lower part of the catchment, may explain the strong variation of the water-table at snowmelt. The aquifer reacts almost immediately (within a few days) to any precipitation/snowmelt event.

The dynamic in the water-table elevation may be explained as follow. In summer, the water table rise is low as most precipitation water is evapotranspirated. In autumn a small rise is monitored due to frequent heavy rain. In particular we notice the maximum measured value in the water-table elevation at 1677 m in October 2000 (Figure 11.5), when flooding caused important damage in the southern part of Switzerland. From November, precipitation is mostly recorded as snow precipitation. No more water infiltrates into the soil and the water table rise stops. From then, the water-table decreases steadily, as groundwater water flows down-gradient and discharges into streams. The water-table recharge begins end of May, early April, period,

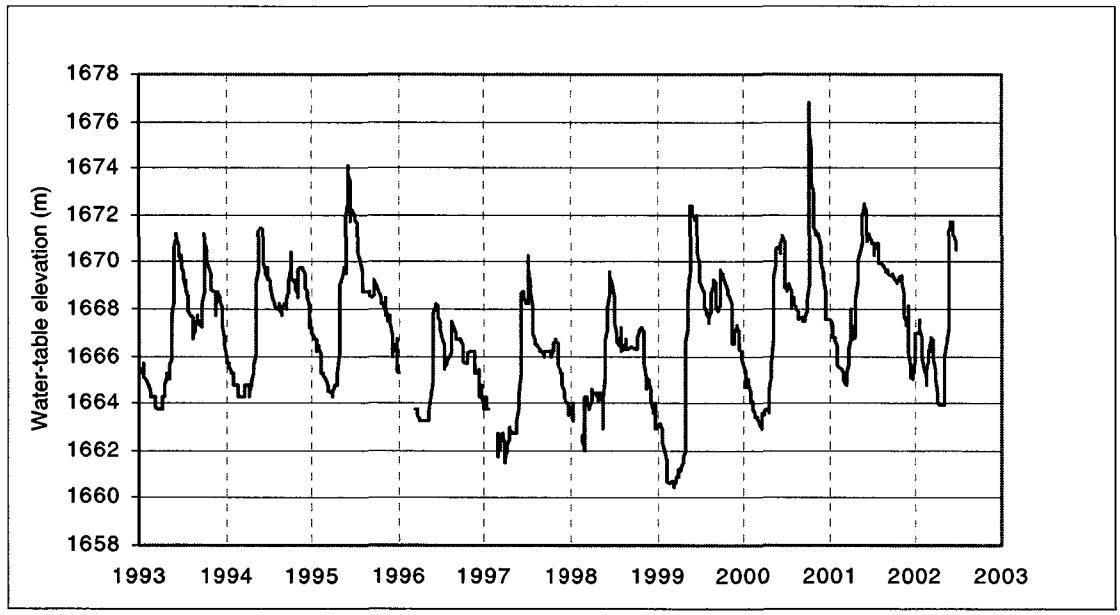

Figure 11.5: Water-table elevation variation at Meisen /Grächen (1700 m) between 1993 and 2001.

when the water-table depth is mostly stable. From mid-April until mid-June, snowmelts is at its highest and the water-table raises significantly.

The aquifer recharge at snowmelt was evaluated using two steps:

(i) In an initial stage, the rate of the water-table decrease in winter was calculated (Figure 11.6).

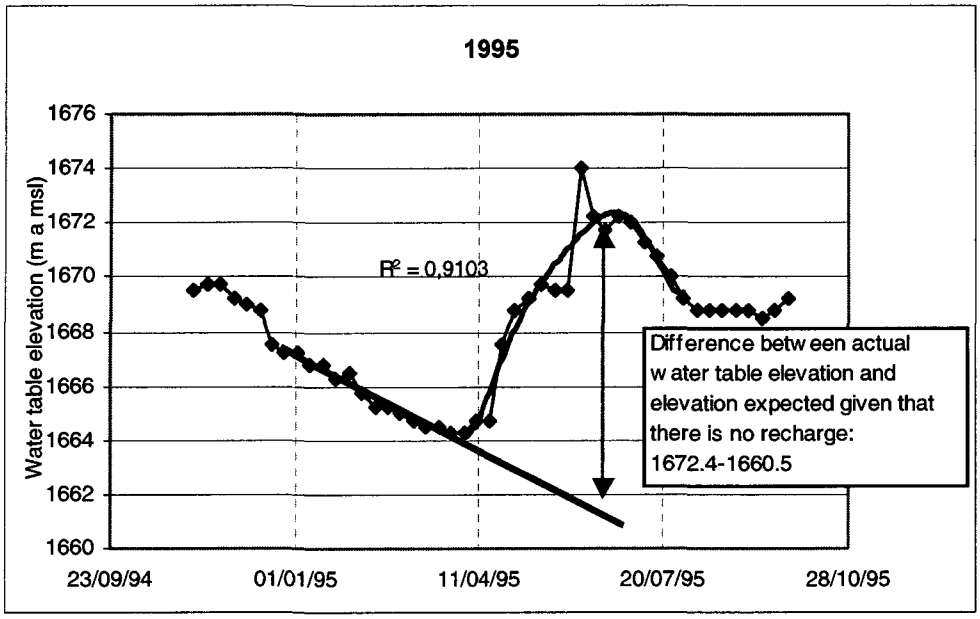

Figure 11.6: Method used to calculate the water-table recharge at snowmelt.

This value varies from year to year as the discharge depends on the water-table elevation (the rate changed between 0.029 m/day and 0.057 m/day), and was used to estimate the distance the water-table would have fallen at the end of the snowmelt period if no recharge would take place. Error on the calculated minimal aquifer depth is quite important (0.5 m), as small snowmelt events in the lower part of the catchment may have taken place in winter, resulting in an underestimation of the rate of the water-table discharge. During winter 1997/1998, no data were available between 19.1.94 and 23.2.94. Due to the fact that the aquifer recharge began already in March, an accurate estimation of the discharge rate was hence difficult, causing a relevant error in the estimated aquifer depth (1.5 m). Same remark applies for winter 1995/1996 and winter 1996/1997, but the estimated rate was improved as data were available prior to the onset of the aquifer recharge (error 1 m).

(ii) In a second step, the variation of the aquifer at snowmelt was obtained by making the difference between the measured maximum water-table elevation and the expected one given no recharge. In order to avoid considering particular rain precipitation events, which would locally influence the water-table elevation during the snowmelt period, the maximum recharge was calculated by approximating the water-table elevation curve with a tendency curve of order 6 (Figure 11.6). *R*- squared values varied between 0.91 and 0.99.

11.5. RESULTS AND DISCUSSION

During the ten measured winters, the water table rise at snowmelt varied between 5.7 m and 17.25 m. In Figure 11.7, we compared the water table rise with the amount of winter precipitation, expressed at the areal snow water equivalent at the start of the snowmelt over the entire catchment.

The rise was lowest for the three «frozen» winters (less than 8 m). For the «unfrozen» winters, the rise was considerable (>10 m), even when comparably little winter precipitation was

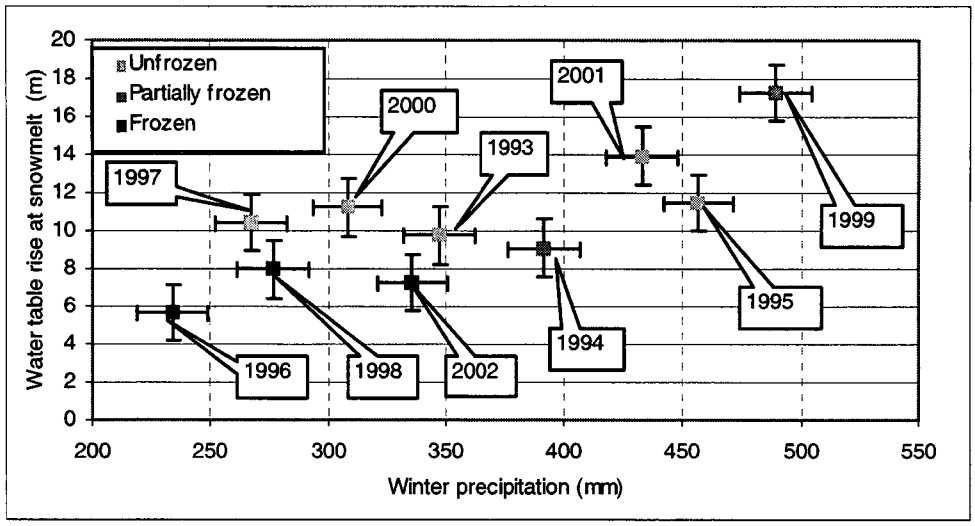

Figure 11.7: Water-table depth variation at Grächen versus winter precipitation (i.e. average SWE at snowmelt over the entire catchment) between winter 1992/1993 and winter 2001/2002. The given number next to each value indicates the spring when the snowmelt took place, e.g. 2002 stands for the water-table recharge in spring 2002.

recorded, as in winter 1997. Especially interesting is the comparison between the two «extreme» winters 1997 and 2002. They were characterized by a contrasting hydraulic cycle and snowmelt dynamic, explaining the differences in the thermal soil state at snowmelt. In 1997, an early and thick snowpack prevented the soil from freezing in November and December, whereas the precipitation between January and May remained far below average. On the other hand, the relatively high amount of winter precipitation in 2002 was mainly caused by a large snowfall in May 2002, when more than 130 mm of precipitation fell within four days. Despite significant differences in the winter precipitation, the water table rise was 31% lower during the frozen winter 2002 than during the unfrozen winter 1997. Such a result may indicate that a partly frozen soil influences the snowmelt discharge over large areas. However, this interpretation should be viewed with caution because, on the one hand, little is known about the hydraulic behaviour of the catchment, and, on the other hand, the error in the winter precipitation is large, due to the strong local variability in the precipitation.

The two "partially frozen" winters 1994 and 1999 illustrate the difficulty in modelling accurately the soil frost depth aerial extension when, at the onset of the winter, large variation in the altitudinal snow depth distribution exists (i.e. a thick snowpack in higher areas and hardly any snow in lower areas). Indeed, despite a similar soil frost extension (the two lowest zones, between 1600 and 2000 m, were simulated as frozen, and the higher areas as unfrozen) the water table rise at snowmelt differed markedly between both winters. In spring 1994 the rise was less than 10 m despite considerable snowfall, and one would expect the soil to be frozen over the entire catchment. In contrast in spring 1999, the rise was the highest ever measured (17.25 m). Such a high recharge tends to show that the soil remained unfrozen during the snowmelt. These two winters shows also the possible influence of the snowmelt dynamic on the recharge, as in spring 1999, similar to spring 2002, a significant late snowmelt event took place. Meltwater was able to infiltrated into the ground in lower areas, which were previously frozen, and which may explain the significant increase in the water-table.

The water table rise was reduced by approx. 20% during frozen winters. However, the number

of analysed years was not high enough to obtain a reliable statistical analysis, and one should proceed with caution in the interpretation. From plot simulations, the lateral runoff varied between 20% and 60% of the total meltwater. Re-infiltration of meltwater in unfrozen areas is hence high (no river above 1800 m), and explains why seasonal soil frost does not influence the recharge over large catchments. Finally, we note that the simulated lateral runoff at plot scale is probably slightly underestimated, as the slope at Hannigalp (23%) is less than the average catchment slope (30%). We may expect a higher proportion of lateral runoff on steep areas.

During the main snowmelt period, we observed that a part of the recorded surface water infiltrated the soil some 100 meters below the experimental plot where the soil was already free of snow and unfrozen. Such a result demonstrates the importance of the soil texture, structure and steepness, as well as the underlying geological structure on the amount of surface runoff.

We did not integrate the variation in the soil physical properties and in the vegetation in our simulation. The given results stand for a vegetation similar to the one encountered at the experimental site of Hannigalp (like grassland and meadow), and we may hence expect a different hydraulic behaviour in forest. Koivusalo (2002) noted that the canopy reduces the amount of snow on the ground by interception and sublimation. It results in deep soil frost and a reduced snow depth. Stadler et al. (1996), showed in his study on sub-alpine regions, that surface runoff is higher in areas below trees than for open fields. As a consequence, using the site of Hannigalp to estimate the soil frost depth and the discharge in forest areas, which made up most part of the are between 1600-2200 m, resulted in an overestimation of the snowmelt discharge, and in an underestimation of the lateral runoff and soil frost. Also, results should not be applied for location above 2600 m, as hydrological behaviour differs markedly when soil cover is made up mainly by rocks (Figure 11.3) and permafrost bodies are present. In such a case, hydrological pathways get much more complicated (Tenthorey 1992).

11.6. CONCLUSION

This chapter was used to investigate the effect of seasonal soil frost on the water table rise at snowmelt for a small aquifer in the area of Grächen. The simulation results showed a highly variable frost depth distribution over the entire catchment, from which we were able to classify each winter as either «frozen», «unfrozen» or «partially frozen».

During the 10 investigated years, «frozen» winters were characterized by a 10-30% decrease in the water table rise at the aquifer of Grächen. The decrease was less marked than the groundwater recharge at Hannigalp, where, from simulation results, the deep seepage diminished between 20% and 50% of the total meltwater during frozen winters. The very permeable soil allowed most meltwater to re-infiltrate the soil in lower areas where soil frost was absent. These results support other studies showing that the effect of seasonal soil frost on the water circulation diminishes with increasing areal extension of the studied field (Thorne, 1998, Cherkauer, 1999). We may hence assume that the combination of different factors, like high winter precipitation, low soil infiltration capacity and low catchment extent can increase the influence of the soil frost on the aquifer recharge.

The change in the water table rise between «frozen» and «unfrozen winters» was within the estimated error. Due to the high annual variability in the winter precipitation, only few winters were directly comparable. It was hence not possible to give a reliable statistical analysis and to show a clear correlation between seasonally frozen soils and water-table-rise. As the water-table

measurements will be still operating in future, we may have to wait a few years to gain a better confidence in the output results. Also further improvement may be achieved by integrating a complete hydrogeological study of the region, which should enable to characterize the aquifer extent, inputs and outflow, and relate the aquifer recharge at snowmelt to seasonal soil frost extent rather than the water table rise. Finally we note that the implication of seasonal soil frost on the water circulation may also be studied on the hydrograph of alpine rivers, as the shape of a streamflow hydrograph is controlled by the amount as surface or interflow water (Beven 1989) (and hence also by seasonal soil frost). At Grächen however, such a study would be difficult, as the only river that could be investigated (Rittigraben) is dangerous and not easy to access (the river was repeatedly affected by debris flow (Lugon and Monbaron 1998)).

12. INFLUENCE OF A CHANGING CLIMATE

12.1. INTRODUCTION

The actual and future change in the earth's climate is a major preoccupation in the field of environmental sciences. As stated in Chapter 4, changes in the climate system are likely to create a sharp increase in the air temperature in alpine regions, which will be accompanied by a change in the hydrological cycle. There is a concern that a climate change resulting in less snow will influence the soil frost depth and consequently also the hydraulic cycle at snowmelt. The objectives of this chapter will hence be to (a) integrate the feedback processes between snow cover and climate at different altitudes, to better forecast long-term effects on the altitudinal snow cover distribution, and (b) to assess possible impacts of climate warming on relevant hydraulic variables at different altitudes.

To investigate possible impacts on catchment recharge, we coupled the one-dimensional model, which takes into account soil freezing, with a two-dimensional groundwater model to simulate the meltwater dynamic at the outlet of an alpine aquifer. With these numerical simulations we did not intend to forecast the exact hydrological response of an alpine aquifer and its sensitivity to a warmer climate, as such a study would have involved much more data and a more sophisticate numerical model. Rather, the simulations were designed to show possible future trends regarding water resources. In particular no downscaling was carried out (Chapter 2: "Global warming effect on the Alps", page 21).

12.2. METHOD

To integrate the altitudinal variability of the snowpack, we divided the catchment into 6 zones between 1200 m and 2600 m, each zone approx. 250 m in vertical extent (Figure 12.1), and simulated the hydraulic response separately for each zone. The COUP model was run for a 30 year period with changed meteorological parameters. We modified the weather inputs from SMA Grächen according to the four scenarios: (a) as measured, (b) air temperature increased by 2°C (c) precipitation increased by 15% (d) air temperature and precipitation increased by 2°C and 15% respectively. Finally, we used the discharge and soil frost depth results obtained as boundary conditions to the two-dimensional transport model FEFLOW (Diersch 1996). We considered a simplified catchment (Figure 12.1), with an altitude range between 1100 m and 2700 m and a horizontal extent of 3 km. The catchment was made up by two geological entities, a quasi-impervious lower structure (bedrock, $k_{sat}=10^{-8}$m/s) and a conductive aquifer layer, 70 m deep. The simulations were carried out for various aquifer permeabilities. Input parameters are listed in Table 12.1. The outlet of the aquifer was located at an altitude of 1150 m.

Boundary conditions are given in Figure 12.1. We used results given by COUP as the upper flow boundary. To take into account the blocking effect of pore ice, the flow at the upper boundary was given by the simulated flux (with COUP) at a depth of one metre. Therefore, we assumed that the (with COUP) simulated lateral meltwater flow drained into rivers and was not allowed to re-infiltrate the ground in lower unfrozen areas (no surface and subsurface flow in the FEFLOW model). Initial conditions were given by the soil condition obtained after a first simulation over a period of 10 years (1967 to 1976), having boundary conditions identical to those shown in Figure 12.1. For this first simulation, initial conditions were given by a constant

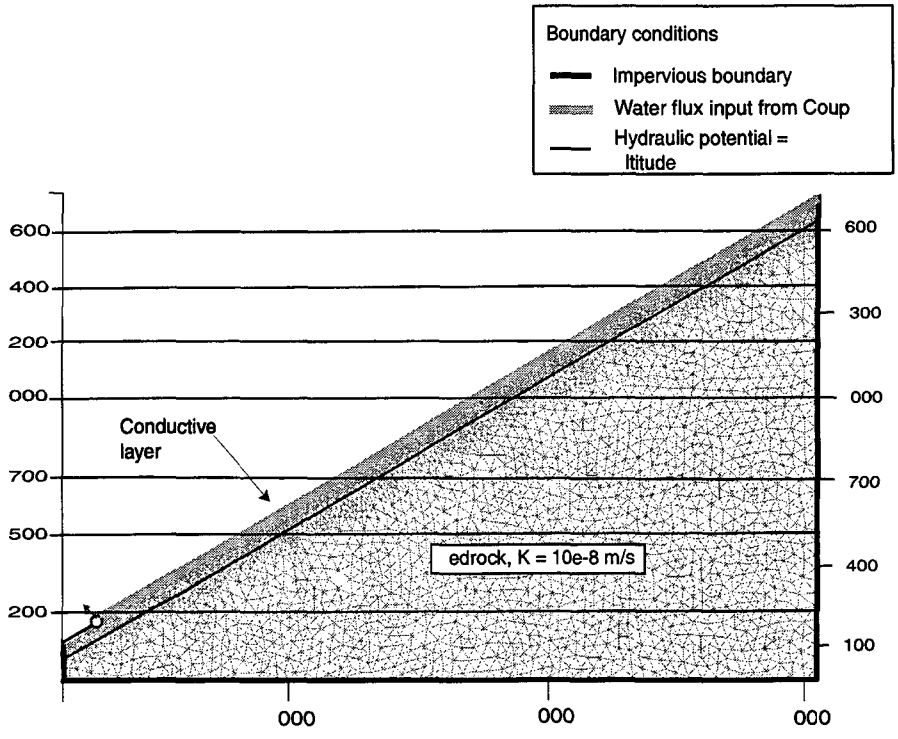

Figure 12.1: Sketch of the simplified aquifer, which was used to investigate the effect of a changing climate on the groundwater recharge dynamic with mesh. The aquifer is made up of a quasi-impervious layer and the conductive aquifer layer.

Zone	k_{sat} *(m/s)*	*Saturated water cont.* θ_s *(% vol.)*	*Unsaturated parameters (Van Genuchten)*		
			n	α (m^{-1})	θ_r *(% vol.)*
Bedrock	10^{-8}	10	1.964	4.1	2.5
Conductive layer	10^{-6}-10^{-3}	30	1.964	4.1	2.5

Table 12.1: Parameters used in simulation. The Van Genuchten parameters are given in eq. 3.3; m=1-1/n.

saturation of 30% for the conductive layer and of 100% for the bedrock. Finally, we used triangular finite elements for the mesh generator (total number of elements = 10343).

Both models are described in Chapter 3.

12.3. RESULTS AND DISCUSSION

12.3.1. CHANGES AT PLOT SCALE

Most results in this section will be presented as density functions, so as to best represent

statistical analyses. In a first step, results for Hannigalp are displayed, followed by a discussion on the relationships between snow depth, soil frost depth and snowmelt discharge at plot scale.

In Table 12.2 the main results for the Hannigalp plot are summarized for the four different climate scenarios. In particular we show changes in the total snow cover length (i.e. number of days with more than 10 cm of snow) and changes in the period length with thick snow (i.e. number of days with more than 70 cm of snow). We note that the percentage of lost due to lateral surface and subsurface runoff is not presented, as this percentage may be deduced from the percentage of percolated water.

	Unchanged climate	ΔT = +2°C	$\Delta Prec$ = +15%	ΔT = +2°C; $\Delta Prec$ = +15%
Mean snow depth (cm) (st. dev.)	86.6 (26)	68.4 (22) (-21%)	91.6 (27) (+6%)	76.2 (23) (-12%)
Max snow depth (cm) (st. dev.)	133 (27)	118 (25) (-12.8%)	145 (28) (+9%)	130 (26) (-2.3%)
#days snow depth > 70 cm	122 (49)	89.8 (45) (-26%)	136 (44) (+12%)	103 (44) (-16%)
#days snow depth > 10 cm	188 (21)	169 (20) (-10%)	192 (20) (+2%)	172 (20) (-8.5%)
Mean soil frost depth (cm) (st. dev.)	11.9 (12.4)	11.6 (12.3) (-2.5%)	11.3 (0.11) (-5.1%)	10.7 (11.8) (-11%)
Max soil frost depth (cm) (st. dev.)	18.4 (20.7)	17.2 (13.4) (-7.1%)	17.7 (18.1) (-7.1%)	16.9 (16.9) (-8.2%)
#days soil frost > 8 cm (cm) (st. dev.)	78.1 (88.4)	70.6 (85.0) (-9.6%)	76.4 (82.2) (-5%)	63.8 (82.5) (-18%)
Deep percolation (%) (st. dev.)	85.7 (28.2)	85.9 (20) (+0.2%)	85.6 (28) (-0.1%)	85.5 (24) (-0.2%)

Table 12.2: Different values for selected snow and soil frost variables at Hannigalp for current climate and three modified climate (ΔT=+2°C; $\Delta Prec$=+15% and ΔT=+2°C $\Delta Prec$=+15%). Simulations are based on daily data between 1968 and 2000. The mean snow depth and mean soil frost depth are taken between the beginning of November and the end of March. The deep percolation is taken between the beginning of November and the end of May.

Increasing the air temperature by 2°C had an abrupt effect on the mean snow depth, which diminished by 21% from 86.6 to 68.4 cm on the average. The change in the maximum snow depth was, however, less pronounced (-11.28%). This behaviour is explained by the fact that a rise in the number of snowmelt events in spring due to a warmer climate primarily affects the mean snow depth, as the maximum snow depth is usually measured before the first snowmelt. A change in the precipitation only slightly increases the yearly snow depth maximum as well as the snow cover period. In particular, it does not compensate for the loss in the snow depth due to a higher air temperature, when additionally the air temperature is increased by 2°C (-12% in the mean snow depth).

A change in the climate acts mainly on the thickness of the snowpack rather than on the length of the snow period. For a warmer climate, we noted for example a greater decrease in the number of days with a snow depth > 70 cm (-26%) than in the number of days with a snow depth >10 cm (-10%). The final snowmelt occurs after a short time lapse (approx. two weeks), releasing nearly all accumulated winter snow. As a result, the snow cover length is little affected by a change in the meteorological inputs, since the snow disappears/remains only a couple of days earlier/longer than for an unchanged climate.

In Figure 12.2 we show the maximum/mean snow depth density function at Hannigalp for the

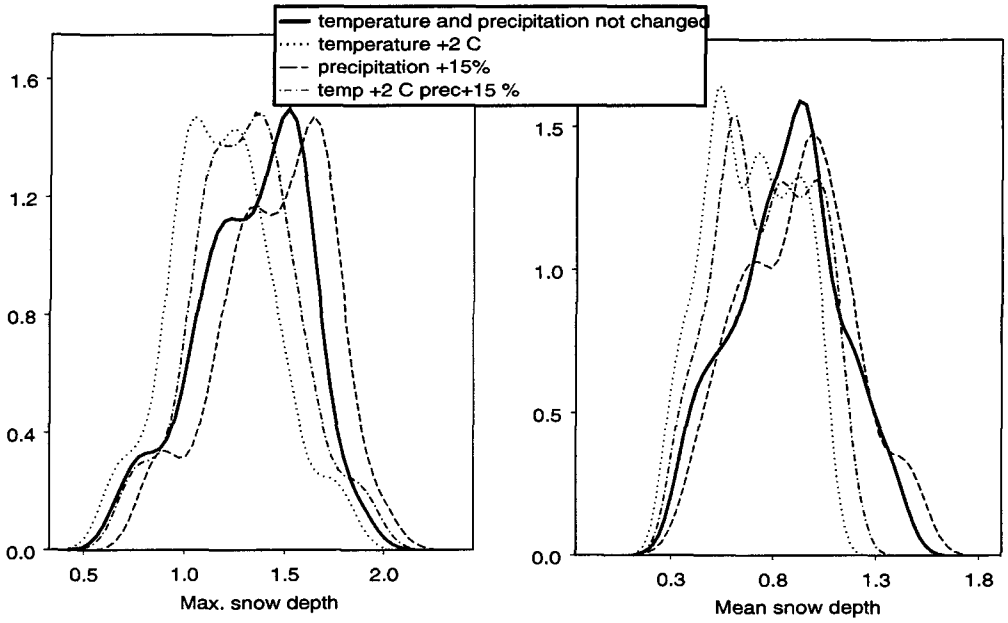

Figure 12.2: Density function of the maximum and mean snow depth at Hannigalp for four different climatic scenarios over 33 years.

four simulated scenarios. The shape of the different curves is very similar. However, the change in the air temperature dilates the yearly maximum/mean snow depth distribution, whereas a change in the precipitation induces a shift of approx. 20 cm in the distribution. This spreading is probably a consequence of the disparate influence of a warmer climate on the snow depth, as an increase in the air temperature affects the snow cover more during warm winters than during severe winters.

It is interesting to note that, in spite of different responses of the snow depth to the three climatic scenarios, the soil frost depth diminished for all scenarios. Increased precipitation created a higher ground insulation, reducing the soil frost. With a warmer air temperature, the soil frost depth was also reduced, as the reduced insulation was compensated for by warmer air temperatures, modifying the energy balance. The reduction was particularly marked when both scenarios were combined, as for example, the number of days with a soil frost depth >8 cm decreased by 18%. From the max/mean frost depth density function (Figure 12.3), we note that most winters were either unfrozen or only slightly frozen. For such winters, a warmer climate slightly increased the max/mean soil frost depth (approx. 5 cm), whereas for winters with deep soil frost (>70 cm), a change in the air temperature reduced the soil frost depth by approx. 30 cm.

The soil infiltration capacity depends on the pore ice content and hence is greatly influenced by the soil frost extent. It is therefore somewhat surprising that on the average the simulated percolation remained constant for all weather scenarios, as the mean soil frost depth diminished for all modified climatic scenarios. Nevertheless, the fact that on the one hand, more meltwater is released by the snowpack under wetter climatic conditions, and on the other hand, melt

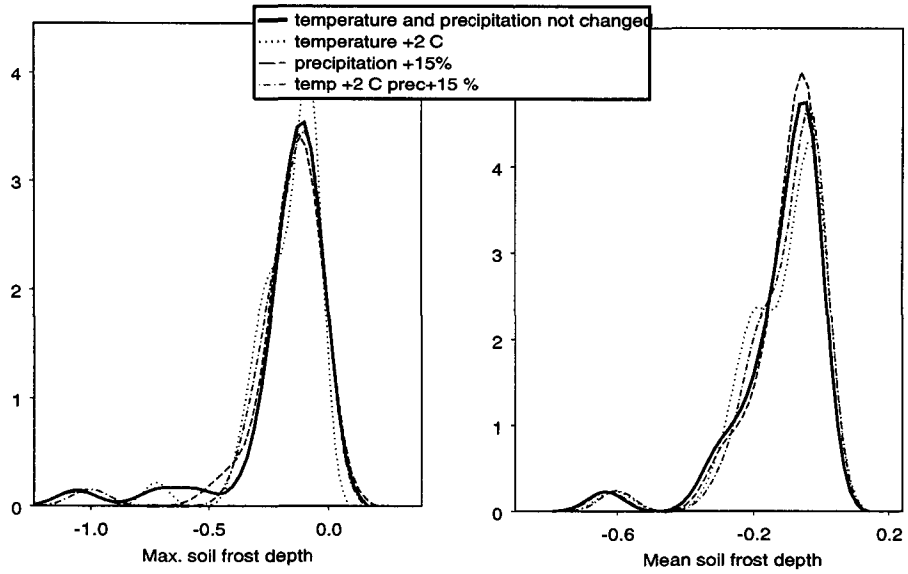

Figure 12.3: Density function of the maximum and mean soil frost depth at Hannigalp for four different climatic scenarios over 33 years.

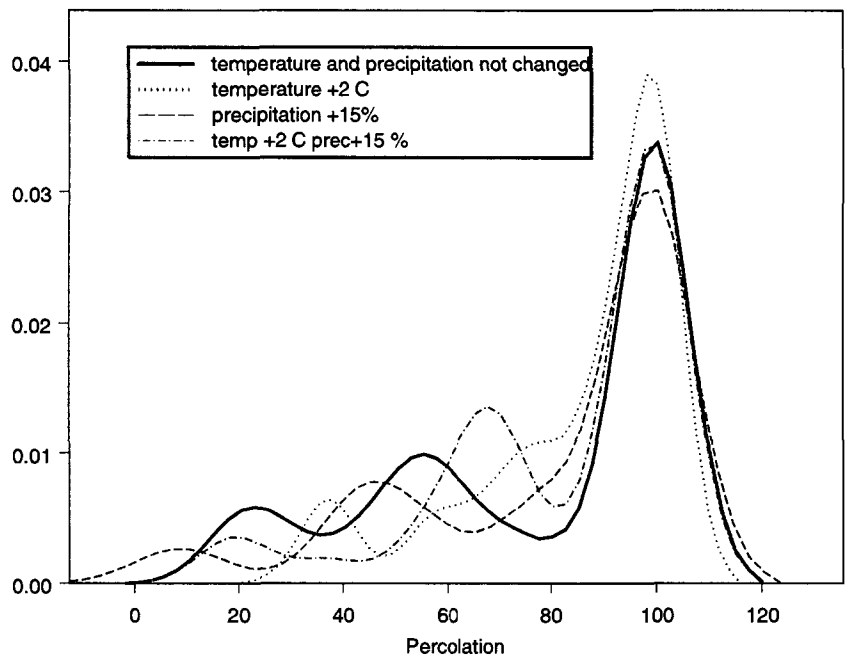

Figure 12.4: Density function of the mean deep seepage during the snowmelt at Hannigalp for four different climatic scenarios over 33 years.

intensity becomes higher under a warmer climate may under certain circumstances saturate the soil infiltration capacity and increase the amount of surface runoff.

The shape of the density function (Figure 12.4) can be explained as follows. Most meltwater infiltrates into the unfrozen soil, creating the sharp increase in the function around zero. If the soil is frozen at snowmelt, the infiltration is reduced, and approximately 40% of snowmelt discharge runs off laterally. Finally, when a deep soil is simulated (< 60 cm), the amount of lateral runoff increases to approx. 80% of total runoff. However, these general explanations have to be relativized, as during some winters all meltwater infiltrated into the ground, despite a soil frost depth of 20 cm at the end of the winter. As stated in Chapter 6, the soil infiltration capacity depends on the soil water content at freezing and on the snowmelt dynamic. It explains why a change in the climate input data did not act linearly on the discharge data.

Most winters were only marginally affected by a change in the meteorological input. However, during specific winters the water balance changed drastically. For example, in 1999/2000, a temperature increase of 2°C created a sharp decrease in the snow depth from 55 cm to 17 cm in December, allowing the soil to freeze down to a depth of 30 cm, which considerably affected the snowmelt discharge pathways. Under unchanged conditions, no soil frost was simulated and all meltwater infiltrated into the ground. Another example occurred in winter 1995/1996. Under the assumption that temperature and precipitation increased, the soil did not freeze, whereas a soil frost depth of 25 cm was found for the unchanged scenario. In contrast to winter 1999/2000, the change in the temperature did not transform snowfall into rain at the beginning of the winter, and the higher snow precipitation insulated the soil from freezing.

Figure 12.5 shows the altitudinal variation in the snow depth, the soil frost depth and the deep percolation obtained using the COUP model for each altitudinal zone. In Appendix G the main results for each altitudinal zone are summarized for the four different climate scenarios. When going from lower to higher altitudes, the differences in the simulated snow depth for an unchanged, and a wetter and warmer climate become negligible. At high altitudes (2600 m), the increased snowmelt due to the warmer climate is compensated for by the higher snow precipitation. For the soil frost depth variation, the model indicates interesting behaviour. For an unchanged climate scenario, the soil frost depth is shallowest at 1900 m, and deepest at 2600 m and 1300 m. As already explained in Chapter 11, the ground is still warm enough at that altitude to inhibit deep soil frost, whereas the snow cover is thick enough to insulate the soil from the atmosphere. At lower altitudes, the mean soil frost increases, as the snow depth is shallow, and soil freezing is possible all winter, whereas at higher altitudes, the mean soil temperature is close to freezing point, allowing frost to penetrate deeply into the ground. Increased precipitation will further insulate the soil and hence decrease the soil frost. The scenario with an increased air temperature resulted in greater changes. In particular, the soil frost depth was deeper at low altitudes where there was hardly any snowpack, whereas at higher altitudes the opposite effect was simulated, as the snowpack was still thick, and the mean soil temperature increased. The variation in the percentage of deep percolation follows an opposing trend to the variation in the soil frost depth. The deeper and the more frequent the soil frost, the higher the lateral runoff. This could be confirmed by the simulated discharge pathways, as shown in Figure 12.5.

12.3.2. CHANGES AT THE CATCHMENT SCALE

Figure 12.6 shows the changes in monthly discharge according to scenarios (a) (no change) and (c) (prec. +15%) (conductivity in the aquifer layer k_{sat} = 5 10^{-5} m/s). The flow changes at the

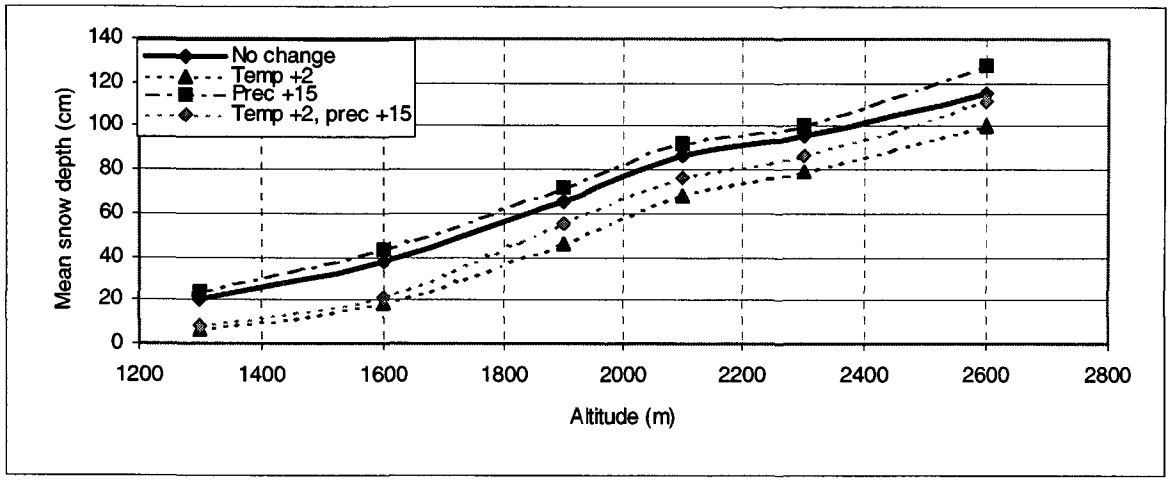

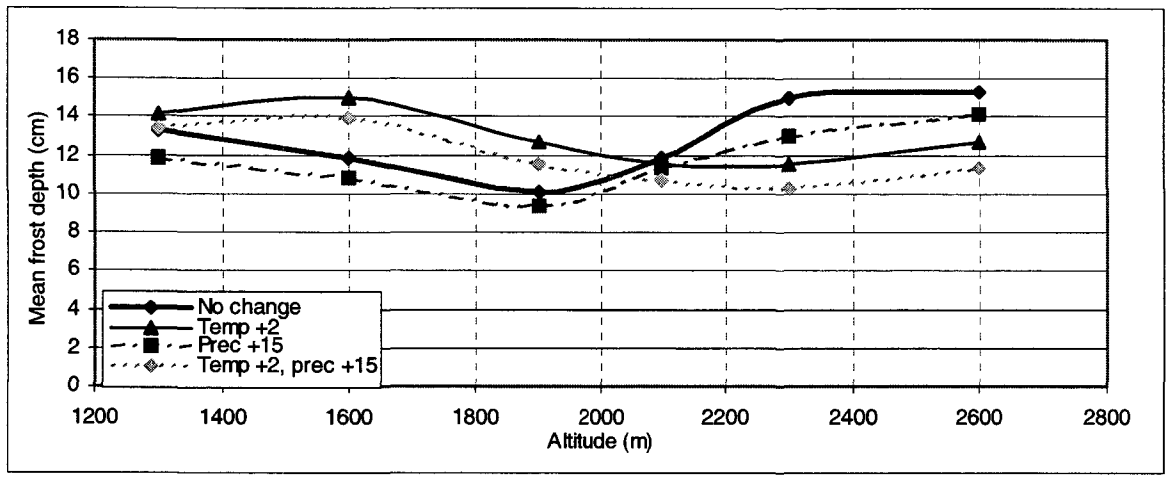

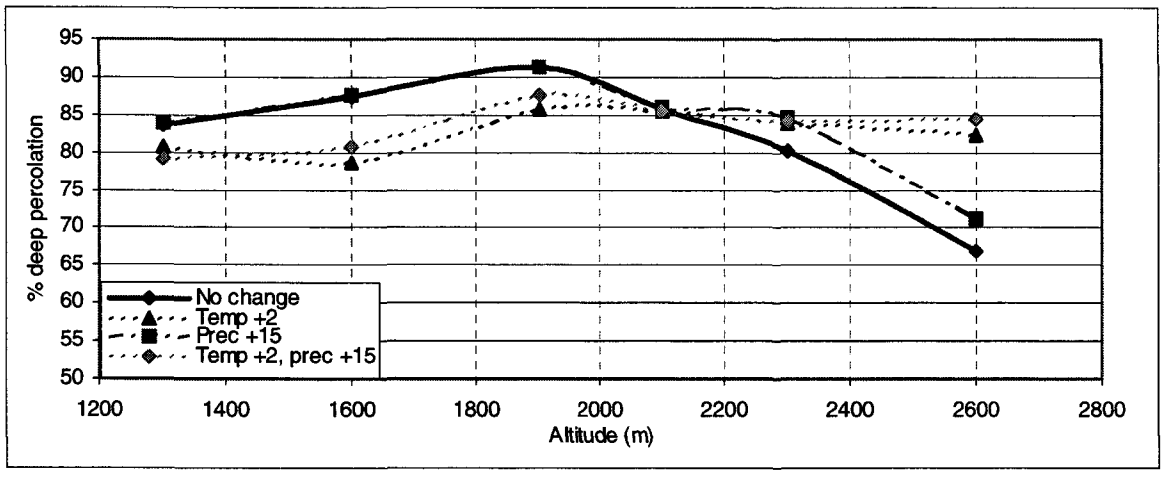

Figure 12.5: Altitudinal variation of (a) mean snow depth, (b) mean soil frost, and (c) percentage of deep percolation. Simulations were carried out over 30 years.

outlet of the catchment hardly changed during the year. A slight increase was noted between May and August on both hydrographs; however, no specific trend could be seen regarding the effect of the snowmelt on the general hydrologic circulation. In fact, by assuming a low permeable aquifer the water residence time in the aquifer was high, and the discharge function

did not show any strong variations on an annual basis. Differences between both hydrographs arose mainly from the differences in the total amount of infiltrating water between both scenarios.

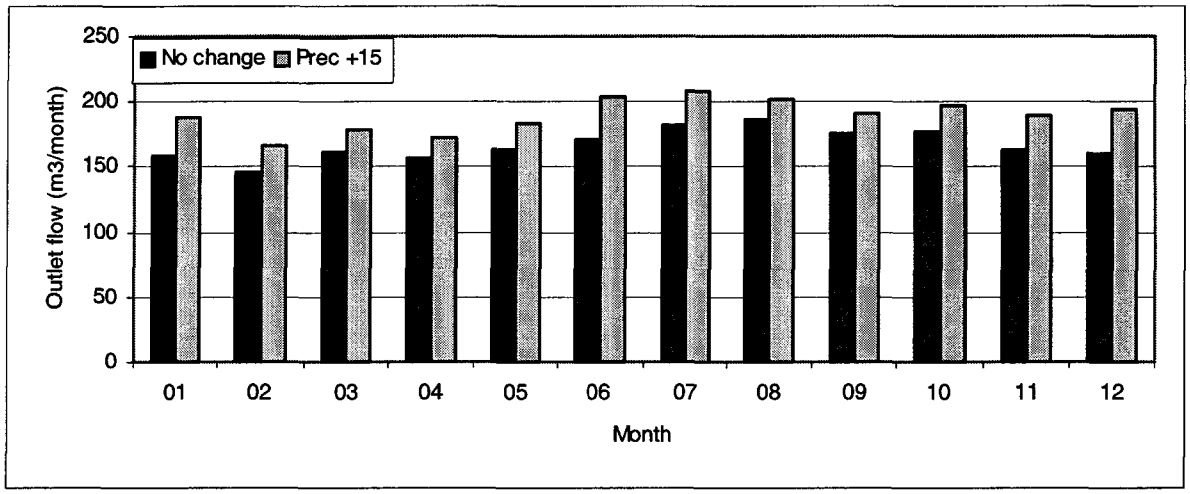

Figure 12.6: Mean monthly flow at the outlet of the catchment between 1967-2002, assuming climatic scenarios (a) (no change) and (c) (Δ ***Prec*** = +15%) in the water flux at the upper boundary of the model.

We continued to test the impact of variable aquifer conductivity using sensitivity analyses. The permeability was varied by a factor 10 between $k_{sat} = 10^{-6}$ m/s and $k_{sat} = 10^{-3}$ m/s. Fluctuations in the simulated hydrograph were minor for all cases, indicating that even for a high conductive aquifer, the water residence time in the aquifer was high enough to lower the hydrograph response to any snowmelt events. As a result, the long-term spatial and temporal variations of the snowmelt recharge determine the response of groundwater level, rather than short annual variation.

In addition, a sensitivity analysis was carried out on the intensity of the upper boundary flux, as the extent of the aquifer may be smaller than the recharge area extent. To simulate this case, we increased the upper boundary flux by a factor of 10. The new hydrograph (for climatic scenario (a)) is shown in Figure 12.7 (the monthly flux was divided by a factor of 10 to be able to compare it with the hydrograph for the unchanged precipitation boundary conditions). The change in the input flow hardly affected the hydrograph. The only difference was a slight increase of the water discharge in May and June, some three months earlier than previously. This reflects a faster transitory flow (i.e. input water causing a displacement of old water at the outlet of the catchment), as a greater part of the catchment stayed saturated, when we assumed a higher water input flux.

Finally, to reproduce a fast transmission similar to that measured at Grächen, the input flux had to be multiplied by a factor of 100, and the conductivity in the conductive layer set to 10^{-3} m/s. The resultant hydrograph is shown in Figure 12.8. It indicates that the strong variation in the water table recorded in the previous chapter is a probable consequence of (a) the coarse-textured soil, which enables a fast transfer of infiltrating water to the aquifer surface, (b) the relatively steep slope of the aquifer, which produces high flow velocities in the aquifer, and (c) the significant difference between the aquifer extent and the water supply catchment.

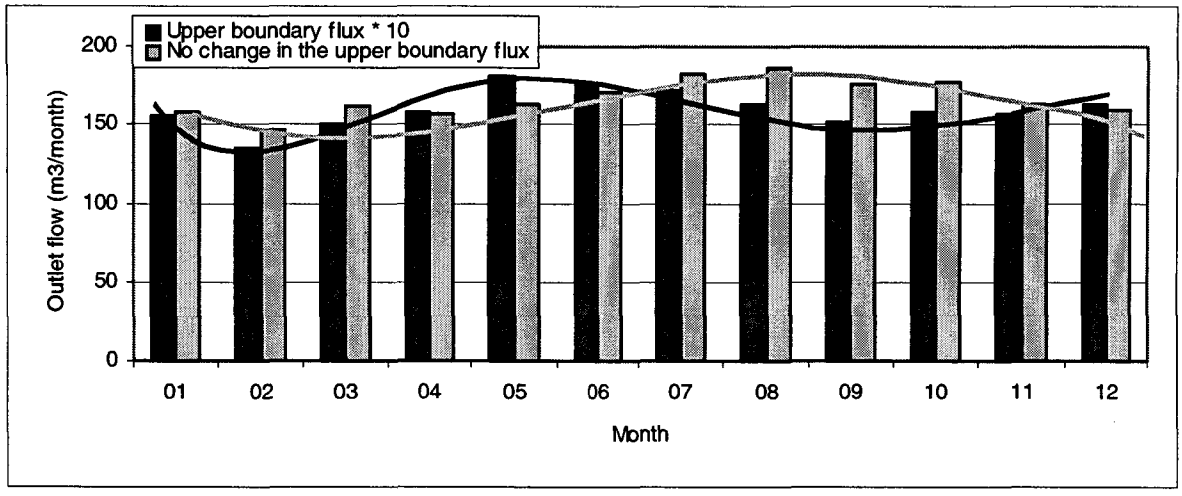

Figure 12.7: Mean monthly flow at the outlet of the catchment between 1967-2002, assuming climatic scenario (a) (no change). The flux at the upper boundary is either unchanged or multiplied by a factor of 10.

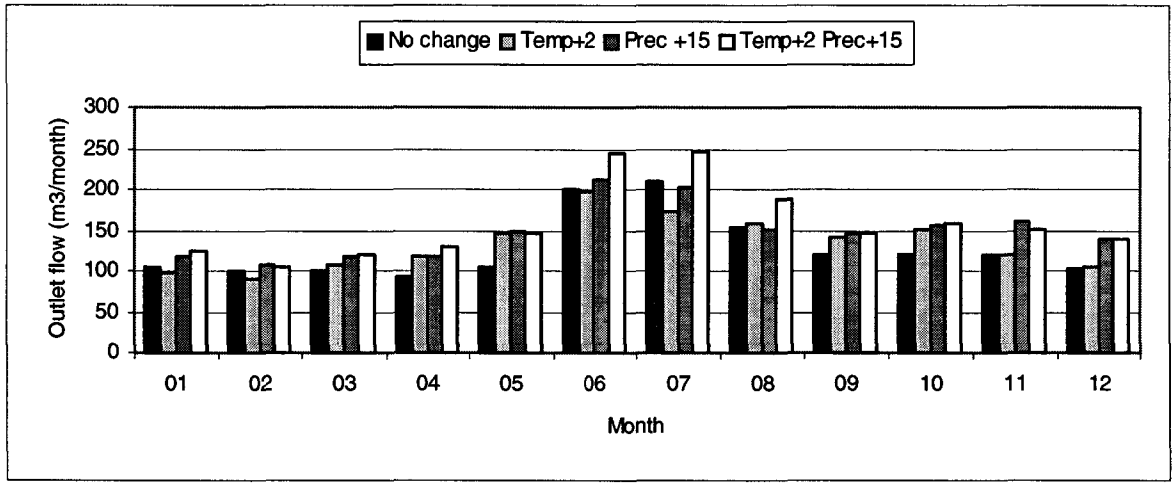

Figure 12.8: Mean monthly flow at the outlet of the catchment between 1967-2002, assuming four different climatic scenarios. The flux at the upper boundary was corrected by a factor of 100.

12.3.2.1. IMPACTS ON WATER RESOURCES AND WATER MANAGEMENT

The different climate scenarios and the numerical and conceptual model applied contain great uncertainties, and interpretation should be carried out with care. Nevertheless, a general trend in the results indicates that a change in the local scale discharge regime may become apparent in the future. This may lead to the following economic problems:

- As confirmed by numerous studies (Cooley 1990, Bultot et al. 1994), the mean snow cover will drastically decrease in lower alpine areas (< 1800 m in our study, see Figure 12.5), thus diminishing the alpine ski season at such locations.
- More precipitation will increase the groundwater recharge at snowmelt. As recharge processes are a main activating factor of landslides (Tullen 2002), one may expect an

increased danger of landslides during unfrozen winters. In areas below 2000 m, the frequency of winters with soil frost is expected to increase in future, which will reduce the risk of sliding, as less water infiltrates into the ground.

- The groundwater recharge as a whole will hardly be affected by a change in the air temperature. Whereas a change in the climate affects the discharge pathways locally, little change was simulated when the catchment was considered as a unique entity (Figure 12.5), the reduction in the deep percolation values at lower altitudes being compensated for by the increase at higher altitudes. Hence water availability (for tourism, agriculture or domestic use) will not be influenced by a spatial change of the seasonal soil frost extent. Nevertheless, a warmer climate will increase the demand for water, especially for artificial snow production in winter when water availability is low, which will in turn require greater sustainable water resources management.
- Similarly, hydropower generation will not be affected by a change in the air temperature, except for dams located at high altitudes (> 2000m): in such regions the percentage of percolated water will increase on the average at snowmelt, reducing the stream flow (Figure 12.5). This reduction will partly be compensated for if the climate change is accompanied by an increase in precipitation.
- The frequency of flooding is expected to increase. In lower-lying areas, the soil will be frozen more often (Figure 12.5), and due to the warmer air temperature, the number of rain on snow events will increase. Rain on snow and frozen ground are two activating factors for flooding (Singh et al. 1998, Loukas, 2002), hence increasing markedly the potential danger of flooding in the future.

12.4. CONCLUSION

In this chapter an assessment was made of the impact of a changing climate on the hydrological regime at an alpine catchment with soil pedological properties similar to those at Hannigalp. The chosen methodology provided detailed discharge results for representative bands located at different altitudes in the catchment.

A climate change is expected to increase the snow-line limit, as well as the snowpack dynamic. This change in the snow depth will induce differences in the soil frost extent and in the discharge regime particularly at both ends of the catchments, where contrasting behaviour may be expected: less/more melt water infiltrates into the soil in lower/higher areas. Due to more frequent rain on snow events at lower altitudes, the frequency of peak flow will increase. In regions located above 2500 m, the warmer climate will reduce the seasonal soil frost, and more water may infiltrate into the ground. This rise in the 0°-line will also result in a melting of the permafrost body, which will further affect the infiltration capacity of higher areas.

At a catchment scale, the effect of seasonal soil frost on the aquifer fluctuation depends on the catchment's geological structure, on the aquifer extent, on the pedological properties of the overlaying soil layer and on the extent of the supply catchment. The aquifer reacts quickly to any change in the input flux, when the water residence time in the aquifer is short (high conductivity), when the aquifer has a high altitudinal extent, or when the supply area is much larger than the aquifer extent. Otherwise, the aquifer depth will depend on long-term, rather than annual variation in the groundwater recharge.

A changing climate will have an economic impact on alpine regions. Although the water supply in the Alps will not be affected as a whole, we may expect an increase in the number of extreme

events. This increase should be considered in future natural danger management, in particular in infrastructure planning. The reduction of snow at lower areas will also increase the water demand for artificial snow, which may lead to excessive use of some aquifers.

Finally, the methodology applied needs some improvement to give a better confidence in the output results. In particular it should integrate:

- A multi-dimensional heat and water transport model integrating in its settings a snow module as well as a water/ice phase-transition, so as to allow a better spatial resolution of the soil frost extent.
- Changes in the water balance due to evapotranspiration, if interest is focused on long-term changes of the groundwater recharge.
- A better spatial resolution of the input data, as well as more complex climatic scenarios. For an accurate estimation of extreme events, one should consider the increase in the intensity and frequency of precipitation, rather than an identical percentage increase over the whole range of precipitation days.

In particular, application to an actual case would be desirable. This would involve a complete hydrogeological study of an alpine aquifer to characterize the aquifer's extent and the hydrologic properties of the geological structure, as well as measurements of the different water balance component during several years, so as to be able to calibrate/validate a numerical model.

13. GENERAL CONCLUSION

The main goal of this study was to assess the effect of seasonal soil frost on the groundwater recharge. This chapter summarizes the main results obtained and discusses how the objectives presented in Chapter 1 were met. Each objective is listed and discussed. Finally we propose some areas for future research.

Objective 1: to investigate the influence of soil frost on local snowmelt runoff at high altitude

The first stage of this work consisted in finding two locations with contrasting meteorological conditions, so as to assess the snowmelt runoff characteristics that may be representative for various alpine locations. The two alpine sites of Hannigalp (2100 m) and Gd St Bernard (2500 m) met this criterion, as Hannigalp may be considered as typical for protected, internal alpine valleys, whereas Gd St Bernard, with it's wet climate, was representative for the climate in the southern Alps.

The two contrasting winters allowed corroboration of the very sensitive relation between snow cover and soil frost. In particular, a shallow snowpack enabled the ground to freeze deeply, whereas a thick snowpack insulated the ground preventing soil frost - regardless of the altitude and the exposure. When the soil was deeply frozen, the snowmelt discharge changed dramatically. With regard to the lateral runoff, an increase from zero (unfrozen winters) to approx. 35% (frozen winters) of the total meltwater was observed. This drastic change was mainly caused by the presence of pore ice as well as by the occurrence of a basal ice layer. We believe that the formation of the basal ice sheet is favoured by the rather cold mean soil temperature, the long snow cover period and the early snowmelt events, as the snow cover period is long enough to allow a substantial latent heat transfer between the wet basal snowpack and the upper frozen soil boundary. However, further investigations of the formation of basal ice-layers are needed, especially its spatial extent.

Objective 2: to assess the local water infiltration pathways at snowmelt

The dye tracer infiltration tests offered the possibility to study the various infiltration pathways at both sites. The difficulty in making use of the fluorescence method *in situ* prevented us from obtaining quantitative information about the infiltration pathways. However, such information may be provided in the laboratory, as, with respect to the areal dye tracer coverage profiles, laboratory and *in situ* results were similar, and thus validated the laboratory results. Differences were noted in the infiltration pathways between frozen and unfrozen soils, as a frozen soil did not prevent meltwater from infiltrating into the ground. However, under frozen soil conditions, the penetration of the infiltrating wetting front was delayed compared to unfrozen conditions. Also, stained water was discovered during the frozen winter some 20 m downslope of the experimental site at Hannigalp, caused by surface runoff over a basal ice sheet. Finally, the dye tracer experiments were successful in differentiating the various infiltration processes between Gd St Bernard and Hannigalp; the infiltration occurring fairly uniformly at the former and in a strongly preferential manner at the latter.

Objective 3: to assess the soil hydrological characteristics at Hannigalp

The hydrophobic nature of the Hannigalp soil was demonstrated with the water drop penetration time procedure. The time needed for a water drop to infiltrate the soil greatly exceed 5 seconds,

which is considered as defining a water-repellent soil. A specific characteristic of hydrophobic soils is their ability to develop preferential infiltration pathways. This could be confirmed when we reproduced infiltration tests by using two different one-dimensional models. The one domain model COUP was unable to simulate the wetting front dynamic, whereas significant improvement was achieved when the two-flow domain MACRO model, integrating preferential flow, was applied. Nevertheless, we did not apply MACRO further, as on the one hand important conceptual differences exist between a macropore and a hydrophobic induced preferential flow, and on the other hand, MACRO does not include the phase transition in its settings. Hydrophobic preferential flow is a consequence of the strong hysteresis, which is typical for water repellent soil. Opposition between the pressure gradient and the flow direction inhibits the infiltrating water from flowing from the wet part towards the dry un-wetted part of the soil. Consequently a further development of COUP, integrating a second Richard's flow domain, would be desirable for future investigations.

Objective 4: to estimate the impact of the spatial, altitudinal, and textural variability on soil frost and snowmelt, so as to regionalize obtained results

Despite the previously mentioned restrictions, the one-dimensional numerical model COUP was used to study the snowmelt dynamic at the four experimental fields for various climatic conditions. The model was calibrated and validated with data from both winter seasons. In a first step, we tested two different methods to simulate the snowmelt dynamic, a surface energy balance approach against an empirically based approach. The different processes taking place under frozen and unfrozen soil conditions, such as snow formation and ablation or meltwater dynamic, were mostly accurately reproduced by the model. Nevertheless, both approaches produced systematic errors, which reduced their applicability to specific conditions. Different modes of energy transfer dominated the melt process at different times through the years. At the onset of the winter, melting was mainly caused by sensible heat transfer, whereas the radiation heat exchange became predominant at the end of the winter. The surface energy balance approach under estimated the snow surface temperature, causing deep soil frost and no snowmelt until spring, regardless of the exposure, whereas in the empirical approach, where the air and the snow surface temperature were set equal, shallow soil frost and excessive snowmelt were reproduced. Best results were achieved by applying the surface energy balance approach to protected areas and the empirical approach to more exposed locations. Prediction of both models indicated that soil frost was sporadic on all plots examined. During most winters the soil remained unfrozen.

The four plots investigated were chosen to allow monitoring of the spatial soil frost variability, with respect to the orientation, the altitude and the soil texture. Simulation results suggest that the first two factors mainly influenced the snowmelt dynamic, as well as the soil frost formation, whereas the last one affected the extent of the soil frost penetration into the soil. Soil frost showed a general tendency to be more present at northerly and rather dry locations. On well-exposed sites, a shallow soil frost was present during most winters, but the underneath heat flux melted most pore ice until the final snowmelt. On a northerly and wet exposed site, the soil was mostly protected by an early snow cover, and consequently soil frost was rare. The altitudinal variation in the soil frost depth was governed by the same factors, i.e. the mean soil temperature and the precipitation. A critical altitude (1900 m) was determined, where the still warm soil and the already thick snowpack prevent the soil from freezing deeply, in contrast to other altitudes. The texture mainly affected the soil frost depth extent, as the presence of large conductive slate stone created a much deeper soil frost at Gd St Bernard than at Hannigalp. During the main snowmelt period, we observed that a part of the recorded surface water infiltrated the soil some

100 meters below the experimental plot where the soil was already free of snow and unfrozen. Such a result demonstrates the importance of the soil texture, structure and steepness, as well as the underlying geological structure on the amount of surface runoff. Although the soil infiltration capacity was similar at both experimental sites, considerably more lateral runoff was measured at Gd St Bernard, as the experimental plot was located on a much steeper slope than at Hannigalp.

Objective 5: to estimate the effect of seasonal soil frost on the alpine aquifer recharge

In our plot studies, the seasonal soil frost affected the groundwater recharge. The simulation results showed that during frozen winters, the seepage diminished by between 20% and 50% of the total meltwater at Hannigalp. However, the decrease was reduced when we looked at fluctuations in the underneath groundwater table. The water table rise at snowmelt in Grächen diminished by 10-30% during frozen winters. Different factors may explain these opposing results. First of all, large there was great uncertainty associated with the estimated water-table recharge, and results should be analysed with great care. Also, only a few winters were directly comparable, and statistical interpretation was hence difficult. This problem may be solved in future, as the water-table measurements at Grächen will be carried on during the next years, providing additional data. Finally, the very permeable Hannigalp soil (till and slope deposit) allowed most meltwater to re-infiltrate the soil in lower areas where soil frost was absent. This last result especially emphasizes the importance of the soil texture, structure and steepness on the amount of surface runoff. One may expect less water to re-infiltrate in steeper and less permeable soils.

Objective 6: to evaluate the influence of the greenhouse effect on the aquifer recharge

By using modified input data, we were able to estimate possible impacts of a changing climate on the global and local water balance. Increased air temperature (+2°C) will mainly affect the snow depth at a lower altitude, generating a deeper soil frost and a higher portion of surface runoff. Frequent winter snowmelt events cause higher ice content in the top soil and inhibit meltwater from infiltrating into the ground. For higher locations, the simulations showed that the snow depth was less influenced by the increased air temperature. Consequently, the simulated soil frost depth was less deep, as more heat was stored in the soil in summer, and as freezing was less severe in early winter. More precipitation (+15%) will reduce the soil frost depth at all altitudes. The proportion of lateral runoff will diminish overall. However, during specific snowmelt events, we may expect an increase in the total surface runoff due to the increased meltwater, and the longer snowmelt period.

The aquifer recharge on a catchment scale will only be slightly affected by a warmer and wetter climate. Reduced infiltration in the lower part of the catchment will be compensated for by infiltration rates in the upper part. However, the simulations showed that significant differences would occur in the discharge dynamic of certain winters. This may lead to an increase in extreme events, as heavy rain precipitation may fall on frozen soils, even at high altitudes like Hannigalp or Gd St Bernard.

Perspective

Considerable progress has been made during the last decades in understanding and describing the heat and water processes of frozen and unfrozen soils. Most processes are now reasonably well understood at the pore scale, as most studies have been carried out at that scale or in the laboratory. But, there is an evident lack of observations at the large scale, arising from the

difficulty in collecting data in large and remote areas. In my opinion future work should emphasize then following topics: (a) comprehensive hydrogeological studies of alpine catchments to characterize the main processes affecting the groundwater recharge, (b) development of a multidimensional numerical model to simulate large-scale processes, and (c) an improved description of the snowpack both at the plot scale and over large areas.

The next step of this project should include an advanced description of the different recharge processes of an alpine aquifer. This description should allow calibration and validation of a groundwater flow model of both mass and heat transfers. Several methods exist to characterize the structure and processes of a catchment, such as hydrological and geological cartography, a complete water balance, piezometric measurements, and hydro-chemistry or artificial tracers. To simulate these hydraulic processes, we may further develop FEFLOW. This would include the addition of a snow and a soil evaporation component to the model, or we may scale up the physical processes from single points to a large scale using the COUP-model in a multi-run mode. However, such an option would imply integrating parameters accounting for the spatial variability of the snow cover, like the topography or the wind speed. Another solution would be to derive this information from Remote Sensing, which maps the spatial distribution of the snow depth, the snow cover area and the soil surface temperature.

Final remarks

Finally, we should be aware of the potential danger of seasonal soil frost, which may have relevant implications for the general water circulation, in particular with respect to flooding. During rain on snow events, the soil infiltration capacity is further reduced by the presence of soil frost. This results in an acceleration of the outflow from the snowpack, which in turn increases the amount of surface runoff, hence potentially increasing the risk for flooding. Warmer air temperatures and higher precipitation will further accentuate this danger in the future, because more rain on snow events will occur.

References

Abbott, M.B., J.C. Bathurst, J.A. Cunge, P.E. O'Connell, and J. Rasmussen (1986). "An introduction to the european hydrological system - système hydrologique européen 2: structures of a physically-based, distributed modelling system." Journal of Hydrology 87: 61-77.

Aeby, P., U. Schultze, D. Braichotte, M. Bundt, F. Moser-Boroumand, H. Wydler, and H. Flühler (2001). "Fluorescence Imaging of tracer distribution in soil profiles." Environment Science and Technology **35**(4): 753-760.

Anderson, D.M. and A.R. Tice (1972). "Predicting unfrozen water contents in frozen soils from surface area measurements." Highway Research Record **393**: 12-18.

Audry, P., A. Candeau, F.X. Humbel, E. Roox, and J.F. Vizier (1973). Essai sur les études de dynamique actuelle des sols. Bulletin du groupe de travail sur la dynamique actuelle des sols. Orston. **2:** 20-31.

Baker, J.M., K.L.Davis, and G.C. Liknes (1999) "Surface energy balance and boundary layer development during snowmelt." Journal of Geophysical Research **104**(D16): 19,611-19,621.

Baker, J.M. and E.J.A. Spaans (1997). "Mechanics of meltwater movement above and within frozen soil." *In* I.K. Iskandar, E.A. Wright, J.K. Radke, B.S. Sharratt, P.H. Groenevelt and L.D. Hinzman (ed.), Proceedings of the International Symposium on Physics, Chemistry and Ecology of Seasonally Frozen Soils, Fairbanks, AK, 31-36.

Bauters, T.W.J., T.S. Steenius, D.A. DiCarlo, J.L. Nieber, L.W. Dekker, C.J. Ritsema, J.-Y. Parlange, and R. Haverkamp (2000). "Physics of water repellent soils." Journal of Hydrology **231-232**: 233-243.

Bengtsson, L. and V.P. Singh (2000). "Model sophistication in relation to scales in snowmelt runoff modeling." Nordic Hydrology **31**(4/5): 267-286.

Beniston, M., A. Ohmura, M. Rotach, P. Tschuck, M. Wild, and T.M. Marinucci (1995). Simulation of climate trends over the alpine region - Development of a physically-based modeling system for application to regional studies of current and future climate. Report. ETHZ Zurich, Department of Geography, 198 pp.

Bergström, S. (1992). The HBV model - its structure and applications. SMHI Report Hydrology. Norrkoping, Sweden. Vol. 4, 32 pp.

Beskow, G. (1935). Soil freezing and frost heaving with special application to roads and railroad, Swe. Geol. Society. Serie C 375, 242 pp.

Beven, K. (1982). "Macropores and water flow in soils." Water Resources Research **18**(5): 1311-1325.

Beven, K. (1989). "Interflow." *In* H.J. Morel-Seytoux (ed.), Unsaturated Flow in Hydrologic Modeling Theory and Practice,191-219.

Benoit, J.R. (1974). "Frost depth and distribution from a heat flow model." *In* Proceedings of Eastern Snow Conference: 123-134.

Bisdom, E.B.A., L.W. Dekker, and J.F. Schoute (1993). "Water repellency of sieve fractions from sandy soils and relationships with organic material and soil structure." Geoderma **56**: 105-118.

Blöscht, G., R. Kirnbauer, and D. Gutknecht (1991). "Assessment of snowmelt simulations in Alpine terrain on the basis of depletion paterns." Trans. AGU 70 **43**(1113).

Braun, L. N. (1985). Simulation of snowmelt-runoff in lowland and lower alpine regions of Switzerland. Zürcher Geographische Schriften. Zürich **21**.

Brooks, R.H. and A.T. Corey (1964). Hydraulic properties of porous media. Hydraulic paper N°3. Fort Collins, Colorado State University. 27 pp.

Brun, E., P. David, M. Sudul, and G. Brunot (1992). "A numerical model to simulate snow-cover stratigraphy for operational avalanche." Journal of Glaciology **38**: 13-22.

Buckingham, E. (1907). Studies on the movement of soil moisture. US Depart. of Agriculture. Bur. of soils N° 38.

Bultot, F., G.L. Durpiez, and D. Gellens (1988). "Estimated regime of energy-balance components evapotranspiration and soil moisture for a drainage basin the case of a CO2 doubling." Climatic Change **12**: 39-56.

Bultot, F., D. Gellens, and B. Schädler (1994). "Effects of climate change on snow accumulation and melting in the Broye catchment (Switzerland)." Climatic Change **28**: 339-363.

Burt, T.P. and P.J. Williams (1976). "Hydraulic conductivity in frozen ground." Earth Surface Processes **1**: 349-360.

Carey, S. and M.-K. Woo (2001). "Slope runoff processes and flow generation in a subarctic, subalpine catchment." Journal of Hydrology **253**: 110-129.

Cary, J.W., G.S. Campbell, and R.I. Papendick (1978). "Is the soil frozen or not? An algorithm using weather records." Water Resources Research. **14**(6): 1117-1122.

Casagrande, A. (1932). "Discussion of frost heaving." HRB Proc. Vol. 2(part 1).

Castelle, T. (1995). Transport de la neige par le vent en montagne: approche expérimentale du site du col du lac Blanc. Dissertation. EPFL. Génie Civil. Lausanne, 183 pp.

Chacho, E.F. and S. Bredthauer (1983). "Runoff from a small subarctic watershed, Alaska." *In* Proceedings, Fourth International Conference on Permafrost, National Academy Press: Washington D.C: 115-120.

Chen, J. (1991). Changes of Alpine Climate and Glacier Water Resources. Zürcher Geographische Schriften. Zürich, Geographisches Institut ETH. Vol. 46, 196 pp.

Cherkauer, K.A. and D.P. Lettenmaier (1999). "Hydrologic effects of frozen soils in the upper Mississippi." Journal of Geophysical Research **104**(D16): 19,599-19,610.

Church, J.E. (1914). "Recent studies on snow in the United States." Quarterly Journal of the Royal Meteorological Society **40**: 43-52.

Colbeck, S.C. (1972). "A theory of water percolation in snow." Journal of Glaciology **11**(63): 369-385.

Colbeck, S.C. (1973 a). Effects of stratigraphic layers on water flow through snow. Research Report 311. Hanover, New Hampshire, U.S. Army Cold Reg. Res. and Engg.

Colbeck, S.C. (1973 b). "Water flow through snow overlaying an impermeable boundary." Water Resources Research **10**(1): 119-123.

Colbeck, S.C. (1978). "The physical aspects of water flow through snow." Advances in Hydrosciences: 165-206.

Colbeck, S.C. (1987). "History of snow cover research." Journal of Glaciology (Special Issue): 60-65.

Coléou, C., K. Xu, B. Lesaffre, and J.B. Brzoska (1999). "Capillary rise in snow." Hydrological Processes **13**(12/13): 1721-1732.

Cooley, K.R. (1990). "Effects of CO2-induced climatic changes on snowpack and streamflow." Hydrological Sciences Journal **35**(5): 511-522.

De Gaetano, A.T., S. Wilks, and M. McKay (1996). "A physically based model of soil freezing in humid climates using air temperature and snow cover data." Journal of Applied Meteorology **35**: 1009-1027.

De Vries, D.A. (1975). Heat transfer in soils. *In* D.A. De Vries and N.H. Afgan (eds.), Heat and Mass Transfer in the Biosphere. I. Transfer Processes in Plant Environment, Washington D.C., 5-28.

Delesse, A. (1848). Procédé mécanique pour déterminer la composition des roches. Ann. Mines Vol. 13, 379 pp.

Diersch, H. (1996). Interactive, graphics based finite element simulation system FEFLOW for modelling groundwater flow, contaminant mass and heat transport processes. Wasy Ltd. Berlin.

Dysli, M. (1991). Le gel et son action sur les sols et les fondations. Walther R. (ed.), Traité de Génie Civil, Presse Polytechnique et Universitaire Romande, 250 pp.

Dysli, M., V. Lunardini, and L. Stenberg (1997). "Related effects on frost action: Freezing and solar radiation indices (invited lecture)." *In* Knutsson (ed.), Inter. Symp. on Ground Freezing and Frost Action in Soils, Lulea, Sweden April.

Easterling, D.R., T.R. Karl, and K.P. Gallo (2000). "Observed climate variability and change of relevance to the biosphere." Journal of Geophysical Research **105**(D15): 20,101-20,114.

Ehrler, C. Klimaänderung und alpine Schneedecke. NRP 31. Zürich, Vdf, 134 pp.

Engelmark, H. (1984). "Infiltration in unsaturated frozen soil." Nordic Hydrology **15**: 243-252.

Engelmark, H. (1987). "Rates of infiltration into frozen and unfrozen fine sand." Can. J. Earth Sci. **25**: 343-347.

Etchevers, P., C. Golaz, and F. Habets (2001). "Simulation of the water budget and the river of the Rhone basin form 1981 to 1994." Journal of Hydrology **244**: 60-85.

Ferrer, M (2000). "Meshing of complex shapes in Earth Sciences." Dissertation. EPFL, ENAC. Lausanne, Switzerland, 110 pp.

Flerchinger, G.N. and K.E. Saxton (1989). "Simultaneous heat and water model of a freezing snow-residue-soil system I. Theory and development." Transaction of the ASAE **32**(2): 565-571.

Flerchinger, G.N., K.R. Colley, and Y. Deng (1994). "Impacts of spatially and temporally varying snowmelt on subsurface flow in a mountainous watershed: 1. Snowmelt simulation." Hydrological Sciences **39**(5): 507-520.

Flury, M., H. Flühler, W.A. Jury, and J. Leuenberger (1994). "Susceptibility of soils to preferential flow of water: A field study." Water Resources Research. **30**: 1945-1954.

Forrer, I., A. Papritz, M. Flury, and H. Flühler (2000). "Quantifying dye tracers in soil profile by image processing." Eur. J. Soil Sci. **51**(2): 313-322.

Fox, J.D. (1992). "Incorporating freeze-thaw calculation into a water balance model." Water Resources Research. **28** (9): 2229-2244.

Fuhrer J. (1997). Klimaänderung und Grünland (Schlussbericht NFP 31), vdf, Hochschulverlag AG an der ETH Zürich, 311 pp.

Fujino, K. (1971). "Measurement of flow down speed of melt water in snow cover, 2. Flow of melt water in snow cover on a slope." Low Temperature Sci. **29**(Ser. A): 151-158.

Furbish, D.J. (1988). "The influence of ice layers on the travel time of meltwater flow through a snowpack." Artic and Alpine Research **20**(3): 265-272.

Gardaz, J.-M., R. Lugon, and M. Monbaron (1995). Prospection du pergélisol de montagne à l'aide de la méthode BTS (Alpes valaisannes, Suisse). Ukpik, Cahiers de l'Institut de Géographie de Fribourg, Suisse: 93-105.

Gerber, E. and G. Tenthorey (1990). Hydrologie du glacier rocheux de Murtèl (Grisons): Description et interaction de traçages d'eau. Report. Modelle in der Geomorphologie. Berichte und Forschungen Geographisches Institut Freiburg/CH: 119-121.

Glen, J.W. (1982). Hydrological Aspects of Alpine and High Mountain Areas. IAHS. Vol. 138, 350 pp.

Granger, R.J., D.M. Gray, and B.D. Dyck (1984). "Snowmelt infiltration to frozen prairie soils." Can. J. Earth Sc. **23**: 696-704.

Gray D.M. and R.J. Granger (1985). "In situ measurements of moisture and salt movement in freezing soils." Can. J. Earth Sc. **21**: 669-677.

Gustafsson, D., M. Stähli, and P.-E. Jansson (2001). "The surface energy balance of a snow cover: comparing measurements to two different simulation models." Theoretical and

Applied Climatology **70**(1-4): 81-96.
Gustafsson, D., P.A. Waldner, and M. Stähli (2002). "Factors governing the formation and persistence of layers in a sub-alpine snow pack." Hydrological Processes. (submitted).
Gyalistras, D. (1998). Projecting Scenarios of Climatic Change and Future Weather for Ecosystem Models: Derivation of Methods and Their Application to Forests In the Alps. Dissertation. ETHZ. Institute of Terrestrial Ecology. Zurich, 103 pp.
Haeberli, W. (1973). "Die Basis-Temperatur der winterlichen Schneedecke als möglicher Indikator für die Verbreitung von Permafrost in den Alpen." Zeitschrift für Gletscher und Glaziologie **9**: 221-227.
Haeberli, W., and M. Hoelzle (1996). Simulation der Permafrostverbreitung in den Alpen mit geographischen Informationssystemen. Zurich, vdf Hochschulverlag an der ETH Zürich, 58 pp.
Haines, B.L., J.B. Waide, R.L. Todd (1982). "Soil solution nutrient concentrations sampled with tension and zero-tension lysimeters: report of discrepancies." Soil Sci. Soc. Am. J. **46**: 658-661.
Hanson, C.L. (1982). "Distribution and stochastic generation of annual and monthly precipitation on a mountainous watershed in southwest Idaho." Water Resources Bulletin **18**: 875-883.
Harlan, R.L. (1973). "Analysis of coupled heat-fluid transport in partially frozen soil." Water Resources Research **9**: 1314-1323.
Hardy, J.P., P.M. Groffman, R.D. Fitzhugh, K.S. Henry, A.T. Welman, J.D. Demers, T.J. Fahey, C.T. Driscoll, G.L. Tierney, and S. Nolan (2001). "Snow depth manipulation and its influence on soil frost and water dynamics in a northern hardwood forest." Biogeochemistry **56**: 151-174.
Hartman, M.D., J.S. Baron, R.B. Lammers, D.W. Cline, L.E. Band, G.E. Liston, and C. Tague (1999). "Simulation of snow distribution and hydrology in a mountain basin." Water Resources Research **35**(5): 1587-1603.
Hendrickx, J.M., L.W. Dekker, and O.H. Boersma (1993) "Unstable wetting fronts in water repellent field soils." Journal of Environmental Quality **22**: 109-118.
Herz, T., H. Gubler, L. King (2002). Microclimate within coarse debris of talus slopes in the alpine periglacial belt, Mattertal, Valais, Swiss Alps. not published. Giessen, Institute of Geography.
Hoersch, B., G. Braun, and U. Schmidt (2001). "Relation between landform and vegetation in alpine regions of Wallis, Switzerland. A multiscale remote sensing and GIS approach." Computers, Environments and Urban Systems **26**: 113-139.
Hood, E., M. Williams, and D. Cline (1999). "Sublimation from a seasonal snowpack at a continental, mid-latitude alpine site." Hydrological Processes **13**: 1781-1797.
Hulme, M., K. Briffa, P.D. Jones, and C.A. Senior (1993). "Validation of GCM control simulations using indices of daily airflow types over the British Isles." Clim. Dynamics **9**: 95-105.
Ippisch, O., I. Cousin, and K. Roth (1998). "Wärmeleitung in porösen Medien. Auswirkungen der Bodenstruktur auf Wärmeleitung und Temperaturverteilung." Mitteilungen DT Bodenkunkl. Gesellsch. **87**: 405-408.
Ippisch, O. and K. Roth (2001). Coupled transport in natural porous media. Dissertation, University of Heidelberg, Germany, 145 pp.
Jansson, P.-E. and L. Karlberg (2001). Coupled heat and mass transfer model for soil-plant-atmosphere systems. Royal Institute of Technology, Dept. of Civil and Environmental Engineering, Stockholm: 325 pp.
Jansson, P.-E., Gustafsson D., G. Alvenäs, and L. Lewan (2002). Soil evaporation, snow and radiation processes. *In* P.-E. Jansson and L. Karlberg (eds.), Coupled Heat and Mass

Transfer Model for Soil-Plant-Atmosphere Systems, Royal Institute of Technology, Dept. of Civil and Environmental Engineering, Stockholm, 145-185.

Jarvis, N. and M. Larsson (1990). The MACRO model (version 4.1). Uppsala, SLU, Department of Soil Sciences: 32 pp.

Johnsson, H. and L.-C. Lundin (1991). "Surface runoff and soil water percolation as affected by snow and soil frost." Journal of Hydrology **122**: 141-159.

Jones, H.G., J.W. Pomeroy, D.A. Walker, and R.W. Hoham (2001). Snow Ecology, Cambridge University Press, 378 pp.

Kane, D.L., S.R. Bredthauer, and J. Stein (1981). "Subartic snowmelt runoff generation." *In* Proceedings of the Sixth International Conference on Permafrost: 257-271.

Kane, D.L. and E.F. Chacho (1990). Frozen ground effects on infiltration and runoff. *In* W.L. Ryan and R.D. Crissman (eds.), Cold Regions Hydrology and Hydraulics, New York, ASCE, 259-300.

Kane, D.L. and J. Stein (1983). "Water movement into seasonally frozen soils." Water Resources Research **19**: 1547-1557.

Kennedy, I. and B. Sharratt (1997). "A Comparison of three models for predicting frost in soils." *In* I.K. Iskandar, E.A. Wright, J.K. Radke, B.S. Sharratt, P.H. Groenevelt and L.D. Hinzman (eds.), Proceedings of the International Symposium on Physics, Chemistry and Ecology of Seasonally Frozen Soils, Fairbanks, AK, 531-536.

Kersten, M.S. (1949). Thermal properties of soils, Uni. of Minnesota. Stat.Bull. N° 28.

Konzelmann T, R.S.W Van de Wal, W. Greuell, R. Bintanja, E.A.C. Henneken, A. Abe-Ouchi (1994). "Parametrization of global and longwave incoming radiation for the Greenland Ice Sheet." Global and Planetary Change **9**: 143-164.

Koivusalo, H. (2002). "Snow processes in a forest clearing and in a coniferous forest." Journal of Hydrology **262**(1-4): 145-164.

Koren, V.I., Q.Y. Duan, J.C. Schaake(1995). Modeling of the effect of frozen ground on snowmelt/rainfall runoff processes. *In* T. Krauss and T. Carroll (eds.), International GEWEX Workshop on Cold Season/Region Hydrometeorology, Banff Alberta, National Oceanic and Atmospheric Administration, 78-82.

Koren, V.I., J.C. Schaake, K. Mitchell, Q.Y. Duan, F. Chen, and J.M. Baker (1999). "A parametrization of snowpack and frozen ground intended for NCEP weather and climate models." Journal of Geophysical Research **104**(D16): 19,569-19,585.

Lang, H. (1998). Forecasting meltwater runoff from snow-covered areas and from glacier basins. *In* D.A. Kraijenhoff and J.R. Moll (eds.), River Flow Modelling and Forecasting, Dordrecht, Reidel Publishing Company, 99-127.

Lehning, M., P. Bartelt, and B. Brown (1998). Operational use of a snowpack model for the avalanche warning service in Switzerland: model development and First Experience. NGI Anniversary Conference, Norwegian Geotechnical Institute: 169-174.

Levine, E.R., and R.G. Knox (1997). "Modeling soil temperature and snow dynamics in northern forests." Journal of Geological Research **112**(D24): 29,407-29,416.

Liston, G.E. and M. Sturm (1998). "A snow-transport model for complex terrain." Journal of Glaciology **44, n°148**: 498-516.

Loukas, A., L. Vasiliades, and N.R. Dalezios (2002). "Potential climate change impacts on flood producing mechanisms in southern British Columbia, Canada using the CGCMA1 simulation results." Journal of Hydrology **259**: 163-188.

Lugon, R. and M. Monbaron (1998). Stabilité des terrains meubles en zone de pergélisol et changements climatiques. Deux études de cas en Valais: le Rittigraben (Mattertal) et la moraine du Dolent (Val Ferret). NRP 31. Zürich, Vdf, 94 pp.

Lundin, L.-C. (1990). "Hydraulic properties in an operational model of frozen soil." Journal of Hydrology **118**: 289-310.

Mac Adam, J. (1816). Remarks on the present system of road making with observations, deduced from practice and experience, with a view to an introduction of improvement in the method of making, repairing and preserving roads, and defending the roads funds from misapplication. 1st ed.

Maisch, M., A. Wipf, B. Denneler, J. Battaglia, C. Benz (2000). Die Gletscher der Schweizer Alpen. NRP 31. Zürich. Vdf: 378 pp.

Malevsky-Malevich, S.P., E.K. Molkentin, E.D. Nadyozhina, and O.B Shklyarevich,.(2001). "Numerical simulation of permafrost parameters distribution in Russia." Cold Regions Science and Technology **32**: 1-11.

Mann, M.E. and R.S. Bradley (1999). "Northern hemisphere temperatures during the past millennium: inference, uncertainties, and limitation." Geophysical Research Letters **26**(6): 759-762.

Martinec, J. (1975). "Snowmelt runoff model for streamflow forecasts." Nordic Hydrology **6**: 145-154.

Marsh, P. and M.-K. Woo (1985). "Soil heat flux, wetting front advance and ice layer growth in cold dry snow cover." Snow property measurement workshop, Lake Louise, Alberta: 285-311.

Marty, C. (2001). Surface radiation, cloud forcing and greenhouse effect in the Alps. Dissertation. ETHZ Institute for Climate Research. Zurich, 122 pp.

Middelkoop, H., K. Daamien, D. Gellens, W. Grabs, J.C. Kwadijk, H. Lang, B.W.Parmet, B. Schädler, J. Schulla, and K. Wilke (2001). "Impact of climate change on hydrological regimes and water resources management in the Rhine Basin." Climatic Change **49**: 105-128.

Miller, C. and J.Y. Lee (1999). "Response of landfill clay liners to extended periods of freezing." Engineering Geology. **51**: 231-302.

Miller, R. D. (1980). Freezing phenomena in soils. *In* Hillel (ed.), Application of Soil Physics, New York, Academic Press, 254-299.

Miller, R.H. and J.F. Wilkinson (1977). "Nature of the organic coating on sand grains of nonwettable golf greens." Soil Sci. Soc. Am. J. **41**: 1203-1204.

Monteith, J.L. (1965). Evaporation and environment. *In* Fogg, G.E. (ed.), The State and Movement of Water in Living Organisms, 19th Symp. Soc. Exp. Biol., Cambridge: The Company of Biologists, 205-234.

Morris, E.M. (1989). "Turbulent transfer over snow and ice." Journal of Hydrology **105**: 205-223.

Mualem, Y. (1976). "A new model for predicting the hydraulic conductivity of unsaturated porous media." Water Resources Research **12**(3): 513-522.

Musy, A. and M. Soutter (1991). Physique du sol. Lausanne, Presse Polytechnique et universitaires romandes: 335 pp.

Nieber, J.L. (1996). "Modeling finger development and persistence in initially dry porous media." Geoderma **70**: 207-229.

Noverraz, F., C. Bonnard, H. Durpraz, and L. Huguenin (1998). Grands glissements de versants et climat. Bern, NRP 31. Zürich. Vdf: 312 pp.

Nyberg, L., M. Stähli, P.E. Mellander, and H. Bishop (2001). "Soil frost effects on soil water and runoff dynamics along a boreal forest transect: 1.Field investigations." Hydrological Processes **15**: 909-926.

Ohmura, A., M. Beniston, M. Rotach, P. Tschuck, M. Wild, and M.R. Marinucci (1998). Simulation of climate trends over the Alpine Region. Bern, NRP 31, 210 pp.

Or, D. and M. Tuller (1999). "Liquid retention and interfacial area in variably saturated porous media -liquid retention and interfacial configurations in angular pores." Water Resources Research **35**(12): 3591-3606.

Parriaux, A. and Nicoud (1988). Hydrological behaviour of glacial deposits in mountainous areas. Communication, International Workshop on Hydrology in Mountainous Areas, Tatra, Czechoslovakia.

Parviainen, J. and J.W. Pomeroy (2000). "Multiple-scale modelling of forest snow sulbimation: initial findings." Hydrological Processes **14**: 2669-2681.

Perfect, E. and Williams, P.J. (1980). "Thermally induced water migration in frozen soils." Cold Regions Science and Technology. **3**: 101-109.

Petrascheck, A., and C. Hegg (2000). Hochwasser 1999: Analyse der Ereignisse. Studienbericht, Vol. 10, Schweizerisches Bundesamt für Wasser und Geologie, Bern, 148 pp.

Pikul Jr., J.L. and J.K. Aase (1998). "Fall Contour Ripping Increases Water Infiltration into Frozen Soil." Soil Sci. Soc. Am. J. **62**: 1017-1024.

Pikul Jr., J.L., J.F. Zuzel, and D.E. Wilkins (1992). "Infiltration into frozen soils as affected by ripping." Transactions of the ASAE **35** (1): 83-90.

Plüss, C. and R. Mazzoni (1994). "The role of turbulent heat flux in the energy balance of high alpine snow cover." Nordic Hydrology **25**: 25-38.

Plüss, C (1997). The energy balance of an alpine snow cover. Point measurements and areal distribution. Geographisches Institut ETH Zürich, Heft 65.

Pomeroy, J.W. (1991). Transport and sublimation of snow in wind-scoured alpine terrain. Vienna Symposium, Vienna, IAHS **205**: 131-140.

Pomeroy, J.W. and R.L. H. Essery (1999). "Turbulent fluxes during blowing snow: field tests of model sublimation predictions." Hydrological Processes **13**: 2963-2975.

Quick, M.C. and A. Pipes (1977). "UBC watershed model." Hydrological Sciences Bulletin **22**: 153-161.

Raats, P.A.C. (1973). "Unstable wetting fronts in uniform and non-uniform soils." Soil Sci. Soc. Am. Proc. **39**: 681-685.

Rango, A. (1992). "Worldwide testing of the Snowmelt Runoff Model with applications for predicting the effects of climate change." Nordic Hydrology **23**: 155-172.

Rango, A. and J. Martinec (1979). "Application of a Snowmelt-Runoff Model using Landsat data." Nordic Hydrology **10**: 225-238.

Richards, L.A. (1931). "Capillary conduction of liquids in porous mediums." Physics **1**: 318-333.

Richardson, S.G., and F.B. Salisbury (1977). "Plant response to the light penetrating snow." Ecology **58**: 1152-1158.

Ritsema, C.J. and L.W. Dekker (2000). "Preferential flow in water repellent sandy soils principles and modeling implications." Journal of Hydrology **231-232**: 308-319.

Ritsema, C.J., L.W. Dekker, J.M. Hendrickx, and W. Hamminga. (1993). "Preferential flow mechanism in a water repellent sandy soil." Water Resources Research **29**: 2183-2193.

Roberge, J. and A.P. Plamondon (1987). "Snowmelt runoff pathways in a boreal forest hillslope, the role of pipe throughflow." Journal of Hydrology **95**: 39-54.

Ross, B. (1990). "The diversion capacity of capillary barriers." Water Resources Research **26**(10): 2625-2629.

Rovina, H. and F. Zuber (1997). Wasserbeschaffung für die Gemeinde Grächen. Trinkwasserbohrungen in den Regionen "Meisen" und "Taa". Hydrogeologischer Bericht. Brig-Glis, 23 pp.

Sand, K. and D.L. Kane (1986). Effects of seasonally frozen ground in snowmelt modeling. Cold Regions Hydrology Symposium, American Water Resources Association: 321-327.

Schaap, M.C., F.J. Leij, and M.T. Van Genuchten (2001). "ROSETTA: a computer program for estimating soil hydraulic parameters with hierarchical pedotransfer functions." Journal of Hydrology **251**: 163-176.

Schlachter, I. (2000). Infiltration into partly frozen soil - its dependence on soil tillage treatments. Diploma thesis. ETHZ Institute for Terrestrial Ecology. Zurich, 39 pp.

Schneebeli, M. (1995). "Development and stability of preferential flow paths in a layered snowpack. *In* Tonnessen K.A., M. W. Williams, and M. Tranter (eds.), Biochemistry of Seasonally Snow-Covered Catchments, Boulder, July 1995. International Association of Hydrological Publication (228), 89-95.

Schneebeli, M., H. Flühler, T. Gimmi, H. Wydler, H.-P. Läser, and T. Baer (1995). "Measurements of water potential and water content in unsaturated crystalline rock." Water Resources Research **31**(8): 1837-1843.

Seligman, G. (1936). Snow structure and ski fields. London, Macmillan.

Seyfried, M.S. and M.D. Murdock (1997). "Use of air permeability to estimate infiltrability of frozen soil." Journal of Hydrology **202**: 95-107.

Shanley, J.B. and A. Chalmers (1998). "The effect of frozen soil on snowmelt runoff at Sleepers River, Vermont." Hydrological Processes **13**: 1843-1857.

Singh, P., G. Spitzbart, H. Hübl, and H.W. Weinmeister (1997). "Hydrological response of snowpack under rain-on-snow events: a field study." Journal of Hydrology **202**(1-4): 1-20.

Singh, P., G. Spitzbart, H. Hübl, and H.W. Weinmeister (1998). "The role of snowpack in producing floods under heavy rainfall." *In* Hydrology, Water Resources and Ecology In Headwaters (Proceedings of the Head Water 98 Conference), N°248, Meran/Merano (Italy): 89-95.

Singh, P. and V.P. Singh (2001). Snow and glacier hydrology. Baton Rouge, Kluwer Academic Publishers, 742 pp.

Spaans, E.J. and J.M. Baker (1996). "The soil freezing characteristic: its measurement and similarity to the soil moisture characteristic." Soil Sci. Soc. Am. J. **60**: 13-19.

Speck, C.K. (1994). "Änderung des Grundwasserregimes unter dem Einfluss von Gletschern und Permafrost." Mitteilungen der VAW (Versuchsanstalt für Wasserbau, Hydrologie und Glaziologie der ETHZ) Vol.134, 164 pp.

Stadler, D, H. Flühler, and P.-E. Jansson (1997). "Modelling vertical and lateral water flow in frozen and sloped forest soil plots." Cold Regions Science and Technology **26** (3): 181-194.

Stadler, D., M. Stähli, P. Aeby, and H.Flühler (2000). "Dye tracing and image analysis for quantifying water infiltration into frozen soils." Soil Sci. Soc. Am. J. **64**: 505-516.

Stadler, D., H. Wunderli, A. Auckenthaler, and H. Flühler (1996). "Measurement of frost-induced snowmelt runoff in a forest soil." Hydrological Processes **10**: 1293-1304.

Stähli, M., D. Bayard, H. Wydler, and H. Flühler (2002). "Snowmelt infiltration into alpine soils visualized by dye tracer technique." Arct. Antarct. Alp. Res. (submitted).

Stähli, M., P.-E. Jansson, and L.C. Lundin (1996). "Preferential water flow in a frozen soil - a two domain model approach." Hydrological Processes **10**: 1305-1316.

Stähli, M. and P.-E. Jansson (1998). "Test of two SVAT snow submodels during different winter conditions." Agricultural and Forest Meteorology **92**: 29-41.

Stähli, M., P.-E. Jansson, and L.C. Lundin (1999). "Soil moisture redistribution and infiltration in frozen sandy soils." Water Resources Research **35**: 95-103.

Stähli, M., L. Nyberg, P.-E.Mellander, P.-E. Jansson, and K.H. Bishop (2001). "Soil frost effects on soil water and runoff dynamics along a boreal transect: 2. Simulations." Hydrological Processes **15**: 927-941.

Stähli, M., J. Schaper, and A. Papritz (2002). "Towards a snow-depth distribution model in a heterogeneous subalpine forest using a Landsat TM image and an aerial photograph." Annals of Glaciology **34**: 65-70.

Stein, J. and D.L., Kane (1983). "Monitoring the unfrozen water content of soil and snow using

Time Domain Reflectometry." Water Resources Research **19**: 1573-1584.
Sturm, M., J. Holmgren, and G.E. Liston. (1995). "A seasonal snow cover classification system for local to global application". J. Climate **8**: 1261-1283.
Taber, S. (1930). "The mechanism of frost heaving." Journal of Geology **38**(4): 303-317.
Tabler, R.D., N.H. Berg, D.C. Trabant, H.S. Santeford, and P.A. Rechard (1990). Measurement and evaluation of winter precipitation. *In* W. L. Ryan and R. D. Crissman (eds.), Cold Regions Hydrology and Hydraulics, New York, American Society of Civil Engineers: 9-30.
Tabler, R. D., J. W. Pomeroy, and B.W. Santana (1990). Drifting snows. *In* W. L. Ryan and R. D. Crissman (eds.), Cold Regions Hydrology and Hydraulics, New York, American Society of Civil Engineers, 95-146.
Tappeiner, U., Tappeiner G., J. Aschenwald, E. Tasser, and B. Ostendorf (2001). "GIS-based modelling of spatial pattern of snow cover duration in an alpine area." Ecological Modelling **136**: 265-275.
Tenthorey, G. (1992). "Perennial névés and the hydrology of rock glaciers." Permafrost and Periglacial Processes **3**(3): 247-254.
Thompson, M.L. and R.L. Scharf (1994). "An improved zero-tension lysimeter to monitor colloid transport in soils." J. Environ. Qual. **23**: 378-383.
Thorne, G.A., J. Laporte, and D. Clarke (1998). "The effects of frozen soils on groundwater recharge and discharge in granitic rock terrane of the Canadian shield." Nordic Hydrology **29**(4/5): 371-384.
Topp, G. C., J.L. Davis, and A.P. Annan,(1980). "Electromagnetic determination of soil water content: measurements in coaxial transmission lines." Water Resources Research **16**(3): 574-582.
Trimble, G.R., R.S. Sartz, R.S. Pierce. (1958). "How type of soil frost affects infiltration." Journal of Soil and Water Conservation **13**: 81-82.
Tseng, P.-H. and T.H. Illangasekare (1994). "Modeling of snow melting and uniform wetting front migration in a layered subfreezing snowpack." Water Research **30**(8): 2363-2376.
Tullen, P. (2002). Méthode d'analyse du fonctionnement hydrogéologique des versants instables. Dissertation. EPFL, ENAC. Lausanne, Switzerland, 192 pp.
U.S. Army Corps of Engineers (1956). Snow hydrology, summary report on the snow investigation. Portland, Oregaon, Corps of Engg.
Van Genuchten, M.T. (1980). "A closed-form equation for predicting the hydraulic conductivity of unsaturated soils." Soil Sci. Soc. Am. J. **44**: 892-898.
Venäläinen, A., H. Tuomenvirta, R. Lahtinen, and M. Heikinheimo (2001). "The influence of climate warming on soil frost on snow-free surfaces in Finland." Climatic Change **50**: 111-128.
Waldner, P.A., M. Stähli, M. Schneebeli, M. Schwikowski, and H. Flühler (2000). "Melt water and nitrate release from a snow pack on a marshy subalpine meadow." Swiss Forestry Journal **151**: 198-204.
Waldner, P.A., M. Schneebeli, U. Schultze-Zimmermann, and H. Flühler (2002). "Effect of snow structure on water flow and solute transport." Hydrological Processes. (submitted).
Werner, P. (1994). La flore. Martigny, Edition Pillet, 257 pp.
Williams, K.S. and D.G. Tarboton (1999). "The ABC's of snowmelt: a topographically factorized energy component snowmelt model." Hydrological Processes **13**: 1905-1920.
Williams, M.W. and J.M. Melack (1991). "Solute chemistry of snowmelt and runoff in an alpine basin, Sierra Nevada." Water Resources Research. **27** (7): 1575-1588.
Williams, P.J. and T.P. Burt (1974). "Measurement of hydraulic conductivity of frozen soils." Can. Geotech. J. **11**: 647-650.
Williams, P.J. and W. Smith (1989). The Frozen Earth. Cambridge University Press, 306 pp.

Woo, M. K., R. Heron, and P. Marsh (1982). "Basal ice in high arctic snowpacks." Arctic and Alpine Research **14**: 251-260.

Woo, M.K., P. Marsch, and W. Pomeroy (2000). "Snow, frozen soils and permafrost hydrology in Canada 1995-1998." Hydrological Processes **14**: 1591-1611.

Zimmermann, M., P. Mani, and P. Gamma (1997). Murganggefahr und Klimaänderung -ein GIS- basierter Ansatz 4. NRP 31. Zürich, Vdf, 162 pp.

Zuzel, J.F. and J.L. Pikul Jr. (1987). "Infiltration into a seasonally frozen agricultural soil." Journal of Soil and Water Conservation: 447-450.

Appendix

APPENDIX A: PORCHET INFILTRATION TESTS

The Porchet infiltration tests are used to calculate the soil saturated hydraulic conductivity k_{sat}. It consists of pouring out water into a small trench. The water level is then measured steadily until all water infiltrated into the soil.

To calculate k_{sat}, a unitary hydraulic gradient **i=1** is assumed in all direction. This strong simplification is rarely supported in reality, and the obtained results should hence be regarded as a first order approximation.

k_{sat} is calculated using the following equation:

$$Q = -\frac{dV}{dt} = k_{sat} \cdot i \cdot S \qquad \text{(A.1)}$$

with **Q** : flow rate,
V : water volume,
t : time,
S : infiltration surface.

By making explicit **V**, **S**, which depends on the geometry of the trench, and integrating eq. A.1, we find k_{sat}.

A.1. PORCHET TEST: HANNIGALP

Time (s)	Water depth (cm)	Sat. hydr. cond. k_{sat} (m/s)	Time (s)	Water depth (cm)	Sat. hydr. cond. k_{sat} (m/s)
0	16	3.8E-5	0	16	6.4E-5
30	15	1.6E-5	30	15	4.1E-5
60	14.6	2.5E-5	60	14.4	4.2E-5
90	14.0	2.1E-5	90	13.8	4.4E-5
120	13.5	2.6E-5	120	13.2	4.6E-5
150	12.9	4.6E-5	150	12.6	4.0E-5
180	11.9	4.0E-5	180	12.1	4.2E-5
210	11.1	2.6E-5	210	11.6	4.4E-5
240	10.6		240	11.1	
Mean k_{sat} (m/s)		3.0E-5			4.6E-5

Table A.1: Two Porchet tests at Hannigalp.

A.2. PORCHET TEST: GD ST BERNARD

Time (s)	Water depth (cm)	Sat. hydr. cond. k_{sat} (m/s)	Time (s)	Water depth (cm)	Sat. hydr. cond. k_{sat} (m/s)
0	16.5	5.6E-5	0	24.7	5.8E-5
30	15.6	4.6E-5	30	23.3	5.2E-5
60	14.9	4.1E-5	60	22.1	6.1E-5
90	14.3	5.0E-5	90	20.8	6.4E-5
120	13.6	6.0E-5	120	19.5	5.8E-5
150	12.8	4.8E-5	150	18.4	5.6E-5
180	12.2	5.0E-5	180	17.4	5.9E-5
210	11.6		210	16.4	
Mean k_{sat} (m/s)		5.0E-5			5.8E-5

Table A.2: Two Porchet tests at Gd St Bernard.

APPENDIX B: TRACER APPLICATION QUANTITIES

B.1. TRACER APPLICATION QUANTITIES AT HANNIGALP

Location	Amount (g)	Surface (m^2)
Bottom	288	2.4
Middle	480	2.4
Top	960	2.4
Reserve	512	2.4

Figure B.1: Tracer application quantities at Hannigalp. The tracer application area was divided into three sub-areas (Figure 4.5) and a reserve area.

B.2. TRACER APPLICATION QUANTITIES AT GD ST BERNARD

Location	Amount (g)	Surface (m^2)
Bottom	240	1.15
Middle	400	1.15
Top	800	1.15

Table B.1: Tracer application quantities at Gd St Bernard. The tracer application area was divided into three sub-areas.

APPENDIX C: SIMULATION RESULTS FOR UNFROZEN SOIL COLUMN IRRIGATION TEST

The comparison between simulated and measured matric potential and soil liquid water content for the first irrigation at a depth of 5, 20 and 35 cm is shown in Figure C.1. Results for the second

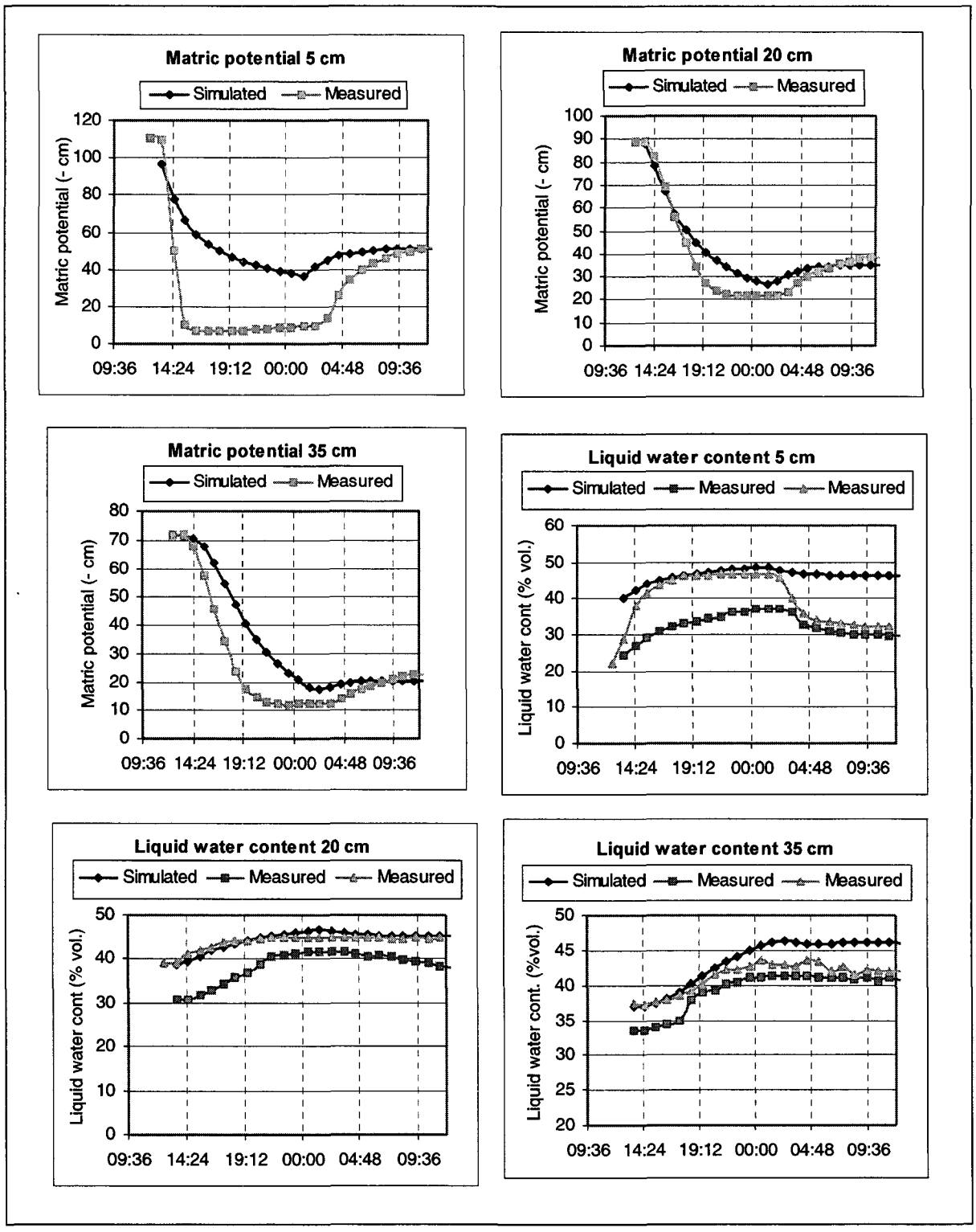

Figure C.1: Comparison between simulated and measured matric potential and liquid water content at a depth of 5, 20 and 35 cm for the first irrigation. Simulation was carried out with COUP.

irrigation at a depth of 20 and 45 cm are given in Figure C.2.

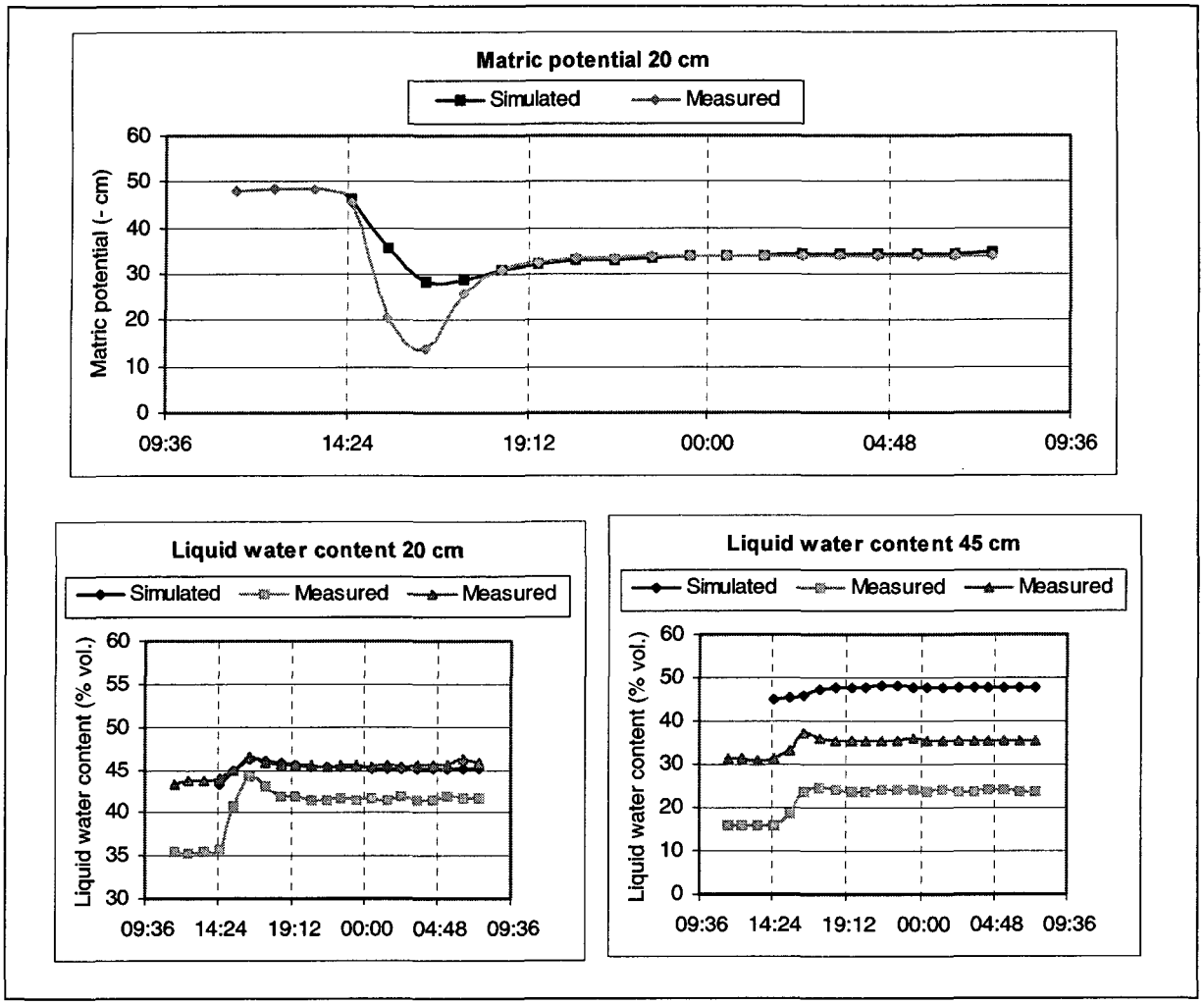

Figure C.2: Comparison between simulated and measured matric potential and liquid water content at a depth of 5 and 35 cm for the second irrigation. Simulation was carried out with COUP.

APPENDIX D: SIMULATION RESULTS FOR UNFROZEN SOIL COLUMN IRRIGATION TEST

The simulated matric potential (20 and 45 cm) and soil liquid water content (20 cm) are shown in Figure D.1.

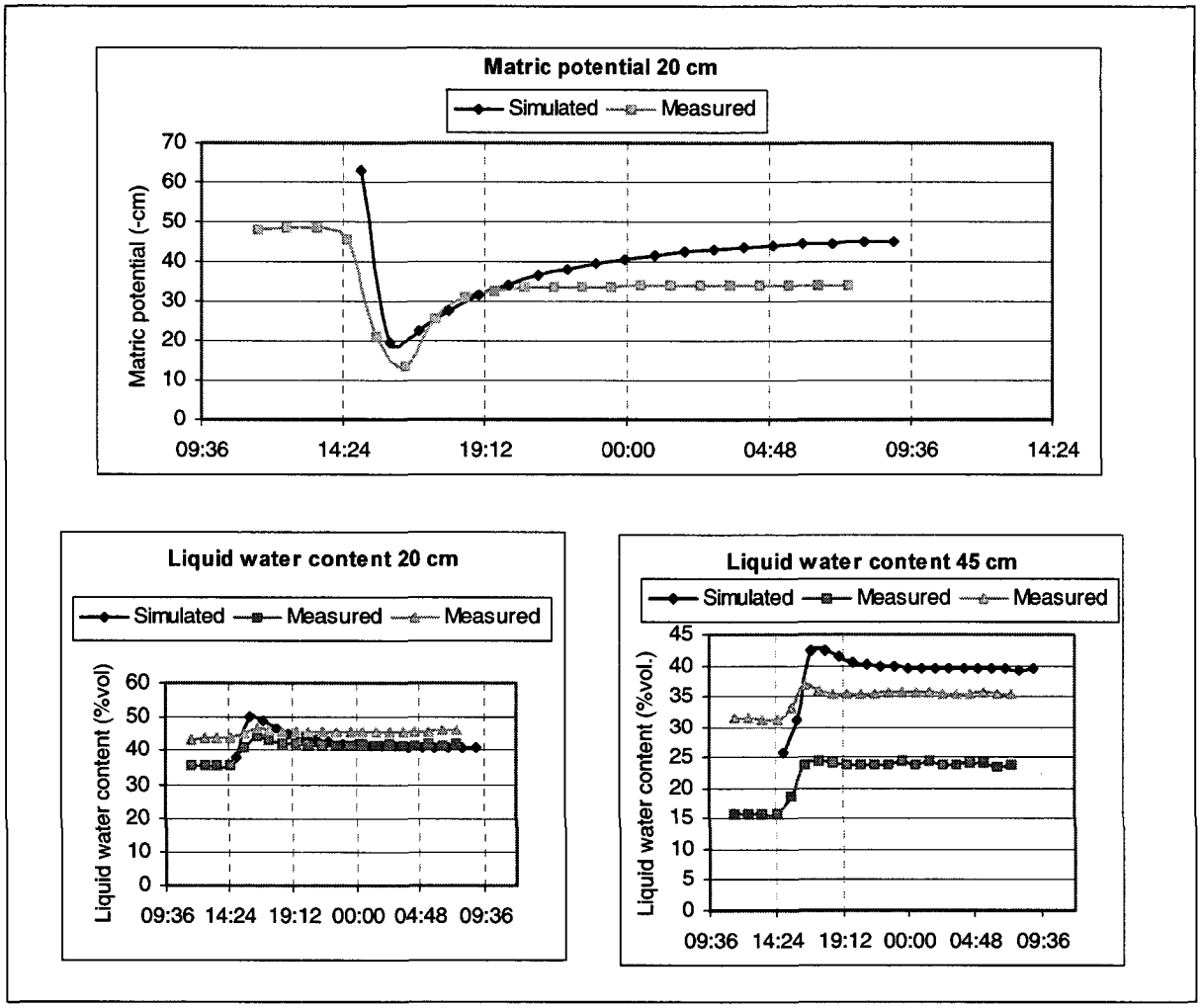

Figure D.1: Comparison between simulated and measured matric potential (20 cm) and liquid water content (20 and 45 cm). Simulation was carried out with COUP.

APPENDIX E: SCALING FACTORS USED IN THE CALIBRATION OF THE THERMAL CONDUCTIVITY AT HANNIGALP FOR UNFROZEN SOIL COLUMN IRRIGATION TESTS AS WELL AS SIMULATION RESULTS

The thermal conductivity was adjusted for each soil layer (see eq. 3.12). Scaling factors are given in Table E.1.

Layer	1	2	3	4	5	6	7	8	9	10	11	12
Thermal scale log	-0.2	-0.1	0.3	0.5	0.5	0.5	0.5	0.5	0.5	0.5	0.5	0.5

Table E.1: Scaling factor of thermal conductivity for different soil layers (see also Table 8.3).

The simulated and measured soil temperatures and liquid water contents at a depth of 20 and 35 cm are shown in Figure E.1.

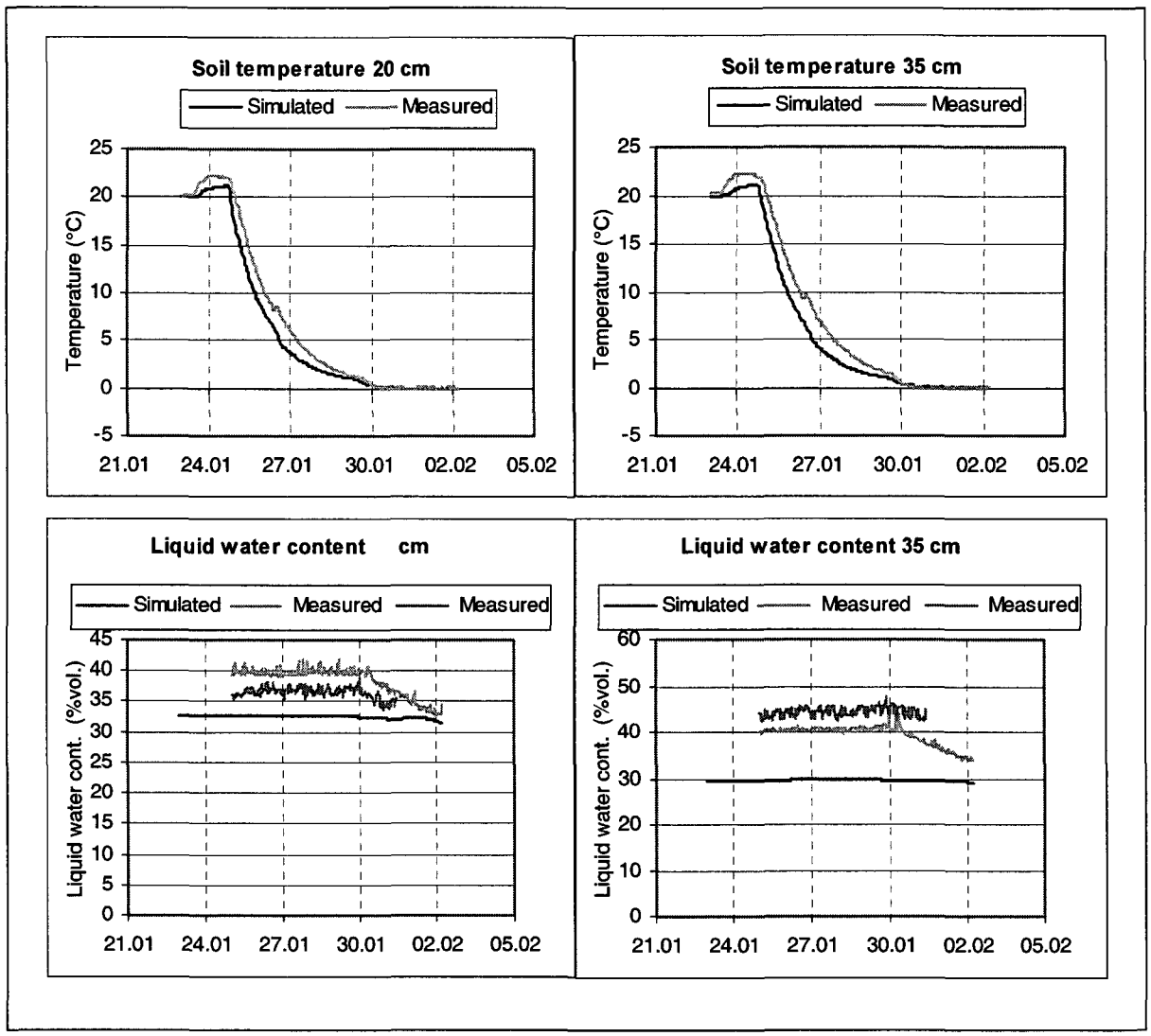

Figure E.1: Simulated soil temperature and liquid water content at a depth of 20 and 35 cm compared with measurements.

APPENDIX F: SCALING PARAMETERS USED IN THE CALIBRATION OF THE THERMAL CONDUCTIVITY AT HANNIGALP AND AT GD ST BERNARD

The thermal conductivity scaling factor (see eq. 3.12) for each soil layer is given for Hannigalp in Table F.1 and Table F.2, and for Gd St Bernard in Table F.3 and Table F.4.

layer	1	2	3	4	5	6	7	8	9	10	11
layer thickness (m)	0.075	0.05	0.05	0.05	0.05	0.05	0.05	0.05	0.05	0.05	0.05
Thermal scale log	-0.3	-0.1	0	0	0	0	0	0	0	0	0

Table F.1: Scaling factor for the thermal conductivity at Hannigalp.

layer	12	13	14	15	16	17	18	19	20	21	22
layer thickness (m)	0.225	0.25	0.25	0.25	0.25	0.25	1	1	1	2	2
Thermal scale log	0	0.55	0.55	0.55	0.55	0.55	0.55	0.55	0.55	055	0.55

Table F.2: Scaling factor for the thermal conductivity at Hannigalp.

layer	1	2	3	4	5	6	7	8	9	10	11
layer thickness (m)	0.075	0.05	0.05	0.05	0.05	0.05	0.05	0.05	0.05	0.05	0.05
Thermal scale log	0.5	0.5	0.5	0.5	0.5	0.5	0.5	0.5	0.5	0.5	0.5

Table F.3: Scaling factor of thermal conductivity at Gd St Bernard.

layer	12	13	14	15	16	17	18	19	20	21	22
layer thickness (m)	0.225	0.25	0.25	0.25	0.25	0.25	1	1	1	2	2
Thermal scale log	0.5	0.6	0.6	0.6	0.6	0.6	0.6	0.6	0.6	0.6	0.6

Table F.4: Scaling factors for thermal conductivity at Gd St Bernard.

F.1. NUMERICAL SIMULATION OF SOIL TEMPERATURE AND LIQUID WATER CONTENT AT A DEPTH OF 10 AND 20 CM AT HANNIGALP AND GD ST BERNARD

The different Figures are explained in the footnotes.

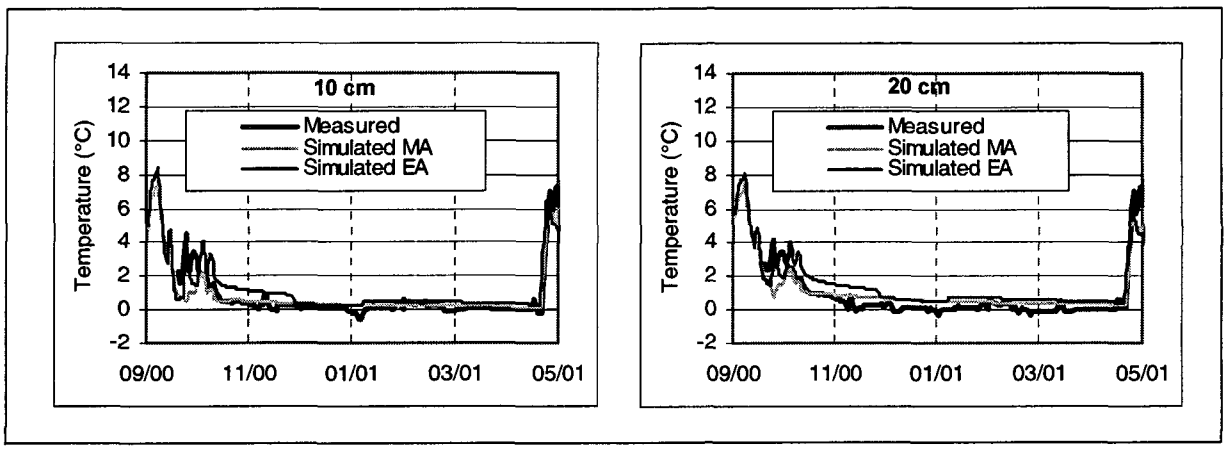

Figure F.1: Simulated and measured soil temperature (°C) at a depth of 10 and 20 cm at Hannigalp from September 2000 to June 2001 using either the **EA** or the **MA**.

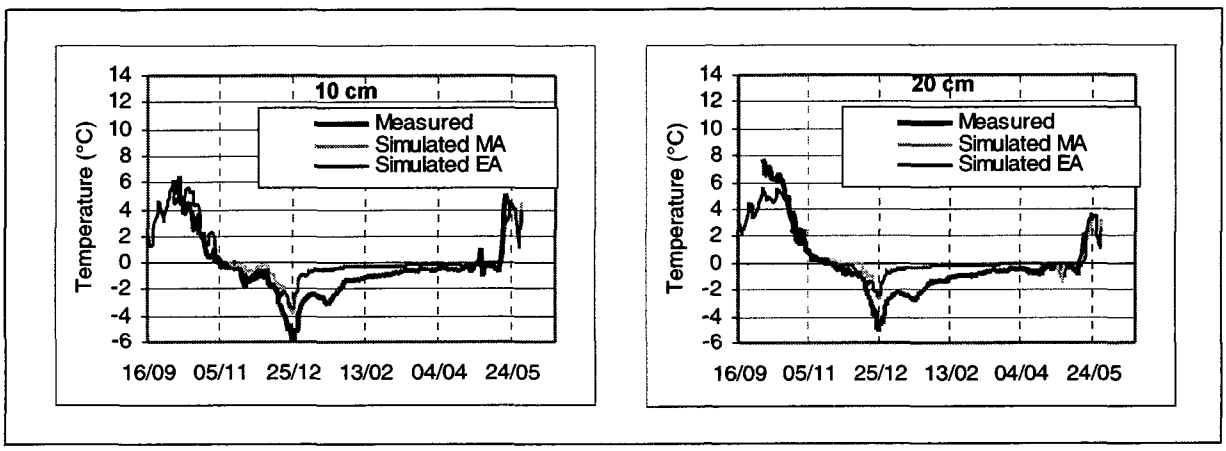

Figure F.2: Simulated and measured soil temperature (°C) at a depth of 10 and 20 cm at Hannigalp from September 2001 to June 2002 using either the **EA** or the **MA**.

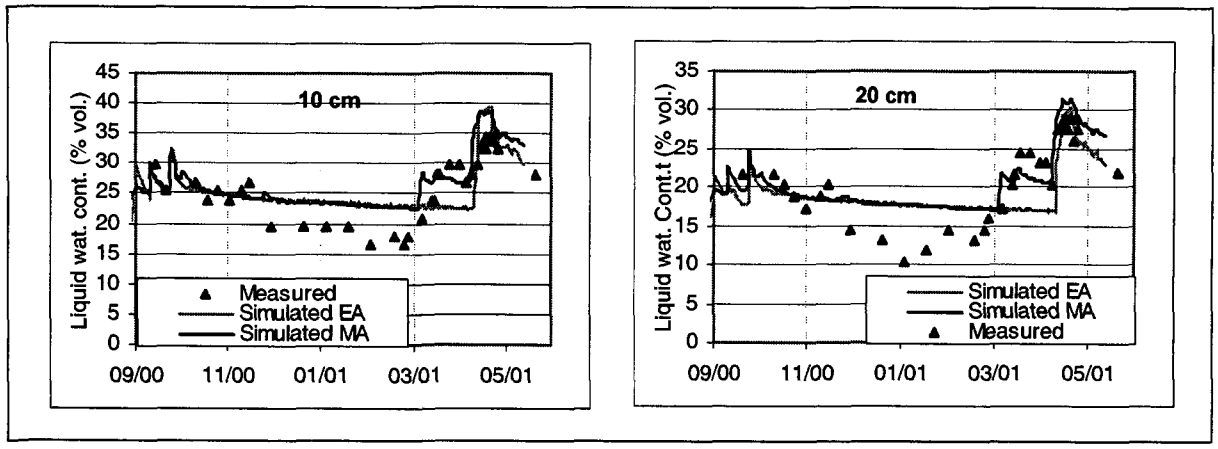

Figure F.3: Simulated and measured soil liquid water content (% vol.) at a depth of 10 and 20 cm at Hannigalp from September 2000 to June 2001 using either the **EA** or the **MA**.

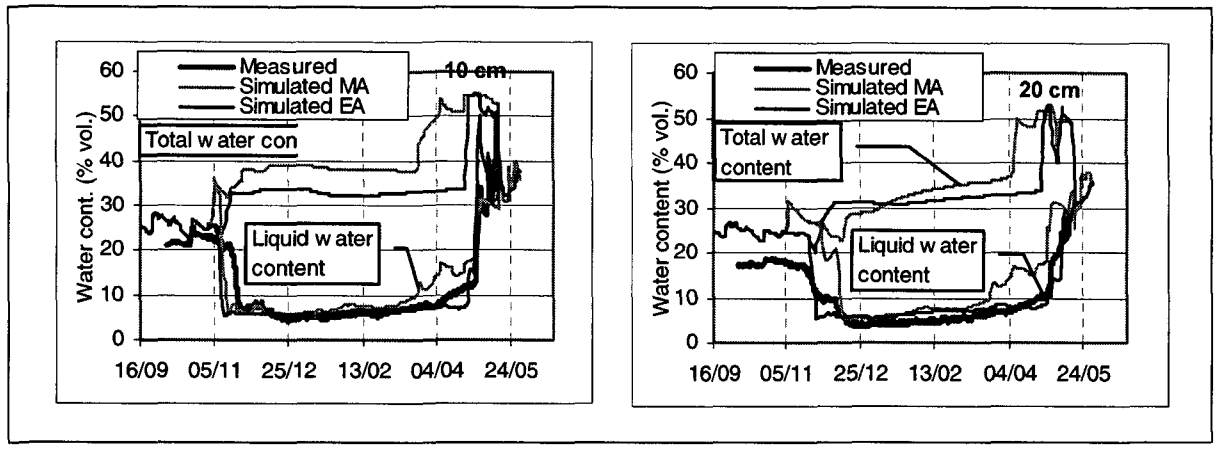

Figure F.4: Simulated and measured soil liquid water content (% vol.) at a depth of 10 and 20 cm at Hannigalp from September 2001 to June 2002 using either the **EA** or the **MA**.

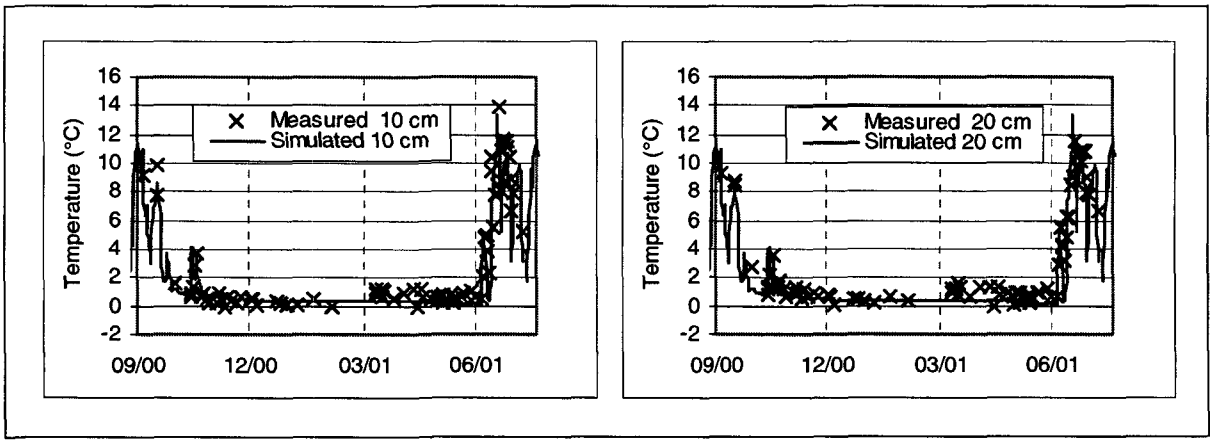

Figure F.5: Simulated and measured soil temperature at a depth of 10 and 20 cm during winter 2000/2001 at Gd St Bernard south plot using the **MA**.

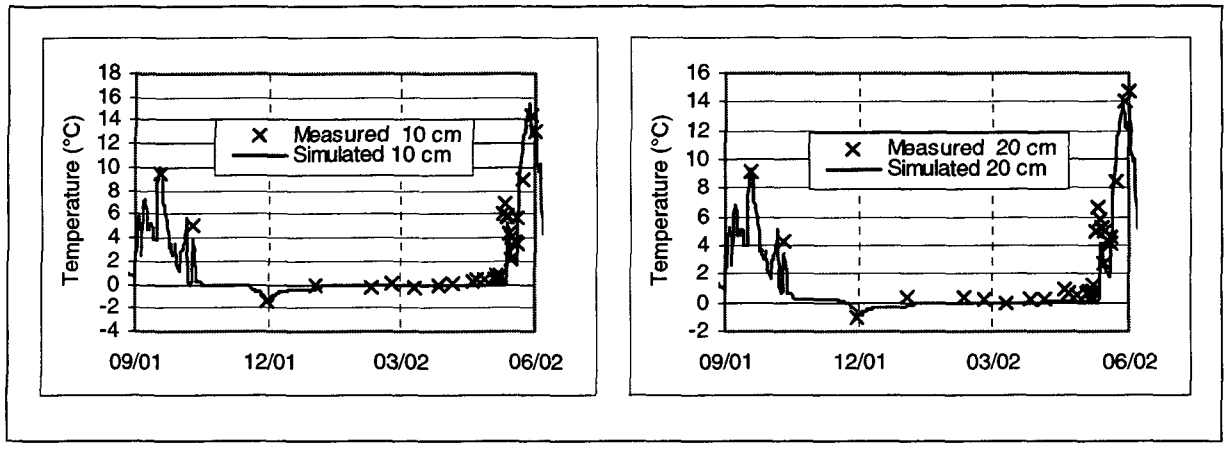

Figure F.6: Simulated and measured soil temperature at a depth of 10and 20 cm during winter 2001/2002 at Gd St Bernard south plot using the MA.

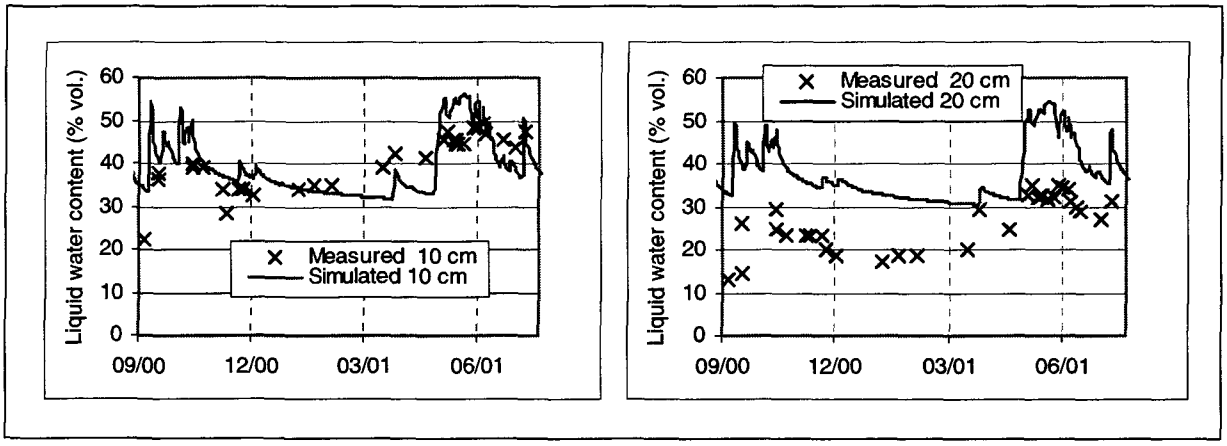

Figure F.7: Simulated and measured liquid water content at a depth of 10 and 20 cm during winter 2000/2001 at Gd St Bernard south plot using the MA.

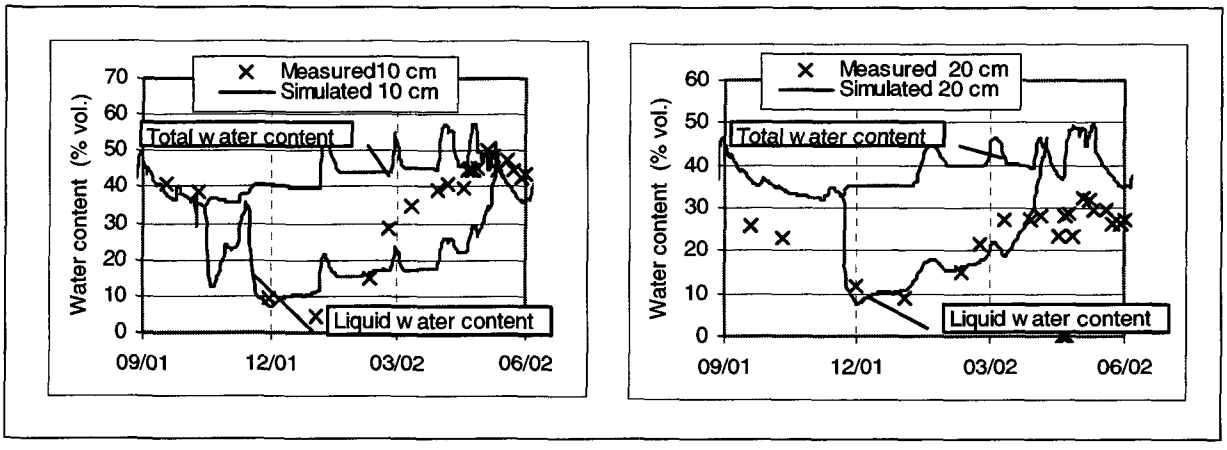

Figure F.8: Simulated liquid/total water content compared with measured liquid water content at a depth of 10 and 20 cm during winter 2001/2002 at Gd St Bernard south plot using the MA.

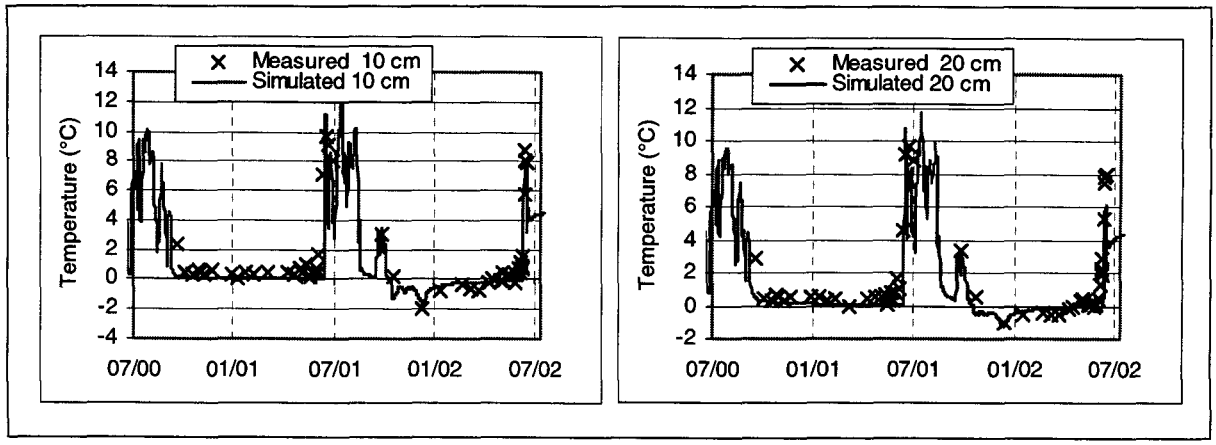

Figure F.9: Simulated and measured soil temperature (°C) at a depth of 10 and 20 cm at Gd St Bernard north plot from October 2000 to July 2002 using the **EA**.

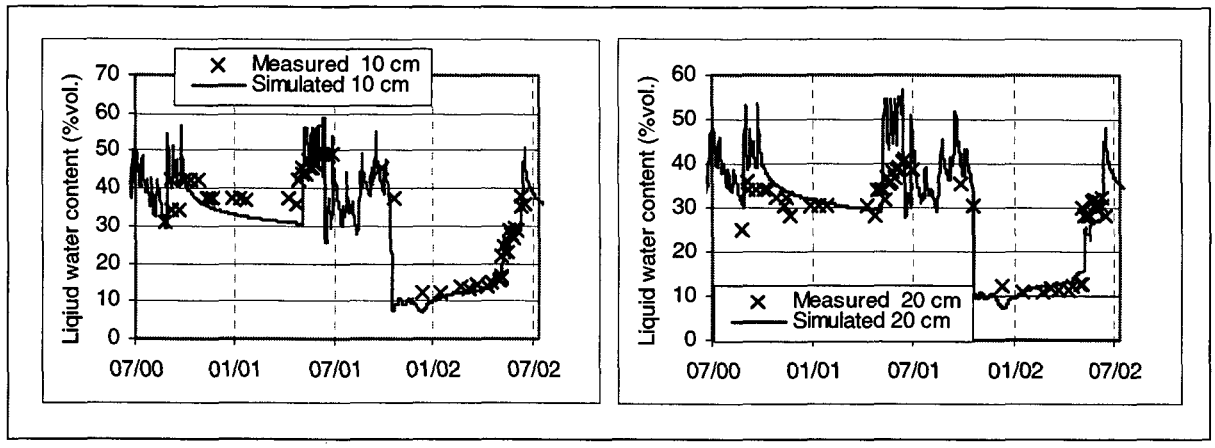

Figure F.10: Simulated and measured liquid water content (% vol.) at a depth of 10 and 20 cm at Gd St Bernard north plot from October 2000 to July 2002 using the **EA**.

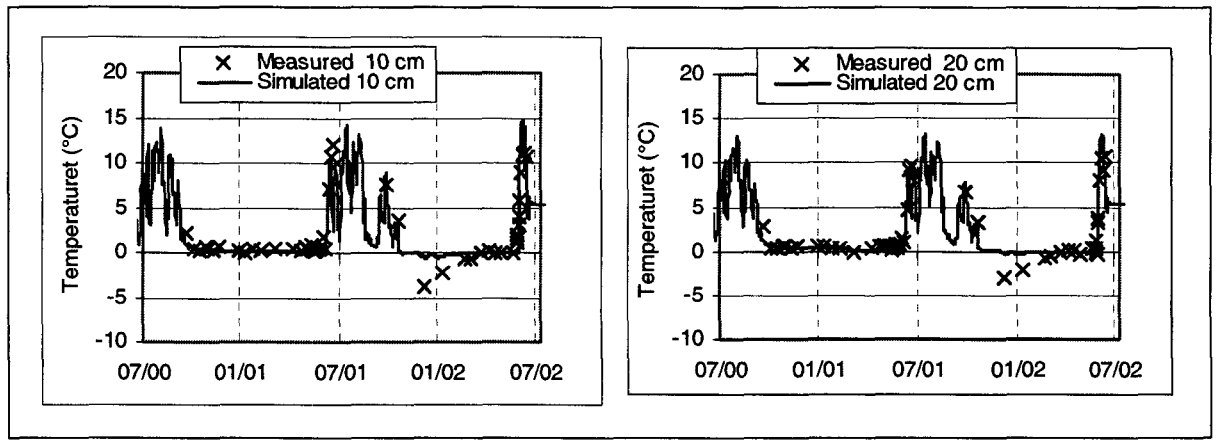

Figure F.11: Simulated and measured soil temperature (°C) at a depth of 10 and 20 cm at Gd St Bernard east plot from October 2000 to July 2002 using the **MA**.

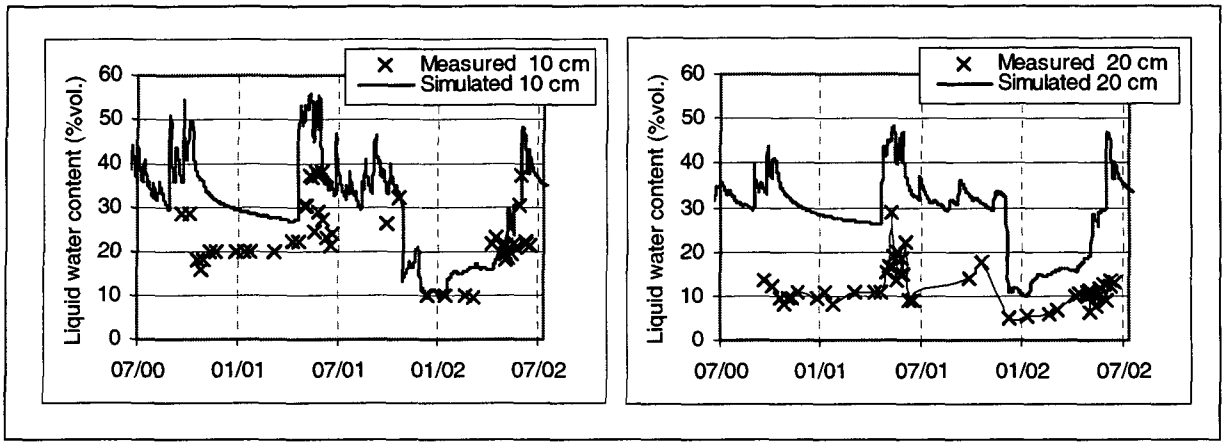

Figure F.12: Simulated and measured liquid water content (% vol.) at a depth of 10 and 20 cm at Gd St Bernard east plot from October 2000 to July 2002 using the **MA**.

APPENDIX G: IMPACT OF A CHANGING CLIMATE ON SELECTED PARAMETERS AT DIFFERENT ALTITUDES

At 1300 m

	Unchanged climate	$\Delta T = +2°C$	$\Delta P = +15\%$	$\Delta T = +2°C$; $\Delta P = +15\%$
Mean snow depth (cm) (st. dev.)	20.4 (13)	6.3 (7) (-69%)	23.7 (14) (+16%)	7.6 (8) (-62%)
Max snow depth (cm) (st. dev.)	51.1 (23)	23.1 (16) (-55%)	57.7 (24) (+13%)	26.6 (19) (-48%)
#days snow depth > 70 cm	6.1 (15)	0 (0) (-100%)	10.1 (21) (+66%)	0.5 (2) (-91%)
#days snow depth > 10 cm	87.1 (39)	34.0 (36) (-61%)	96.1 (37) (+10%)	38.8 (38) (-55%)
Mean soil frost (cm) (st. dev.)	13.3 (9)	14.2 (6) (+6.2%)	11.9 (8) (-10.5%)	13.4 (6) (+0.7%)
Max soil frost (cm) (st. dev.)	24.5 (14)	27.5 (10) (+12.5%)	22.0 (12) (-10%)	25.4 (9) (+3.7%)
#days soil frost > 8 cm (cm) (st. dev.)	72.0 (46)	83.1 (34) (+15%)	64.1 (50) (-11%)	75.1 (38.4) (+4%)
Deep percolation (%) (st. dev.)	83.5 (33)	80.8 (23) (-3%)	83.8 (30) (+0%)	80.0 (21.4) (-4%)

Table G.1: Different values for selected snow and frost variables at 1300 m for current climate and three modified climate (Δ T=+2°C; Δ Prec=+15% and Δ T=+2°C Δ Prec=+15%). Simulation are based on daily data between 1968 and 2000. The mean snow depth and mean soil frost depth are taken between the beginning of November and the end of March. The percolation is taken between the beginning of November and the end of May.

At 1600 m

	Unchanged climate	$\Delta T = +2°C$	$\Delta P = +15\%$	$\Delta T = +2°C$; $\Delta P = +15\%$
Mean snow depth (cm) (st. dev.)	38.1 (15)	18.8 (12.4) (-50%)	42.9 (16) (+13%)	20.9 (14) (-45%)
Max snow depth (cm) (st. dev.)	73.8 (25)	47.6 (24) (-36%)	83.6 (22) (+13%)	54.3 (26) (-26%)
#days snow depth > 70 cm	29.8 (32)	5.7 (14) (-81%)	42 (38) (+45%)	8.9 (18) (-70%)

Table G.2: Different values for selected snow and frost variables at 1600 m for current climate and three modified climate (Δ T=+2°C; Δ Prec=+15% and Δ T=+2°C Δ Prec=+15%). Simulation are based on daily data between 1968 and 2000. The mean snow depth and mean soil frost depth are taken between the beginning of November and the end of March. The percolation is taken between the beginning of November and the end of May.

#days snow depth > 10 cm	124.5 (39)	80.9 (40) (-35%)	131 (31) (+5%)	86.7 (41) (-30%)
Mean soil frost (cm) (st. dev.)	11.9 (13)	15.0 (10) (+26%)	10.8 (13) (-9%)	13.9 (10) (+17%)
Max soil frost (cm) (st. dev.)	21.4 (18)	26.8. (13) (+25%)	19.8 (18) (-7%)	25.3 (14) (+18%)
#days soil frost > 8 cm (cm) (st. dev.)	63.0 (64)	84.4 (42) (+33%)	58.9 (66) (-7%)	77.7 (48) (+23%)
Deep percolation (%) (st. dev.)	87.2 (42)	78.7 (39) (-10%)	87.7 (39) (+1%)	80.7 (36) (-7%)

Table G.2: Different values for selected snow and frost variables at 1600 m for current climate and three modified climate (Δ T=+2°C; Δ Prec=+15% and Δ T=+2°C Δ Prec=+15%). Simulation are based on daily data between 1968 and 2000. The mean snow depth and mean soil frost depth are taken between the beginning of November and the end of March. The percolation is taken between the beginning of November and the end of May.

At 1900 m

	Unchanged climate	Δ T = +2°C	Δ P = +15%	Δ T = +2°C; Δ P = +15%
Mean snow depth (cm) (st. dev.)	65.3 (20)	46.2 (17) (-29%)	71.7 (21) (+10%)	52.0 (19) (-20%)
Max snow depth (cm) (st. dev.)	108 (21)	89.2 (25) (-17%)	117 (21) (+8%)	98.2 (25) (-9%)
#days snow depth > 70 cm	88.6 (48)	47.9 (37) (-46%)	102 (44) (+15%)	59.7 (39) (-32%)
#days snow depth > 10 cm	172 (21)	139 (30) (-13%)	175 (21) (+2%)	144 (29) (-16%)
Mean soil frost (cm) (st. dev.)	10.1 (14)	12.7 (15) (+26%)	9.4 (13) (-7%)	11.5 (14) (+14%)
Max soil frost (cm) (st. dev.)	16.9 (18)	20.6 (20) (+22%)	15.8 (18) (-7%)	19.4 (20) (+15%)
#days soil frost > 8 cm (cm) (st. dev.)	63.0 (83)	71.6 (73) (+14%)	55.6 (83) (-12%)	68.3 (73) (+8%)
Deep percolation (%) (st. dev.)	91.3 (43)	85.9 (4) (-6%)	91.2 (40) (+0%)	85.5 (42) (-6%)

Table G.3: Different values for selected snow and frost variables at 1900 m for current climate and three modified climate (Δ T=+2°C; Δ Prec=+15% and Δ T=+2°C Δ Prec=+15%). Simulation are based on daily data between 1968 and 2000. The mean snow depth and mean soil frost depth are taken between the beginning of November and the end of March. The percolation is taken between the beginning of November and the end of May.

At 2300 m

	Unchanged climate	ΔT = +2°C	ΔP = +15%	ΔT = +2°C; ΔP = +15%
Mean snow depth (cm) (st. dev.)	93.8 (30)	78.8 (24) (-16%)	100 (28) (+6%)	87.2 (26) (-7%)
Max snow depth (cm) (st. dev.)	139 (36)	129 (26) (-7%)	155 (27) (+11%)	141 (27) (+1%)
#days snow depth > 70 cm	140 (49)	112 (46) (-20%)	155 (42) (+11%)	123 (45) (-12%)
#days snow depth > 10 cm	202 (20)	181 (21) (-10%)	206 (20) (+2%)	185 (21) (-9%)
Mean soil frost (cm) (st. dev.)	15.0 (18)	11.6 (17) (-23%)	13.0 (18) (-13%)	10.3 (16) (-31%)
Max soil frost (cm) (st. dev.)	20.1 (20)	19.8 (20) (-1%)	20.4 (19) (+1%)	19.4 (19) (-3%)
#days soil frost > 8 cm (cm) (st. dev.)	83.6 (100)	76.6 (96) (-8%)	73.3 (101) (-12%)	63.9 (94) (-16%)
Deep percolation (%) (st. dev.)	80.2 (47)	84.0 (45) (-5%)	84.6 (44) (+5%)	84.2 (42) (+5%)

Table G.4: Different values for selected snow and frost variables at 2300 m for current climate and three modified climate (Δ T=+2°C; Δ Prec=+15% and Δ T=+2°C Δ Prec=+15%). Simulation are based on daily data between 1968 and 2000. The mean snow depth and mean soil frost depth are taken between the beginning of November and the end of March. The percolation is taken between the beginning of November and the end of May.

At 2600 m.

	Unchanged climate	ΔT = +2°C	ΔP = +15%	ΔT = +2°C; ΔP = +15%
Mean snow depth (cm) (st. dev.)	115 (35)	99.4 (32) (-19%)	128 (38) (+4%)	111 (34) (-10%)
Max snow depth (cm) (st. dev.)	183 (39)	165 (36) (-10%)	201 (42) (+10%)	182 (38) (-1%)
#days snow depth > 70 cm	169 (46)	139 (43) (-17%)	177 (41) (+5%)	152 (40) (-10%)
#days snow depth > 10 cm	212 (21)	193 (21) (-9%)	215 (21) (+1%)	197 (21) (-7%)
Mean soil frost (cm) (st. dev.)	15.3 (15.9)	12.7 (17.1) (-17%)	14.2 (13.9) (-7%)	11.3 (17.0) (-26%)

Table G.5: Different values for selected snow and frost variables at 2600 m for current climate and three modified climate (Δ T=+2°C; Δ Prec=+15% and Δ T=+2°C Δ Prec=+15%). Simulation are based on daily data between 1968 and 2000. The mean snow depth and mean soil frost depth are taken between the beginning of November and the end of March. The percolation is taken between the beginning of November and the end of May.

Max soil frost (cm) (st. dev.)	23.6 (25.3)	20.1 (25) (-15%)	21.5 (22) (-9%)	17.9 (22) (.24%)
#days soil frost > 8 cm (cm) (st. dev.)	97.9 (112)	76.3 (97) (-22%)	93.3 (114) (-5%)	63.4 (93) (-35%)
Deep percolation (%) (st. dev.)	67.0 (33)	82.3 (27) (+23%)	71.1 (33) (+6%)	84.5 (36) (+26)

Table G.5: Different values for selected snow and frost variables at 2600 m for current climate and three modified climate (Δ T=+2°C; Δ Prec=+15% and Δ T=+2°C Δ Prec=+15%). Simulation are based on daily data between 1968 and 2000. The mean snow depth and mean soil frost depth are taken between the beginning of November and the end of March. The percolation is taken between the beginning of November and the end of May.

CURRICULUM VITAE

Daniel Bayard

Né le 01.01.73, de nationalité suisse

Formation professionnelle

1987-1992: Maturité type scientifique: Lycée Collège des Creusets, Sion.
1993-1995: Ecole Polytechnique Fédérale de Lausanne (EPFL): Etude de Physique.
1995-1998: Eidgenössische Technische Hochschule Zürich (ETHZ): Etude de Physique: spécialisation en physique de l'environnement (Glaciologie et Physique de l'atmosphère).

Expérience professionnelle

1999-2002: Assistanat/Doctorat à l'Ecole Polytechnique Fédérale de Lausanne (EPFL).

Liste des publications

Bayard, D., and M. Stähli (2002). The effect of frozen soil on the groundwater recharge in alpine areas. *In* Collins, D., C. de Jong, and R. Ranzi (eds.), Hydrological and Meteorological Coupling in Mountain Areas: Experiments and Modelling (submitted).

Stähli, M., D. Bayard, H. Wydler, and H. Flühler (2002). "Snowmelt infiltration into alpine soils visualized by dye tracer technique." Arct. Antarct. Alp. Res (submitted).

Bayard, D., M. Stähli, A. Parriaux, H. Flühler (2002). "Snowmelt in alpine regions. How does a partly frozen soil affect the snowmelt runoff ?" Journal of Hydrology (in prep.).

Participations en Congrès, Symposium et Colloques

Symposium International, «Snowmelt Erosion and Related Problems», 28th to 30th March 2001, Oslo, Norway. Travail présenté: Water infiltration in a partly frozen ground and groundwater recharge in alpine catchments. Bayard D., M. Stähli, V.Maître, A. Parriaux.

General Assembly of the EGS, «Hydrology and rainfall processes: Hydrological and meteorological coupling in mountain areas.» 26th to 30th March 2002, Nice, France. Travail présenté: Snowmelt processes at high altitude. How does a partly frozen ground affect the groundwater recharge during snowmelt? Bayard, D., M. Stähli, P. Turberg, A. Parriaux.

SGHL-Symposium, «Wasser in den Alpen», 20th September 2002, Davos, Switzerland. Travail présenté: Hydrogeolgische Prozesse im Alpenbereich. Wie beeinflusst ein teilweise gefrorener Boden den Wasserverlauf während der Schneeschmelze? Bayard, D., M. Stähli, P. Turberg, A. Parriaux.